

The role of novel protein-protein interactions in the function and mechanism of the sarcomeric protein, myosin binding protein H (MyBPH)

By

Jacoba Martina Mouton



Dissertation presented for the degree Doctor of Philosophy (Human Genetics) in the Faculty of Medicine and Health Sciences, at Stellenbosch University

Supervisor: Dr CJ Kinnear

Co-Supervisor: Prof JC Moolman-Smook

April 2014

Declaration

By submitting this thesis electronically, I declare that the entirety of the work contained therein is my own, original work, that I am the authorship owner thereof (unless to the extent explicitly otherwise stated) and that I have not previously in its entirety or in part submitted it for obtaining any qualification.

Signatures:

Date:

Abstract

Left ventricular hypertrophy (LVH) is a major risk factor for cardiovascular morbidity and mortality, and is a feature of common diseases, such as hypertension and diabetes. It is therefore vital to understand the underlying mechanisms influencing its development. However, investigating the mechanisms underlying LVH in such complex disorders can be challenging. For this reason, many researchers have focused their attention on the autosomal dominant cardiac muscle disorder, hypertrophic cardiomyopathy (HCM), since it is considered a model disease in which to study the causal molecular factors underlying isolated cardiac hypertrophy.

HCM is a heterogeneous disease that manifests with various phenotypes and clinical symptoms, even in families with the same genetic defects, suggesting that additional factors contribute to the disease phenotype. Despite the identification of several HCM-causing genes, the genetic factors that modify the extent of hypertrophy in HCM patients remain relatively unknown.

The gene encoding the sarcomeric protein, cardiac myosin binding protein C, cMyBPC (*MyBPC3*) is one of the most frequently implicated genes in HCM. Identification of proteins that interact with cMyBPC has led to improved insights into the function of this protein and its role in cardiac hypertrophy. However, very little is known about another member of the myosin binding protein family, myosin binding protein H (MyBPH). Given the sequence homology and similarity in structure between cMyBPC and MyBPH, we propose that MyBPH, like cMyBPC, may play a critical role in the structure and functionality of the cardiac sarcomere and could therefore be involved in HCM pathogenesis.

The present study aimed to identify MyBPH-interacting proteins by using yeast two-hybrid (Y2H) analysis and to verify these interactions using three-dimensional (3D) co-localisation and co-immunoprecipitation (Co-IP) analyses. We further hypothesized that both MyBPH and cMyBPC may be involved in autophagy. To test this hypothesis, both MyBPH and cMyBPC were analysed for co-localisation with a marker for autophagy, LC3b-II. The role of MyBPH and cMyBPC in cardiac cell contractility were analysed by measuring the planar cell surface area of differentiated H9c2 rat cardiomyocytes in response to β -adrenergic stress after individual and concurrent siRNA-mediated knockdown of MyBPH and cMyBPC.

In the present study we employed a family-based genetic association analysis approach to investigate the contribution of genes encoding the novel MyBPH-interacting proteins in modifying the hypertrophy phenotype. This study investigated the hypertrophy modifying effects of 38 SNPs and haplotypes in four candidate HCM modifier genes, in 388 individuals from 27 HCM families, in which three unique South African HCM-causing founder mutations segregate.

Yeast two-hybrid analysis identified three putative MyBPH-interacting proteins namely, cardiac β -myosin heavy chain (MYH7), cardiac α -actin (ACTC1) and the SUMO-conjugating enzyme UBC9 (UBC9). These interactions were verified using both 3D co-localisation and Co-IP analyses. Furthermore, MyBPH and cMyBPC were implicated in autophagy, since both these proteins were being recruited to the membrane of autophagosomes. In addition, a cardiac contractility assay demonstrated that the concurrent siRNA-mediated knockdown of MyBPH and cMyBPC resulted in a significant reduction in cardiomyocyte contractility, compared to individual protein and control knockdowns under conditions of β -adrenergic stress. These results indicated that MyBPH could compensate for cMyBPC, and vice versa, further confirming that both these proteins are required for efficient sarcomere contraction.

Results from genetic association analyses found a number of SNPs and haplotypes that had a significant effect on HCM hypertrophy. Single SNP and haplotype analyses identified SNPs and haplotypes within genes encoding MyBPH, MYH7, ACTC1 and UBC9, which contribute to the extent of hypertrophy in HCM. In addition, we found that several variants and haplotypes had markedly different statistical significant effects in the presence of each of the three HCM founder mutations.

The results of this study ascribe novel functions to MyBPH. Cardiac MyBPC and MyBPH play a critical role in sarcomere contraction and have been implicated in autophagy. This has further implications for understanding the patho-etiology of HCM-causing mutations in the gene encoding MyBPH and its interacting proteins.

This is to our knowledge the first genetic association analysis to investigate the modifying effect of interactors of MyBPH, as indication of the risk for developing LVH in the context of HCM. Our findings suggest that the hypertrophic phenotype of HCM is modulated by the compound effect of a number of variants and haplotypes in *MyBPH*, and genes encoding protein interactors of MyBPH. These results provide a basis for future studies to investigate the risk profile of hypertrophy development in the

context of HCM, which could consequently lead to improved risk stratification and patient management.

Opsomming

Linker ventrikulêre hipertrofie (LVH) is 'n primêre risikofaktor vir kardiovaskulêre morbiditeit en mortaliteit asook 'n kenmerk van algemene siektes soos hipertensie en diabetes. Daarom is dit van kardinale belang om te verstaan wat die onderliggende meganismes is wat die ontwikkeling van LVH beïnvloed. Die ondersoek na die onderliggende meganismes wat lei tot LVH in sulke komplekse siektes is 'n uitdaging. Om hierdie rede fokus baie navorsers hul aandag op die autosomaal dominante hartspier siekte, hipertrofiese kardiomiopatie (HKM), wat beskou word as 'n model siekte om die molekulêre oorsake onderliggend tot geïsoleerde kardiovaskulêre hipertrofie te ondersoek.

HKM is 'n heterogene siekte wat manifesteer met verskeie fenotipes en kliniese simptome, selfs in families met dieselfde genetiese defekte, wat impliseer dat addisionele faktore bydra tot die modifisering van die siekte fenotipe. Ten spyte van die identifisering van verskeie HKM-versoorsakende gene, bly die genetiese faktore wat die mate van hipertrofie in HKM pasiente modifiseer relatief onbekend.

Die geen wat kodeer vir die sarkomeriese proteïen, kardiaale miosien-bindingsproteïen C (*kMyBPC*) is die algemeenste betrokke in HKM. Die identifisering van proteïene wat bind met *kMyBPC* het gelei tot verbeterde insigte tot die funksie van hierdie proteïen en die rol wat hierdie proteïen in hipertrofie speel. Ten spyte hiervan, is daar baie min inligting beskikbaar oor 'n ander lid van die miosien-bindingsproteïen families, miosien-bindingsproteïen H (*MyBPH*). Gegewe die ooreenstemming tussen die DNA basispaar-volgorde en struktuur tussen hierdie twee proteïene, stel ons voor dat *MyBPH*, net soos *kMyBPC*, 'n kritiese rol in die struktuur en funksie van die kardiaale sarkomeer speel en kan daarom betrokke wees in die patogenese van HKM.

Die huidige studie het beoog om proteïene wat met *MyBPH* bind te identifiseer deur die gebruik van gis-twee-hibried (G2H) kardiaale biblioteek sifting en om hierdie interaksies te verifieer met behulp van drie-dimensionele (3D) ko-lokalisering en ko-immunopresipitasie eksperimente. Ons het verder gehipotiseer dat beide *MyBPH* and *kMyBPC* betrokke kan wees in outofagie. Om hierdie hipotese te toets is beide *MyBPH* en *kMyBPC* geanaliseer vir ko-lokalisering met 'n merker vir outofagie, LC3b-II.

Verder het ons beplan om die rol van MyBPH en kMyBPC in kardiaale spiersel-sametrekking te ondersoek deur die oppervlak van gedifferensieerde H9c2 rot kardiomyosiete in reaksie op β -adrenergiese stres te meet, na individuele en gesamentlike siRNA-bemiddelde uitklopping van MyBPH en kMyBPC.

In hierdie studie het ons 'n familie-gebaseerde genetiese assosiasie analise benadering gevolg om vas te stel of *MyBPH* en gene wat kodeer vir die geverifieerde bindingsgenote van MyBPH bydra tot die modifisering van die hipertrofiese fenotipe. Die doel van hierdie studie was om die hipertrofiese effek van 38 enkel nukleotied polimorfismes (SNPs) en haplotipes in vier kandidaat HKM modifiserende gene in 388 individue van 27 HCM families te toets, waarin drie unieke Suid-Afrikaanse HKM-stigters mutasies segregeer.

G2H analise het drie verneemde MyBPH bindingsgenote geïdentifiseer, naamlik miosien (MYH7), alfa kardiaale aktien (ACTC1) en die SUMO-konjugerende ensiem UBC9 (UBC9). Hierdie interaksies is geverifieer deur middel van 3D ko-lokalisering en ko-immunopresipitasie analyses. Verder is bewys dat MyBPH en kMyBPC betrokke is in outofagie, siende dat beide proteïene gewerf is tot die membraan van die outofagosoom. 'n Kardiaale sametrekking eksperiment het gevind dat die gesamentlike siRNA-bemiddelde uitklopping van MyBPH en kMyBPC 'n merkwaardige vermindering in die kardiomyosiet sametrekking veroorsaak het in reaksie op β -adrenergiese stres kondisies, in vergelyking met die individuele proteïen en kontrole uitkloppings eksperimente. Hierdie resultate bevestig dat MyBPH vir kMyBPC kan instaan en ook andersom, wat verder bevestig dat beide proteïene benodig word vir effektiewe sarkomeer sametrekking.

Resultate van die genetiese assosiasie studie het gevind dat 'n aantal SNPs en haplotipes 'n beduidende effek of HKM hipertrofie het. Enkel SNP en haplotipe analyses in gene wat kodeer vir MyBPH, MYH7, ACTC1 en UBC9 het SNPs en haplotipes geïdentifiseer wat bydra tot die omvang van hipertrofie in HKM. Verder het ons gevind dat sekere SNPs en haplotipes kenmerkend verskillende statistiese beduidende effekte in die teenwoordigheid van elk van die drie HKM-stigter mutasies gehad het.

Die resultate van hierdie studie skryf twee nuwe funksies aan MyBPH toe. Kardiaale MyBPC en MyBPH speel 'n kritiese rol in sarkomeer sametrekking en is betrokke in outofagie. Hierdie resultate

het verdere implikasies vir die verstaan van die pato-etologie van die HKM-veroorsakende mutasies in die *MyBPH*, *MYH7*, *ACTC1* en *UBC9* gene.

So vêr dit ons kennis strek is dit die eerste genetiese assosiasie studie wat die modifiserende effek van bindingsgenote van *MyBPH* ondersoek as risiko aanduiding vir die ontwikkeling van LVH in die konteks van HKM. Ons bevindinge bewys dat die hipertrofiese fenotipe van HKM gemoduleer word deur die komplekse effekte van SNPs en haplotipes in die *MyBPH* geen en gene wat *MyBPH* proteïen-bindingsgenote encodeer. Hierdie resultate verskaf dus 'n basis vir toekomstige studies om die risiko profiel van hipertrofie ontwikkeling met betrekking tot HKM te ondersoek, wat gevolglik kan bydra tot die verbeterde risiko stratifikasie en pasiënte bestuur.

Acknowledgements

I would like to extend my sincerest gratitude to the following individuals who have assisted me in this study.

My supervisors, Dr CJ Kinnear and Prof JC Moolman-Smook. Thank you for your invaluable insight, scientific input, guidance and patience, without which this study would not have been possible.

Professor Lize van der Merwe. My gratitude for your guidance, assistance and patience was not only very helpful but also very encouraging. You challenged my understanding of statistical analysis and gave me a new appreciation for genetic association analyses.

Dr Ben Loos at the Department of Physiology, Stellenbosch University. Your technical insight and help with the microscopy experiments and analyses were very valuable to me. The challenging scientific questions you posed and discussions you prompted were particularly challenging, but equally rewarding.

Susan Cooper and Professor Dirk Lang at the Imaging Facility located at the University of Cape Town. Thank you for your advice, assistance and guidance with the analysis in using the confocal microscope.

Stefanie Malan, my colleague and dear friend, thank you for standing by me during the course of this project. Your endless encouragement and good naturedness were often a source of inspiration for me.

Professor P van Helden. In addition to providing the necessary financial support and superb infrastructure, I thank you for this opportunity that allowed me to undertake this study while working.

Harry Crossley Foundation. Thank you for the funding that allowed this project to happen.

My friend Delia (and Jacques). Thank you for reading through and editing many copies of this thesis. Your friendship and encouragement have surely been a great motivation during this study.

My dear friends and colleagues in the Department of Biomedical Sciences. Thank you for your friendly smiles and always being available to help seek an answer to a question.

My parents and family. Your love, encouragement, unexpected visits and motivating phone calls have helped shape me into the person I am today. I am truly blessed to have parents and family like you.

My loving husband Pierre. For motivating me to always keep going, inspiring me to always give my best and for loving me every day as much as the day before.

Finally, thank you God, for providing me with the ability, determination, courage and motivation to give my best every day.

TABLE OF CONTENTS

LIST OF FIGURES.....	xi
LIST OF TABLES.....	xvi
LIST OF ABBREVIATIONS.....	xix
INTRODUCTION.....	4
MATERIALS AND METHODS: PROTEIN INTERACTION STUDY.....	49
MATERIALS AND METHODS: MODIFIER STUDY	75
RESULTS: PROTEIN INTERACTION STUDY	89
RESULTS: MODIFIER STUDY.....	114
DISCUSSION: PROTEIN INTERACTION STUDY.....	152
DISCUSSION: MYBPH AND INTERACTORS AS MODIFIERS OF HYPERTROPHY	168
APPENDIX I.....	190
APPENDIX II.....	203
APPENDIX III.....	205
REFERENCES.....	208

LIST OF FIGURES

CHAPTER ONE: INTRODUCTION

- Figure 1.1 Pathology of hypertrophic cardiomyopathy. In comparison to the normal heart (A), the HCM heart (B) shows left ventricular hypertrophy with reduced left ventricular cavity size. On histology, the normal heart (C), as compared to the HCM heart (D), shows enlarged myocytes and myocyte disarray.....6
- Figure 1.2 A representation of the cardiac sarcomere in a relaxed and contracted state. (A) The basic organisation of the sarcomere sub-regions; the A band represents the central location of myosin and actin and the Z-discs are shown in red. (B) A theoretical diagram that represents the connection between molecules within the sarcomere. For example, a person (which represents myosin (M)) pulls the bookcases (which represent Z-discs) via ropes (which represent actin).....13
- Figure 1.3 Premyofibril model of myofibrillogenesis. Mature myofibrils are formed through three steps; pre-myofibrils that contain non-muscle myosin II, nascent myofibrils that contain both non-muscle myosin II and muscle specific myosin II, and mature myofibrils that contain muscle-specific myosin II but no non-muscle myosin II.....14
- Figure 1.4 Schematic representation of myofibril. Sarcomeric proteins assemble to form a sarcomere. Sarcomeres combine to form a myofibril.15
- Figure 1.5 The series of reactions involved in the cross-bridge cycle.....17
- Figure 1.6 Sumoylation is regulated by conjugation and deconjugation pathways.....19
- Figure 1.7 Calcium cycling in cardiomyocytes and regulation by PKA phosphorylation. Phosphorylation influences cardiac functioning by phosphorylation of proteins essential for cardiac functioning.21
- Figure 1.8 The ubiquitination of target substrates for degradation involves three steps. These are: Initial activation (catalysed by E1 enzyme), covalent linking of ubiquitin to a conjugating enzyme, E2, and conjugating ubiquitin to the target substrate (facilitated by E3 ligase).23
- Figure 1.9 Ubiquitination in the normal heart compared to the cardiomyopathic heart.....25
- Figure 1.10 Autophagy plays a role in recycling amino acids, removing damaged proteins and organelles and maintaining the ER.....28

Figure 1.11 The activity of autophagy in response to pressure overload in the heart.	29
Figure 1.12 Schematic diagram of striated muscle sarcomere. This image indicates the localisation of cMyBPC (blue) that is restricted to the C-zone of the A-band, titin (dashed green lines), myosin (thick filament) in red and actin in black (thin filament).....	33
Figure 1.13 Schematic representation of cardiac myosin binding protein C (cMyBPC), indicating domains of known function..	34
Figure 1.14 Schematic representation of the asymmetric myosin molecule indicating the heavy meromyosin (HMM) and the light meromyosin (LMM).	36
Figure 1.15 Two models predicting the C-terminal arrangement of cMyBPC in the sarcomere, the trimeric collar model (A) as proposed by Moolman-Smook et al., 2002 and the rod model (B) as proposed by Squire et al., 2003.....	41
Figure 1.16 Schematic representation of cardiac myosin binding protein H (MyBPH), indicating domains of known function..	42

CHAPTER TWO: MATERIALS AND METHODS

Figure 2.1 Formula for calculating the overlap coefficient.	73
Figure 2.2 Formula for calculating the Pearson's correlation.	73
Figure 2.3. A representation of 8-well borosilicate glass-bottomed chambers (Nunc, New York, USA) and the experimental preparation of the contractility assay, indicating which siRNAs were used and how they were treated.....	75
Figure 2.4 A graphical representation of the three levels of the heart muscle at which wall thickness was measured. (A) The blue dotted lines on the long axis view of the left ventricle indicate the mitral valve, papillary muscle and apex levels at which echocardiographic parameters were measured. (B) A representation of a 2D echocardiographic ultrasound of the left ventricle.....	77
Figure 2.5 Formula used to estimate LVM from 2D left ventricle linear dimensions	78

CHAPTER THREE: RESULTS

Figure 3.1 Linear growth curves of yeast strain GOLD transformed with non-recombinant pGBKT7, pGBKT7-53 and pGBKT7-MyBPH bait constructs. The growth rate of the pGBKT7-MyBPH transformant were compared to the non-recombinant pGBKT7 and pGBKT7-53, in an attempt to determine if the bait constructs had any toxic effects on the GOLD strain.....90

Figure 3.2 Fluorescent imaging and co-localisation analysis of MyBPH and MYH7 in differentiated H9c2 cardiomyocytes. (A) MyBPH labelled with a donkey anti-mouse Cy5 secondary antibody (Yellow). (B) MYH7 labelled with a donkey anti-rabbit Alexa Fluor 488 antibody (Green). (C) Nucleus labelled with Hoechst H-33342 (Blue). (D) Overlay of images A-C. (E) Co-localisation of MyBPH and MYH7 generated from merged images (Pink). (F) Scatter diagram generated by co-localisation analysis with quadrant three representing the degree of co-localisation.....97

Figure 3.3 Fluorescent imaging and co-localisation analysis of MyBPH and ACTC1 in differentiated H9c2 cardiomyocytes. (A) MyBPH labelled with a donkey anti-mouse Cy5 secondary antibody (Yellow). (B) ACTC1 labelled with a donkey anti-rabbit Alexa Fluor 488 secondary antibody (Green). (C) Nucleus labelled with Hoechst H-33342 (Blue). (D) Overlay of images A-C. (E) Co-localisation of MyBPH and ACTC1 generated from merged images (Pink). (F) Scatter diagram generated by co-localisation analysis with quadrant three representing the degree of co-localisation... ..98

Figure 3.4 Fluorescent imaging and co-localisation analysis of MyBPH and UBC9 in differentiated H9c2 cardiomyocytes. (A) MyBPH labelled with a donkey anti-mouse Cy5 secondary antibody (Yellow). (B) MYH7 labelled with a donkey anti-goat Cy3 secondary antibody (Red). (C) Nucleus labelled with Hoechst H-33342 (Blue). (D) Overlay of images A-C. (E) Co-localisation of MyBPH and UBC9 generated from merged images (Pink). (F) Scatter diagram generated by co-localisation analysis with quadrant three representing the degree of co-localisation.....99

Figure 3.5 Western blots of Co-IP of MyBPH and putative interactors (A) MYH7, (B) ACTC1 and (C) UBC9 in differentiated H9c2 rat cardiomyocytes. Reciprocal Co-IPs were performed for each interaction.101

Figure 3.6 Fluorescent imaging of MyBPH and ACTC1 in differentiated H9c2 rat cardiomyocytes. (A) MyBPH labelled with a donkey anti-mouse Cy3 secondary antibody (Red). (B) ACTC1 labelled with a donkey anti-rabbit Alexa Fluor 488 secondary antibody (Green). (C) Nucleus labelled with Hoechst H-33342 (Blue). (D) Overlay of images A-C.....102

- Figure 3.7 Super resolution imaging and co-localisation analysis of MyBPH and LC3b-II_GFP in differentiated H9c2 rat cardiomyocytes. (A) MyBPH labelled with a donkey anti-mouse Cy3 secondary antibody (Red), GFP-tagged LC3b-II (Green). (B, C) Enlarged image. (D) Co-localisation of MyBPH and GFP-tagged LC3b-II generated from merged images (Yellow).....103
- Figure 3.8 Super resolution imaging and co-localisation analysis of cMyBPC and LC3b-II_GFP in differentiated H9c2 rat cardiomyocytes. (A) cMyBPC labelled with a donkey anti-rabbit Cy3 secondary antibody (Red), GFP-tagged LC3b-II (Green). (B, C) Enlarged image. (D) Co-localisation of MyBPH and GFP-tagged LC3b-II generated from merged images (Yellow).....104
- Figure 3.9 Fluorescent imaging of MyBPH in differentiated H9c2 rat cardiomyocytes after 24 hours of differentiation (A-C), after 5 days of differentiation (D-F) and after 8 days of differentiation (G-I). (A, D, G) MyBPH labelled with a donkey anti-mouse Cy3 secondary antibody (Red). (B, E, H) Nucleus labelled with Hoechst H-33342 (Blue). (C, F, I) Overlay images.....106
- Figure 3.10 Fluorescent imaging of Alexa Fluor 488-labelled NSC siRNA after 24 hours of transfection in H9c2 rat cardiomyocytes that was differentiated for 5 days (A, B) and 8 days (C, D). (A - D) NSC siRNA tagged with Alexa Fluor 488 (Green) and nucleus labelled with Hoechst H-33342 (Blue).....107
- Figure 3.11 Western blotting quantification of MyBPH in differentiated H9c2 rat cardiomyocytes transfected with either a NSC or a particular MyBPH siRNA. The siRNA H3 resulted in optimal knockdown of MyBPH.....108
- Figure 3.12 Western blotting quantification of cMyBPC in differentiated H9c2 rat cardiomyocytes transfected with either a NSC or a particular cMyBPC siRNA. The siRNA C3 resulted in optimal knockdown of cMyBPC.....109
- Figure 3.13 Western blotting quantification of MyBPH in differentiated H9c2 rat cardiomyocytes transfected with either a NSC or H3, and C3 MyBPH and cMyBPC siRNAs concurrently. The concurrent transfection of siRNA H3 and C3 resulted in optimal knockdown of MyBPH.....110
- Figure 3.14 Western blotting quantification of cMyBPC in differentiated H9c2 rat cardiomyocytes transfected with either a NSC or H3, and C3 MyBPH and cMyBPC siRNAs concurrently. The concurrent transfection of siRNA H3 and C3 resulted in optimal knockdown of MyBPC.....111
- Figure 3.15 Effect of MyBPH and cMyBPC knockdown in differentiated H9c2 rat cardiomyocytes in response to β -adrenergic stimulation. (A) siRNA transfected H9c2 cells before (0 minutes) and after (60 minutes) stimulation by isoproterenol, representing the change in planar cell surface area in each

group. (B) The differences between the four groups as the mean \pm SEM (n=6 per group) of three independent experimental repeats. The percentage planar cell surface area differed significantly in the double knockdown group from the NSC (**p<0.05)..	113
Figure 3.16 The p-values for tests of association between single SNPs in <i>MyBPH</i> and individual hypertrophy traits.	125
Figure 3.17 The p-values for tests of association between <i>MYBPH</i> haplotypes and individual hypertrophy traits.	128
Figure 3.18 The p-values for tests of association between single SNPs in <i>MYH7</i> and individual hypertrophy traits.	132
Figure 3.19 The p-values for tests of association between <i>MYH7</i> haplotypes and individual hypertrophy traits.	135
Figure 3.20 The p-values for tests of association between single SNPs in <i>ACTC1</i> and individual hypertrophy traits.	137
Figure 3.21 The p-values for tests of association between <i>ACTC1</i> haplotypes and individual hypertrophy traits.	140
Figure 3.22 The p-values for tests of association between single SNPs in <i>UBC9</i> and individual hypertrophy traits.	143
Figure 3.23 The p-values for tests of association between <i>UBC9</i> haplotypes and individual hypertrophy traits.	147

LIST OF TABLES

CHAPTER ONE: INTRODUCTION

Table 1.1 Known HCM genes and their OMIM references.	8
Table 1.2 Physiological and pathological role of calpains in the heart.	32
Table 1.3 List of cMyBPC domains that interact with cardiac actin.	39

CHAPTER TWO: MATERIALS AND METHODS

Table 2.1 Oligonucleotide primers used for the generation of inserts for Y2H cloning.	51
Table 2.2 Oligonucleotide primers used for the amplification of inserts from cloning vectors.	52
Table 2.3 Transfer conditions of the IBlot system for the different proteins.	54
Table 2.4 Primary and secondary antibody concentrations for western blot analyses.	70
Table 2.5. Antibodies and antibody concentrations for co-localisation assays.	72
Table 2.6 Excitation and emission spectra of fluorescent proteins used in co-localisation assays.	72
Table 2.7 Candidate genes selected for gene association analysis.	79
Table 2.8 The SNP position and nucleotide change of SNPs selected for genotyping.	80

CHAPTER THREE: RESULTS

Table 3.1 Effect of the pGBKT7-MyBPH bait construct on the GOLD mating efficiency.	91
Table 3.2 Activation of nutritional and colourimetric reporter genes by interaction between MyBPH and prey clones. Below is a representative subset of the scoring of the 400 clones that activated the <i>HIS3</i> reporter gene and were resistant to AbA, the 76 clones that activated the <i>ADE2</i> reporter gene and the remaining 12 clones that were able to activate the <i>MEL1</i> reporter gene.	92

Table 3.3 Interaction between MyBPH preys with heterologous baits in specificity tests. The scores of the clones considered as putative interactors are detailed below.	94
Table 3.4 Identification of MyBPH putative interactor clones from Y2H cardiac library screen. Putative MyBPH interactors are arranged according to interactors represented by multiple clones from highest to lowest activity of nutritional and colourimetric reporter genes. Putative interactors represented by a single clone are arranged similarly. Putative interactors highlighted in pink were chosen for verification based on their cellular localisation and physiological role in the cardiac sarcomere	95
Table 3.5 Quantification of co-localisation for the interaction between MyBPH and MYH7.	97
Table 3.6 Quantification of co-localisation for the interaction between MyBPH and ACTC1.....	98
Table 3.7 Quantification of co-localisation for the interaction between MyBPH and UBC9.....	99
Table 3.8 Quantification of co-localisation for the interaction between MyBPH and LC3b-II.....	103
Table 3.9 Quantification of co-localisation for the interaction between cMyBPC and LC3b-II.	104
Table 3.10 Basic characteristics of the study cohort. Individuals are grouped according to the relevant HCM founder mutation and mutation status as either mutation carrier (MC) or non-carrier (NC).	115
Table 3.11 The SNPs chosen for investigation in this study and their MAF in the CEU and YRI populations.....	116
Table 3.12 Cohort-specific descriptives. Hardy-Weinberg equilibrium test p-values and MAF for the SNPs investigated.....	118
Table 3.13 Pair-wise LD structure for <i>MyBPH</i> . D' values = 1 are highlighted in red, D' values between 0,60 and 0,99 are highlighted in dark pink and D' values < 0,60 are highlighted in light pink.	120
Table 3.14 Pair-wise LD structure for <i>MyH7</i> . D' values = 1 are highlighted in red, D' values between 0,60 and 0,99 are highlighted in dark pink and D' values < 0,60 are highlighted in light pink.	121
Table 3.15 Pair-wise LD structure for <i>ACTC1</i> . D' values = 1 are highlighted in red, D' values between 0,60 and 0,99 are highlighted in dark pink and D' values < 0,60 are highlighted in light pink.	122
Table 3.16 Pair-wise LD structure for <i>UBC9</i> . D' values = 1 are highlighted in red, D' values between 0,60 and 0,99 are highlighted in dark pink and D' values < 0,60 are highlighted in light pink.	122

Table 3.17 The PC1 score defined in terms of its weighted composition: the weight of each wall thickness measurement.....	123
Table 3.18 The environment and heritability estimates detailed as estimated percentage contribution to trait variance, as well as the p-values for heritability.....	124
Table 3.19 The p-values obtained for the analysis of the additive allelic models inside the mutation groups in <i>MyBPH</i> , illustrating the allelic effect of the particular variants within these groups..	126
Table 3.20 The p-values obtained for the analysis of the association with <i>MyBPH</i> haplotypes within the mutation groups.	129
Table 3.21 The p-values obtained for the analysis of the additive allelic models inside the mutation groups in <i>MYH7</i> , illustrating the differences in allelic effect of the particular variants within these groups.	133
Table 3.22 The p-values obtained for the analysis of the association with <i>MYH7</i> haplotypes within the mutation groups.	136
Table 3.23 The p-values obtained for the analysis of the additive allelic models inside the mutation groups in <i>ACTC1</i> , illustrating the differences in allelic effect of the particular variants within these groups..	138
Table 3.24 The p-values obtained for the analysis of the association with <i>ACTC1</i> haplotypes within the mutation groups.	141
Table 3.25 The p-values obtained for the analysis of the additive allelic models inside the mutation groups in <i>UBC9</i> , illustrating the differences in allelic effect of the particular variants within these groups.	144
Table 3.26 The p-values obtained for the analysis of the association with <i>UBC9</i> haplotypes within the mutation groups.	148

LIST OF ABBREVIATIONS

α	alpha
α 1ARs	alpha 1 receptors
α 2ARs	alpha 2 receptors
β	beta
β ARs	beta adrenergic receptors
γ	gamma
$^{\circ}$ C	degrees Celsius
#	number
2D	two-dimensional
3'	three prime
5'	five prime
A	alanine
A	adenine
AbA	aureobasidin a
A-band	anisotropic band
ABI	Applied Biosystems Incorporated
AC	adenylyl cyclase
ACC	ascending aortic constriction
Acc #	accession number
ACE	angiotensin-converting enzyme
<i>ACE1</i>	angiotensin-converting enzyme 1
<i>ACE2</i>	angiotensin-converting enzyme 2
<i>ACTC1</i>	cardiac alpha actin
ACTC1	cardiac alpha actin
AD	activating domain

Ade	adenine
<i>ADE2</i>	phosphoribosylaminoimidazole carboxylase gene
ADP	adenosine diphosphate
AF488	Alexa Fluor 488
<i>AGT</i>	angiotensinogen
<i>AGTR1</i>	angiotensin II type I receptor gene
Ala	alanine
ALP	autophagy-lysosome pathway
Aivs	anterior interventricular septum thickness
AMP	adenosine monophosphate
AMPK	AMP-activated protein kinase
Ang	angiotensin
<i>ANKRD1</i>	ankyrin repeat domain 1
ANOVA	analysis of variance
Aos1/Uba2	SUMO-activating enzyme e1
Arg	arginine
ASE	American Society of Echocardiography
Asn	asparagine
Asp	aspartic acid
ATCC	American Type Culture Collection
ATG1	autophagy-related 1
ATG3	autophagy-related 3
ATG5	autophagy-related 5
ATG6	autophagy-related 6
ATG7	autophagy-related 7
ATG8	autophagy-related 8

ATG10	autophagy-related 10
ATG12	autophagy-related 12
ATG13	autophagy-related 13
ATG16L	autophagy-related 16l
ATG101	autophagy-related 101
ATP	adenosine triphosphate
ATPase	adenosine triphosphatase
AV	aortic valve
AW	anterior wall thickness
BLAST	Basic Local Alignment Search Tool
BP	blood pressure
BSA	body surface area
©	copyright
C	cytosine
C1	siRNA type c1 specific to myosin binding protein c
C2	siRNA type c2 specific to myosin binding protein c
C3	siRNA type c3 specific to myosin binding protein c
C4	siRNA type c4 specific to myosin binding protein c
Ca ²⁺	calcium
CaCl ₂	calcium chloride
Calpain	calcium ion-dependent papain-like protease
CaM	calmodulin
CaMK	calmodulin-dependent kinase
cAMP	cyclic adenosine monophosphate
CaN	calcineurin
CapZ	capping protein (actin filament) muscle z line, alpha 2

CASQ2	calsequestrin 2
CAV3	caveolin 3
cDNA	complementary DNA
CEU	HapMap population: parent-offspring trios with Northern and Western European Ancestry
Ch2-T1	channel 2, track 1
CH3-T2	channel 3, track 2
Ch3-T3	channel 3, track 3
cm ²	cubic centimetre
cMyBPC	cardiac myosin binding protein c
Co.	company
CO ₂	carbon dioxide
Co-IP	co-immunoprecipitation
COX15	cytochrome c oxidase assembly protein 15
CSRP3	muscle LIM protein
C-terminus	carboxy-terminus
C-terminal	carboxy-terminus
Cy3	cyanine dye 3
Cy5	cyanin dye 5
dATP	deoxy-adenosine triphosphate
DBP	diastolic blood pressure
DCM	dilated cardiomyopathy
dCTP	deoxy-cytidine triphosphate
ddH ₂ O	distal deionised water
DES	desmin
dGTP	deoxy-guanosine triphosphate
DMEM	Dulbecco's Modified Eagle media

DMSO	dimethyl sulphoxide
DNA	deoxyribo nucleic acid
dNTP	deoxy-nucleotide triphosphate
dTTP	deoxy-thymidine triphosphate
E1	ubiquitin-activating ligase
E2	ubiquitin-conjugating ligase
E3	ubiquitin ligase
E4	elongation factor
<i>E.coli</i>	<i>Escherichia coli</i>
EDTA	ethylene-diamine-tetra-acetic acid
EGF-like	epidermal growth factor like
ER	endoplasmic reticulum
F-actin	filamentous actin
FAF1	fas (TNFRSF6) associated factor 1
FBN1	fibrillin 1
FIP200	focal adhesion kinase (FAK) family interacting protein of 200kda
FLNC	filamin c, gamma
FnIII	fibronectin type III
FRET	föster resonance energy transfer
<i>FXN</i>	frataxin
g	grams
G	guanine
GAPDH	glyceraldehyde 3-phosphate dehydrogenase
g/cc	gram per cubic centimetre
GC	genomic control
GFP	green fluorescent protein

Gln	glutamine
Glu	glutamic acid
Gly	glycine
GRK	G protein-coupled receptor kinase
H ⁺	hydrogen
<i>H1</i>	siRNA type h1 specific to myosin binding protein h
<i>H2</i>	siRNA type h2 specific to myosin binding protein h
<i>H3</i>	siRNA type h3 specific to myosin binding protein h
<i>H4</i>	siRNA type h4 specific to myosin binding protein h
HA	hemagglutinin
HCM	hypertrophic cardiomyopathy
Hg	mercury
His	histidine
<i>HIS3</i>	imidazoleglycerolphosphate dehydratase
H ₂ O	water
HR	heart rate
HRM	high resolution melt
HRP	horseradish peroxidase
HMM	heavy meromyosin
HWE	Hardy-Weinberg equilibrium
Hz	hertz
I-band	isotropic band
Ig	immunoglobulin i-like
Ile	isoleucine
Inc.	incorporated
IP	immunoprecipitation

IPneg	immunoprecipitation using “non-relevant” antibody as negative control
IQ	domain within myosin
ITC	isothermal titration calorimetry
IVS	interventricular septum thickness
IW	inferior wall thickness
<i>JPH2</i>	junctionophilin-2
K ⁺	potassium
KASP	kompetitive allele specific PCR
Kb	kilo bases
kDa	kilo dalton
KI	knock-in
KO	knockout
L	litre
LA	left atrium
<i>LAMP2</i>	lysosomal-associated membrane protein 2
LAMP2	lysosomal-associated membrane protein 2
LB	luria bertani
LC3b	marker for autophagy
LC3b-I	non-lipidated form of LC3b
LC3b-II	lipidated form of LC3b, pe-conjugated form of LC3b
LD	linkage disequilibrium
LDU	linkage disequilibrium unit
LiAc	lithium acetate
LIMK1	lim domain kinase 1
LMM	light meromyosin
LOD	logarith of odds

Log	logarithm
LSM	laser scanning microscopy
Ltd.	limited
LV	left ventricle
LVH	left ventricular hypertrophy
LVIDd	left ventricular internal dimension at end-diastole
LVM	left ventricular mass
LVOT	left ventricular outflow tract
LWW/BW	left ventricular weight and body weight
LWWT	left ventricular wall thickness
LW	lateral wall thickness
Lys	lysine
M	molar
MAF	minor allele frequency
MAFbx	muscle atrophy F-box
MC	mutation carrier
MCS	multiple cloning sites
MEF2C	myocyte enhancer factor 2C
<i>MEL1</i>	alpha-galactosidase
Met	methionine
mg	milligram
MgCl ₂	magnesium chloride
miRNA	micro RNA
min	minute
mIVST	maximal interventricular septum thickness
ml	millilitre

MLC2v	myotilin and ventricular myosin light chain 2
mLVWT	maximal left ventricular wall thickness
mm	millimetre
mM	millimolar
m-mode	motion mode
mTOR	mammalian target of rapamycin
mPWT	maximal posterior wall thickness
MRI	magnetic resonance imaging
mRNA	messenger ribonucleic acid
MTRNR2L2	MT-RNR2-like 2 protein
MuRF	muscle ring finger
MuRF1	muscle ring finger 1
MuRF2	muscle ring finger 2
MuRF3	muscle ring finger 3
MV	mitral valve
<i>MyBPH</i>	myosin binding protein H
MyBPH	myosin binding protein H
MyBPC	myosin binding protein C
<i>MYBPC3</i>	cardiac myosin binding protein C
<i>MYH6</i>	alpha-myosin heavy chain
<i>MYH7</i>	cardiac beta-myosin heavy chain
MYH7	cardiac beta-myosin heavy chain
MYO6	myosin VI
MYOZ	myozenin 2
MYL2	myosin regulatory light chain
MYL3	myosin essential light chain

<i>MYLK2</i>	myosin light chain kinase
n	number of clinically evaluated samples
Na ⁺	sodium
Na ⁺ /K ⁺ -ATPase	sodium-potassium pump
NaCl	sodium chloride
NC	non-carrier
NCBI	National Centre for Bioinformatics
NCX	sodium-calcium exchanger
NH ₂ -terminus	amino-terminus
NHE	sodium-proton exchanger
ng	nanogram
NLO	non-linear optics
nm	nanometer
nM	nanomolar
NMR	nuclear magnetic resonance
<i>NSC</i>	non-silencing control
N-terminal	amino-terminus
<i>OBSCN</i>	obscurin
OD	optimal density
OR	odds-ratio
p	short chromosomal arm
p62	nucleoporin 62
P13K	phosphatidylinositol-3-kinase
PAGE	polyacrylamide gel electrophoresis
PBS	phosphate buffered saline
PCA	principal component analysis

PC1	first principal component
Pc2	polycomb-2 protein
PCI	phenol-chloroform-isoamyl alcohol
PCR	polymerase chain reaction
PD	Parkinson's disease
PE	phosphatidylethanolamine
PEG	polyethylene glycol
pH	power of hydrogen
Pi	inorganic phosphate
PIAS	protein inhibitor of activated stat (signal transducer and activator of transcription)
PIPES	piperazine-N, N-bis (2-ethanesulfonic acid) 1.5 sodium
pIVS	posterior interventricular septum thickness
<i>PLN</i>	phospholamban
PML	promyelocytic leukemia protein
PMSF	phenylmethanesulphonyl fluoride
PKA	protein kinase A
PP	protein phosphatase
PPARG	peroxisome proliferator-activated receptor gamma
PRKAG2	AMP-activated protein kinase, gamma 2 non-catalytic subunit
protG	protein G agarose control
PVDF	polyvinylidene fluoride
PW	posterior wall thickness
PWTd	posterior wall thickness at end-diastole
q	long chromosomal arm
QDO	quadruple dropout

QTD	quantitative transmission disequilibrium test
®	registered
R	arginine
<i>RAF1</i>	v-raf-1 murine leukemia viral oncogene homolog 1
RanBP2	ran-binding protein 2, sumo E3 ligase
RNA	ribonucleic acid
ROCK1	rho kinase 1
rpm	revolution per minute
RSA	Republic of South Africa
RT-PCR	realtime PCR
RyR	ryanodine receptor
RVOT	right ventricular outflow tract
S1	myosin S1 sub-fragment of myosin heavy chain
S2	myosin S2 sub-fragment of myosin heavy chain
SB	sodium borate
SBP	systolic blood pressure
SCD	sudden cardiac death
<i>S. cerviae</i>	<i>Saccharomyce cerviae</i>
SD	synthetic dropout
SDS	sodium dodecyl-sulphate
sec	second
SEM	standard error of mean
SENPs	sentrin-specific proteases
Ser	serine
SERCA	sarcoplasmic reticulum calcium atpase
siRNA	small interfering ribonucleic acid (RNA)

<i>SLC5A4</i>	solute carrier family 25 member 24
SNP	single nucleotide polymorphism
SR-SIM	super resolution structured illumination microscopy
STAT	signal transducer and activator of transcription
SUMO	small ubiquitin-related modifier
SUMO1	small ubiquitin-related modifier 1
SWTd	intraventricular septum thickness at end-diastole
T	thymine
T	threonine
T_a	annealing temperature
T_m	melting temperature
™	trademark
TAC	transverse aortic constriction
TagSNP	tagging single nucleotide polymorphism
TB	domain within fibrillin 1
TBST	tris-buffered saline tween 20
<i>TCAP</i>	telethonin or titin-cap
TDO	triple dropout
Thr	threonine
TIF	triton-insoluble filamentous actin
<i>TNNIC</i>	cardiac troponin c
<i>TNNI3</i>	cardiac troponin I type 3
<i>TNNT2</i>	cardiac troponin T type 2
<i>TPM1</i>	alpha-tropomyosin
Trp	tryptophan
<i>TTN</i>	titin

U	unit
Ub	ubiquitin
<i>UBC9</i>	SUMO-conjugating enzyme UBC9, ubiquitin-conjugating enzyme E2, UBE2I
UBC9	SUMO-conjugating enzyme UBC9, ubiquitin-conjugating enzyme E2, UBE2I
UCT	University of Cape Town
UK	United Kingdom
UPS	ubiquitin-proteasome system
Ura	uracil
USA	United States of America
UT	transfection control
UTR	untranslated region
UV	ultra-violet
V	volts
v	version
Val	valine
<i>VCL</i>	vinculin
VNTR	variable number tandem repeat
Vps34	a phosphatidylinositol 3-kinase
W	tryptophan
WB	western blot
WFS1	wolframin
WT	wild type
W/V	weight per volume
www	world wide web
X- α -gal	x-alpha-galactosidase

YRI	HapMap population: parent-offspring trios from the Yoruba people in Ibadan, Nigeria
Y2H	yeast two-hybrid
YPDA	yeast peptone dextrose adenine
μl	microliter
μg	microgram

Chapter One

Introduction

CHAPTER ONE

INTRODUCTION

TABLE OF CONTENTS

INTRODUCTION.....	4
1.1 Left ventricular hypertrophy	4
1.1.1 Hypertrophic cardiomyopathy	5
1.1.2 Genetics of HCM.....	6
1.1.3 Phenotype modification	9
1.1.4 South African HCM founder mutations	10
1.2 HCM as a disease of the sarcomere and impaired cardiac contractility	11
1.2.1 Sarcomeric development and maintenance	11
1.2.2 Sarcomerogenesis	13
1.2.2.1 Premyofibril model	14
1.2.3 Cardiac contraction.....	16
1.2.3.1 The cross-bridge cycle.....	16
1.2.4 Sarcomeric protein modification and regulation	17
1.2.4.1 Sumoylation.....	17
1.2.4.2 Adrenergic stimulation and contractile protein phosphorylation	20
1.2.5 Sarcomeric protein integration and exchange.....	22
1.2.6 Sarcomeric protein degradation	22
1.2.6.1 The ubiquitin-proteasome system.....	23
1.2.6.2 Autophagy	26
1.2.6.3 Calpain system.....	30
1.3 Cardiac myosin binding protein C.....	32
1.3.1 cMyBPC as a regulatory protein found in the sarcomere	32
1.3.2 The role of cMyBPC in the thick filament	34

1.3.3	Interactions of cMyBPC	35
1.3.3.1	Myosin	35
1.3.3.2	Titin	37
1.3.3.3	Actin	37
1.3.4	The arrangement of cMyBPC in the sarcomere.....	39
1.3.4.1	The rod model	39
1.3.4.2	The trimeric collar model.....	40
1.4	Myosin binding protein H.....	41
1.4.1	MyBPH as a relatively unknown member of the MyBP family	41
1.4.2	Interactions with MyBPH in the sarcomere	42
1.4.2.1	Myosin	42
1.5	The present study.....	43
1.5.1	Study hypothesis and aim.....	43

INTRODUCTION

1.1 Left ventricular hypertrophy

Left ventricular hypertrophy (LVH) is acknowledged as a major risk factor for cardiovascular morbidity and mortality (Frey and Olson, 2003; Lorell and Carabello, 2000). The reason for this is that LVH is considered a feature of, and precursor to, many common diseases also prevalent in South African populations, such as congestive heart failure (Mathew et al., 2001), coronary heart disease (Devereux and Roman, 1993), stroke (Verdecchia et al., 2001), cardiac arrhythmias (McLenachan et al., 1987), sudden cardiac death (SCD) (Haider et al., 1998) and hypertension (Levy et al., 1990b). It is therefore important to understand the mechanisms influencing the development of LVH and identifying markers indicative of the risk of developing extensive hypertrophy before its occurrence. In doing so, screening families for molecular markers associated with LVH would allow for improved management and therapeutic intervention in susceptible individuals. However, identifying these molecular markers for LVH in complex disorders, such as those listed above, is rather challenging. It is much easier to identify and investigate molecular mechanisms leading to LVH in disorders in which LVH is the primary feature.

One such disorder is hypertrophic cardiomyopathy (HCM), a cardiac muscle disorder. Given that its primary feature is the development of LVH in the absence of any other external loading conditions (Elliott et al., 2008), HCM has been viewed as a model in which to study the causal molecular factors underlying isolated cardiac hypertrophy. The cardiac phenotype of HCM is extremely heterogeneous, and past studies have shown that the clinical presentations observed in HCM varies greatly between individuals from the same and different families (Thierfelder et al., 1994).

This chapter will briefly describe HCM as a disease of the sarcomere and in doing so provide a more detailed overview of the sarcomere, sarcomerogenesis and the processes in the heart responsible for protein degradation. Furthermore, the implication of cardiac myosin binding protein C (cMyBPC) in HCM, followed by an overview of the latter-mentioned protein, its location, structure and function within the sarcomere and its similarity to another myosin binding protein, myosin binding protein H (MyBPH), will follow. This serves as background for the current study.

1.1.1 Hypertrophic cardiomyopathy

Hypertrophic cardiomyopathy is a dominant primary myocardial disease, mostly caused by defects in the cardiac sarcomere, and affects approximately 0.2% of individuals between the ages of 25 and 35 years (Maron et al., 1995). Previously, the prevalence of HCM in African countries was considered to be extremely low (Lewis et al., 1973). However, echocardiography results from more recent investigations in Ghana, Ethiopia and South Africa have demonstrated that this may not be the case (Abegaz, 1990; Amoah and Kallen, 2000). One of these studies were conducted over a period of four years where 572 patients were evaluated for heart failure at the National Cardiothoracic Centre in Accra, Ghana. Two-dimensional Doppler echocardiography identified heart failure in 50.5% of patients, which was caused by hypertension (21.3%), rheumatic heart disease (20.1%), cardiomyopathies (16.8%), congenital heart disease (9.8%) and coronary artery disease (10%). Interestingly, dilated cardiomyopathy (DCM) and HCM accounted for 67.7% and 9.4% of cardiomyopathies identified in this cohort, respectively (Amoah and Kallen, 2000).

Clinically, HCM is characterised by a wide spectrum of phenotypic expression ranging from asymptomatic or mildly symptomatic disease (which presents with symptoms such as dyspnoea, chest pain, palpitations and episodes of syncope) to heart failure and sudden cardiac death (Maron et al., 1986). On gross morphology HCM presents with left ventricular hypertrophy, reduced volume of left ventricular cavity and dilated atria, mitral valve thickening and abnormal intra-mural coronary arteries (Schoen, 2008), while on histology, interstitial fibrosis, cardiac myocyte hypertrophy and myocyte and myofibril disarray is observed (Seidman and Seidman, 2001) (Figure 1.1). It should be noted that this inappropriate myocardial hypertrophy occurs in the absence of any obvious cause, such as hypertension or aortic stenosis (Maron, 1993). Myocyte disarray is considered the pathognomic hallmark of the disease (Maron et al., 1981).

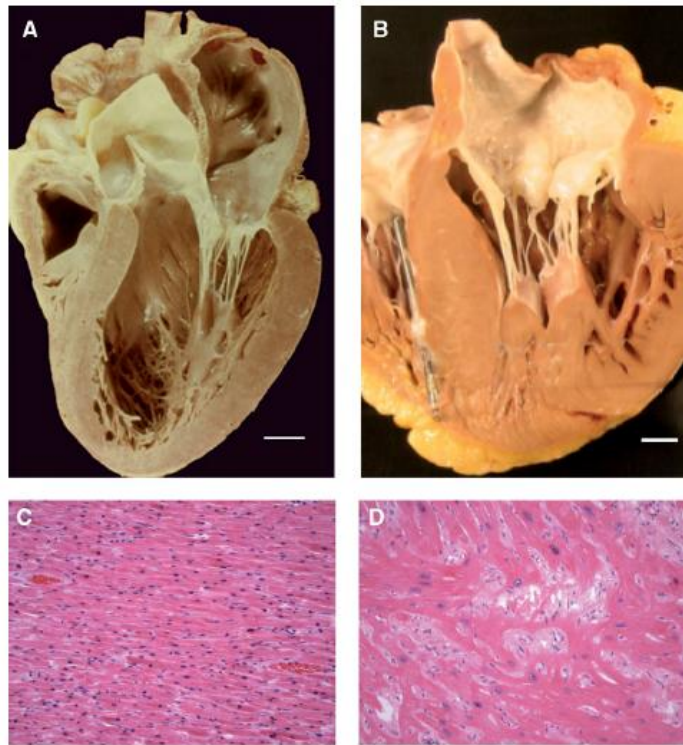


Figure 1.1 Pathology of hypertrophic cardiomyopathy. In comparison to the normal heart (A), the HCM heart (B) shows left ventricular hypertrophy with reduced left ventricular cavity size. On histology, the normal heart (C), as compared to the HCM heart (D), shows enlarged myocytes and myocyte disarray (This image was taken and adapted from Wang et al., 2010).

1.1.2 Genetics of HCM

HCM is an autosomal dominantly inherited disease and a higher prevalence is expected in older individuals, as the penetrance of HCM is age-dependent (Niimura et al., 2002). The Ala403Gln missense mutation, located within the cardiac β -myosin heavy chain gene (*MYH7*), was the first HCM-causing mutation identified (Geisterfer-Lowrance et al., 1990). Since the identification of this mutation in a French Canadian family with HCM in 1990, more than 1 000 mutations in genes encoding various components of the thin and thick filament of the sarcomere have been discovered (Ho, 2010).

HCM is a heterogeneous disease that manifests with various phenotypes and clinical symptoms, even in families with the same genetic defects (Thierfelder et al., 1994). Over the past decades, several genes encoding sarcomeric proteins have been investigated for mutations associated with HCM (Marian, 2002). Currently, more than 1 000 mutations in 13 genes encoding sarcomere or sarcomere-related proteins can be screened for by clinical genetic testing of HCM patients (<http://genepath.med.harvard.edu/~seidman/cg3/>) (Ho, 2010; Marian and Roberts, 2001;

Seidman and Seidman, 2011, 2001). In 40% to 60% of sporadic and familial cases that are subjected to genetic screening, mutations are identified in one of the genes mentioned in Table 1.1 (Thierfelder et al., 1994; Van Driest et al., 2004). Despite the identification of several hundred causal mutations, the frequency of these mutations remain low globally (Marian, 2010). In most laboratories thorough screening of known HCM-causing genes typically identify causal mutations only in ~50 to 60% of cases, implying that as-yet unknown genes contribute to the patho-etiology of the condition (Girolami et al., 2006). For this reason, there is a large percentage of HCM patients for whom no genetic diagnosis can be made, which highlights the need for novel HCM-causing mutation identification in an attempt to identify the underlying cause of HCM.

Mutations in the three genes encoding the troponin complex; cardiac troponin T (*TNNT2*), cardiac troponin I (*TNNI3*) and α -tropomyosin (*TPM1*) collectively account for approximately 10% to 15% of genetic causes of HCM (Richard et al., 2003; Thierfelder et al., 1994; Van Driest et al., 2004). Rare variants in the titin (*TTN*) (Bos et al., 2006), myozenin 2 (*MYOZ2*) (Osio et al., 2007), cardiac actin (*ACTC1*), muscle LIM protein (*CSRP3*) (Bos et al., 2006), myosin essential and regulatory light chains (*MYL3* and *MYL2*, respectively) (Andersen et al., 2012; Flavigny et al., 1998), cardiac troponin C (*TNNC1*) (Landstrom et al., 2008), alpha myosin heavy chain (*MYH6*) (Carniel et al., 2005), myosin light chain kinase (*MYLK2*) (Davis et al., 2001), phospholamban (*PLN*) (Chiu et al., 2007; Landstrom et al., 2011), telethonin or titin-cap (*TCAP*) (Bos et al., 2006), junctophilin-2 (*JPH2*) (Landstrom et al., 2007) and Caveolin 3 (*CAV3*) (Hayashi et al., 2004) genes have also been shown to cause HCM (Marian, 2008) (Table 1.1). Mutations in the genes that encode the sarcomeric proteins cardiac myosin binding protein C, cMyBPC (*MyBPC3*) and cardiac β -myosin heavy chain (*MYH7*), have been most frequently implicated in HCM.

Mutations in *MyBPC3* and *MYH7* account for approximately 50% of the genetic cause of HCM (Keren et al., 2008; Van Driest et al., 2005a). Interestingly, about 70% of mutations described in *MyBPC3* are nonsense mutations and 30% are missense mutations, compared to mutations identified in *MYH7*, of which most are missense mutations (Marian et al., 2001).

Table 1.1 Known HCM genes and their OMIM references (Table was taken and adapted from Bos et al., 2009; Hershberger et al., 2009; Ho and Seidman, 2006).

Genetic Causes of Hypertrophic Cardiomyopathy (HCM)				
Gene Symbol	Genes	Locus	OMIM	Prevalence
<i>MyH7</i>	β -myosin heavy chain	14q12	160760	~ 30%
<i>MyBPC3</i>	Myosin binding protein	11p11.2	600958	~ 30%
<i>TNNT2</i>	Cardiac Troponin T	1q32	191045	~ 2% - 5%
<i>TNNI3</i>	Cardiac Troponin I	19q13.4	191044	~ 2% - 5%
<i>TPM1</i>	α -tropomyosin	15q22.1	191010	~ 2% - 5%
<i>MYOZ2</i>	Myozenin 2 (calsarcin 1)	4q26-q27	605602	< 1%
<i>ACTC1</i>	Cardiac α -actin	15q14	102540	< 1%
<i>TTN</i>	Titin	2q31	188840	< 1%
<i>MYL3</i>	Essential myosin light chain	3p21.3-p21.2	160790	< 1%
<i>MYL2</i>	Regulatory myosin light chain	12q23-q24.3	160781	< 1%
<i>MYH6</i>	α -myosin heavy chain	14q12	160710	< 1%
<i>TCAP</i>	T-cap (telethonin or titin-cap)	17q12	604488	Rare
<i>PLN</i>	Phospholamban	6q22.1	172405	Rare
<i>CAV3</i>	Caveolin 3	3p25	601253	Rare
<i>MYLK2</i>	Cardiac myosin light peptide kinase	20q13.3	606566	?
<i>JPH2</i>	Junctophilin 2	20q13.12	605267	?
<i>TNNIC</i>	Cardiac troponin C	3p21.3-3p14.3	191040	Rare
<i>OBSCN</i>	Obscurin	1q42.13	608616	?
<i>DES</i>	Desmin	2q35	125660	?
<i>CSPR3</i>	Muscle LIM protein (MLP)	11p15.1	600824	?
<i>VCL</i>	Vinculin	10q22.2	193065	?
<i>CASQ2</i>	Calsequestrin 2	1p13.1	114251	?
<i>MYO6</i>	Myosin VI	6q13	600970	?
<i>SLC5A4</i>	Solute carrier family 25 member 4	4q35	103220	?
<i>COX15</i>	Cytochrome C oxidase assembly protein 15	10q24	603646	?
<i>PRKAG2</i>	AMP-activated protein kinase, gamma 2 non-catalytic subunit	7q36.1	602743	?
<i>RAF1</i>	V-raf-1 murine leukemia viral oncogene homolog 1	3p25	164760	?
<i>FXN</i>	Frataxin	9q21.11	606829	?
<i>LAMP2</i>	Lysosomal-associated membrane protein 2	Xq24	309060	?

Abbreviations: α , alpha; p, short chromosomal arm; q, long chromosomal arm

Furthermore, the majority of mutations described in *MYH7* are located within the gene region that encodes for the globular head of the myosin protein (Marian et al., 2001). Interestingly, two HCM-causing mutations, known to segregate in South African HCM families, have been identified in *MYH7* (Moolman et al., 1993, 1995; Posen et al., 1995).

It should be noted that, in contrast to the findings of earlier studies, there is in fact little correlation between genotypes and the HCM phenotype. Different HCM-causing mutations exhibit highly variable clinical, electrographic and echocardiographic manifestations and no specific mutation underlies a particular phenotype consistently (Marian et al., 2001). Despite the low genotype-phenotype correlation in HCM, mutations in several genes have been associated with certain general HCM traits. For example, mutations in *MYH7* have been associated with more extensive hypertrophy, early onset of the disease and a higher incidence of SCD (Charron et al., 1998; Niimura et al., 1998), while mutations in *MyBPC3* have been associated with a mild phenotype manifesting later in life (Charron et al., 1998; Niimura et al., 1998). Furthermore, mutations in *TNNT2* have been associated with less extensive LVH, a high incidence of SCD and more extensive myocyte disarray (Varnava et al., 2001; Watkins et al., 1995).

1.1.3 Phenotype modification

In addition to the variability in phenotype between patients harbouring different HCM-causing mutations, there is also a great deal of phenotypic variability in individuals harbouring the same causal mutation, suggesting that the phenotype is modified by other genetic factors (Marian, 2002). These modifier genes are known to affect the severity of the phenotype, although they are not necessary, nor sufficient, to cause the phenotype observed (Alcalai et al., 2008). Individual modifier genes for HCM are largely unknown, although an insertion/deletion polymorphism in the angiotensin-1 converting enzyme 1 gene (*ACE1*) has commonly been associated with risk of SCD (Marian et al., 1993) and the severity of hypertrophy (Lechin et al., 1995). Furthermore, results from a study by Van der Merwe and colleagues confirmed that components of the renin-angiotensin-aldosterone system are plausible candidate hypertrophy modifiers, since they identified an association between the G-allele of rs879922 in the *ACE2* gene and increased left ventricular mass, maximal interventricular septal thickness and posterior wall thickness (Van der Merwe et al., 2008).

Another gene coding for components in the renin-angiotensin-aldosterone system, the angiotensin (Ang) II type I receptor (*AGTR1*) gene, was found to play a modifying role in HCM (Carstens et al., 2011). Results from the latter study proved an association between the functional

single nucleotide polymorphism (SNP) rs1403543 in the *AGTR1* gene, and heritable composite hypertrophy scores in HCM families, since this SNP was found to significantly decrease the hypertrophy composite score (Carstens et al., 2011).

A recent study investigated the role of the gene encoding myocyte enhancer factor 2C (*MEF2C*) in the progression of hypertrophy in a cohort consisting of 209 Caucasian HCM patients and 313 control individuals. In this study, a variable number tandem repeat (VNTR) polymorphism c.-450C (8_10) and a 15bp insertion/deletion was found to be associated with left ventricular outflow tract (LVOT) obstruction. More specifically, HCM patients homozygous for the 10C allele of c.-450C (8_10) showed a significantly greater LVOT obstruction compared to patients carrying any of the other possible genotypes at this locus (Alonso-Montes et al., 2012). Intriguingly, one patient who harboured the p.Asp175Asn HCM-causing mutation in *TPM1* and was homozygous for the 10C allele of c.-450C (8_10), as well as for the 15bp deletion allele, presented with a significantly thicker ventricular wall compared to family members who harboured the same disease-causing mutation.

The above-mentioned studies provide good evidence for the role of modifier genes and variants in the development of hypertrophy in HCM. It is thought that a large number of genes and their functional variants play a role in modifying the expression of the cardiac phenotype in HCM because of the complexity of the regulation of gene expression and the molecular biology of cardiac hypertrophy.

1.1.4 South African HCM founder mutations

A founder mutation is a mutation that is inherited from a common ancestor. Consequently, a founder mutation is observed at high frequency in a geographically or culturally isolated population. In South Africa three founder mutations have been identified and found to cause the disease in 45% of genotyped HCM patients of European and Mixed Ancestry descent (Moolman-Smook et al., 1999). These three founder mutations are the p.Ala797Thr (Moolman et al., 1995) and p.Arg403Trp (Moolman et al., 1993; Posen et al., 1995) mutations located within *MYH7* and the p.Arg92Trp mutation located within *TNNT2* (Moolman et al., 1997). South African HCM patients are therefore screened for these three founder mutations and only in their absence is more extensive screening performed. Findings from a previous study (Moolman-Smook et al., 1999) indicated that the p.Ala797Thr mutation accounts for 25% of HCM cases in South Africa, compared to the p.Arg92Trp mutation in *TNNT2* and the p.Arg403Trp mutation in *MYH7*, which accounts for 15% and 5% of South African HCM cases, respectively. Currently, a mutation-screening programme is in place at Tygerberg Hospital in the Western Cape to screen any referred patients for these three founder mutations. Extensive mutation screening involves screening for a selection of genes previously associated with

HCM by using high resolution melt analysis (HRM; Table 1.1). *MYH7*, *TNNT2*, *MyBPC3*, *TNNI3* and *TPM1* are screened for mutations in this programme.

1.2 HCM as a disease of the sarcomere and impaired cardiac contractility

HCM is classically described as a disease of the sarcomere, which, as the basic component of the myofibrils, constitutes the contractile elements in cardiac muscle (section 1.2.1). The literature indicates that, among others, disturbances in sarcomeric contractility and energy homeostasis are involved in the development of LVH. A recent article demonstrated the effect of HCM-causing mutations in the ankyrin repeat domain 1 (*ANKRD1*) gene that were transferred into engineered heart tissue impair cardiac mechanics. The p.Ile280Val-transduced engineered heart tissue resulted in prolonged relaxation after epoxomicin (a potent and selective proteasome inhibitor) treatment and p.Thr123Met-transduced engineered heart tissue demonstrated higher force and velocities of contraction and relaxation compared to the wild type (Crocini et al., 2013). To elaborate on impaired energy homeostasis in HCM, a study by Blair and colleagues investigated mutations in genes involved in the energy homeostasis in the heart in HCM families and observed two mutations, one missense and one in-frame single codon insertion in *PRKAG2*, that impaired energy homeostasis in the heart (Blair, 2001). These are just two examples to highlight the diversity of molecular and cellular mechanisms involved in the pathogenesis underlying HCM. A brief discussion of the cardiac sarcomere will follow to provide an overview of the complex integration of the development, maintenance, regulation and degradation of sarcomeric proteins.

1.2.1 Sarcomeric development and maintenance

Three important properties of the sarcomere, that are critical for performing its function, is its ability to shorten rapidly and efficiently, its ability to switch on and off very quickly, and its precision for self-assembly and structural regularity. In addition to these properties, the structure and interaction of proteins within the sarcomere are fundamental for sarcomere functioning.

The sarcomere is composed of three major functional classes; contractile, regulatory and structural (Squire et al., 2005). The major contractile protein myosin, which assembles into the thick filament, and actin, which assembles into the thin filament, play a critical role in generating force and shortening of the sarcomere (Huxley and Niedergerke, 1954) (Figure 1.2). Troponin, titin, cMyBPC, tropomyosin, α -tropomyosin and myomesin are, among others, some of the major contractile, structural and regulatory proteins. Some of these are involved in regulating cardiac contraction through actin-myosin interaction in response to changes in calcium concentration, some play an integral role in the

development of an integrated and stable sarcomere, some regulate activity, and some organise myosin and actin into thick and thin filaments (Squire et al., 2005).

Myosin binding proteins, such as cMyBPC, are vital for sarcomeric structure, since they organise sarcomeric molecules during development and modulate contraction in the sarcomere (De Lange et al., 2012; Gautel et al., 1995a; Harris et al., 2002; Stöhr et al., 2013; Weisberg and Winegrad, 1996). Furthermore, capping proteins, such as capZ, attach to the ends of the thin filament and prevent polymerisation and development of actin filaments (Caldwell et al., 1989). The capZ protein plays a vital role in the assembly of the thin filament and regulation within the Z-disc (Pappas et al., 2008).

The thick and thin filaments are linked by cross-linking proteins in the M and Z-lines to form organised three-dimensional lattices (Craig and Padron, 2004). Adjacent sarcomeres are linked to each other in a longitudinal or transversal manner by intermediate filaments that attach to the M and Z-lines. Although the full contribution of Z-disc components in the assembly and maintenance of Z-disc is not known, titin has been implicated in the assembly and maintenance of the Z-disc structure (Seeley et al., 2007; Zou et al., 2006).

Lastly, the giant protein nebulin plays a regulatory role in the assembly of thick and thin filaments in the sarcomere (Bang et al., 2006; Wang and Williamson, 1980; Witt et al., 2006).

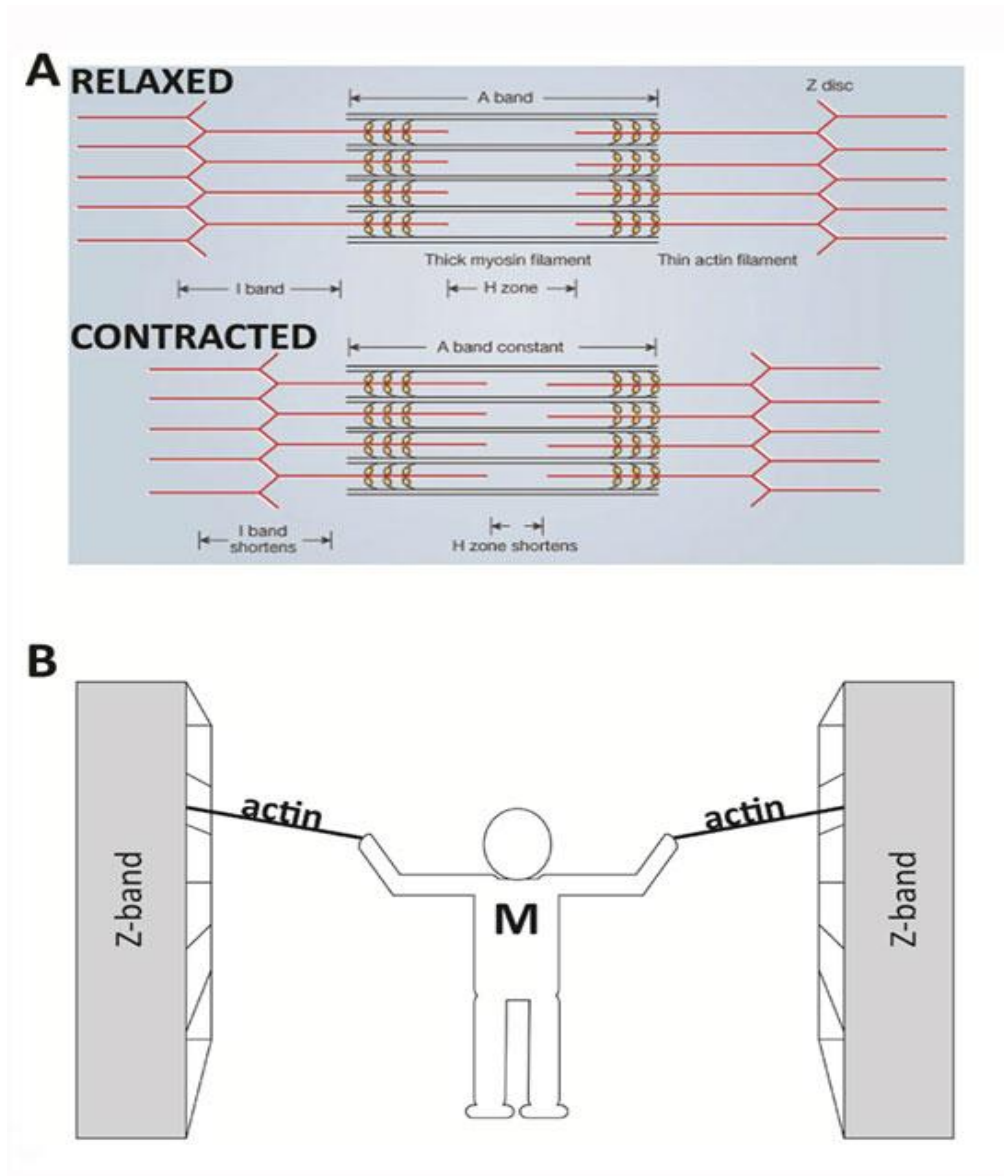


Figure 1.2 A representation of the cardiac sarcomere in a relaxed and contracted state. **(A)** The basic organisation of the sarcomere sub-regions; the A band represents the central location of myosin and actin and the Z-discs are shown in red. **(B)** A theoretical diagram that represents the connection between molecules within the sarcomere. For example, a person (which represents myosin (M)) pulls the bookcases (which represent Z-discs) via ropes (which represent actin) (This image was taken and adapted from Huxley and Niedergerke, 1954).

1.2.2 Sarcomerogenesis

Sarcomerogenesis is the assembly of highly ordered sarcomeric proteins to form a structured, three-dimensional longitudinal alignment of multiprotein complexes, which are regulated at the transcriptional, translational and post-translational levels. Cardiac muscle cells are composed of

tubular myofibrils, which are repeating sections of basic units of a muscle, viz., the sarcomeres. Although there is still some uncertainty as to how proteins assemble to form myofibrils (Sanger et al., 2005), there is growing evidence that myofibrillogenesis involve three myofibril stages in cardiomyocytes (Du et al., 2008). These three stages will be discussed in more detail below.

1.2.2.1 Premyofibril model

The process of assembling the myofibril is not fully understood, although it is known that the process involves filament formation, association of binding proteins with filaments and integration of filaments into contractile sub-units to form myofibril arrays (Sanger et al., 2005). The arrangement of the myofibril in terms of its major components; the thin filament, thick filament and the Z-bands, are similar across species, although the lengths of the striated muscle differs between species (Figure 1.3). The importance of myofibrillar protein interactions have been documented, since mutant sarcomeric proteins in which such interactions are affected have been implicated in cardiomyopathies (Morimoto, 2007; Piston and Kremers, 2007).

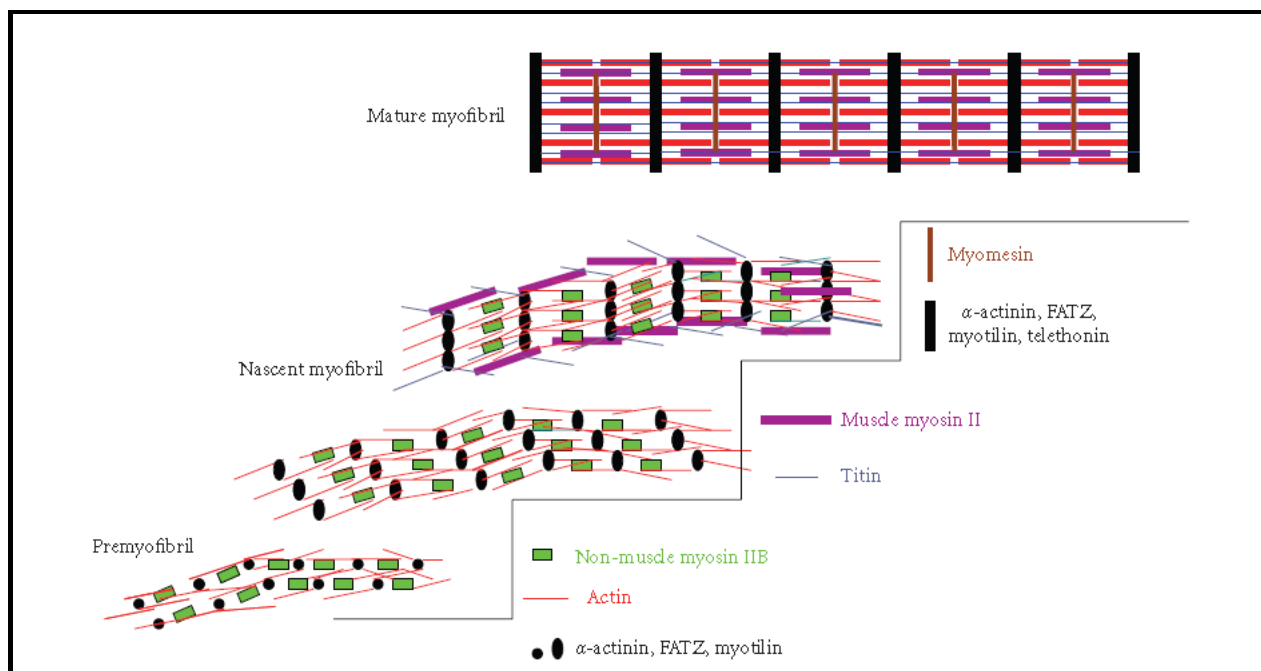


Figure 1.3 Premyofibril model of myofibrillogenesis. Mature myofibrils are formed through three steps; pre-myofibrils that contain non-muscle myosin II, nascent myofibrils that contain both non-muscle myosin II and muscle specific myosin II, and mature myofibrils that contain muscle-specific myosin II but no non-muscle myosin II (This image was taken from Sanger et al., 2005).

In vertebrates, the thin filaments and titin molecules are embedded in the Z-bands (approximately 2 μ m in length) that bind the sarcomere. The thin filaments and titin molecules both interact with the thick filament (Figure 1.4). Actin binding proteins, such as nebulins, tropomyosin and troponins, form the thin filament and myosin binding proteins such as cMyBPC, myomesin and creatine kinase form the thick filament. The titin molecule stretches from the Z-band to the middle of the A-band of the sarcomere. Z-band proteins, such as α -actinin, provide a scaffold for integrating the sarcomere with the plasma membrane.

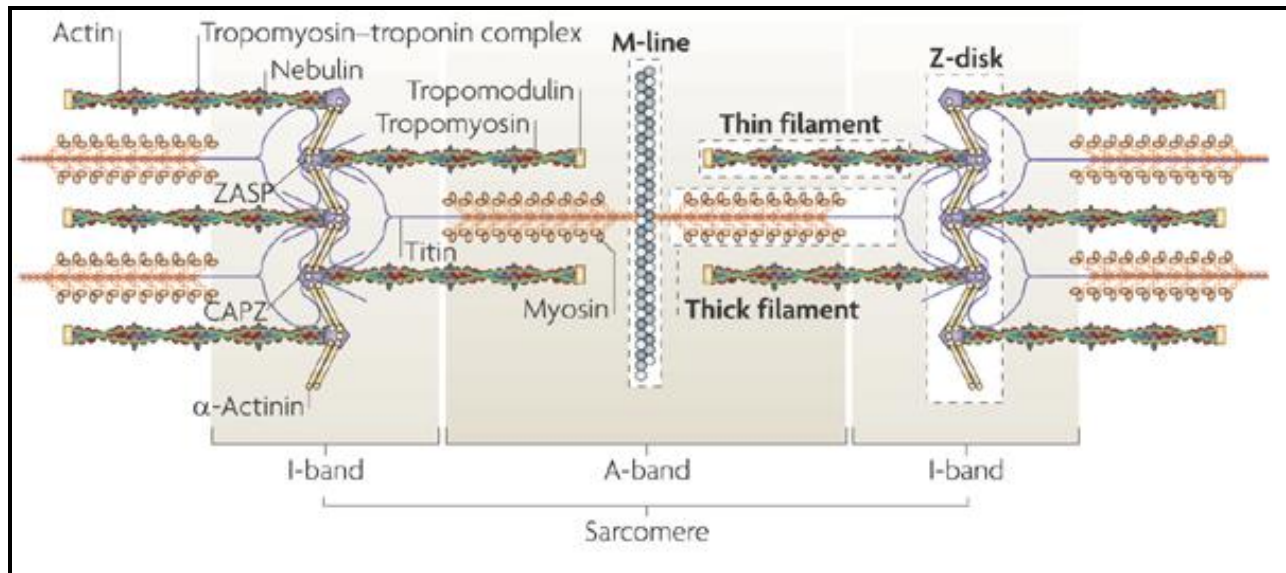


Figure 1.4 Schematic representation of myofibril. Sarcomeric proteins assemble to form a sarcomere. Sarcomeres combine to form a myofibril (This image was taken from Sparrow and Schöck, 2009).

Currently, there are three proposed ways as to how sarcomeric proteins assemble to form myofibrils in avian cardiomyocytes (Sanger et al., 2005). Firstly, it is proposed that two subunits, the A-bands and I-Z-I (thin filament/Z-band) bands, assemble in tandem on a temporary stress fibre-like template (Dlugosz et al., 1984). Secondly, it is proposed that sarcomeres could assemble and subsequently combine to create a myofibril (Gregorio and Antin, 2000; Schultheiss et al., 1990). Finally, myofibrils form through three steps, premyofibrils containing non-muscle myosin II, nascent myofibrils containing both non-muscle myosin II, and muscle-specific myosin II and mature myofibrils containing the muscle specific myosin II but no non-muscle myosin II (Du et al., 2008; Rhee et al., 1994; Wang et al., 2005). Sarcomeres and sarcomeric proteins that make up myofibrils, as described above, are known to be complexly regulated and modified by various processes and pathways, such as sumoylation and phosphorylation, which will be discussed in more detail later (section 1.2.4).

1.2.3 Cardiac contraction

During the differentiation of cardiac muscles, thousands of structural and regulatory proteins assemble into sarcomeric contractile units. Subsequently, many different classes of proteins function in concert to efficiently convert molecular interactions of proteins, such as actin and myosin, into contractile activity (Gregorio and Antin, 2000).

1.2.3.1 The cross-bridge cycle

The cross-bridge cycle is a series of reactions that generate the force required to shorten and lengthen the sarcomere during muscle contraction and relaxation, respectively (Figure 1.5, Steps 1 to 4). At diastolic levels of intracellular calcium, the troponin complex, and more specifically troponin I, inhibits the interaction between myosin and actin. Binding of calcium, released from the sarcoplasmic reticulum, to troponin C during systole, result in a change in the conformation of the troponin-tropomyosin complex. Tropomyosin slides over and exposes myosin-binding sites on actin, which allows the myosin cross-bridge from the thick filament to bind to an actin molecule in the surrounding thin filaments.

In order for the cross-bridge cycle to begin, the myosin head needs to be activated. This occurs when an adenosine triphosphate (ATP) molecule binds to the myosin head and is hydrolysed to adenosine diphosphate (ADP) and inorganic phosphate (Pi). The energy liberated from the hydrolysis of ATP activates the myosin head, forcing it into its cocked position and allowing the myosin head to bind to actin and form the cross-bridge. Upon binding of the myosin head to an actin molecule, the conformation of the cross-bridge is altered to bend inwards (bending), resulting in the “power stroke”. The release of inorganic phosphate (Pi) increases the affinity of the myosin cross-bridge for actin. Following this, ADP is released, causing the myosin head to pivot, which results in the sliding of the thin filament towards the centre of the sarcomere and exposing the ATP-binding site on myosin. The cross-bridge detaches once another ATP molecule attaches to myosin at the end of the power stroke. This prepares the cross-bridge for another cycle, allowing it to return to its unbent conformation. In the absence of Ca^{2+} , troponin and tropomyosin remain in their blocking positions and the myosin cross-bridges and actin cannot bind and no power stroke takes place (Au, 2004).

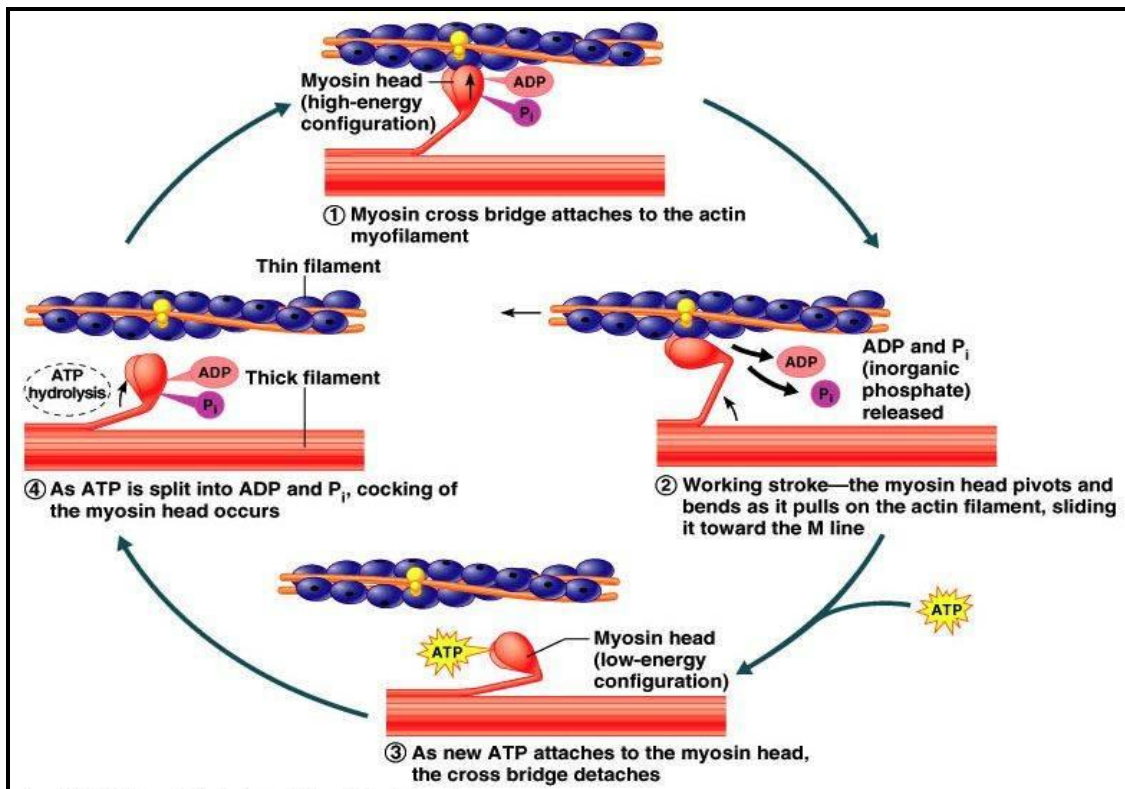


Figure 1.5 The series of reactions involved in the cross-bridge cycle (This image was taken from: <http://www.flashcardmachine.com/hosmolecular-mechanisms-ofmusclecontractionlecture16.html>).

Abbreviations: ADP, adenosine diphosphate; ATP, adenosine triphosphate; P_i , inorganic phosphate

1.2.4 Sarcomeric protein modification and regulation

1.2.4.1 Sumoylation

Sumoylation is the post-translational modification of proteins by the small ubiquitin-related modifier (SUMO). SUMO covalently attaches to specific target proteins and affect their functional properties during cell regulatory processes, such as attaining a particular sub-cellular localisation, DNA-binding and transcriptional activation (Geiss-Friedlander and Melchior, 2007; Hilgarth et al., 2004). Although sumoylation (section 1.2.4.1) and ubiquitination (section 1.2.6.1) compete for the lysine residues of substrates for proteosomal degradation, and although the series of enzymatic reactions involved are very similar, sumoylation is regulated by different enzymes to those involved in ubiquitination (Bergink and Jentsch, 2009; Hoege et al., 2002). Most of these enzymes are evolutionary, conserved from yeast to humans (Nacerddine et al., 2005).

Sumoylation is a reversible reaction regulated by conjugation and deconjugation pathways (Figure 1.6). The mature form of SUMO is activated by an E1-activating enzyme, an Aos1/Uba2

heterodimer, in an ATP-dependent manner (Johnson et al., 1997). Subsequently, the activated SUMO is transferred to UBC9 to form a thioester bond that is conjugated to a lysine residue on the substrate (Johnson and Blobel, 1997). The human SUMO-conjugating enzyme, UBC9, is homologous to ubiquitin-conjugating enzymes (E2s), although UBC9 conjugates to SUMO1 instead of ubiquitin. UBC9 is the only E2 conjugase involved in sumoylation and has been studied in different species in an attempt to elucidate the physiological role of sumoylation (Hayashi et al., 2002; Jones et al., 2002; Nacerddine et al., 2005; Seufert et al., 1995).

In one such study by Nacerddine and co-workers, UBC9-deficient mouse embryos at the blastocyst stage have been shown to die in early post-implantation due to developmental defects. Furthermore, these blastocysts had abnormal nuclear organisation, chromosome segregation, promyelocytic leukemia protein (PML) nuclear bodies and RanBP2-dependent nuclear pore complex (Nacerddine et al., 2005). It is thus evident that SUMO substrates are nuclear proteins that play an important role in proper nuclear architecture, accurate chromosome segregation and embryonic viability (Nacerddine et al., 2005).

Although UBC9 associates with SUMO and aids in transferring SUMO to targets, several SUMO E3 ligases, such as protein inhibitors of activated STAT (signal transducer and activator of transcription) (PIAS) family members (Johnson and Gupta, 2001; Sachdev et al., 2001), polycomb-2 protein (Pc2) (Kagey et al., 2003), or RanBP2 nucleoporin (Pichler et al., 2002), are required for efficient SUMO modification. A family of isopeptidases, namely sentrin-specific proteases (SENPs), which have both hydrolase and isopeptidase activity, are responsible for removing SUMO from target substrates regulating deconjugating reactions (Li and Hochstrasser, 1999; Yeh, 2009).

Defects in the SUMO pathway have been implicated in several disorders, such as cleft lip and/or palate, prostate and breast cancer, neurodegenerative diseases, and cardiovascular diseases (Dorval and Fraser, 2007; Pauws and Stanier, 2007; Song et al., 2008; Wu and Mo, 2007; Zhang and Sarge, 2008). Additionally, sumoylation has been proposed as an important modulator of cardiac function and gene regulation (Wang and Schwartz, 2010).

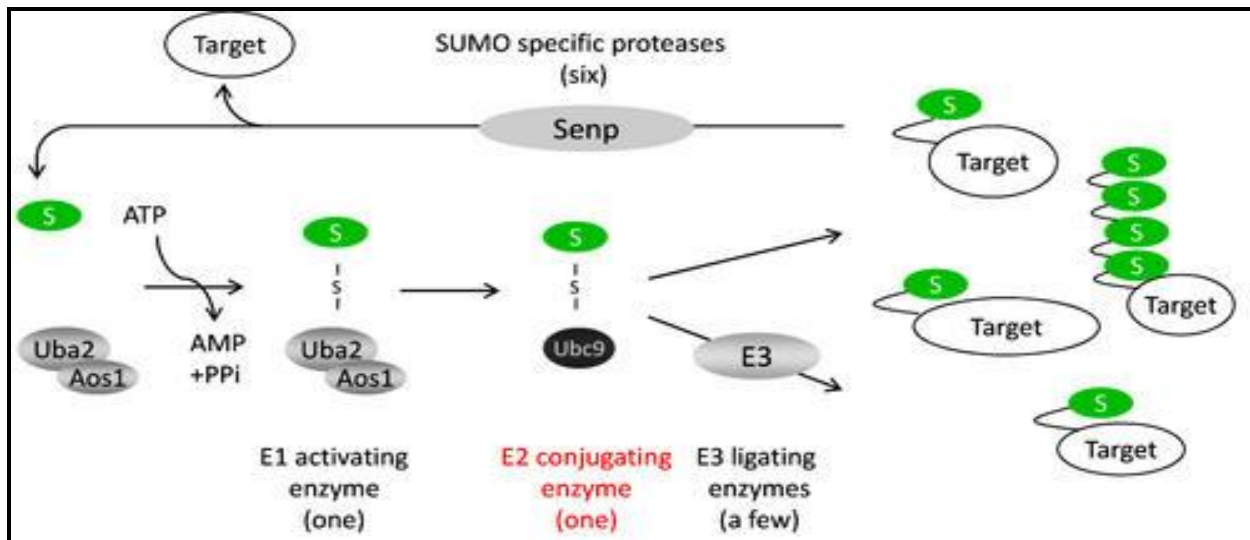


Figure 1.6 Sumoylation is regulated by conjugation and deconjugation pathways (Image was retrieved from The Max Planck Institute of Immunobiology and Epigenetics' website; <http://www3.ie-freiburg.mpg.de/research-groups/epigenetics/pichler/regulation-of-sumoylation-by-its-sole-e2-enzyme-ubc9/>).

Abbreviations: AMP, adenosine monophosphate; ATP, adenosine triphosphate; Aos/Uba2, SUMO-activating enzyme E1; **senp**, sentrin-specific proteases; **UBC9**, SUMO-conjugating enzyme UBC9

Accumulated evidence suggests that sarcomeric proteins tropomyosin and troponin can localise to the nucleus of cardiomyocytes (Asumda and Chase, 2012; Bergmann et al., 2009, 2011; Franklin et al., 2011). Additionally, a recent study by Chase and colleagues used a bioinformatics approach (WoLF PSORT) and predicted the localisation of some tropomyosin and troponin to the nucleus, based on their primary sequence (Chase et al., 2013). In the nucleus, tropomyosin and troponin is suggested to play a role in Ca^{2+} regulation in processes that involve nuclear actin. Furthermore, nuclear actin is thought to be involved in the regulation of transcription and chromatin remodelling (De Lanerolle and Serebryanny, 2011; Grummt, 2006).

Mutations in the sarcomeric proteins tropomyosin and troponin have been associated with HCM, and such mutations in both tropomyosin and troponin have been associated with altered calcium sensitivity and/or binding (Karibe et al., 2001; Kataoka et al., 2007). It is thus thought that mutations in nuclear tropomyosin and troponin could alter Ca^{2+} binding and sensitivity, which would indirectly influence various signaling pathways that modulate gene expression (Kataoka et al., 2007). Interestingly, the study by Chase and colleagues predict that HCM- and DCM-associated mutations in tropomyosin and troponin could affect the functioning of the sarcomere by altering the nuclear structure, function and sumoylation (Chase et al., 2013).

There is thus growing evidence that sarcomeric proteins, such as those mentioned above, are localised in the nucleus of cardiomyocytes and that these proteins could play an important role in the structure, function and regulation of nuclear functions. It is thus not surprising that alterations, such as HCM-causing mutations, in sarcomeric proteins localised to the nucleus could affect processes such as sumoylation.

1.2.4.2 Adrenergic stimulation and contractile protein phosphorylation

Phosphorylation and de-phosphorylation is known to regulate cellular function via a variety of physiological stimuli. Phosphorylation of target substrates result in small conformational changes in protein structure, which consequently affect biological properties. Processes such as membrane transport and permeability, metabolism, ionic fluxes, contractility and transcription and translation of genes, are regulated by phosphorylation (Kurosawa, 1994).

It is suggested that the classical pathway of cardiac protein phosphorylation is via cyclic adenosine monophosphate (cAMP) dependent processes (Lindemann et al., 1983; Rapundalo et al., 1989; Solaro et al., 1976). This process involves the activation of adenylyl cyclases via Gs proteins, resulting in increased cAMP levels. It is thought that cAMP-dependent processes underlie the mechanical effects of catecholamines on cardiac muscle, namely systolic shortening and enhanced contractility. The primary target for cAMP is protein kinase A (PKA), which is suggested to influence cardiac function through specific phosphorylation of regulatory proteins at various levels (Bartel et al., 1993) (Figure 1.7). More specifically, PKA phosphorylates proteins essential for cardiac functioning, such as L-type calcium channels (Gerhardstein et al., 1999; Zhao et al., 1994), phospholamban (Simmerman and Jones, 1998), troponin (Sulakhe and Vo, 1995), ryanodine receptors (Marx et al., 2000), MyBPC (Kunst et al., 2000), and protein phosphatase inhibitor 1 (Zhang et al., 2002).

Adrenergic receptors play an essential role in regulating cardiac function in response to a constantly changing environment. Adrenergic receptors are divided into three sub-classes; firstly, the α 1 receptors (α 1ARs), which include subtypes α 1_A, α 1_B, α 1_D (Docherty, 2010), secondly, the α 2 receptors (α 2ARs), which include subtypes α 2_A, α 2_B, α 2_C (Civantos Calzada and Aleixandre de Artiñano, 2001) and thirdly, the β adrenergic receptors (β ARs), which include subtypes β 1, β 2, β 3 (Xiao, 2001). All three subtypes of α 1ARs and β ARs are expressed in the heart (Brodde and Michel, 1999; Pönicke et al., 2001) and it has been shown that both α and β receptors regulate contractile rate and force, and play a vital role in regulating blood pressure, airway reactivity and metabolic functions.

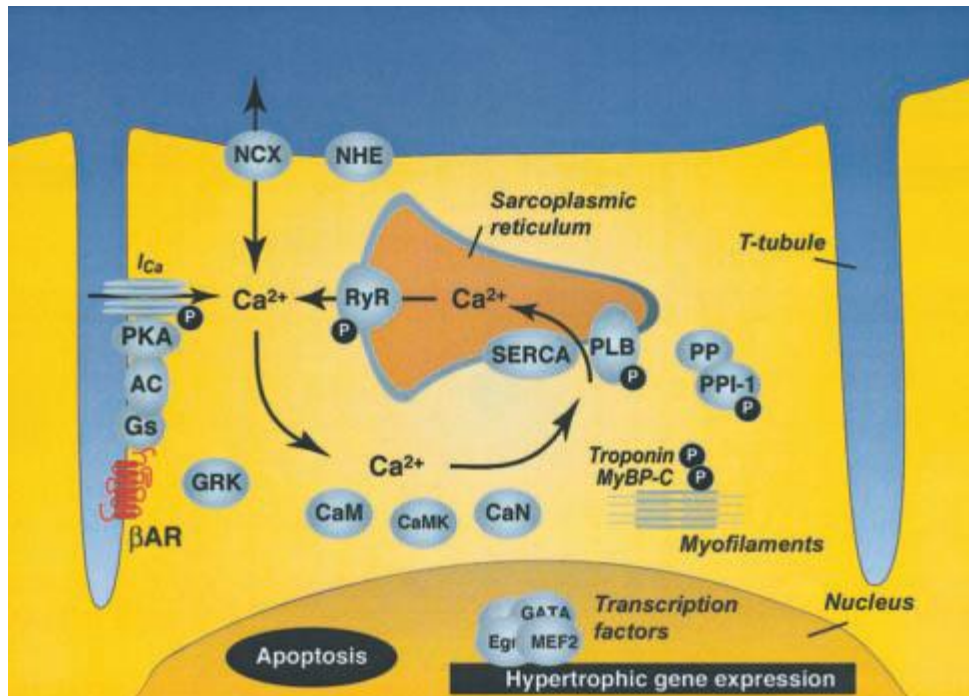


Figure 1.7 Calcium cycling in cardiomyocytes and regulation by PKA phosphorylation. Phosphorylation influence cardiac functioning by phosphorylation of proteins essential for cardiac functioning (Image was taken from Lohse, 2003). **Abbreviations:** AC, adenylyl cyclase; RyR, ryanodine receptor; PLB, phospholamban; SERCA, sarcoplasmic reticulum calcium ATPase; CaM, calmodulin; CaMK, calmodulin-dependent kinase; CaN, calcineurin; GRK, G protein-coupled receptor kinase; NCX, sodium-calcium exchanger; NHE, sodium-proton exchanger; PP, protein phosphatase

The stimulation of β -adrenergic receptors and activation of adenylyl cyclase result in increased cAMP levels. This, in turn, activates PKA, which phosphorylate sarcolemmal slow Ca^{2+} (Sperelakis et al., 1994), which causes a conformational change, causing elevated Ca^{2+} influx (via L-type channels). Increased calcium levels “trigger” the release of more calcium (Fabiato, 1983), which results in increased Ca^{2+} re-uptake into the sarcoplasmic reticulum (phospholamban/sarcoplasmic reticulum calcium ATPase) and modulation of myofilament Ca^{2+} sensitivity (troponin I and MyBPC). Thus, the increased Ca^{2+} concentrations cause Ca^{2+} to bind to troponin C, which results in greater affinity for the interaction of troponin I with troponin C, resulting in a weakened actin-troponin I interaction. This permits actin-myosin interaction, allowing cross-bridge cycling to take place. The amount of Ca^{2+} delivered to troponin C determines the number of cross-bridge cycles that are responsible for “contractility” of the cardiomyocyte.

It is unclear whether the myocardial hypertrophy results from an extended increase in cardiac workload caused by neurohormonal stimulation, or from acute cardiac damage, and whether this could

play a protective role in the prevention of deterioration of ventricular functioning (Barki-Harrington and Rockman, 2003; Chien, 1999; Esposito, 2002; Grossman et al., 1975). However, several studies have shown that sustained hypertrophy is a predictor of heart failure (Ho et al., 1993; Levy et al., 1990a). Furthermore, alterations in components of the adrenergic system have been associated with heart failure and hypertrophy (Bristow, 1998; Engelhardt, 2001).

1.2.5 Sarcomeric protein integration and exchange

The integration and exchange of new sarcomeric proteins into the sarcomere precedes the formation of sarcomeres and myofibrils. This continuous process requires a careful balance between protein synthesis and protein degradation (protein turnover). Protein turnover is, for example, regulated and controlled by the activation of protein synthesis during cardiac hypertrophy or by activating protein degradation during ventricle unloading (Hedhli et al., 2005).

The half-life of contractile proteins, such as myosin, has been proven to differ significantly from that of myofibrillar proteins, such as troponin. The half-life of myosin in the heart is approximately 15 days (Papageorgopoulos et al., 2002), while the half-life of the troponin is approximately three to five days (Martin, 1981). It is thus evident that these sarcomeric proteins have different protein turnover rates within the heart and that the constant integration of proteins into the sarcomere, as well as the synthesis and degradation of these proteins, warrant tight regulation.

Deregulation of protein synthesis and degradation has been linked to the pathogenesis of multiple forms of heart disease, such as cardiac ischemia (Cadete et al., 2013), hypertrophy (McDermott et al., 2012) and heart failure (Letavernier et al., 2012), therefore controlling the activity of these pathways present an opportunity for novel therapeutic avenues or strategies.

1.2.6 Sarcomeric protein degradation

Proteolysis is defined as the hydrolytic breakdown of proteins into simpler, soluble substances, such as peptides and amino acids. This process is also termed protein degradation, which, in the heart, is achieved by three main systems; the ubiquitin-proteasome system (UPS), autophagy/lysosomal degradation and the calpain system (Ord et al., 1983). These three systems function in distinct ways.

The UPS targets specific proteins and labels them with multiple ubiquitin molecules, which then allows recognition and subsequent degradation by the 26S proteasome. During autophagy, larger damaged or misfolded proteins and damaged organelles that cannot be degraded by the UPS system, are

degraded. The calpain system is mediated by a family of calcium-dependent, non-lysosomal cysteine proteases that are expressed ubiquitously within all cells and appear to play a role in cardiac pathophysiology (Singh et al., 2004).

1.2.6.1 The ubiquitin-proteasome system

The ubiquitin protein degradation system is mediated by an enzyme cascade that is responsible for the degradation of abnormal proteins (proteins that are unfolded or damaged) and short-lived proteins (Goldberg, 2003). Several enzymes are involved in the ubiquitination process, the ubiquitin-activating (E1), ubiquitin-conjugating (E2) and ubiquitin ligase (E3) (Figure 1.8). The UPS is considered to be the major pathway of protein degradation, since approximately 80% to 90% of intracellular bulk proteins in mammalian cells are degraded via the UPS. Ubiquitin is a highly conserved 76 amino acid protein that is covalently linked to target substrates for degradation via the UPS.

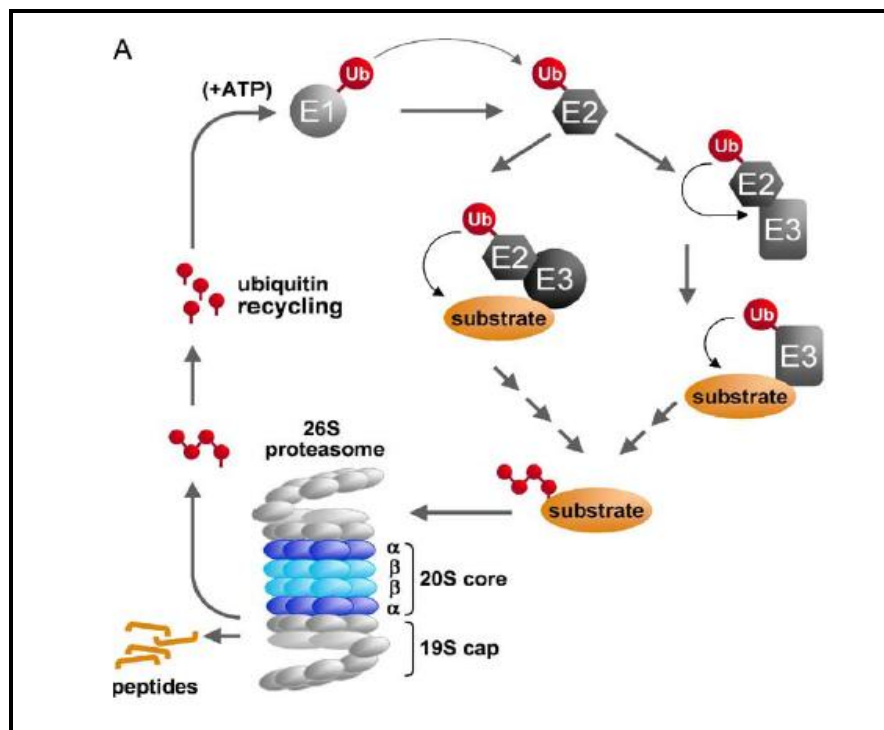


Figure 1.8 The ubiquitination of target substrates for degradation involves three steps. These are: Initial activation (catalysed by E1 enzyme), covalent linking of ubiquitin to a conjugating enzyme, E2, and conjugating ubiquitin to the target substrate (facilitated by E3 ligase) (This image was taken and adapted from Zolk et al., 2006). **Abbreviations:** ATP, adenosine triphosphate; E1, ubiquitin-activating enzyme; E2, ubiquitin-conjugating enzyme; E3, ubiquitin ligase; Ub, ubiquitin

Ubiquitin covalently attaches to ubiquitin-activating enzyme (E1) in an ATP-dependent manner. Subsequently, the ubiquitin-conjugating enzyme (E2) catalyses the transfer of ubiquitin from E1 to the active cysteine site of the E2. A third enzyme, ubiquitin ligase E3, is required to transfer ubiquitin from E2 to a lysine residue on the target substrate. E3 ligases ensure substrate specificity of ubiquitination by conjugating directly to target substrates for protein degradation (Powell, 2006) (Figure 1.8) (Haglund et al., 2003). An elongation factor (E4) is needed to polyubiquitate a substrate for degradation by the 26S proteasome. In order to transport the polyubiquitinated target to the proteasome, the target needs to be recognised by the proteasome directly or needs to bind to a transport protein, such as a chaperone (Powell, 2006).

One E1, approximately 12 different E2 and hundreds of E3 ubiquitin ligases have previously been described; nine of these have been found to be expressed in the heart (Rodríguez et al., 2009). Muscle-specific ubiquitin ligases, such as the muscle RING finger (MuRF) protein family and muscle atrophy F-box (atrogin-1/MAFbx) proteins (Gomes et al., 2001; Spencer et al., 2000), have been shown to play a role in the development of cardiac conditions, such as cardiac atrophy.

MuRF1, MuRF2 and MuRF3 are members of a muscle-specific RING finger protein family that are expressed in striated muscles. More specifically, these three MuRF family members localise to the M-line and Z-disc of the sarcomere (Centner et al., 2001; McElhinny, 2004; Spencer et al., 2000). Although it is not clear what role MuRF1 plays in normal growth, it has shown to be essential in activating skeletal muscle atrophy (Bodine et al., 2001), mediating cardiac atrophy *in vivo* and inhibiting cardiac hypertrophy (Arya et al., 2004; Willis et al., 2009). Furthermore, MuRF1 and MuRF2 interact with the sarcomeric proteins titin, troponin T, myotilin and ventricular myosin light chain 2 (MLC2v) and T-cap (Witt et al., 2005), of which mutations in all but myotilin have previously been implicated in HCM (Table 1.1). MuRF2 plays a critical role in the maintenance of microtubules, intermediate filaments and the sarcomeric M-line in striated muscle (McElhinny, 2004). MuRF2 and MuRF3 have also been shown to be important for normal cardiac contraction and maintenance (Fielitz et al., 2007; Witt et al., 2007). Interestingly, MuRF3 does not interact with the same binding partners as MuRF1 and MuRF2, as mentioned above (Witt et al., 2005), which suggests specificity for targets of MuRF in the sarcomere.

A recent study by Predmore and colleagues investigated the function of the UPS in human heart failure and HCM (Predmore et al., 2010) (Figure 1.9). Distinctly reduced proteasome activity, which

was indicated by measuring chymotrypsin-like and caspase-like activities, was observed in hearts with heart failure and HCM, compared to healthy hearts. Interestingly, protease activity was significantly reduced in HCM hearts containing defined disease-causing mutations (HCM-causing mutations in *MyBPC3*, *TNNT2* or *TPM1*), compared to HCM hearts without these mutations. Furthermore, protease activity in failing hearts was partially reversed by mechanical unloading (Predmore et al., 2010). These results indicate that post-translation modifications to the proteasome may account for defective protein degradation in human cardiomyopathies.

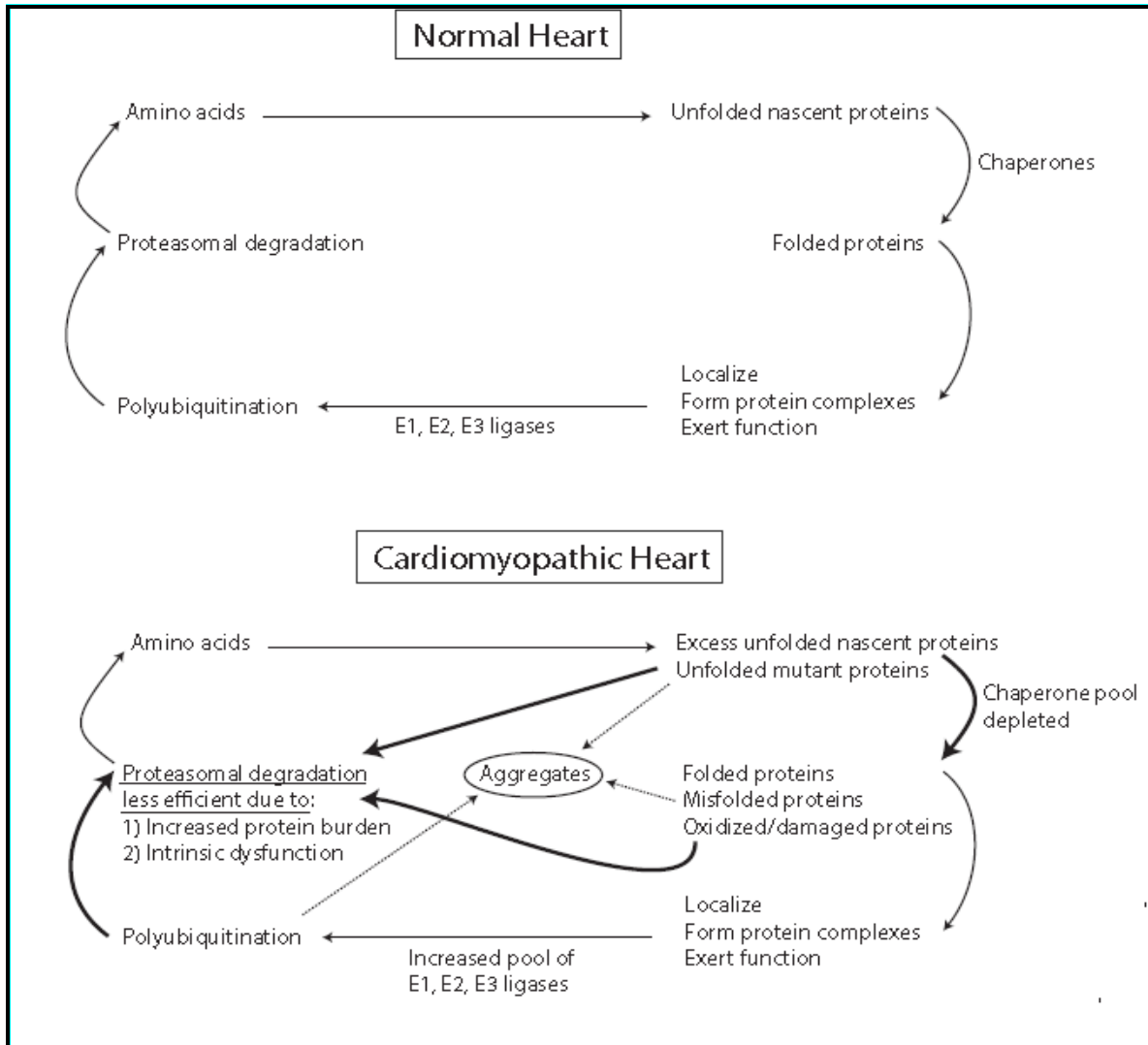


Figure 1.9 Ubiquitination in the normal heart compared to the cardiomyopathic heart (This image was taken from Day, 2013). **Abbreviations:** **E1**, ubiquitin-activating enzyme; **E2**, ubiquitin-conjugating enzyme; **E3**, ubiquitin ligase

Several studies have shown that altered cMyBPC protein expression, as a result of either truncated cMyBPC (Sarikas et al., 2005) or missense mutations (Bahrudin et al., 2008, 2011), could contribute

to HCM cardiac dysfunction through impaired proteasome activity. A study by Vignier and colleagues investigated the mechanisms that regulate cardiac MyBPC expression by looking at the effect of a missense mutation (p.Glu264Lys) in a knock-in (KI) mouse model (Vignier et al., 2009). This mutation corresponds to the human mutation p.Glu258Lys and is located within the last base pair of exon 6 of *MyBPC3*, in a conserved splice site. Interestingly, this mutation resulted in three altered mRNA isoforms in the mouse; one containing a missense mutation, another containing nonsense mutations resulting in a premature stop codon, exon skipping or frameshift, and the third containing a deletion/insertion, which results in almost full length cMyBPC cDNA. Furthermore, truncated cMyBPC was significantly increased after inhibition of nonsense-mediated mRNA decay, whereas the two full-length cDNA isoforms were detected at higher concentrations after inhibition of the UPS, suggesting that nonsense-mediated mRNA decay and the UPS work together to degrade mutant proteins.

More recently, the UPS system in a KI mouse model, containing a HCM-causing mutation that results in low levels of mutant cMyBPC, and a knockout (KO) model, which results in absence of cMyBPC, was investigated. Results indicated impaired ubiquitin-proteasome activity with age in only the KI mouse model and defective autophagy-lysosomal activity in the KI and KO model (Schlossarek et al., 2012).

1.2.6.2 Autophagy

Autophagy is a proteolytic system used for bulk degradation and recycling of long-lived proteins and organelles (Kim et al., 2007). Furthermore, autophagy has shown to be important for the maintenance of endoplasmic reticulum (ER), since autophagosomes are thought to emerge from the ER (Arstila and Trump, 1968; Dunn, 1990; Ericsson, 1969; Hayashi-Nishino et al., 2009, 2010; Ylä-Anttila et al., 2009).

There are three main autophagic pathways, viz., microautophagy (Kunz, 2003), in which the cytosol is directly engulfed by lysosomes; chaperone-mediated autophagy (Dice, 2007), where chaperone proteins recognise target proteins and direct them to lysosomes, and finally, macroautophagy (Yorimitsu and Klionsky, 2005) (hereafter referred to as autophagy), in which cytosolic material is engulfed in an autophagosome and delivered to lysosomes for degradation. While autophagy is an important mechanism for the degradation of unwanted proteins and damaged organelles, it also serves to maintain cellular homeostasis during periods of nutrient and energy deprivation (Klionsky and Emr, 2000). Through the process of excessive self-digestion and degradation of

essential cellular constituents, autophagy is thought to modulate cell death (Levine and Yuan, 2005; Shimizu et al., 2004).

A distinct vesicle, sequestering cytoplasm in a double-unit limiting membrane with the intention of degrading its contents, is known as an autophagosome (Klionsky and Emr, 2000) (Figure 1.10). During autophagy, autophagosomes lose their distinctive membrane by fusing with late endosomes and lysosomes to deliver their contents for degradation (Ericsson, 1969). There are several protein complex groups with specific functions that are responsible for mediating autophagy (Levine and Kroemer, 2008). One of these protein complexes is composed of the proteins ATG1 (autophagy-related-1), FIP200 (focal adhesion kinase [FAK] family interacting protein of 200kDa), ATG101 and ATG13, and possesses serine/threonine kinase activity (Hosokawa et al., 2009; Jung et al., 2009). The mammalian target of rapamycin (mTOR) and AMP-activated protein kinase (AMPK) is responsible for regulating this complex through phosphorylation of ATG1, which regulates the autophagy rate according to the metabolic needs of the cell (Kim et al., 2011).

The ATG1-containing complex controls the activity and localisation of another multiprotein complex, vps34, which contains phosphatidylinositol-3-kinase (P13K) activity. P13 moieties are required for the formation of autophagosomes (Blommaert et al., 1997; Suzuki et al., 2007). Another member of the vps34 protein complex, ATG6/Beclin-1 protein, is critical for the formation of autophagosomes (Funderburk et al., 2010; Zeng et al., 2006). The previously mentioned P13-phosphate moieties are essential for maturation of autophagosomes and play an important role in changing the membrane of the autophagosomes by changing its physical properties, (Fan et al., 2011; Matsunaga et al., 2010) to form a cup-like structure called an “omegasome” (Axe et al., 2008; Hayashi-Nishino et al., 2009, 2010).

An ubiquitin-like ligase system composed of ATG3, ATG7, ATG10 and a trimeric complex composed of ATG5, ATG12 and ATG16L, which localises to the omegasome (Fujita et al., 2008a); (Ichimura et al., 2004), is involved in conjugating the ATG8/LC3b protein to the lipid phosphatidylethanolamine (PE). This lipid is abundant in the autophagosome membrane (Tanida et al., 2004a). PE-conjugated LC3b (LC3b-II) specifically associates with autophagosome membranes (Kabeya et al., 2000) and is required for autophagosome membrane elongation (Fujita et al., 2008b; Weidberg et al., 2010). LC3b is targeted to the autophagosome by PE conjugation and co-operates in autophagosome maturation and sealing (Weidberg et al., 2010). Additionally, luminal-facing LC3b-II, the lipidated form of LC3b, is degraded by lysosomal hydrolases (Ueno and Takahashi, 2009), whereas protein on the cytosolic-facing side of autophagosome is

recovered by delipidation (Tanida et al., 2004b). LC3b-I is the cytoplasmic, non-lipidated form of LC3b and can be recruited for the formation of new autophagosomes (Tanida et al., 2004a). LC3b-II serves as a marker for autophagy as it is uniquely targeted to autophagosome membranes (Kabeya et al., 2000).

Autophagy is known to play an important role in the heart. Basal levels of autophagy are involved in the turnover of organelles in the normal heart (Kim et al., 2007; Levine and Klionsky, 2004), which is altered in response to stress, such as ischemia/reperfusion (Hamacher-Brady et al., 2006; Matsui et al., 2007), cardiovascular diseases such as cardiac hypertrophy (Dämmrich and Pfeifer, 1983) and heart failure (Shimomura et al., 2001).

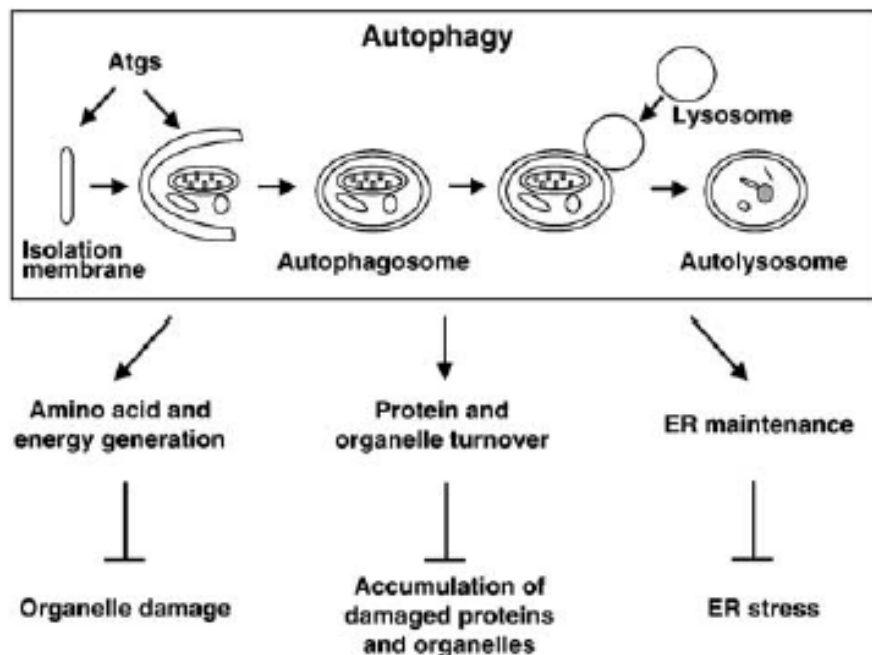


Figure 1.10 Autophagy plays a role in recycling amino acids, removing damaged proteins and organelles and maintaining the ER (This image was taken from Nishida et al., 2009). **Abbreviations:** ER, endoplasmic reticulum

Constitutive cardiomyocyte autophagy is not only essential for degrading and recycling cytoplasmic components, such as long-lived proteins and organelles, but also serves a cytoprotective role by disposing of damaged mitochondria under the basal state (Levine and Yuan, 2005; Maiuri et al., 2007). Moreover, autophagy has the ability to prevent activation of apoptosis (Decker and Wildenthal, 1980); (Hamacher-Brady et al., 2007), since pro-apoptotic factors, such as cytochrome c, is released from damaged mitochondria (Gustafsson and Gottlieb, 2003).

Furthermore, autophagy is thought to play a protective role in the heart, given that past studies have observed a cardiomyopathy phenotype in lysosome-associated membrane protein 2 (LAMP2)-deficient mice, caused by an accumulation of autophagic vacuoles and impaired autophagic degradation of long-lived proteins (Nishino et al., 2000; Tanaka et al., 2000). Despite increased protein turnover during cardiac hypertrophy, reduced autophagy in response to aortic stenosis and isoproterenol infusion have been observed (Pfeifer et al., 1987).

An increase in the rate of protein synthesis and cardiac hypertrophy seem to be a response to pressure overload (Imamura et al., 1994). Interestingly, when wild type mice were subjected to pressure overload by transverse aortic constriction (TAC), they converted to hypertrophic mice, with no visible cardiac dysfunction one week after exposure (Yamaguchi, 2003). In fact, a more recent study compared TAC-induced hypertrophied hearts to sham-operated hearts and confirmed that reduced autophagic activity is observed in response to hypertrophy (Nakai et al., 2007) (Figure 1.11).

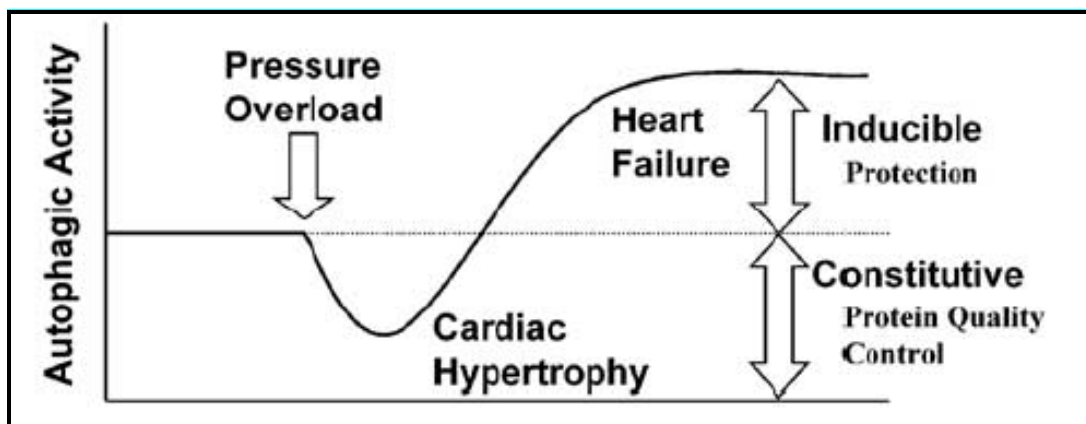


Figure 1.11 The activity of autophagy in response to pressure overload in the heart (This image was taken from Nishida et al., 2009).

Autophagy is thought to play an important role in mediating regression of cardiac hypertrophy upon unloading (Hariharan et al., 2013; McMullen, 2004). Results from a recent study demonstrated the up-regulation of autophagy and a decrease in heart size in transgenic mice in which forkhead box protein 01 (FOXO1) was over-expressed (Hariharan et al., 2013). More specifically, cardiac hypertrophy was observed in mice subsequent to releasing transverse aortic constriction (TAC) that was administered for one week. Cardiac hypertrophy was indicated by a reduced left ventricular weight and body weight LVW/BW ratio and a reduction in the cross-sectional area of cardiomyocytes in these mice. Markers for autophagy (LC3b-II expression, p62 degradation and GFP-LC3 dots/cell) demonstrated that autophagy was induced along with the regression of cardiac

hypertrophy, and subsequently cardiac-specific FOXO1 was found to be up-regulated during increased autophagy (Hariharan et al., 2013). These effects were found to be attenuated upon inhibition of autophagy or downregulation of FOXO1. This indicates that FOXO1 and autophagy mediate regression of cardiac hypertrophy during mechanical unloading and that FOXO1 could be used as molecular marker to indicate regression of cardiac hypertrophy.

A study by McMullen (2004) induced autophagy using the mTOR inhibitor, rapamycin and found that this promoted the regression of cardiac hypertrophy. Mice that were subjected to ascending aortic constriction (ACC) overload for one week, followed by rapamycin treatment for another week, presented with a heart weight/body weight ratio decreased by 68% and 41% in mice with either compensated or decompensated cardiac hypertrophy, respectively. Interestingly, improved cardiac function was observed in mice with decompensated cardiac hypertrophy, suggesting a cardiac hypertrophic response during down-regulated autophagy in a hypertrophic state. Furthermore, the beneficial effects of rapamycin was confirmed in a more recent study (Marin et al., 2011), suggesting that rapamycin-induced autophagy could prevent and aid in the management of cardiac hypertrophy (Shioi, 2003).

1.2.6.3 Calpain system

Approximately 16 members of the **calcium** ion-dependent **papain**-like protease (calpain) family, which localise to the cytosol, have previously been described. Calpains are inactive pro-enzymes that translocate to membranes in response to increased intracellular calcium levels. Calpain 1 and calpain 2 are localised to the Z-disc (Dayton and Schollmeyer, 1981; Kumamoto et al., 1992) and once at the membrane, they are activated by calcium and phospholipids. Calpastatin is an endogenous inhibitor that consists of four inhibitory domains that regulate calpain 1 and 2 (Goll et al., 2003). Furthermore, post-translational modification by phosphate groups can inhibit calpain activity (Goll et al., 2003).

Under normal cardiac functioning, calpain 1 and calpain 2 are active and are responsible for proteolysis of substrates such as desmin and protein kinase C α , increased ubiquitination and protein turnover by the 26S proteasome (Galvez et al., 2007). Calpains are known to regulate cleavage and play an important role in various calcium-regulated cellular processes, such as muscle contraction, neuronal excitability, secretion, signal transduction, cell proliferation, differentiation, cell cycle progression and apoptosis (Carafoli and Molinari, 1998; Huang and Wang, 2001; Saïdo et al., 1994; Sorimachi and Suzuki, 2001; Sorimachi et al., 1997) (Table 1.2). Disrupted calcium homeostasis in

cardiac conditions, such as atrial fibrillation, heart failure, hypertrophy and ischemia-reperfusion, result in deregulation of calpain (Table 1.2). Consequently, deregulation of calpain has been implicated in myocardial damage.

In a study by Galvez and colleagues, the over-expression of calpastatin, the calpain inhibitor, in mice hearts resulted in a decrease in the levels of ubiquitination of myocardial calpain 1 activity by 58%, although the general proteasome activity was not affected. Taking into account that only calpain 1 was affected by the over-expression of calpastatin, it was suggested that calpain 1 affects the ubiquitination step specifically (Galvez et al., 2007). Moreover, the inhibition of calpain 1 activity by the over-expression of calpastatin resulted in progressive DCM with the presence of autophagosomes, accumulated protein complexes and the loss of sarcomere integrity (Galvez et al., 2007). These findings suggest that calpain 1 activity is essential for normal cardiac functioning and is critical for the regulation of protein turnover of specific cardiac proteins, including sarcomeric proteins.

Calpain activity has been implicated in the progression of cardiac pathophysiology (Singh et al., 2004), since calpain 1-dependent degradation of sarcomeric contractile proteins, such as troponin I, has been implicated in myocardial stunning (Gao et al., 1997). In a study by Gao and colleagues, troponin I was observed to be degraded in the stunned myocardium, but this could be prevented by perfusion resulting in decreased Ca^{2+} and pH. In parallel experiments, normal skinned trabeculae were found to be degraded by calpain 1 in a similar way. Interestingly, calpastatin was able to prevent troponin degradation, suggesting that myocardial stunning is caused by calcium-dependent myofilament proteolysis (Gao et al., 1997).

Inhibition of calpain has been suggested as a possible therapeutic intervention for cardiac diseases such as atrial fibrillation (Ke et al., 2008). In an attempt to identify the proteases involved in the degradation of myofibrillar proteins during atrial fibrillation, degradation of myofibrillar proteins (cardiac troponin I, cardiac troponin T and cardiac troponin C) were investigated in tachy-paced human cardiac troponin T-overexpressing HL-1 cardiomyocytes. Furthermore, contractile function was evaluated by analysing cell-shortening measurements. Results from this study demonstrated that contractile cardiac troponins were significantly degraded and contractile dysfunction was clearly visible (Ke et al., 2008). Interestingly, both these effects could be inhibited by calpain, but not by caspases or proteases, suggesting that human cardiac troponin degradation was mediated by calpain. It was thus suggested that the inhibition of calpain could therefore prove to be an effective treatment for the structural and functional remodelling associated with atrial fibrillation (Ke et al., 2008).

Table 1.2 Physiological and pathological role of calpains in the heart (This table was taken and adapted from Bukowska et al., 2012).

Calpains in the Heart			
Regulated by	Calcium, calpastatin		
Physiological role	Regulatory role in calcium dependent process: <ul style="list-style-type: none"> • Muscle contraction • Signal transduction • Gene expression • Cell cycle • Apoptotic pathway 		
Patho-physiological role (calpain over-activation)	Myocardial remodelling and contractile dysfunction: <ul style="list-style-type: none"> • Degradation of contractile proteins • Loss of regular sarcomere structure • Down regulation of L-type calcium channel • Swelling of mitochondria • Damage of cardiomyocytes 		
Cardiac pathologies	Atrial fibrillation	Heart failure	Ischemia reperfusion
Calcium level	[Ca ²⁺] _i overload	[Ca ²⁺] _i overload	[Ca ²⁺] _i overload
Involved calpain	Calpain 1	Calpain 2	Calpain 1 and Calpain 2

Abbreviations: Ca²⁺ - calcium

1.3 Cardiac myosin binding protein C

MyBPC3, encoding cardiac MyBPC, is one of the most frequently mutated genes in HCM and interactors of this protein have previously been investigated (Ababou et al., 2007; Freiburg and Gautel, 1996; Gruen et al., 1999; Koretz et al., 1993; Kulikovskaya et al., 2003; Labeit et al., 1992; Moolman-Smook et al., 2002). The localisation, expression and interactions of this protein will be discussed in more detail, as the similarity of cMyBPC with our protein of interest in this study, myosin binding protein H (MyBPH), warrants investigation into the structure and function of this protein.

1.3.1 cMyBPC as a regulatory protein found in the sarcomere

cMyBPC is one of three isoforms of MyBPC, namely fast skeletal, slow skeletal and cardiac, each of which are encoded by separate genes (Yamamoto and Moos, 1983; Vaughan et al., 1993a, 1993b).

cMyBPC (approximately 130 kDa) is a multi-domain sarcomeric protein that resides in the thick filaments of the striated muscle. It is arranged within the C-zone along the length of the A-band in nine to 11 transverse stripes that are 43nm apart, with approximately two to four molecules of cMyBPC associated with each myosin cross-bridge (Bennett et al., 1986; Pepe et al., 1986) (Figure 1.12).

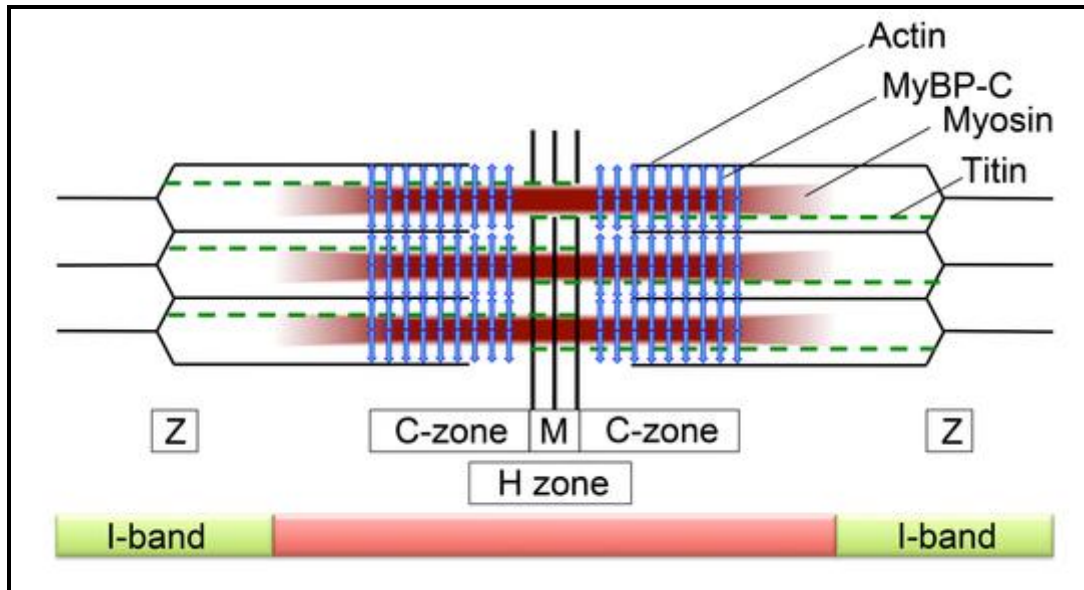


Figure 1.12 Schematic diagram of striated muscle sarcomere. This image indicates the localisation of cMyBPC (blue) that is restricted to the C-zone of the A-band, titin (dashed green lines), myosin (thick filament) in red and actin in black (thin filament) (This image was taken and adapted from Lin et al., 2013).

In terms of its structure, cMyBPC consists of ten globular domains; seven immunoglobulin I-like (Ig) domains and three fibronectin type III (Fn_{III}) repeats. These domains are designated C1-C10, C1 being on the amino-terminus (NH₂-terminus) (Einheber and Fischman, 1990) and C10 on the carboxy-terminus (C-terminus) (Figure 1.13). The cMyBPC-motif, a conserved linker, is located between domains C1 and C2, with the N-terminal of domain C1 extending into a proline/alanine-rich sequence. All isoforms of MyBPC have a similar domain organisation, with high sequence conservation, particularly in the C-terminal domains (Okagaki et al., 1993).

However, the cardiac isoform is different from the skeletal MyBPC isoform in three important ways. Firstly, cMyBPC contains a unique C0 domain at the NH₂-terminus, present only in the cardiac isoform of MyBPC. Secondly, a LAGGRRIS-amino acid sequence insertion containing phosphorylation sites is located within the MyBPC-motif, which is necessary for the role that cMyBPC plays in phosphorylation, and thirdly, the C5 domain contains a 28-amino acid sequence insertion (Gautel et al., 1995a; Yasuda et al., 1995).

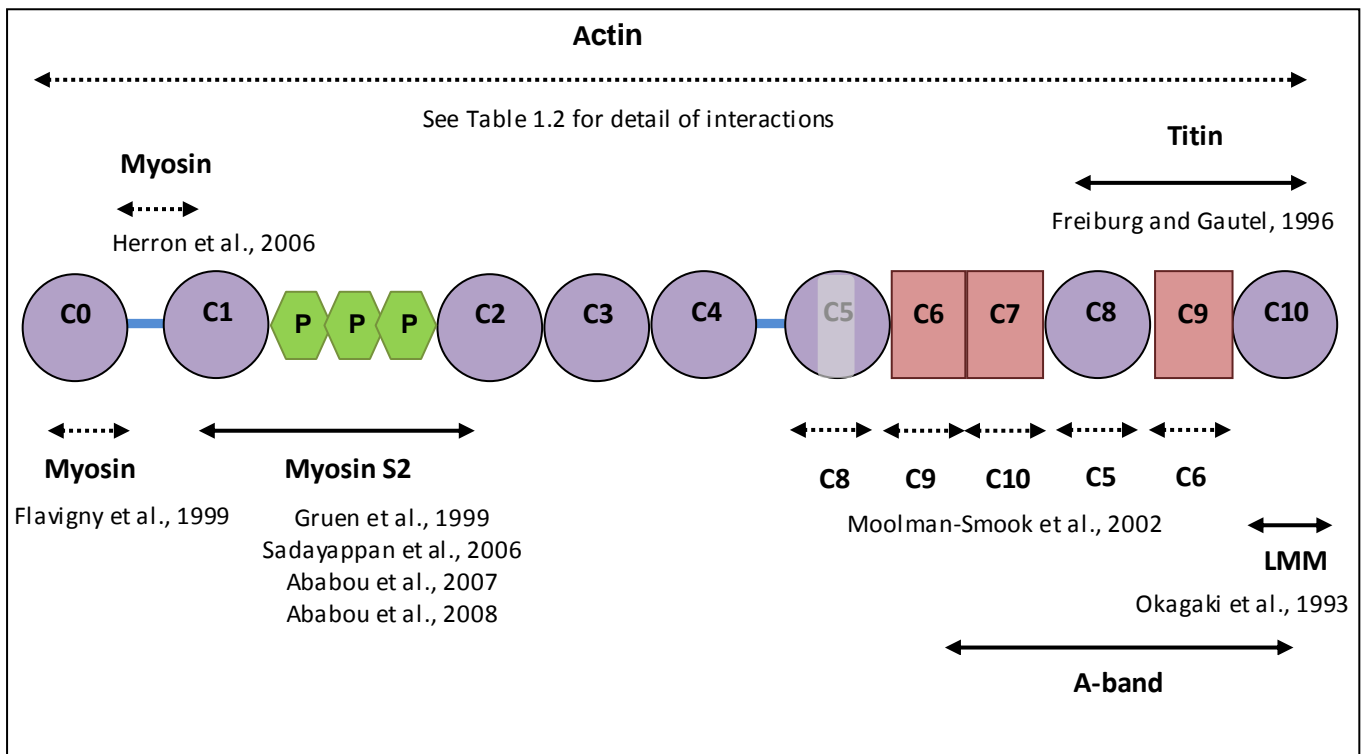


Figure 1.13 Schematic representation of cardiac myosin binding protein C (cMyBPC), indicating domains of known function. The purple circles represent immunoglobulin-like domains, the pink squares represent fibronectin type-III domains, the green hexagons represent phosphorylation sites in the cMyBPC motif located between domains C1 and C2, the solid blue lines represent linker sequences, the white rectangle in domain C5 represents a cardiac-specific insert, the solid black line represents established interactions and the dashed black line represents interactions that require independent verification. **Abbreviations:** **Myosin S2**, Myosin S2 subfragment of myosin heavy chain; **LMM**, light meromyosin

1.3.2 The role of cMyBPC in the thick filament

Although cMyBPC is thought to play a structural and regulatory role in the sarcomere, its function is not completely understood (Gautel et al., 1995a; Okagaki et al., 1993). Past studies have shown that although myosin filaments are still able to form in the absence of cMyBPC, the addition of physiological ratios of cMyBPC increased filament length and structural organisation of the filament (Davis, 1988; Koretz, 1979), substantiating its role in thick filament structure. Furthermore, when skeletal cMyBPC and myosin were co-expressed in non-mammalian non-muscle cells, long and compact myosin filaments formed around the nucleus, while diffuse spindle-shaped structures formed in the absence of cMyBPC (Seiler et al., 1996; Welikson and Fischman, 2002).

Results from the above-mentioned studies raised the question as to whether cMyBPC is necessary for filament assembly. Several studies have since investigated cMyBPC KO models in an attempt to elucidate the function of cMyBPC in cardiac muscle function (Harris et al., 2002; Korte et al., 2003; Luther et al., 2008).

A study by Harris and co-workers involved generations of KO mouse models that lack the coding region of cMyBPC via homologous recombination (Harris et al., 2002). Although this study demonstrated that wild type mice and mice heterozygous for the KO allele were indistinguishable from each other upon histology, the homozygous null mice exhibited significant hypertrophy, myocyte disarray and fibrosis (Harris et al., 2002). Furthermore, transmission electron microscopy observed regular striated muscle with clear Z-lines, M-lines and A-bands in all mice with and without KO alleles, although the Z-lines were often misaligned in the homozygous null mice. Functionally, echocardiography results demonstrated a significant decrease in diastolic and systolic function in the homozygous null mice (Harris et al., 2002).

Furthermore, a study by Luther and colleagues found normal distribution of cMyBPC in the A-band of cardiac and skeletal muscle in wild type mice and cMyBPC-deficient mice, showing that the A-band of cardiac and skeletal muscle is very similar. However, in cMyBPC-deficient mice the cMyBPC stripes were significantly suppressed (Luther et al., 2008). The above-mentioned experiments indicated that although cMyBPC is not essential for sarcomere assembly or maintenance, it may play a critical role in thick filament stability or regulation of such processes.

1.3.3 Interactions of cMyBPC

1.3.3.1 Myosin

In vitro binding studies demonstrated that domain C10 in the C-terminal of cMyBPC contains light meromyosin (LMM)-binding sites (Okagaki et al., 1993; Alyonycheva et al., 1997a). Myosin is a hexamer that consists of two heavy chains and two non-identical regulatory and essential light chains (Figure 1.14). Furthermore, myosin has two globular head domains and one long rod domain. The light meromyosin (LMM) domain comprises the larger part of the C-terminal region of the rod domain and directs the assembly of myosin into thick filaments (Sohn et al., 1997). The globular head domains protrude from the thick filaments and are also known as heavy meromyosin (HMM), which is subdivided into sub-fragments S1 and S2. Sub-fragment S2 in the N-terminal region of the rod connects the neck and the head portions of myosin. Additionally, a more recent study demonstrated that the

C-terminal Igl domain of cMyBPC is necessary for the intracellular cross-linking of sarcomeric myosin in transfected non-muscle cells (Welikson and Fischman, 2002).

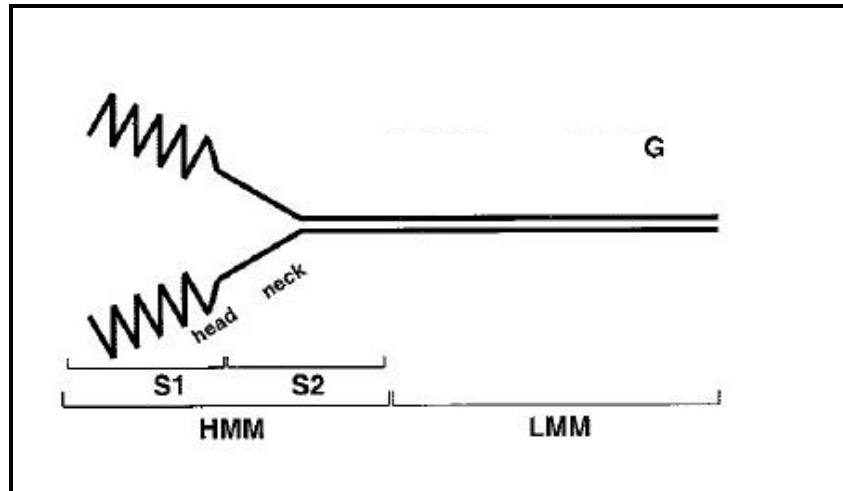


Figure 1.14 Schematic representation of the asymmetric myosin molecule indicating the heavy meromyosin (HMM) and the light meromyosin (LMM) (This image was taken and adapted from McNally, 2002). **Abbreviations:** **S1**, myosin S1 sub-fragment of myosin heavy chain; **S2**, myosin S2 sub-fragment of myosin heavy chain

Furthermore, results from co-sedimentation assays and isothermal titration calorimetry (ITC) demonstrated that the cMyBPC-motif located between cMyBPC domains C1 and C2 interacts with the myosin S2 domain (Gruen et al., 1999). In addition to this, it was observed that this interaction is regulated in an “on-off” fashion by PKA triphosphorylation of the cMyBPC-motif. It was thus proposed that cMyBPC could regulate cardiac contractility through this particular interaction, since cMyBPC phosphorylation would enhance the removal of steric constraints from myosin heads. Triphosphorylation of cMyBPC not only allows myosin heads to extend into a position that is more favourable for binding to actin, but also transforms the tightly packed myosin rod in the thick filament to a more loosely packed myosin rod (Levine et al., 2001; Winegrad, 1999).

In a study by Herron and colleagues, N-terminal fragments of cMyBPC were investigated in skinned cardiomyocyte preparations from rodent and human ventricles to determine their effect on force production and cross-bridge activity. In previous studies, domains C0 and C1C2 were shown not to be involved in either the activation of the cross-bridge cycle (section 1.2.3.1) or the rate of force development (Harris, 2004; Kulikovskaya et al., 2003). However, Herron and co-workers showed that fragment C0C2 and C0C1 induced calcium-independent activation of cross-bridge cycling and force development (Herron, 2006). Thus, from these results, it was suggested that cMyBPC provides a

calcium-independent regulatory pathway, by which activation of the thin filament can be influenced by the thick filament. This interaction was further confirmed with results from nuclear magnetic resonance spectroscopy (NMR) and ITC analyses, which observed a low affinity and high specificity binding of cMyBPC domains C1C2 to myosin (Ababou et al., 2007).

Interestingly, a novel myosin-binding site was identified in the cMyBPC C0 domain. This interaction was proposed based on findings that N-terminal truncated cMyBPC fragments (C0C1, C0C3, C0C4; all containing domain C0C1), after transfection into foetal rat cardiomyocytes, demonstrated A-band localisation in 10% of the mutant-expressing cardiomyocytes (Flavigny et al., 1999).

1.3.3.2 Titin

Cardiac MyBPC not only binds to myosin, but also to another thick filament component, titin (Fürst et al., 1992; Koretz et al., 1993; Labeit et al., 1992; Soteriou et al., 1993). A study by Freiburg and Gautel found that domains C8 to C10 of cMyBPC interact with a part of titin that is restricted to the C-zone of the A band (Freiburg and Gautel, 1996). Titin consists of a series of 11-domain super-repeats, which are made up of Igl-like and FnIII domains (Labeit and Kolmerer, 1995; Labeit et al., 1992), and cMyBPC binds exclusively to the first domain in each repeat (Freiburg and Gautel, 1996). Although cMyBPC is located, similar to titin, in the C-zone, it does not localise to stripes 1 and 2, which suggest that additional factors are required to direct cMyBPC to particular positions within the C-zone. However, in contrast to the interactions with myosin (Moos et al., 1975; Offer et al., 1973; Okagaki et al., 1993), the interaction with titin was found to be fairly weak (Freiburg and Gautel, 1996). Despite these findings, the complex interactions of titin and myosin with the C-terminal of cMyBPC could form a stable structure, which is likely to be instrumental in the arrangement of the sarcomere.

1.3.3.3 Actin

Early studies identified interactions between cMyBPC and actin in both regulated and unregulated filaments (Moos et al., 1978; Yamamoto and Moos, 1983). Since then, several cMyBPC domains have been proven to interact with actin; these are indicated in Table 1.3.

The C0 domain was shown to directly bind to actin (Kulikovskaya et al., 2003). Another study by Shaffer and colleagues identified two additional actin-binding sites in cMyBPC (C1 domain and the region containing the three phosphorylation sites (M-domain)) within the N-terminal region of cMyBPC (Shaffer et al., 2009). However, the interaction of actin with the M-domain of cMyBPC was found to be

reversible and phosphorylation-dependent, while the interaction of actin with domain C1 was unaffected by phosphorylation. The actin-C1-interaction could provide stable coupling of thick and thin filaments, regardless of the MyBPC phosphorylation state. Such coupling could ensure optimal lattice spacing as sarcomere shortening ensues and thereby help to maintain efficient cross-bridge interactions throughout the cardiac cycle. Recently, several other studies focused their attention on the interaction between the cMyBPC M-domain and actin (Howarth et al., 2012; Kensler et al., 2011; Lu et al., 2011; Mun et al., 2011; Orlova et al., 2011), and confirmed that the M-domain binds to both actin and myosin in a phosphorylation dependent manner (Razumova et al., 2006; Shaffer et al., 2009).

In contrast to the above-mentioned studies, a novel interaction was found between actin and domains C6-C10 at the C-terminus of cMyBPC (Rybakova et al., 2011). Furthermore, results from the aforementioned study by Rybakova and colleagues proved that the actin-binding sites in domains C0-C1, C0-C4 and C0-C5, were weak and without saturation (Rybakova et al., 2011). Interestingly, in contrast to the binding of the M-domain with actin (Shaffer et al., 2009), neutron contrast variation data demonstrated that domains C0-C2, containing the M-domain, and actin do not interact; instead, domains C0-C1 were shown to interact with actin. From these contradicting results, the precise actin-binding regions in cMyBPC is not clear and warrants further interaction and verification studies.

Table 1.3 List of cMyBPC domains that interact with cardiac actin.

cMyBPC Domain	Interaction Assay	Reference
C0	Immunoprecipitation	(Kulikovskaya et al., 2003)
C0-C1	In vitro motility, co-sedimentation binding and acto-myosin ATPase assays	(Razumova et al., 2006)
C0-C2	Electron microscopy	(Kensler et al., 2011)
C1, M-domain	Co-sedimentation binding assay	(Shaffer et al., 2009)
C1-C2	In vitro motility, co-sedimentation binding and acto-myosin ATPase assays	(Razumova et al., 2006)
C-C10	Co-sedimentation binding assay	(Rybakova et al., 2011)

1.3.4 The arrangement of cMyBPC in the sarcomere

Currently two models, the rod model (Squire et al., 2003) and the trimeric collar model (Flashman et al., 2004, 2008; Moolman-Smook et al., 2002), describe the arrangement of the C-terminal of cMyBPC in the sarcomere. Despite the contradicting data supporting each model, both models suggest the interaction of cMyBPC with the thick and thin filament systems.

1.3.4.1 The rod model

The rod model proposes that three C-terminal domains of cMyBPC interact along the axis of the thick filament with the N-terminal domains extended perpendicularly towards the thin filament (Squire et al., 2003) (Figure 1.15). The projection in which titin and cMyBPC lie parallel to each other takes into consideration the interaction between domains C8-C10 of cMyBPC with titin (Freiburg and Gautel, 1996). However, this model does not consider the interaction between domains C5-C8 and C7-C10 of cMyBPC, nor the fact that titin might only bind one, or at most two, of the three C-terminal domains of cMyBPC (Flashman et al., 2004). Three-dimensional image analyses of electron micrographs confirmed that three to four domains of cMyBPC form a rod-like structure by C-terminal interaction along the thick filament (Al-Khayat et al., 2009; Zoghbi et al., 2008).

1.3.4.2 The trimeric collar model

The trimeric collar model is based on *in vitro* binding studies that suggested interactions between cMyBPC domains C5 and C8 and additional interactions between domains C7 and C10 (Flashman et al., 2004, 2008; Moolman-Smook et al., 2002) (Figure 1.13). Interactions between three parallel staggered cMyBPC molecules at the C5-C10 domains form a collar-like structure around the core of the thick filament (Flashman et al., 2008) (Figure 1.15), which is thought to be stabilised by interactions between domains C5-C8 and C7-C10.

Findings from yeast two-hybrid (Y2H) and plasma resonance interaction assays suggested that interactions between C5-C8 and C8-C10 are similar to interactions observed in cardiac isoforms, although the binding affinity were found to be much lower between C5-C8 in fast skeletal muscle compared to cardiac muscle. Thus, the findings from the above-mentioned study suggested that a similar trimeric collar arrangement exists in fast skeletal muscle, but that either no collar is present in slow skeletal muscle or other domains could be involved in such an arrangement (Flashman et al., 2008).

Interestingly, both the collar and the rod models propose that the arrangement of the N-terminal domains (C0-C4) extend into the interfilament space, which allows for interaction with the thin filament (Moolman-Smook et al., 2002; Squire et al., 2003). Recent small-angle X-ray scattering data confirmed the predictions of both these models (Moolman-Smook et al., 2002; Squire et al., 2003), since the cMyBPC N-terminus (in its unphosphorylated state) adopted an extended tandem arrangement in a solution that could span interfilament cross-bridge distances (Jeffries et al., 2008).

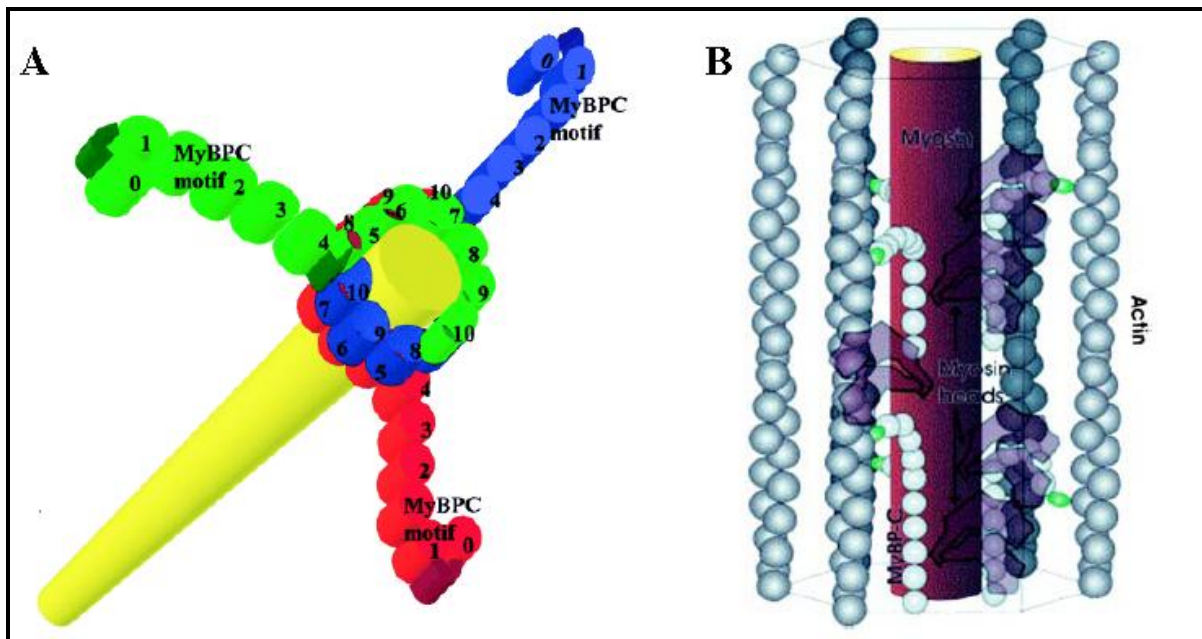


Figure 1.15 Two models predicting the C-terminal arrangement of cMyBPC in the sarcomere, the trimeric collar model (A) as proposed by Moolman-Smook et al., 2002 and the rod model (B) as proposed by Squire et al., 2003 (This image was taken from Flashman et al., 2004).

1.4 Myosin binding protein H

The MyBPH protein, which is the protein of interest in this study, is similar to cMyBPC in terms of structure, sequence and location within the sarcomere. While cardiac MyBPC has been extensively studied, very little is known about the structure, functions and implications of MyBPH in general, and HCM in particular.

1.4.1 MyBPH as a relatively unknown member of the MyBP family

MyBPH is approximately 55kDa in size and is encoded by a single gene (*MyBPH*). *MyBPH* encodes a single isoform that is expressed in both fast skeletal and cardiac muscle cells, including those that differentiate into Purkinje fibres, which are the primary conduction cells of the heart (Alyonycheva et al., 1997a; Vaughan et al., 1993a, 1993b). Interestingly, although Purkinje fibres contain significant amounts of MyBPH, cMyBPC, which is present in all striated muscles, was shown to be absent from Purkinje fibres (Alyonycheva et al., 1997a).

A study by Bennett and colleagues, in which different types of rabbit muscle fibres were labelled with purified anti-MyBPH antibody, found that MyBPH was localised to stripe 3 in the C-zone (counting from the M-line) in the majority of psoas fibres, a muscle containing mainly fast white fibres

(Bennett et al., 1986). Subsequently, a number of independent studies have confirmed its cellular localisation (Bennett et al., 1986; Starr et al., 1985; Yamamoto, 1984).

Structurally, cMyBPC and MyBPH are very similar, as both are multi-domain proteins consisting of Igl and FnIII domains (Figure 1.13, Figure 1.16). In chickens, the unique N-terminal sequence of MyBPH, which contain motifs of alternating alanine and proline residues, have been found to be the cause of the slow mobility of MyBPH upon electrophoresis (Vaughan et al., 1993a, 1993b). The C-terminal shares 50% identity and 17% conserved amino acids with cMyBPC, and consist of four protein modules, FnIII-Igl-FnIII-Igl, which correspond to domains C7-C10 of cMyBPC (Vaughan et al., 1993b).

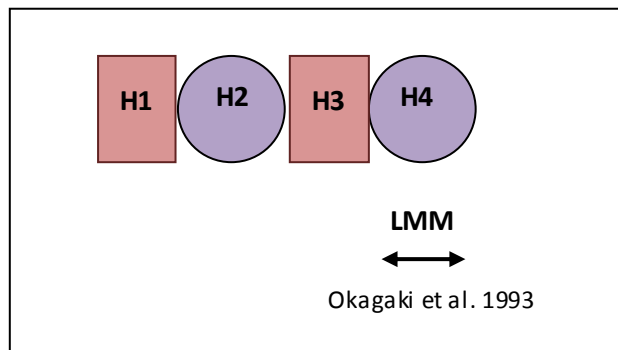


Figure 1.16 Schematic representation of cardiac myosin binding protein H (MyBPH), indicating domains of known function. The purple circles represent immunoglobulin-like domains, the pink squares represent fibronectin type-III domains, the solid blue lines represent linker sequences, the solid black line represent established interactions and the dashed black line represent interactions that require independent verification.

Abbreviations: LMM, light meromyosin

1.4.2 Interactions with MyBPH in the sarcomere

1.4.2.1 Myosin

Past studies demonstrated that the H4 domain in the C-terminal of MyBPH interacts with light meromyosin (LMM)-binding sites within myosin (Alyonycheva et al., 1997b; Okagaki et al., 1993). Similar to domain C10 of cMyBPC (as mentioned in section 1.3.3.1), this Igl domain is necessary for the intracellular cross-linking of sarcomeric myosin in transfected non-muscle cells (Welikson and Fischman, 2002). It seems that even if myosin is saturated by MyBPH, cMyBPC would still be able to bind myosin (Yamamoto, 1984).

As much of the current research has focussed on cMyBPC, very little is known about the binding partners and functions of the molecular mechanisms involving MyBPH.

1.5 The present study

1.5.1 Study hypothesis and aim

In the past much of the focus of our research group has been on identifying cMyBPC-interacting proteins in an effort to better understand the function and incorporation of this protein into the sarcomere and its role in the pathogenesis of HCM (Flashman et al., 2004; Moolman-Smook et al., 2002, 2003). Given the sequence homology and similarity in structure between cMyBPC and MyBPH, and since both proteins are known to bind myosin (Vaughan et al., 1993b; Okagaki et al., 1993), we proposed that MyBPH may also play a crucial role in the cardiac sarcomere and possibly in HCM pathogenesis. However, since the function of this protein remains largely unknown, we considered that identifying novel protein interactors of MyBPH could shed some light on its function. Moreover, we proposed that *MyBPH* and the genes encoding each of the putative interactors of MyBPH could be considered good candidate hypertrophy-modifying genes.

The aims of this study were to contribute to the knowledge of the structure and function of the sarcomeric protein MyBPH by;

- Identifying protein ligands of MyBPH by means of a Y2H analysis
- Verifying interactions between Y2H-identified ligands and MyBPH
- Assessing the structural and functional role these interactions may play within the sarcomere
- Assessing known SNPs in *MyBPH* and genes encoding identified putative interactors of MyBPH for association with hypertrophy in a cohort of HCM founder families, to determine if they modify hypertrophy development

Chapter Two

Materials and Methods

CHAPTER TWO

MATERIALS AND METHODS

TABLE OF CONTENTS

MATERIALS AND METHODS: PROTEIN INTERACTION STUDY	49
2.1 DNA extraction	49
2.1.1 Bacterial plasmid purification using Zyppy™ Plasmid purification kit	49
2.1.2 Bacterial plasmid purification using Qiagen Maxi Plasmid prep kit	49
2.1.3 Yeast plasmid purification	49
2.1.4 DNA purification using the Wizard Mini Plasmid DNA purification kit	50
2.2 Polymerase chain reaction.....	50
2.2.1 Oligonucleotide primer design and synthesis.....	50
2.2.1.1 Primers for generation of inserts for Y2H cloning	51
2.2.1.2 Primers for Y2H insert screening	51
2.2.2 PCR-amplification for the generation of the MyBPH cDNA insert.....	52
2.2.3 Bacterial colony PCR.....	52
2.3 Bradford protein concentration determination	53
2.4 Gel electrophoresis	53
2.4.1 Agarose gel electrophoresis	53
2.4.2 Sodium dodecyl sulphate polyacrylamide gel electrophoresis	54
2.4.3 Transfer of protein from SDS polyacrylamide gels to PVDF membrane	54
2.5 Automated DNA sequencing.....	55
2.6 DNA sequencing analysis	55
2.7 Restriction enzyme digest for cloning.....	55
2.8 Generation of constructs.....	56
2.8.1 Generation of Y2H constructs.....	56
2.8.2 DNA ligation	56

2.9	Bacterial strains, yeast strains and cell lines	56
2.9.1	Bacterial strains.....	56
2.9.2	Yeast strains	57
2.9.3	Cell lines.....	57
2.9.4	Generation of <i>E.coli</i> DH5 α competent cells	57
2.10	Culturing of cell lines	58
2.10.1	Culture of cells from frozen stocks	58
2.10.1.1	Thawing the cells	58
2.10.1.2	Removing the Dimethyl Sulphoxide (DMSO) from stocks and culturing cells.....	58
2.10.1.3	Subculturing cell cultures.....	58
2.10.1.4	Differentiation of cells	59
2.10.2	Cell lysis	59
2.10.2.1	Cell lysis using RIPA buffer	59
2.10.2.2	Cell lysis using Qiagen RNA/DNA/protein extraction kit	60
2.11	Transformations and transfection of plasmids into prokaryotic and eukaryotic cells.....	60
2.11.1	Bacterial plasmid transformation	60
2.11.2	Yeast plasmid transformation	60
2.11.3	Transfection of H9c2 cells for microscopy and siRNA experiments	61
2.12	Assessment of Y2H constructs.....	62
2.12.1	Phenotypic assessment of yeast strains	62
2.12.2	Toxicity tests of transformed cells	62
2.12.3	Testing the mating efficiency	63
2.13	Yeast two-hybrid analysis	63
2.13.1	The cardiac cDNA library	63
2.13.2	Establishment of bait culture.....	64
2.13.3	Library mating	64
2.13.4	Establishing a library titre.....	65

2.13.5	Control matings	66
2.13.6	Detection of activation of nutritional reporter genes	66
2.13.6.1	Selection of transformant yeast colonies	66
2.13.6.2	Selection of diploid yeast colonies containing putative interactor peptides	66
2.13.7	Detection of activation of colourimetric reporter genes via X- α -galactosidase assay	66
2.13.8	Rescuing prey plasmids from diploid colonies	67
2.13.9	Interaction specificity test	67
2.14	Co-immunoprecipitation (Co-IP)	68
2.15	Western blotting	69
2.15.1	Membrane blocking	69
2.15.2	Addition of primary antibody	69
2.15.3	Addition of secondary antibody	70
2.15.4	Chemiluminescent visualisation of membrane proteins	70
2.16	Co-localisation	71
2.16.1	Co-localisation assay	71
2.17	RNA-interference-mediated knockdown	74
2.17.1	siRNA preparation, transfection and optimisation	74
2.17.2	Contractility assay	74
MATERIALS AND METHODS: MODIFIER STUDY		75
2.18	Study participants	75
2.18.1	Clinical evaluation	76
2.19	Blood sample collection and DNA extraction	78
2.20	Bioinformatics	78
2.20.1	Candidate gene selection	78
2.20.2	SNP selection	79
2.21	SNP genotyping by KBioscience	81
2.21.1	Sample preparation	81

2.21.2 Allelic discrimination.....	81
2.22 Statistical analysis.....	81
2.22.1 Descriptive statistics.....	81
2.22.2 Linkage disequilibrium (LD) determination.....	82
2.22.3 Principal component score.....	83
2.22.4 Confounding variables.....	83
2.22.5 Heritability.....	84
2.22.6 Single nucleotide polymorphism association.....	84
2.22.7 Effect sizes.....	85
2.22.8 Haplotype assignment and association analysis.....	85

MATERIALS AND METHODS: PROTEIN INTERACTION STUDY

2.1 DNA extraction

2.1.1 Bacterial plasmid purification using Zyppy™ Plasmid purification kit

Escherichia coli (*E.coli*) colonies containing the plasmid of interest were picked from Luria-Bertani (LB) agar plates (Appendix I) containing the appropriate antibiotics, and inoculated in 10ml of LB media (Appendix I), in a 50ml polypropylene tube (Greiner Bio-One, Frickenhausen, Germany). The culture was subsequently incubated at 37°C, shaking at 250rpm overnight in a YIH DER model LM-530 shaking incubator (SCILAB Instrument Co. Ltd., Taipei, Taiwan). The following morning, the culture was centrifuged for 10 minutes at 3000rpm in an Eppendorf model 5810/5810R centrifuge (Eppendorf, Hauppauge, New York, USA) after which the supernatant was discarded. The plasmid DNA was subsequently extracted using the Zyppy™ Plasmid Miniprep kit (Zymo Research Corporation, California, USA) as per manufacturer's instructions. Afterward, purified plasmid was quantified using a Nanodrop Spectrophotometer (Thermo Fisher Scientific Inc., Massachusetts, USA).

2.1.2 Bacterial plasmid purification using Qiagen Maxi Plasmid prep kit

In order to isolate endotoxin free LC3b-II_GFP DNA plasmids for transfection into H9c2 cells, the Qiagen Maxi Plasmid prep kit (Qiagen, Hilden, Germany) was used. A 10ml LB culture containing 100µl of the bacterial glycerol stock of LC3b-II_GFP, (containing the appropriate antibiotics) was incubated at 37°C, shaking at 250rpm overnight in a YIH DER model LM-530 shaking incubator (SCILAB Instrument Co. Ltd., Taipei, Taiwan). Following incubation, 100µl from the start-up culture was used to inoculate 200ml LB media (Appendix I) (containing the appropriate antibiotics). This 200µl culture was subsequently incubated at 37°C, shaking overnight at 250rpm in a YIH DER model LM-530 shaking incubator (SCILAB Instrument Co. Ltd., Taipei, Taiwan). Following this, the culture was centrifuged for 10 minutes at 3000rpm in an Eppendorf model 5810/5810R centrifuge (Eppendorf, Hauppauge, New York, USA) after which the supernatant was discarded and the plasmid DNA extracted using the Qiagen Maxi Plasmid Prep kit (Qiagen, Hilden, Germany), according to the manufacturer's instructions. The DNA was resuspended in 100µl ddH₂O and the plasmid DNA was quantified using a Nanodrop Spectrophotometer (Thermo Fisher Scientific Inc., Massachusetts, USA).

2.1.3 Yeast plasmid purification

A *Saccharomyce cerviseae* (*S. cerviseae*) GOLD strain (Clontech Laboratories, Inc., Palo Alto, California, USA) colony containing a plasmid of interest was inoculated in 1ml synthetic dropout

media (SD) containing the appropriate dropout supplement (Clontech Laboratories, Inc., Palo Alto, California, USA) (Appendix I). The culture was incubated overnight at 30°C, shaking at 200rpm in a YIH DER model LM-530 shaking incubator (SCILAB Instrument Co. Ltd., Taipei, Taiwan). Following this, 4ml of 1X YPDA (Appendix I) was added to the culture. This culture was further incubated at 30°C for 4 hours, shaking at 200rpm in a YIH DER model LM-530 shaking incubator (SCILAB Instrument Co. Ltd., Taipei, Taiwan). The cells were subsequently centrifuged at 3000rpm for 5 minutes in a Labnet Prism™ microcentrifuge (Labnet International Inc., New Jersey, USA) and the supernatant was discarded. The pellet was resuspended in the remaining supernatant and transferred to a 2ml microcentrifuge tube. The following was added in quick succession to the pellet: 200µl yeast lysis buffer (Appendix I), 200µl phenol-chloroform-isoamyl alcohol (PCI) (Sigma Aldrich Inc., St Louis, USA) and 0.3µg sterile 450-600µm glass beads (Sigma-Aldrich Inc., St Louis, USA). This mixture was mixed by vortexing for approximately 3 minutes using a Whirlimixer vortex (Fisher Scientific UK Ltd., Loughborough, UK). To obtain phase separation, the samples were centrifuged at 14 000rpm for 10 minutes at room temperature in a Labnet Prism™ microcentrifuge (Labnet International Inc., New Jersey, USA). A volume of 500µl of the aqueous phase was transferred to a Wizard PCR purification column (Wizard Purefection Mini Plasmid DNA purification kit, Promega Corp., Madison Wisconsin, USA) for DNA purification (section 2.1.4). The DNA was eluted in 35µl of ddH₂O and used to transform bacterial *E.coli* DH5α cells (section 2.11.1).

2.1.4 DNA purification using the Wizard Mini Plasmid DNA purification kit

Yeast Plasmid DNA preparations (section 2.1.3) and PCR amplified DNA products (section 2.2) were purified using the Wizard Mini Plasmid DNA purification kit (Wizard Purefection Mini Plasmid DNA purification kit, Promega Corp., Madison Wisconsin, USA) according to manufacturer's instructions. The purified products were subsequently sequenced (section 2.5) and used for cloning reactions (section 2.8.2).

2.2 Polymerase chain reaction

2.2.1 Oligonucleotide primer design and synthesis

All gene reference sequences for which primers were to be designed, were obtained from the National Centre for Biotechnology Information (NCBI) Entrez Nucleotides Database (<http://www.ncbi.nlm.nih.gov/nucleotide/>). All primers were designed using Integrated DNA Technologies Software, Primer Quest (<http://www.idtdna.com>). The NCBI Basic Local Alignment Search Tool (BLAST) (<http://www.ncbi.nlm.nih.gov/BLAST/>) was used to examine primer specificity.

Oligonucleotide primers were synthesised according to standard phosphorimidite methodology at the Department of Molecular and Cellular Biology, University of Cape Town (UCT), Cape Town, South Africa.

2.2.1.1 Primers for generation of inserts for Y2H cloning

A pair of oligonucleotide primers were designed to amplify the MyBPH cDNA sequence for cloning into the Y2H pGBKT7 bait vector (Clontech Laboratories, Inc., Palo Alto, California, USA) (Appendix III), containing the appropriate restriction enzyme (*NdeI* and *EcoRI*) sites, as well as a six nucleotide “overhang” tag to facilitate restriction digestion. Primer sequences of the primers used to generate the desired polymerase chain reaction (PCR) fragment for cloning are presented in Table 2.1.

Table 2.1 Oligonucleotide primers used for the generation of inserts for Y2H cloning.

Primer Name	*Primer Sequence (5'-3')	T _a (°C)	T _m (°C)
MyBPH_Forward	ACTGCAGAA CATATG ATGATGGAAAAAACACCTCCGAG	51	55
MyBPH_Rreverse	ACTGCAGAA GAATTC TCAGTGTGCGGCTGAGGC	51	55

Abbreviations: **A**, adenine; **C**, cytosine; **°C**, degrees Celsius; **G**, guanine; **MyBPH**, myosin binding protein H; **T**, thymine; **T_a**, annealing temperature; **T_m**, melting temperature

*The nucleotide sequence in black font represents the sequence of the primer that anneals to the DNA in the PCR reaction. An “overhang” tag to facilitate restriction enzyme digestion is represented in blue font, while the sequence in bold red and orange font represents the *NdeI* and *EcoRI* restriction enzyme sites, respectively.

2.2.1.2 Primers for Y2H insert screening

Primers flanking the multiple cloning sites (MCS) of pGBKT7 (Clontech Laboratories, Inc., Palo Alto, California, USA) (Appendix III) and pGADT7-Rec (Clontech Laboratories, Inc., Palo Alto, California, USA) (Appendix III) Y2H vectors were designed to amplify inserts cloned into the the Y2H cloning vectors. In order to design these primers, sequences from the Clontech™ Matchmaker™ vector handbook (www.clontech.com) were used. The sequences of these primers are presented in Table 2.2.

Table 2.2 Oligonucleotide primers used for the amplification of inserts from cloning vectors.

Primer Name	Primer Sequence (5'-3')	T _a (°C)	T _m (°C)
pGBKT7_Forward	TCATCGGAAGAGAGTAG	45	50
pGBKT7_Reverse	TCACTTTAAAATTTGTATACA	45	50
pGADT7_Forward	CGATGATGAAGATACCCCAA	56	50
pGADT7_Reverse	CACGATGCACAGTTGAAGTGA	56	50

Abbreviations: **A**, adenine; **C**, cytosine; **°C**, degrees Celsius; **G**, guanine; **MyBPH**, myosin binding protein H; **T**, thymine; **T_a**, annealing temperature; **T_m**, melting temperature

2.2.2 PCR-amplification for the generation of the MyBPH cDNA insert

The following PCR conditions were used to amplify the MyBPH cDNA sequence from genomic DNA. The MyBPH fragment was subsequently cloned into the pGBKT7 Y2H cloning vector (section 2.8.2).

For amplification of the MyBPH cDNA, the PCR was performed in a reaction mixture consisting of 100ng genomic DNA, 1X Bioline High Fidelity Velocity Buffer (Bioline UK Ltd., London, UK), 1.5mM MgCl₂ (Bioline UK Ltd., London, UK), 200µM dNTPs (dATP, dCTP, dGTP, dTTP), 1.0U of Velocity Taq Polymerase enzyme (Bioline UK Ltd., London, UK), 0.2µM of each forward and reverse primers (Table 2.1) and ddH₂O to a final volume of 50µl. PCR amplifications were performed using the GeneAmp® PCR System 2700 (Perkin-Elmer, Applied Biosystems Inc., Foster City, California, USA). The standard PCR cycle consisted of initial denaturation at 95°C for 3 minutes, followed by 35 cycles of denaturation at 95°C for 30 seconds, annealing at the T_a (Table 2.1) for 30 seconds, elongation at 72°C for 30 seconds, and a final elongation step at 72°C for 5 minutes. The amplified products were verified by electrophoresis on a 1% (w/v) agarose gel (Appendix I).

2.2.3 Bacterial colony PCR

In order to identify bacterial colonies containing the recombinant plasmid with the desired insert, a bacterial colony PCR was performed. The PCR amplification performed is similar to that described in section 2.2.2, but using primers for the amplification of inserts from Y2H cloning vectors (Table 2.2) instead. Furthermore, instead of using 100ng genomic DNA, a minute amount of an individual *E. coli* colony from an agar plate containing the antibiotic Ampicilin (F. Hoffmann-La Roche Ltd., Basel, Switzerland), was used as template DNA.

PCR amplifications were performed using the GeneAmp® PCR System 2700 (Perkin-Elmer, Applied Biosystems Inc., Foster City, California, USA). The PCR cycle consisted of initial denaturation at 95°C for 3 minutes, followed by 35 cycles of denaturation at 95°C for 30 seconds, annealing at the T_a for the specific PCR primers sets (Table 2.2) for 30 seconds, elongation at 72°C for 30 seconds, and a final elongation step at 72°C for 5 minutes. Electrophoresis on a 1% (w/v) agarose gel (Appendix I) verified the amplified products.

2.3 Bradford protein concentration determination

For co-immunoprecipitation (Co-IP) and western blot analysis protein concentrations of the cell lysates (section 2.10.2) were determined by means of a Bradford assay. For calculation of the standard curve, 10µl of a bovine serum albumin protein dilution series (0-1000µg/µl) were used as protein standards. Then 200µl Bradford reagent (Sigma-Aldrich Inc., St Louis, USA) was added to each of the protein standards and the 1µl lysate sample, in duplicate. The reaction was performed in a 96-well microtitre and the absorbance for each sample was measured at 595 nanometers (A_{595}), using a luminometer (BioTek Instruments Inc., Vermont, USA). The A_{595} was used to calculate the concentration of the protein samples.

2.4 Gel electrophoresis

2.4.1 Agarose gel electrophoresis

PCR-amplified fragments and plasmid preparations were visualised using agarose gel electrophoresis. DNA fragments were also excised from agarose gel electrophoresis for purification. Approximately 10µl of the PCR products or 10µl plasmid preparations were mixed with 3µl cressol loading dye (Appendix I), before loading the total 13µl into separate wells of a 1% (w/v) agarose gel (Appendix I). All agarose gels contained 1µg/ml ethidium bromide (Sigma Aldrich Inc., St Louis, USA) and 1X sodium borate (SB) buffer (Appendix I). To verify the size of the PCR fragments and plasmid preparations, 5µl Kapa Universal Ladder (Kapa Biosystems, Woburn, Massachusetts, USA) was electrophoresed concurrently. The products were resolved at 140V, for 10 to 15 minutes in 1X SB running buffer (Appendix I). The gels were examined under UV light and photographed with the Multigenius Bio Imaging System (Syngene, Cambridge, UK).

2.4.2 Sodium dodecyl sulphate polyacrylamide gel electrophoresis

Protein products derived from Co-IP reactions (section 2.14) were subjected to sodium dodecyl sulphate gel electrophoresis (SDS-PAGE). Prior to SDS-PAGE in Mini-Protean TGX 4-15% resolving precast gels (Bio-Rad, Hercules, CA, USA), 50µg protein was mixed with a 1X SDS loading buffer, containing pre-mixed SDS Laemlli Sample buffer (Bio-Rad, Hercules, CA, USA) and 5% freshly added β-mercaptoethanol (Merck, Darmstadt, Germany). Protein samples were subsequently incubated in a Techne Dri-block DB-3A heating block (Techne Ltd., Duxford, Cambridge, UK) at 95°C for 5 minutes, before loading it onto the gels. Electrophoresis followed at 150V for 1 hour in 1X SDS running buffer (Appendix I). The protein samples in the gel were subsequently transferred to a polyvinylidene fluoride (PVDF) membrane for visualisation by western blotting (section 2.15).

2.4.3 Transfer of protein from SDS polyacrylamide gels to PVDF membrane

Western blotting was performed to visualise the protein bands of the Co-IP experiments. To facilitate this, the proteins separated on the SDS-PAGE gels were transferred to a PVDF membrane. The SDS-PAGE gels were rinsed in TBST buffer (Appendix I) prior to placing the gel on the PVDF membrane, which is attached to the bottom stack of the IBLOT transfer pack, as provided by the manufacturer (Life Technologies, Invitrogen™, Carlsbad, California, USA). Subsequently, the transfer stack was assembled and the proteins transferred to the membrane using the iBLOT (Life Technologies, Invitrogen™, Carlsbad, California, USA) transfer system at different transfer voltages and durations for different proteins (Table 2.3), according to the manufacturer's instructions.

Table 2.3 Transfer conditions of the IBlot system for the different proteins.

Protein Name	Transfer Programme	Duration (min)	Voltage (V)
MyBPH	P3	8	20
cMyBPC	P3	5	20
MYH7	P3	9	20
ACTC1	P3	9	20
UBC9	P6	9	7.5

Abbreviations: **ACTC1**, cardiac α-actin; **cMyBPC**, cardiac myosin binding protein C, **MyBPH**, myosin binding protein H; **MYH7**, cardiac β-myosin heavy chain; **UBC9**, SUMO-conjugating enzyme UBC9

2.5 Automated DNA sequencing

Cloned inserts were bi-directionally sequenced using the BigDye® Terminator v3.1 Cycle Sequencing kit (Perkin-Elmer, Applied Biosystems Inc., Foster City, California, USA), followed by electrophoresis on an ABI 3130XL Genetic Analyzer (Perkin-Elmer, Applied Biosystems Inc., Foster City, California, USA). All automated DNA sequencing reactions were performed at the Core Sequencing Facility of the Department of Genetics at Stellenbosch University, Stellenbosch, South Africa.

2.6 DNA sequencing analysis

Sequences were analysed using BioEdit Sequence Alignment Editor Software v7.0.9.0 (Hall, 1999) to verify the sequence integrity of the MyBPH fragment generated by PCR-amplification, as well as to identify each of the putative MyBPH-interacting prey clones identified by Y2H analysis. The reference sequence (accession number: NP_004988.2, NM_004997.2) in NCBI (<http://www.ncbi.nlm.nih.gov/nucleotide/>, 2010) was aligned to the sequenced MyBPH cDNA (section 2.2.2), used in the present study. The ClustalW v1.4 programme was used to align and analyse the sequence of interest for mismatches to the reference sequence. BLAST (www.ncbi.nlm.nih.gov/BLAST) was used to compare the nucleotide sequences of bait and prey inserts to the appropriate cDNA and mRNA sequences obtained from the Genbank database (www.ncbi.nlm.nih.gov/Entrez) and the Ensemble database (www.ensembl.org). These prey insert sequences were also translated using the BioEdit Sequence Alignment Editor Software v7.0.9.0 (Hall, 1999) in the frame dictated by the GAL4 DNA activating domain reading frame (reading frame 1). The deduced protein sequences were compared to the protein sequences in the NCBI database (<http://blast.ncbi.nlm.nih.gov/protein/>) using BLAST in order to confirm that the prey insert sequences encode for in-frame proteins.

2.7 Restriction enzyme digest for cloning

For cloning of the MyBPH cDNA into the pGBKT7 bait vector, the PCR-generated MyBPH cDNA fragment (section 2.2.2), as well as the Y2H bait vector pGBKT7, were double-digested with *Nde*I and *Eco*RI restriction enzymes (Table 2.1). Digestion reactions consisted of 10µl of the PCR product or 20µl of plasmid vector DNA (100ng/µl), 1X NEBuffer 2, 5U of the *Eco*RI restriction enzyme (New England Biolabs, Ltd., Massachusetts, USA) and ddH₂O to a final volume of 20µl. Samples were then incubated at 37°C for 3 hours in a Techne Dri-block DB-3A heating block (Techne Ltd., Duxford, Cambridge, UK). Following this, the digestion reactions were purified using the Wizard Purefection Mini Plasmid DNA purification kit (Wizard Purefection Mini Plasmid DNA purification kit, Promega

Corp., Madison Wisconsin, USA), as discussed in section 2.1.4. The samples were eluted using 35µl ddH₂O before using it for the second restriction enzyme digest. The second digestion mix contained 35µl purified digestion product, 1X NEBuffer 3, 5U of the *Nde*I restriction enzyme (New England Biolabs Inc., Massachusetts, USA) and ddH₂O to a final volume of 50µl. The samples were again incubated at 37°C for 3 hours in a Techne Dri-block DB-3A heating block (Techne Ltd., Duxford, Cambridge, UK). Following the 3-hour incubation, the samples were again purified using the Wizard Purefection Mini Plasmid DNA purification kit (Promega Corp., Madison Wisconsin, USA).

2.8 Generation of constructs

2.8.1 Generation of Y2H constructs

The MyBPH bait insert was cloned into the pGBKT7 bait vector (Appendix III) and was subjected to automated DNA sequencing to verify sequence integrity and confirm the conservation of the GAL4 DNA binding domain reading frame, before transforming it into the GOLD yeast strain. This construct (pGBKT7-MYBPH:GOLD) was used to screen a CLONTECH MATCHMAKER™ pre-transformed cardiac cDNA library, comprised of cardiac cDNAs cloned into the pGADT7 prey-vector (Appendix III) and transformed into the Y187 yeast strain.

2.8.2 DNA ligation

The double-digested PCR fragment and plasmid vector (section 2.7) were added in a ratio of 5:1 to a mixture containing 5µl T4 DNA ligase buffer (Promega, Madison Wisconsin, USA), 5U T4 DNA ligase (Promega, Madison Wisconsin, USA) and ddH₂O to a final volume of 15µl. This DNA ligation mixture was incubated at room temperature for 16 hours, before 5µl of the sample was transformed into an *E.coli* DH5α bacterial strain (section 2.11.1). Bacterial colonies containing successful ligation reactions were identified by bacterial colony PCR (section 2.2.3).

2.9 Bacterial strains, yeast strains and cell lines

2.9.1 Bacterial strains

In order to facilitate the selection and purification of Y2H cloned constructs, the ligation reactions described in section 2.8.2 were transformed into the *E.coli* DH5α bacterial strain. Transformed bacterial colonies were selected based on their ability to grow on LB agar plates (Appendix I) containing appropriate antibiotics (when selecting for the pGBKT7 vector, kanamycin was used as

selection antibiotic, ampicilin was used to select for the pGADT7 vector). Colonies containing recombinant plasmids were identified by colony PCR (section 2.2.3).

2.9.2 Yeast strains

The recombinant bait plasmid pGBKT7-MyBPH was transformed in the *S.cerevisiae* GOLD strain (Clontech Laboratories, Inc., Palo Alto, California, USA). The cardiac cDNA library (Clontech Laboratories, Inc., Palo Alto, California, USA) was cloned into the pGADT7 prey vector and pre-transformed into the Y187 yeast strain (Clontech Laboratories, Inc., Palo Alto, California, USA) by the manufacturer.

2.9.3 Cell lines

The *Rattus Norvegicus* (rat) cardiac (atrial) myocyte H9c2 cell line, purchased from the American Type Culture Collection (ATCC, Manassas, Virginia, USA), was used for all co-localisation, Co-IP and functional assays.

2.9.4 Generation of *E.coli* DH5 α competent cells

A frozen *E.coli* DH5 α stock was removed from the -80°C and thawed on ice for 20 minutes. A volume of 10ml LB media (Appendix I) was inoculated with 200 μ l of thawed *E.coli* DH5 α stock and incubated at 37°C overnight in a YIH DER model LM-530 shaking incubator (SCILAB Instrument Co. Ltd., Taipei, Taiwan) at 200rpm. The following day, 200 μ l of this overnight culture was inoculated in 200ml LB media (Appendix I) in a sterile 2L Erlenmeyer flask. Consequently, the culture was incubated overnight at room temperature on a STUART orbital shaker model SSL1 shaking at 200rpm (Barloworld Scientific Ltd., Staffordshire, UK). In order to determine whether the cells are in the log growth phase ($OD_{600nm} = 0.6$), the OD_{600nm} were measured the following morning.

The growth culture was pelleted by transferring the culture to four 50ml polypropylene centrifuge tubes (Greiner Bio-One, Frickenhausen, Germany) and centrifuging in an Eppendorf model 5810/5810R centrifuge (Eppendorf, Hauppauge, New York, USA) at 3000rpm for 10 minutes. Subsequently, the supernatant was discarded and the pellet resuspended in 8ml ice-cold CAP buffer (Appendix I). The cells were pelleted using an Eppendorf model 5810/5810R centrifuge (Eppendorf, Hauppauge, New York, USA) at 3000rpm for 10 minutes, before discarding the supernatant. The pellet was resuspended in 4ml ice-cold CAP buffer and kept on ice. The cells in suspension were then

transferred to 1.5ml microcentrifuge tubes (Eppendorf, Happaug, New York, USA) in 200µl aliquots and stored overnight at 4°C before storing them at -80°C until needed.

2.10 Culturing of cell lines

2.10.1 Culture of cells from frozen stocks

2.10.1.1 Thawing the cells

Frozen H9c2 cells were thawed by immersing the vial containing the cells in a waterbath at 37°C for 3 minutes. The vial was then immediately sterilised with 70% ethanol and placed in the Esco Airstream® Class II Biohazard Safety cabinet (Esco Technologies Inc., Missouri, USA) for further use.

2.10.1.2 Removing the Dimethyl Sulphoxide (DMSO) from stocks and culturing cells

Frozen stocks of cells contain DMSO. It was therefore necessary to remove the DMSO to improve the cell viability upon plating. One millilitre of thawed cells were transferred into a 14ml tube (Greiner Bio-One, Frickenhausen, Germany) containing 4ml pre-heated (37°C) complete growth media (Appendix I). The cells were gently mixed before centrifugation at 5000rpm for 1 minute in a Labnet Prism™ microcentrifuge (Labnet International Inc., New Jersey, USA). The supernatant was discarded and the cells were gently resuspended in 2ml complete growth media (Appendix I), before transferring the cells to two 25cm² flasks (Corning Inc., New York, USA) containing 5ml complete growth media (Appendix I) each. The cells were distributed by gently swirling the flasks before incubation at 37°C in a Thermo Scientific Forma Steri-Cycle 5% carbon dioxide humidified incubator (Thermo Fisher Scientific Inc., Massachusetts, USA).

2.10.1.3 Subculturing cell cultures

The H9c2 cell cultures were passaged every 2 to 4 days, at 70-80% confluency. The growth media was removed from the flask and residual media removed by washing cells with 2ml Trypsin-Versene (Lonza Group Ltd., Basel, Switzerland), before adding 4ml Trypsin-Versene (Lonza Group Ltd., Basel, Switzerland) for 5 minutes at room temperature to loosen cells from the growth surface. To deactivate the trypsin enzyme activity, 5ml complete growth media (Appendix I) was added. The cells were transferred to a 14ml tube (Greiner Bio-One, Frickenhausen, Germany), which was centrifuged for 1 minute at 300rpm to pellet cells, in a Sorvall® general laboratory centrifuge model GLC-4 (Thermo Fisher Scientific Inc., Massachusetts, USA). The supernatant was discarded and the pellet

resuspended in 3ml complete growth media (Appendix I), before the cells were evenly distributed into 75cm² flasks (Corning Inc., New York, USA) containing 25ml complete growth media (Appendix I).

2.10.1.4 Differentiation of cells

Cells used in all analyses were differentiated between 5 and 10 days to form elongated myotubes containing multiple nuclei. Cells were grown and passaged in complete growth media (section 2.10.1.3). Twenty four hours after seeding the cells for various analyses, the complete growth media was replaced with differentiation media (Appendix I), to allow for differentiation of cardiomyoblasts to myotubes.

2.10.2 Cell lysis

2.10.2.1 Cell lysis using RIPA buffer

The H9c2 cell lysates used in subsequent Co-IP and western blot analyses (section 2.14 and 2.15) were prepared as follows: cells were trypsinised (section 2.10.1.3) from the growth surface of the flask, 5ml of complete growth media (Appendix I) was added and the cells were transferred to a 50ml polypropylene tube (Greiner Bio-One, Frickenhausen, Germany), prior to centrifugation in an Eppendorf model 5810/5810R centrifuge (Eppendorf, Hauppauge, New York, USA) for 3 minutes at 5000rpm. The supernatant was discarded and the pellet resuspended in 300µl phosphate buffered saline (PBS) (Appendix I) before transferring it to a 1.5ml microcentrifuge tube. The cells were subsequently centrifuged in a Labnet Prism™ microcentrifuge (Labnet International Inc., New Jersey, USA) for 3 minutes at 5000rpm, after which the supernatant was discarded. The pellet was resuspended in 250-500µl passive cell lysis buffer (Appendix I), depending on the pellet size and left on ice for 30 minutes. A small amount of ZR0B05 Ceria Zirconium Oxide Silicate beads (3.8g/cc, 0.5mm) (Next Advance, Inc., New York, USA) was added to the cell mixture on ice, before the cells were subjected to the Bullet Blender® (Gentaur, UK). The blending series consisted of 1 minute blending, 1 minute rest for three cycles at 4°C. The cell mixture was centrifuged in a Labnet Prism™ microcentrifuge (Labnet International Inc., New Jersey, USA) at room temperature, for 5 minutes at 5000rpm. The supernatant was transferred to a clean microcentrifuge tube and stored at -80°C until further use.

2.10.2.2 Cell lysis using Qiagen RNA/DNA/protein extraction kit

For extracting RNA, DNA and proteins using the Qiagen RNA/DNA/Protein extraction kit (Qiagen, Hilden, Germany), H9c2 cells were grown in six well plates (Greiner Bio-One, Frickenhausen, Germany). Cell lysates were used for purification of messenger ribonucleic acid (mRNA) for realtime PCR (RT-PCR) and extraction of proteins for immunoprecipitation and western blotting. The cells were loosened from the growth surface using the RTL PLUS buffer and cell scrapers as recommended in the manufacturer's protocol. The cell lysates necessary for these assays were obtained following the protocol as recommended by the manufacturer (Qiagen, Hilden, Germany).

2.11 Transformations and transfection of plasmids into prokaryotic and eukaryotic cells

2.11.1 Bacterial plasmid transformation

A 200µl aliquot of competent *E.coli* DH5α cells (section 2.9.4) was removed from a -80°C freezer and thawed on ice for 20 minutes. A volume of 1µl plasmid preparation (section 2.1.4) or 3-5µl of the ligation reaction (section 2.8.3) was subsequently added to the competent *E.coli* DH5α cells. Following 20 minutes incubation on ice, the cells were transformed by incubating the reaction at 42°C for 45 seconds in a Techne Dri-block DB-3A heating block (Techne Ltd., Duxford, Cambridge, UK). The samples were left standing at room temperature for 2 minutes before adding 1ml LB media (Appendix I), after which samples were incubated for 1 hour at 37°C, in a 200rpm YIH DER model LM-530 shaking incubator (SCILAB Instrument Co. Ltd., Taipei, Taiwan). The samples were centrifuged for 1 minute at 14 000rpm using a Labnet Prism™ microcentrifuge (Labnet International Inc., New Jersey, USA) and the supernatants were discarded before the pellets were resuspended in 200µl LB media (Appendix I). These samples were plated out onto agar plates (Appendix I) containing the appropriate antibiotics before incubating the plates in an inverted position at 37°C in a model 329 stationary CO₂ incubator (Former Scientific, Marieta, Ohio, USA) for 16 hours.

2.11.2 Yeast plasmid transformation

A volume of 100µl of the yeast strain to be transformed was inoculated from a glycerol stock into 5ml YPDA media (Appendix I) in a 15ml polypropylene tube (Greiner Bio-One, Frickenhausen, Germany). This culture was subsequently incubated overnight at 30°C in a YIH DER model LM-530 shaking incubator (SCILAB Instrument Co. Ltd., Taipei, Taiwan) (200rpm). The following day these cultures were plated onto YPDA agar plates (Appendix I) and incubated at 30°C for 2 to 3 days in a Sanyo MIR262 stationary ventilated incubator (SANYO Electronic Co., Ltd., Ora-Gun, Japan). A volume representing 20-50µl yeast cells were picked from the plates and resuspended in 1ml ddH₂O in a

sterile 2ml microcentrifuge tube (Eppendorf, Hauppauge, New York, USA), before the cells were pelleted by centrifugation at 13 000rpm for 30 seconds in a Labnet Prism™ microcentrifuge (Labnet International Inc., New Jersey, USA). The supernatant was discarded and the pellet resuspended in 1ml 100mM lithium acetate (LiAc) (Appendix I), prior to incubation for 5 minutes at 30°C in a Sanyo MIR262 stationary ventilated incubator (SANYO Electronic Co., Ltd., Ora-Gun, Japan). The cells were then centrifuged at 13 000rpm for 30 seconds to form a pellet. The supernatant was removed after which the following were added, in this order, in quick succession: 240µl of 50% polyethylene glycol (PEG) (Appendix I), 36µl of 1M LiAc (Appendix I), 25µl of 2mg/ml heat denatured and snap-cooled sonicated herring sperm DNA (Promega, Madison Wisconsin, USA), 10-20µl plasmid preparation and ddH₂O to a final volume of 350µl. The samples were then vigorously vortexed using a Whirlimixer vortex (Fisher Scientific UK Ltd., Loughborough, UK) for at least 1 minute, before incubation at 42°C for 20 to 30 minutes in a waterbath. Following incubation, the cells were centrifuged at 13 000rpm for 30 seconds to pellet the cells and the supernatant was discarded before resuspending the pellet in 250µl ddH₂O. These samples were then plated onto the appropriate selection plates and incubated in an inverted position at 30°C for 2 to 4 days in a Sanyo MIR262 stationary ventilated incubator (SANYO Electronic Co., Ltd., Ora-Gun, Japan).

2.11.3 Transfection of H9c2 cells for microscopy and siRNA experiments

To determine if MyBPH plays a role in autophagy, the LC3b-II_GFP construct (kind gift from Dr Ben Loos) was transfected into H9c2 cells in the following manner: approximately 8000 cells per well were seeded (Appendix II) in complete growth media (Appendix I), in 8-well borosilicate glass-bottomed chambers (Nunc, New York, USA). The cells were then incubated at 37°C in a Thermo Scientific Forma Steri-Cycle 5% carbon dioxide humidified incubator (Thermo Fisher Scientific Inc., Massachusetts, USA). At 70-80% confluency, the cells were transfected. For the transfection, 12µl Lipofectamine transfection reagent (Life Technologies, Invitrogen™, Carlsbad, California, USA) was added to 200µl serum free media (Appendix I) and 800ng LC3b-II_GFP plasmid DNA per well was added to 200µl serum free media (Appendix I) in a separate 1.5ml microcentrifuge tube (Eppendorf, Hauppauge, New York, USA). Before incubation at room temperature for 5 minutes, gentle pipetting mixed each solution. The solutions were then combined and mixed in a single 1.5ml microcentrifuge tube (Eppendorf, Hauppauge, New York, USA) before incubating at room temperature for 20 minutes. Afterwards 100µl of the transfection/DNA/media mixture was added drop-wise to the cells in the wells. Twenty four hours after the H9c2 cells were seeded and transfected, the cells were differentiated to cardiac myotubes as described in section 2.10.1.4 and incubated at 37°C in a Thermo Scientific

Forma Steri-Cycle 5% carbon dioxide humidified incubator (Thermo Fisher Scientific Inc., Massachusetts, USA) for 5 days.

Optimal knockdown conditions such as siRNA concentration and time point of transfection, for RNA/protein extractions, were optimised by transfecting H9c2 cells with siRNA constructs (Qiagen, Hilden, Germany). To establish optimised knockdown conditions, the following procedure was followed: 45 000 cells were seeded in six well plates (Appendix II) (Greiner Bio-One, Frickenhausen, Germany), of which one plate was transfected before the cells were differentiated (section 2.10.1.4) and the other plate was differentiated for 5 days before transfection. Once the ideal time-point for transfection was optimised at transfection post differentiation, the siRNA concentration was determined by transfecting H9c2 cells with an Alexa Fluor 488-labelled non-silencing control (*NSC*) (Qiagen, Hilden, Germany) at different concentrations, as recommended by the manufacturer's protocol (5nM, 10nM).

2.12 Assessment of Y2H constructs

2.12.1 Phenotypic assessment of yeast strains

The phenotype of each of the yeast strains used in the Y2H analysis was assessed before transformation of the MyBPH:pGBKT7 bait plasmid and the respective prey plasmids into the GOLD and Y187 strain. Both strains were plated onto different agar plates containing specific selection media (SD-Ade, SD-Trp, SD-His, SD-Leu, SD-Ura) (Appendix I) and the non-transformed yeast cells that were able to grow on SD-Ura and were unable to grow on SD-Ade, SD-Trp, SD-His, SD-Leu were used for transformation and subsequent Y2H analysis.

2.12.2 Toxicity tests of transformed cells

In order to determine whether the pGBKT7-MyBPH bait construct (section 2.8.1) is toxic when expressed in the GOLD yeast strain (section 2.9.2), a growth curve of the GOLD yeast strain transformed with pGBKT7-MyBPH was compared with a growth curve of the GOLD yeast strain transformed with non-recombinant pGBKT7. These growth curves were set up under the same experimental conditions at the same point in time. Each of the aforementioned transformed yeast strains were grown in SD-Trp media (Appendix I) in 50ml polypropylene tubes (Greiner Bio-One, Frickenhausen, Germany) overnight at 30°C, in a YIH DER model LM-530 shaking incubator (SCILAB Instrument Co. Ltd., Taipei, Taiwan) (200rpm) to a stationary growth phase. The growth cultures were

then diluted 1:10 in SD-Trp media (Appendix I) and incubated at 30°C in a shaking incubator (200rpm). A 1ml aliquot of the culture was taken and its OD_{600nm} was measured every 2 hours over a period of 8 hours. A linearised graph of the log of these OD_{600nm} readings versus time was drawn and the slopes of the graphs generated for the recombinant and non-recombinant transformants were compared.

2.12.3 Testing the mating efficiency

Small-scale yeast matings were performed to determine whether the bait construct had any significant effect on the mating efficiency of the GOLD yeast cells. The pGBKT7-MyBPH bait transformed GOLD strain was mated with the Y187 prey host strain, into which either the non-recombinant pGADT7-Rec prey vector (Appendix III) or the control prey vector, pTD1.1 was transformed (Clontech Laboratories, Inc., Palo Alto, California, USA). Control matings, in which either the non-recombinant pGBKT7 or the control pGBKT7-53 vector transformed GOLD strain (Clontech Laboratories, Inc., Palo Alto, California, USA) was mated with Y187 prey host strain, which was transformed with either the non-recombinant pGADT7-Rec prey vector or the pTD1.1 control prey vector, were conducted concurrently with the aforementioned matings. In order to determine the mating efficiency, the yeast strains GOLD pGBKT7-MyBPH and GOLD pGBKT7 were plated onto the SD-Trp nutritional selection agar plates (Appendix I) and the Y187 pGADT7-Rec and Y187 pTD1.1 yeast strains were plated onto SD-Leu agar plates (Appendix I). Plates were incubated at 30°C for 2 to 4 days in a Sanyo MIR262 stationary ventilated incubator (SANYO Electronic Co., Ltd., Ora-Gun, Japan). A single colony from each of the test mating plates were used to inoculate 1ml YPDA media (Appendix I), in a 15ml polypropylene tube (Greiner Bio-one, Frickenhausen, Germany). These matings were incubated overnight at 30°C, shaking at 200rpm in a YIH DER model LM-530 shaking incubator (SCILAB Instrument Co. Ltd., Taipei, Taiwan). Following incubation, serial dilutions (1:10, 1:100, 1:1000 and 1:10 000) of the mating cultures were plated onto SD-Leu, SD-Trp and SD-Trp-Leu agar plates (Appendix I). These plates were incubated in an inverted position at 30°C for 4 to 5 days in a Sanyo MIR262 stationary ventilated incubator (SANYO Electronic Co., Ltd., Ora-Gun, Japan), prior to counting the colonies on each plate and calculating the mating efficiency (Appendix II).

2.13 Yeast two-hybrid analysis

2.13.1 The cardiac cDNA library

The pre-transformed MATCHMAKER™ cDNA human cardiac library (Clontech Laboratories, Inc., Palo Alto, California, USA) in the Y187 *S.cerevisiae* strain, used for the Y2H screen, was constructed by

homologous recombination-mediated cloning in a pGADT7-Rec vector. The library consisted of normal, whole hearts pooled from three Caucasian males of the following ages: 33 and 55 years that died due to trauma. The library contained approximately 1.15×10^7 independent clones and had an insert range of between 0.5 and ≥ 3.0 kb.

2.13.2 Establishment of bait culture

A pGBKT7-MyBPH transformed GOLD colony was streaked out onto SD-Trp agar plates (Appendix I) and four of the resultant colonies were inoculated in four separate 500ml Erlenmeyer flasks containing 50ml SD-Trp media (Appendix I). These cultures were grown to obtain a final pooled bait culture with a titre of at least 1×10^{10} . In order to ensure a high mating efficiency, a 100-fold excess of the bait to prey culture was needed. These 50ml cultures were incubated at 30°C overnight, shaking at 200rpm in a YIH DER model LM-530 shaking incubator (SCILAB Instrument Co. Ltd., Taipei, Taiwan). Following overnight incubation, cells were pelleted in 50ml polypropylene tubes (Greiner Bio-One, Frickenhausen, Germany) using an Eppendorf model 5810/5810R centrifuge (Eppendorf, Hauppauge, New York, USA) at 3000rpm for 10 minutes at room temperature. The supernatants were then discarded and all four the pellets were resuspended in a total volume of 50ml SD-Trp media (Appendix I). The 50ml resuspension was subsequently transferred to a 500ml Erlenmeyer flask and incubated at 30°C for 16 hours in a YIH DER model LM-530 shaking incubator (SCILAB Instrument Co. Ltd., Taipei, Taiwan) (200rpm). Following incubation, the OD_{600nm} of 1ml of the of the bait culture was measured and the cells counted before the cells were centrifuged at 3000rpm at room temperature in an Eppendorf model 5810/5810R centrifuge (Eppendorf, Hauppauge, New York, USA) for 10 minutes. The supernatant was discarded and the pellet resuspended in the residual SD-Trp media (Appendix I). A 10µl aliquot of this culture was removed for control mating experiments.

2.13.3 Library mating

A 1ml pre-transformed cardiac cDNA library (Clontech Laboratories, Inc., Palo Alto, California, USA) aliquot stored at -80°C was thawed and vortexed using a Whirlimixer vortex (Fisher Scientific UK Ltd., Loughborough, UK). Subsequently, 10µl of the thawed library was transferred to a 1.5ml microcentrifuge tube (Eppendorf, Hauppauge, New York, USA) for the library titre. In order to determine the mating efficiency, 100µl aliquots of 1:100, 1:1000, 1:10 000 dilutions were plated out onto 90mm SD-Trp, SD-Leu, SD-Trp-Leu agar plates (Appendix I).

The remaining pre-transformed library culture (990µl) was added to 45ml 2X YPDA media (Appendix I) containing the pGBKT7-MyBPH:GOLD bait culture (section 2.13.2) and 50µg/ml Kanamycin in a 2L Erlengmeyer flask. To ensure all of the remaining growth culture in the 500ml Erlengmeyer flask was being used, the flask was washed out twice with 30ml 2X YPDA (Appendix I), which was then transferred to the culture in the 2L Erlengmeyer flask. The culture was incubated at 30°C in a YIH DER model LM-530 shaking incubator (SCILAB instrument Co. Ltd., Taipei, Taiwan), shaking at 200rpm overnight. The following day a drop of the mating culture was viewed on a slide under the microscope (Nikon Corporation, Tokyo, Japan) to confirm the presence of zygotes before plating out the mated culture.

The content of the 2L Erlengmeyer flask was transferred to a 50ml polypropylene tube (Greiner Bio-One, Frickenhausen, Germany) and centrifuged for 10 minutes at 3000rpm in an Eppendorf model 5810/5810R centrifuge (Eppendorf, Hauppauge, New York, USA). To ensure that all of the remaining mating culture is plated out, the Erlengmeyer flask was rinsed twice with 50ml 2X YPDA (Appendix I). The rinses were used to resuspend pelleted cells and recentrifuged at 3000rpm for 5 minutes to repellet the cells. All pelleted cells were resuspended in 10ml 0.5X YPDA (Appendix I), containing 50µg/ml Kanamycin. The total volume of cells plus media was 13ml.

Serial dilutions (1:10, 1:100, 1:1000 and 1:10 000) of 100µl of the mating culture were plated onto 90mm SD-Leu, SD-Trp and SD-Trp-Leu agar plates (Appendix I) in order to determine the bait: library mating efficiency and the number of library plasmids screened (Appendix II). A volume of 250µl of the remaining mating culture was plated directly onto each of the 58 140mm TDO (SD-Trp-Leu-His) agar plates (Appendix I), before the plates were incubated for 2 weeks in an inverted position at 30°C in a Sanyo MIR262 stationary ventilated incubator (SANYO Electronic Co., Ltd., Ora-Gun, Japan).

2.13.4 Establishing a library titre

The colonies of the mating culture serial dilutions (1:10, 1:100, 1:1000 and 1:10 000) that grew on the selection plates SD-Leu, SD-Trp and SD-Trp-Leu (section 2.12.3) were counted to calculate the mating efficiency of the library mating and the number of library plasmids screened (Appendix II).

2.13.5 Control matings

Control matings were performed to ensure that the recombinant pGBKT7-MyBPH:GOLD construct had no influence on the ability of the transformed GOLD strain to mate with the Y187 library strain. Consequently, 10µl of the pGBKT7-MyBPH:GOLD and the pTD1.1:Y187 cultures were co-innoculated in 1ml 0.5X YPDA (Appendix I) and incubated overnight shaking at 200rpm in a 30°C YIH DER model LM-530 shaking incubator (SCILAB Instrument Co. Ltd., Taipei, Taiwan). Following incubation, cultures were diluted (1:10; 1:100; 1:1000; 1:10 000) and plated onto SD-Trp, SD-Leu and SD-Trp-Leu plates (Appendix I). After incubating the plates at 30°C for 3 to 5 days in a Sanyo MIR262 stationary ventilated incubator (SANYO Electronic Co., Ltd., Ora-Gun, Japan), the colonies were counted and the mating efficiency calculated as previously described (section 2.12.3) (Appendix II).

2.13.6 Detection of activation of nutritional reporter genes

2.13.6.1 Selection of transformant yeast colonies

In order to identify transformant yeast colonies to use in this Y2H library screen, the pGBKT7-MyBPH:GOLD bait construct was plated onto SD-Trp plates (Appendix I), and incubated at 30°C for 3 to 5 days in a Sanyo MIR262 stationary ventilated incubator (SANYO Electronic Co., Ltd., Ora-Gun, Japan). Transformant yeast colonies were picked and used for both small-scale and library mating experiments.

2.13.6.2 Selection of diploid yeast colonies containing putative interactor peptides

In order to identify diploid colonies in which an interaction between the bait- and prey-fusion peptides had taken place, diploid yeast colonies were plated onto TDO and QDO plates, containing Aureobasidin A (AbA) (TDO+AbA) (QDO+AbA) (Appendix I). Growth on TDO+AbA and QDO+AbA plates signify resistance to AbA and the transcriptional activation of the reporter gene *HIS3* and both *HIS3* and *ADE2*, respectively.

2.13.7 Detection of activation of colourimetric reporter genes via X-α-galactosidase assay

Yeast colonies that were resistant to AbA and activated transcription of the *HIS3* and *ADE2* reporter genes, as determined by their growth on QDO+AbA agar plates (Appendix I), were transferred to Hybond N+ nylon membrane. These membranes were subsequently placed, colony side up, onto QDO+AbA plates containing 20mg/ml X-α-galactosidase (Clontech Laboratories, Inc., Palo Alto, California, USA) (Appendix I). Growth of yeast cultures on these plates indicated transcription of the

MEL1 reporter gene by specific interaction between bait and prey peptides. After incubation at 30°C for 3 to 5 days in a Sanyo MIR262 stationary ventilated incubator (SANYO Electronic Co., Ltd., Ora-Gun, Japan), the colour of the yeast colonies were assessed visually.

2.13.8 Rescuing prey plasmids from diploid colonies

All yeast colonies that grew on the QDO+AbA agar plates (section 2.13.6) and turned blue on the plates containing X- α -galactosidase (section 2.13.7) contained putative MyBPH interactors. In order to test the specificity of the putative interaction and to identify the putative interactors, prey plasmids had to be isolated from the diploid colonies. Plasmids were isolated from diploid yeast colonies (section 2.1.3) and then transformed into *E.coli* DH5 α cells (section 2.11.1), before plating the transformed cultures onto LB plates (Appendix I) containing ampicillin (F. Hoffmann-La Roche Ltd., Basel, Switzerland) to select for prey constructs. Subsequently, the prey plasmids were purified (section 2.1.1) and transformed into the Y187 prey yeast strain (section 2.11.2).

2.13.9 Interaction specificity test

Once the prey constructs were isolated, the specificities of the interactions between the MyBPH-pGBKT7 bait construct and each of the prey constructs were assessed by mating each of the prey colonies on agar plates (Appendix I) containing the appropriate selection media. Each of the prey colonies were mated with the following transformed GOLD strains; the recombinant pGBKT7-MyBPH bait construct, the non-recombinant pGBKT7, the pGBKT7-53 control bait-plamid, supplied by the manufacturer (Clontech Laboratories, Inc., Palo Alto, California, USA) and the GOLD strain transformed with a heterologous bait encoding a transmembrane protein, wolframin (WFS1), a protein exclusively expressed in the brain. Diploid clones were selected on SD-Trp-Leu plates (Appendix I), after which positive clones were streaked out onto TDO+AbA and QDO+AbA plates (Appendix I) to test for resistance to AbA and activation of nutritional reporter genes. Clones that were positive on both the TDO+AbA and QDO+AbA plates (Appendix I) and produced a blue colour in the presence of X- α -galactosidase (20mg/ml) (Clontech Laboratories, Inc., Palo Alto, California, USA) were considered true putative interactors of MyBPH, in the absence of any colony growth for any of the control matings. Subsequently, prey constructs considered to be true interactors of MyBPH were subjected to automated DNA sequencing (section 2.5) and sequencing analyses (section 2.6) to reveal their identities.

2.14 Co-immunoprecipitation (Co-IP)

For Co-IP, 150µg prepared lysate (section 2.6 and section 2.10.2) was pre-cleared by transferring it to a 1.5ml microcentrifuge tube (Eppendorf, Hauppauge, New York, USA) containing 30µl protein G agarose beads (KPL, Gaithersburg, Maryland, USA), which were incubated at 4°C for 30 minutes on a LabRoller II rotator wheel (Labnet International Inc., New Jersey, USA) at 60rpm. After centrifugation at room temperature at 7000rpm for 30 seconds in a Labnet Prism™ microcentrifuge (Labnet International Inc., New Jersey, USA), the pre-cleared lysates (supernatant) were transferred to a clean 1.5ml microcentrifuge tube (Eppendorf, Hauppauge, New York, USA). A lysis mixture containing the appropriate amount of pre-cleared lysate (150µg), 1µg primary antibody and passive lysis buffer (Appendix I) to a total volume of 200µl was prepared and incubated overnight at 4°C for 30 minutes on a LabRoller II rotator wheel (Labnet International Inc., New Jersey, USA) at 60rpm. For each experiment two controls were included, the negative control to which a “non-relevant” antibody, HA-probe F-7 AC (sc-7392, Santa Cruz Biotechnology, California, USA), was added to the lysis mixture instead of the antibody of interest, and the second was the protein G agarose control, which contained no antibody at all, only pre-cleared lysate and passive lysis buffer (Appendix I).

Following the overnight incubation, 60µl protein G agarose beads (KPL, Gaithersburg, Maryland, USA) were added to each sample and incubated at 4°C on a LabRoller II rotator wheel (Labnet International Inc., New Jersey, USA) at 60rpm for a further 60 minutes. The beads were then collected by centrifugation at 7000rpm for 30 seconds and the supernatant transferred to clean 1.5ml microcentrifuge tubes (Eppendorf, Hauppauge, New York, USA), which was kept on ice for use as controls in western blot analyses (section 2.15). Passive lysis buffer (200µl) (Appendix I) was used to wash the beads 3 to 5 times, by centrifugation in a Labnet Prism™ microcentrifuge (Labnet International Inc., New Jersey, USA) between each wash step and discarding the supernatant each time, before adding more passive lysis buffer (Appendix I) to wash. After the final wash, the supernatant was removed from the agarose beads and 35µl pre-mixed SDS Laemlli sample buffer (Bio-Rad, Hercules, California, USA), containing 5% β-mercapto-ethanol (Merck, Darmstadt, Germany), was added to each sample. These samples were denatured at 95°C for 5 minutes in a Techne Dri-block DB-3A heating block (Techne Ltd., Duxford, Cambridge, UK) and centrifuged at 7000rpm for 30 seconds in a Labnet Prism™ microcentrifuge (Labnet International Inc., New Jersey, USA). The supernatant for each sample was loaded onto 4-15% TGX resolving pre-cast SDS polyacrylamide gels (section 2.4.2).

2.15 Western blotting

Proteins obtained from Co-IP assays (section 2.14) were visualised on western blots. The optimal primary and secondary antibody concentrations used to detect putative interactions with MyBPH are summarised in Table 2.4. For the immunoprecipitation analyses performed to determine siRNA-mediated knockdowns of MyBPH and cMyBPC (section 2.14), the supernatant of each sample was kept on ice and used to blot for GAPDH (Santa Cruz Biotechnology, California, USA), which served as loading control at the optimised concentrations (Table 2.4).

2.15.1 Membrane blocking

Following the transfer of proteins from the 4-15% TGX resolving pre-cast SDS polyacrylamide gels (section 2.4.2) onto the PVDF membranes (section 2.4.3), the membranes were removed from the iBLOT transfer machine and washed with TBST (Appendix I). The membranes were then blocked in 5% Elite fat-free instant powder milk (Clover, Roodepoort, South Africa) in TBST (Appendix I), containing 0.01% Tween-100 (Merck, Darmstadt, Germany) at room temperature for 60 minutes on a STUART orbital shaker model SSL1 shaking at 200rpm (Barloworld Scientific Ltd., Staffordshire, UK), to reduce the amount of background or non-specific binding of the antibodies.

2.15.2 Addition of primary antibody

After the PVDF membrane was blocked in 5% fat-free milk in TBST (section 2.15.1), the PVDF membrane was incubated overnight at 4°C on a STUART orbital shaker model SSL1 shaking at 200rpm (Barloworld Scientific Ltd., Staffordshire, UK) with the appropriate primary antibody at the optimised concentration (Table 2.4) diluted in either 5% fat-free milk or 5% bovine serum albumin dissolved in TBST, containing 0.01% Tween-100 (Merck, Darmstadt, Germany) (Table 2.4). After primary antibody incubation, the PVDF membrane was washed three times (10 minute washing steps) using fresh TBST on a STUART orbital shaker model SSL1 shaking at 200rpm (Barloworld Scientific Ltd., Staffordshire, UK) at room temperature.

Table 2.4 Primary and secondary antibody concentrations for western blot analyses.

Antigen	Primary Antibody	Catalogue Number	Solution TBST	Optimum Concentration	*Secondary Antibody	Optimum Concentration
MyBPH	#MyBPH	ab55561	5% milk	1:500	Donkey-anti mouse	1:2000
ACTC1	**ACTC1	PA5-21396	5% milk	1:1000	Donkey-anti rabbit	1:2000
UBC9	#UBC9	ab21193	5% milk	1:100	Donkey-anti rabbit	1:2000
MYH7	#MYH7	ab15	5% bovine serum albumin	1:1000	Donkey-anti mouse	1:2000
MyBPC3	*MyBPC3	sc-67353	5% milk	1:400	Donkey-anti rabbit	1:2000
GAPDH	*GAPDH	sc-25778	5% milk	1:2000	Donkey-anti rabbit	1:2000

Abbreviations: **ACTC1**, cardiac α -actin; **GAPDH**, glyceraldehyde 3-phosphate dehydrogenase; **MyBPC3**, cardiac myosin binding protein C, **MyBPH**, myosin binding protein H; **MYH7**, cardiac β -myosin heavy chain; **UBC9**, SUMO-conjugating enzyme UBC9

*All secondary antibodies were HRP-conjugated for chemiluminescent visualisation and supplied by Santa Cruz Biotechnology, California, USA. #Antibodies were supplied by Abcam[®], Massachusetts, USA, **Antibodies were supplied by Thermo Scientific, Pierce Biotechnology, Illinois, USA, +Antibodies were supplied by Santa Cruz Biotechnology, California, USA.

2.15.3 Addition of secondary antibody

Following the wash steps to get rid of the primary antibody, the PVDF membrane was incubated with the appropriate concentration of secondary antibody in 5% milk in TBST containing 0.01% Tween-100 (Merck, Darmstadt, Germany) (Table 2.4) at room temperature for 60 minutes on a STUART orbital shaker model SSL1 at 200rpm (Barloworld Scientific Ltd., Staffordshire, UK). The membrane was then washed three times (10 minute washing steps) with fresh TBST, while shaking at room temperature on a STUART orbital shaker model SSL1 at 200rpm (Barloworld Scientific Ltd., Staffordshire, UK).

2.15.4 Chemiluminescent visualisation of membrane proteins

After washing the PVDF membrane, the membrane was subjected to a working solution of the Supersignal West Pico Chemiluminescent Substrate (Thermo Scientific, Pierce Biotechnology, Illinois, USA), which consists of a 1:1 ratio of two substrates, the Supersignal West Pico Enhancer solution

and the Supersignal West Pico Stable Peroxide solution. Visualisation of the proteins on the membrane took place in the dark room, as reagents were sensitive to light. The membrane was incubated in this working solution for 5 minutes before the membrane was removed and placed between two transparent plastic sheets, within an autoradiography cassette. A glow-in-the-dark sticker was placed in the bottom right corner on the plastic sheet in the cassette to aid in orientation. The membrane was then exposed to autoradiography film (Thermo Scientific, Pierce Biotechnology, Illinois, USA) for 10 seconds to 10 minutes and developed using an automatic Hyperprocessor™ autoradiography film processor (Amersham Pharmacia Biotech UK Ltd., Little Chalfont, Bucks, UK).

2.16 Co-localisation

2.16.1 Co-localisation assay

For co-localisation of putative interactions identified in the Y2H analyses (section 2.13), the appropriate antibodies were used to stain endogenous proteins as indicated in Table 2.5. However, for the autophagy assay the LC3b-II_GFP construct was transfected into H9c2 cells (section 2.11.3), after which the cells were differentiated for 5 to 10 days (2.10.1.4) before proceeding with the co-localisation assay, as described below.

For co-localisation assays, approximately 10 000 to 15 000 H9c2 cells were seeded, and transfected in the case of the autophagy assays, on sterile glass coverslips (section 2.11.3) before differentiation for 5 to 10 days (section 2.10.1.4). The differentiation media was removed and the cells washed with PBS (Appendix I). Subsequently, the cells were fixed to the glass coverslips using 100% methanol at 4°C for 5 minutes and 5% paraformaldehyde at room temperature for an additional 5 minutes. The cells were washed three times (10 minute washing steps) using PBS, before incubation with 1% bovine serum albumin for 60 minutes to reduce non-specific binding of antibodies. After blocking the coverslips, the cells were incubated with the primary antibody at the optimised concentration (Table 2.5), diluted in 1% bovine serum albumin overnight at 4°C in a humidified chamber.

The following day the excess primary antibody was removed by washing the coverslips twice (10 minute washing steps) using PBS. The coverslips were then incubated with the secondary antibody (diluted in PBS) at the optimised concentrations (Table 2.5), at room temperature for 90 minutes in a humidified chamber. Prior to staining the nuclei of the differentiated H9c2 cells with Hoechst H-33342 (Sigma-Aldrich Inc., St Louis, USA) at an optimised concentration of 0.5µg/ml in PBS at room temperature for 10 minutes, the excess secondary antibody was washed off three times

(10 minute washing steps) using PBS. The excess Hoechst H-33342 was washed of with PBS for 10 minutes, before mounting the coverslip to glass slides using 20-30µl Mowiol, containing freshly added n-propylgallate as anti-fade (Appendix I).

Table 2.5 Antibodies and antibody concentrations for co-localisation assays.

Antigen	Primary Antibody	Catalogue Number	Optimum Concentration	*Secondary Antibody	Optimum Concentration
MyBPH	#MyBPH	ab55561	1:20	Donkey-anti mouse (Cy5)	1:500
				Donkey-anti mouse (Cy3)	1:500
ACTC1	**ACTC1	PA5-21396	1:100	Donkey-anti rabbit (AF488)	1:500
UBC9	#UBC9	ab21193	1:10	Donkey-anti rabbit (Cy3)	1:500
MYH7	°MYH7	LS-B5888	1:50	Donkey-anti rabbit (AF488)	1:500
MyBPC3	#MyBPC3	ab140892	1:50	Donkey-anti rabbit (Cy3)	1:500

Abbreviations: **AF488**, Alexa Fluor 488; **Cy3**, cyanine dye 3; **Cy5**, cyanine dye 5; **ACTC1**, cardiac α -actin; **MyBPC**, cardiac myosin binding protein C, **MyBPH**, myosin binding protein H; **MYH7**, cardiac β -myosin heavy chain; **UBC9**, SUMO-conjugating enzyme UBC9

*All secondary antibodies were fluorescently labelled and supplied by Jackson ImmunoResearch Laboratories Inc., USA. #Antibodies were supplied by Abcam®, Massachusetts, USA +Antibodies were supplied by Santa Cruz Biotechnology, California, USA, **Antibodies were supplied by Thermo Scientific, Pierce Biotechnology, Illinois, USA, °Antibodies supplied by Lifespan Biosciences Inc., Washington, USA.

Table 2.6 Excitation and emission spectra of fluorescent proteins used in co-localisation assays.

Fluorescent Protein	Excitation (nm)	Emission (nm)
Hoechst	358	461
GFP	395	509
AF488	496	519
Cy3	550	570
Cy5	650/670	649

Abbreviations: **AF488**, Alexa Fluor 488; **Cy3**, cyanine dye 3; **Cy5**, cyanine dye 5; **GFP**, green fluorescent protein; **nm**, nanometer

The slides were viewed using the Zeiss LSM 510 Meta confocal microscope, with a pulsed infrared laser for 2-photon excitation and imaging (NLO) or the super resolution ELYRA S1, with SR-SIM and LSM 780 technology, located at the Confocal and Light Microscope Imaging Facility, UCT, South Africa and the Central Analytical Facility, Department of Physiological Sciences, Stellenbosch University, South Africa, respectively. The excitation and emission spectra of fluorescent proteins are shown in Table 2.6. All images were captured using a 60X oil immersion objective.

Co-localisation of proteins were quantified using the Zeiss Zen 2011 Lite software package, downloaded from the Carl Zeiss website; http://microscopy.zeiss.com/microscopy/en_de/downloads/zen.html (Carl Zeiss Microscopy GmbH, Jena, Germany). This software allowed calculation of overlap (Figure 2.1) and co-localisation coefficients as derived from Mander's article based on Pearson's correlation coefficient (Figure 2.2) (Zinchuk, 2007; Dunn, 2011).

$$\text{Overlap coefficient} : [\Sigma(\text{Ch1}_i)(\text{Ch2}_i)] / [\sqrt{(\text{sum}(\text{Ch1}_i)^2)(\text{Ch2}_i)^2}]$$

Figure 2.1 Formula for calculating the overlap coefficient.

The values for the overlap coefficient range from 0 to 1. An overlap coefficient with a value of 1 would represent perfectly co-localised pixels.

$$\text{Pearson's correlation} : [\Sigma(\text{Ch1}_i - \text{Ch1}_{\text{avg}})(\text{Ch2}_i - \text{Ch2}_{\text{avg}})] / [\sqrt{(\text{sum}(\text{Ch1}_i - \text{Ch1}_{\text{avg}})^2)(\text{Ch2}_i - \text{Ch2}_{\text{avg}})^2}]$$

Figure 2.2 Formula for calculating the Pearson's correlation.

Because each pixel is subtracted by the average pixel intensity, the value for correlation R can range from -1 to 1. A value of 1 would mean that the patterns are perfectly similar (co-localised), while a value of -1 would mean that the patterns are perfectly opposite.

For each co-localisation image, three images of each of the bait protein and prey proteins were taken and the average baseline threshold was determined for each channel, which was used to calculate the average co-localisation of the respective bait and prey protein pairs in at least 20 overlay images, which included z-stack images.

2.17 RNA-interference-mediated knockdown

2.17.1 siRNA preparation, transfection and optimisation

For the siRNA-mediated knockdown assay, cells were seeded and transfected with siRNA constructs as described in section 2.11.3. For both MyBPH and cMyBPC, four different siRNA constructs (Qiagen, Hilden, Germany) were prepared and diluted according to the manufacturer's instructions with RNase free H₂O to a concentration of 20µM. Each assay included a well which was transfected with a NSC siRNA construct, which consisted of scrambled RNA sequence. An Alexa Fluor 488-labelled NSC was used to transfect the cells (section 2.11.3) at different concentrations and viewed using the Zeiss LSM 510 meta two-photon laser scanning confocal microscope, located at the Confocal and Light Microscope Imaging Facility, UCT, South Africa. The concentration of siRNA used to transfect the cells was optimised at 200ng per well, for a final concentration of 10nM. To determine whether the cells should be transfected with siRNA constructs before the cells were differentiated (pre-differentiation) or after the cells were differentiated (post-differentiation) (section 2.10.1.4), cells were seeded onto glass coverslips (section 2.11.3) and transfected with the optimised concentration of Alexa Fluor 488-labelled NSC (10nM). Cells were visualised using the Zeiss LSM 510 meta two-photon laser scanning confocal microscope at the Confocal and Light Microscope Imaging Facility, UCT, South Africa.

Significant individual and concurrent knockdown of MyBPH and cMyBPC in the siRNA-treated groups compared to the NSC-treated group were determined by unpaired, two-tailed t-test, where a p-value <0.05 indicated significance. Graphpad Prism software version 5.03 for Windows was used for statistical analyses (Graphpad Software Inc., California, www.graphpad.com). Data presented are the mean ± SEM, representative of three independent experiments.

2.17.2 Contractility assay

To investigate the role of MyBPH and cMyBPC in cardiac cell contractility, the planar cell surface area of the seeded and transfected cells (section 2.11.3) were measured using the Axiovert fluorescent microscope, located at the Central Analytical Facility, Stellenbosch University, South Africa, as

previously described (Chen et al., 2004, 2011). A concentration of 0.1 μ M of the β -adrenergic stimulant, isoproterenol (Sigma-Aldrich Inc., St Louis, USA) was added to four of the eight wells (Figure 2.3) and the marked cells within each well were captured every 20 minutes to calculate the planar cell surface area upon isoproterenol stimulation.

An average of six cells in each well were used to calculate the percentage contractility over time. The experiment was repeated three times and the data pooled to achieve an average percentage for each group. The planar surface area of each cell was measured at time point 0, 20 minutes, 40 minutes and 60 minutes. The isoproterenol treated groups were normalised with the non-isoproterenol treated groups. For statistical analysis, a mixed model repeated measures ANOVA test was used by Professor Martin Kidd, at the Centre for Statistical Consultation, Department of Statistics and Actuarial Sciences, Stellenbosch University, Stellenbosch, South Africa to determine whether there is a significant difference in percentage contractility between the siRNA treated groups over time.

H3 siRNA <i>Isoproterenol treated</i>	C3 siRNA <i>Isoproterenol treated</i>	H3 + C3 siRNA <i>Isoproterenol treated</i>	NSC siRNA <i>Isoproterenol treated</i>
H3 siRNA	H3 siRNA	H3 + C3 siRNA	NSC siRNA

Figure 2.3. A representation of 8-well borosilicate glass-bottomed chambers (Nunc, New York, USA) and the experimental preparation of the contractility assay, indicating which siRNAs were used and how they were treated. **Abbreviations:** **H3**, siRNA type H3 specific to myosin binding protein H; **C3**, siRNA type C3 specific to myosin binding protein C; **siRNA**, small interfering RNA; **NSC**, non-silencing control

MATERIALS AND METHODS: MODIFIER STUDY

2.18 Study participants

The Ethical Review Committee of the Faculty of Health Science at Stellenbosch University, South Africa, (N04/C3/062) granted institutional approval for this study and informed, written consent was obtained from all the participants.

A panel of 115 South African HCM unrelated probands, who were consecutively recruited from Tygerberg Hospital in the Western Cape, South Africa, or were referred to us from elsewhere, were previously screened for mutations in 11 sarcomeric genes. This led to the identification of 27 probands harbouring three South African HCM founder mutations, namely R304W in *MYH7*, A797T in *MYH7* and R92W in *TNNT2*, as previously described by Moolman-Smook et al., 1999.

The modifier gene study consisted of consenting relatives older than 18 years, for whom HCM-founder mutation carrier-status was determined. The South African HCM founder-mutation familial cohort used in this modifier gene study consisted of 388 genetically and clinically affected and unaffected individuals, from 27 South African HCM families of self-reported Caucasian or Mixed Ancestry descent.

2.18.1 Clinical evaluation

All participating individuals were clinically characterised by an experienced echocardiographer (Dr Miriam Revera from Pavia University, Italy), who was blinded to patient mutation carrier status. Echocardiography data obtained were M-mode, transthoracic 2-dimensional (2D) echocardiography and Doppler imaging using a GE Healthcare Vivid7 cardiovascular ultrasound system. More specifically echocardiographic imaging was measured using a 2.5Hz transducer in standard parasternal long- and short-axis orientations and apical four- and two-chamber views. Echocardiograms were analysed using measurement conventions as outlined in the American Society of Echocardiography (ASE) (Schiller et al., 1989) for the assessment of patients with HCM, as previously described by Revera et al., 2008.

Ventricle wall thickness (left ventricular wall thickness [LVWT], maximal posterior wall thickness [mPWT] and maximal intraventricular septum thickness [mIVST]) were assessed by 16 2D-echocardiographic measurements taken at the mitral valve-, papillary muscle- and supra-apex levels (Figure 2.4). Six of these 16 segments were measured at the mitral valve- and papillary muscle levels (at the anterior interventricular septum [IVS], posterior IVS and anterior wall [AW], lateral wall [LW], inferior wall [IW] and posterior wall [PW] of the left ventricle) and four at the supra-apex level (at the IVS, AW, LW and PW as per 4 chamber view).

Past medical records were obtained for deceased family members and, if relevant, in living individuals who had had previous contact with medical services. In addition, medical history and additional cofounders for cardiac hypertrophy such as age, sex, body surface area (BSA), heart rate (HR) and arterial blood pressure (in sitting position after 5 minutes of rest) were recorded for each individual. When participants had blood pressure of more than 140mm and 90mm Hg systolic and diastolic pressure, respectively, or were being treated for hypertension, they were considered hypertensive.

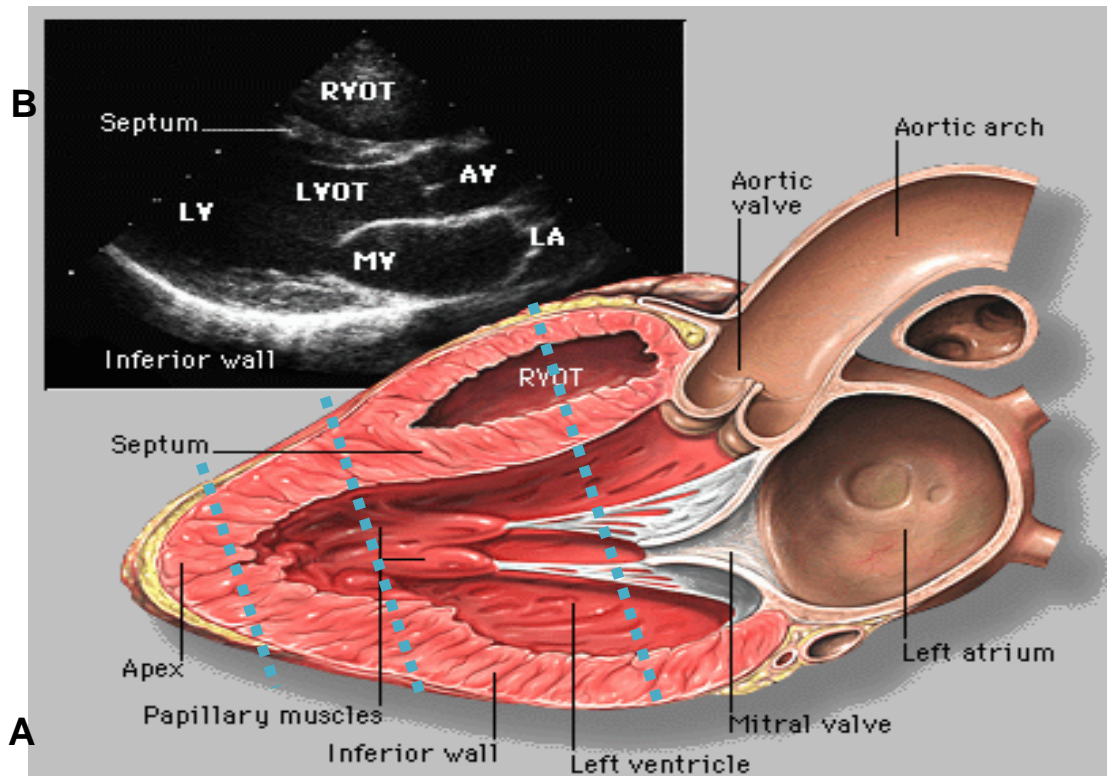


Figure 2.4 A graphical representation of the three levels of the heart muscle at which wall thickness was measured (The image was taken from http://www.med.yale.edu/.../aortic_regurgitation.html, with modifications by JC Moolman-Smook.). (A) The blue dotted lines on the long axis view of the left ventricle indicate the mitral valve, papillary muscle and apex levels at which echocardiographic parameters were measured. (B) A representation of a 2D echocardiographic ultrasound of the left ventricle. **Abbreviations:** AV, aortic valve; LA, left atrium; LV, left ventricle; LVOT, left ventricular outflow tract; MV, mitral valve; RVOT, right ventricular outflow tract

In the present cohort principal component analysis (PCA) was used to derive PC1 (principal component score), which is a weighted sum of 16 wall thickness measurements or composite scores of hypertrophy to best define ventricle-wide hypertrophy and LVH variability.

Due to the variable extent and distribution of hypertrophy, the measurement of hypertrophy was described by left ventricular mass (LVM), instead of a single wall thickness measurement. Left ventricular mass was calculated to estimate the LVM from two-dimensional LV linear dimensions according to ASE's formula (Figure 2.5).

$$\text{LVM (g)} = 0.8 \times 1.04 \times [(\text{LVID}_d + \text{PWT}_d + \text{SWT}_d)^3 - (\text{LVID}_d)^3] + 06\text{g}$$

Figure 2.5 Formula used to estimate LVM from 2D left ventricle linear dimensions. Abbreviations: g, gram; LVID_d, left ventricular internal dimension at end-diastole; LVM, left ventricular mass; PWT_d, posterior wall thickness at end-diastole; SWT_d, intraventricular septum thickness at end-diastole

2.19 Blood sample collection and DNA extraction

A total of two 5ml ethylene-diamine-tetra-acetic acid (EDTA) tubes (Vacutainer, South Africa) and one 10ml heparin tube (Vacutainer, South Africa) of blood was collected for DNA extraction and establishment of permanent lymphocyte cell lines, respectively. Blood obtained from patients at other centres in South Africa was transported to the laboratory and extracted within 24 hours of sampling. The DNA extraction method used to extract the DNA from peripheral blood lymphocytes is an adapted method previously described by Corfield et al., 1993. The protocol used to establish the permanent lymphocyte cell line is a method previously described by Neitzel, 1986.

2.20 Bioinformatics

2.20.1 Candidate gene selection

The candidate genes selected for genotyping in the South African HCM founder-mutation familial cohort, were genes encoding the proteins involved in the protein interactions, as identified in the Y2H assay and confirmed with co-localisation and Co-IP analyses. The gene information for the genes encoding the three prey proteins MYH7, ACTC1, UBC9 and the bait protein, MyBPH and their functions are summarised in Table 2.7.

Table 2.7 Candidate genes selected for gene association analysis.

Gene Symbol	Gene	Size (bp)	Protein Function
<i>MYBPH</i>	myosin binding protein H	8004	<i>Binds to myosin.</i>
<i>UBC9</i>	(SUMO-conjugating enzyme UBC9) ubiquitin-conjugating enzyme E2I, UBE2I	21 472	Involved <i>in sumoylation</i> , accepts the <i>ubiquitin-like proteins</i> from UBLE1A-UBLE1b E1 complex and <i>catalyses</i> their covalent attachment to other proteins with the help of an <i>E3 ligase</i> .
<i>MYH7</i>	Myosin heavy chain	22 981	Involved in <i>cross bridge cycling and contraction</i> .
<i>ACTC1</i>	Cardiac alpha actin	8044	Involved in various types of <i>cell motility</i> .

Abbreviations: *ACTC1*, cardiac α -actin; **bp**, base pairs; *MyBPH*, myosin binding protein H; *MYH7*, cardiac β -myosin heavy chain; *UBC9*, SUMO-conjugating enzyme UBC9

2.20.2 SNP selection

SNPs spanning *MyBPH*, *MYH7*, *ACTC1* and *UBC9* were selected using the SNPbrowser™ v4.1 software (De La Vega et al., 2006). The SNPbrowser™ software creates metric linkage disequilibrium (LD) maps similar to the genetic map expressed in centi-Morgans (cM) from the HapMap NCBI 36 assembly, by using the LDMAP programme (Kuo et al., 2007). SNPs can then be selected based on their additive position as markers for population-based disease association studies (Collins et al., 2004). Accordingly, there is no distance between SNPs in perfect LD in contrast to the distance of three or more linkage disequilibrium units (LDUs) between SNPs with no significant correlation (De La Vega et al., 2006). In this study, SNPs were selected to achieve an even coverage of 0.5 LDUs in the HapMap CEU and YRI populations. Markers were further prioritised with a minor allele frequency (MAF) of ≥ 0.05 (De La Vega, 2007). LDU is a measurement that represent the genetic map distance between SNPs which depends on the allelic association between these SNPs (Maniatis et al., 2004). Details of the SNPs selected for genotyping are presented in Table 2.8.

Table 2.8 The SNP position and nucleotide change of SNPs selected for genotyping.

<i>MyBPH (NM_004997)</i>			
SNP ID (rs number)	Chromosome Locus	Chromosome Position (bp)	Nucleotide Change
2642531		201401348	A/C
4950926		201403289	G/A
7545750		201405399	T/A
2250509	1q32.1	201405593	G/A
2791718		201408047	C/A
3737872		201410018	T/C
762625		201411924	C/T
<i>MYH7 (NM_000257)</i>			
SNP ID (rs number)	Chromosome Locus	Chromosome Position (bp)	Nucleotide Change
12147570		22951760	G/T
3729833		22953024	C/T
765019		22953688	T/C
3729832		22953977	T/A
7140721		22955534	G/A
3729825		22956104	C/T
7159367		22957485	T/C
10136106		22957705	G/A
2277475		22958505	A/T
12147533	14q12	22960531	A/G
743567		22960822	T/G
7157087		22962790	C/T
7155989		22962874	G/A
1951154		22967306	G/A
2754163		22967347	T/C
3729810		22969565	A/G
2239578		22973220	A/G
2239577		22973792	C/G
17092326		22973988	G/A
<i>ACTC1 (NM_005159)</i>			
SNP ID (rs number)	Chromosome Locus	Chromosome Position (bp)	Nucleotide Change
1370154		32869517	C/T
3729755		32871507	C/G
2070664	15q14	32872493	T/C
7165006		32873189	C/G
7166484		32873658	G/A

<i>UBC9</i> (NM_003345)			
SNP ID (rs number)	Chromosome Locus	Chromosome Position (bp)	Nucleotide Change
2281226		1304768	C/A
11248866		1305342	A/G
9933497		1309731	G/A
8052688	16p13.3	1312184	G/C
761059		1314525	G/A
761060		1314657	G/A
8063		1314819	G/A

Abbreviations: **A**, adenine; **ACTC1**, cardiac α -actin; **bp**, base pairs; **C**, cytosine; **G**, guanine; **MyBPH**, myosin binding protein H; **MYH7**, cardiac β -myosin heavy chain; **T**, thymine; **UBC9**, SUMO-conjugating enzyme UBC9

2.21 SNP genotyping by KBioscience

2.21.1 Sample preparation

The SNPs selected for genotyping were genotyped using PCR-based KASP™ genotyping assays designed by KBiosciences (LGC Genomics Ltd., Hertz, UK). DNA samples were diluted to 20ng/ μ l and 60 μ l were transferred to a 96 well plate (Axygen, Scientific, Inc., California, USA) and sealed with a Eppendorf heat sealer (Eppendorf AG, Hamburg, Germany) using peelable heat sealing foil sheets (Thermo Scientific, ABgene House, Surrey, UK) before sending the samples to KBiosciences (LGC Genomics Ltd., Hertz, UK) for genotyping.

2.21.2 Allelic discrimination

The software programme SNPviewer2 v3.2.2.16 supplied by LGC KBiosciences, Herts, UK provided for allele discrimination and viewing of allelic discrimination plots. The genotyping data was provided in a grid format for easy transfer into a database, minimising errors associated with transferring data.

2.22 Statistical analysis

2.22.1 Descriptive Statistics

Pedstats v6.11 (Wigginton and Abecasis, 2005) was used to verify and assess the Mendelian inheritance within families, the conformance of genotype data of unrelated, individuals with Hardy-Weinberg equilibrium (HWE) and the distribution of quantitative traits and covariates.

Subsequently, the data obtained served as a check for genotyping inconsistencies, which were then re-genotyped.

Minor allele frequencies (MAF) and genotype efficiency for SNPs investigated in the present HCM cohort were determined using Haploview v4.2 (Barrett et al., 2005). Haploview reports the genotyping efficiency for the entire cohort after individuals for whom no DNA was available were excluded, while the MAFs were determined on a set of unrelated individuals.

Since linear models and variance components analyses are sensitive to kurtosis and skewness in trait distribution, all traits were quantile-normalised to approximate normal distributions (Pilia et al., 2006) prior to association analysis.

2.22.2 Linkage disequilibrium (LD) determination

Genotyping data described in sections 2.21.1 and 2.21.2 were to determine pairwise LD statistics for our cohort applying Haploview v4.2 (Barrett et al., 2005). Since our cohort consisted of complex families with multiple generations, a set of maximally informative unrelated individuals were selected by Haploview for analyses. This was to ensure an accurate estimate of LD, as variants in related individuals are in tight LD by definition.

Haploview selects potentially different “informative subsets” with consecutive runs, but there are sometimes multiple, equally valid unrelated sample sets, which can result in different LD estimates from the same data. This could result in variable LD values when the same data is analysed a number of times. In this study, we report on the median of the normalised disequilibrium coefficient (D') values, which were obtained from 100 consecutive Haploview runs.

If two SNPs are in complete LD the following is true; individuals genotyped for two SNPs in complete LD with possible alleles a, A, b and B, would have genotypes ab or AB. When genotyping both these SNPs, any association or frequency observed for alleles of one SNP would be true for the alleles of other SNP. Complete LD is thus deterministic and if the above-mentioned is true, $r^2 = 1$ (Jarvik, 2003; Pittman, 2005).

Linkage disequilibrium can also be determined by a D' value, for example when the LD between two SNPs are being described by $D' = 0$, there is no inheritance pattern between these two SNPs, thus these two SNPs would act completely independent of one another. Furthermore, the higher the D' value, the higher the relation or association between these SNPs would be.

Only if all possible haplotypes are observed in a sample, the D' could be less than 1. For example, if the $D' = 1$, it means that at least one of the haplotypes, such as aB or Ab are not present in the sample. Thus, D' is not a strict measure of linkage and in our study cohort LD indicated by D' is not deterministic, as pair-wise LD was estimated on a selected subset of unrelated individuals every time, to give an idea of the LD in the underlying population. It is therefore possible that only one SNP can be associated with a hypertrophy trait and the other not, although they are in complete LD ($D'=1$) and it is thus clear that the allelic effects of these SNPs would not be the same.

2.22.3 Principal component score

Finding a single echocardiographic measure to quantify the extent of hypertrophy in all HCM patients accurately is very difficult, since the hypertrophy phenotype observed in HCM patients is extremely variable.

The five hypertrophy traits chosen to represent the HCM hypertrophic phenotype were viz. LVM, mIVST, mLWWT (maximal left ventricular wall thickness), mPWT and PC1. Although the use of echocardiographically derived LVM is most often used to quantify hypertrophy in HCM, it is known that it may not be an accurate account of the variable and asymmetric nature of hypertrophy in HCM. Principal component analysis provides a means to derive a single score that comprehensively describes the person-to-person variability in hypertrophy, regardless of the variability in the distribution of the hypertrophy. The principal component score outcome variable, PC1, is a single score, which is a weighted sum of 16 wall thickness measurements and define the largest quantity of variability in this data. It is a measure of hypertrophy, which takes into account the variability in distribution, and extent of hypertrophy between patients in the cohort, in all 16 measurements combined.

2.22.4 Confounding variables

All analyses were adjusted for covariates that are known to modulate cardiac hypertrophy. These included the mutation carrier status and the identity of HCM-causing founder mutations viz. R92W

mutation in the *TNNT2* gene, R403W and A797T mutations in the *MYH7* gene, hypertension (including treatment for hypertension), mean arterial blood pressure, sex, age, ethnicity (as proxy for recent population stratification), BSA and HR (as proxy measure for tachycardia). These known confounders were included in the models as fixed effects. Consequently, the effect of the variant were being estimated after the effects of the covariates have been removed from the phenotype.

Furthermore possible clustering of the phenotype within families, the extent of relatedness and phenotype correlation between each pair of individuals were adjusted for by including random effects for family and individuals in the models. The coefficients of the random effects were an indicator of family-membership, and a function of the kinship coefficients, respectively.

2.22.5 Heritability

The definition of broad sense heritability is the ratio of inherited variance to total phenotypic variance. A variance components model, the Abecasis pedigree-based QTDT (Abecasis et al., 2000), was used to define hypertrophy variability into either environmental or additive genetic effects. Taking into account hypertrophy cofounders, this model furthermore estimated the components of variance of the quantile normalised hypertrophy traits.

2.22.6 Single nucleotide polymorphism association

Genetic association between each variant and the five hypertrophy traits chosen to represent the HCM hypertrophic phenotype were assessed with a specialised mixed-effects linear model (lme4 function, coxme: Mixed Effects Cox Models, R package v2.2-3 (<http://CRAN.R-project.org/package=coxme>) and the kinship2 function: Pedigree functions, R package v1.5.0 (<http://CRAN.R-project.org/package=kinship2>). This model enabled us to adjust for per family, as well as per individual, random effects, so that they included environmental (individual and per family) and polygenic variance components. SNPs were numbered 0, 1 or 2 according to their number of minor alleles. A significant association between a bi-allelic variant and a phenotype trait (p -value <0.05) indicates that the mean phenotype trait value is significantly different between wild type homozygotes (no minor alleles) and heterozygotes (1 minor allele) and that this is equal to the difference between heterozygotes and minor homozygotes (2 minor alleles), the so-called additive allelic model.

2.22.7 Effect sizes

In order for the conclusions, specifically p-values, from the linear mixed effect models used for these analyses to be valid, the trait values have to be approximately normally distributed. Therefore the traits were quantile normalised to approximate normality for appropriate statistical inference (i.e. they deliver valid p-values), but these models provide the effect estimates in quantile-normalised units, which are not clinically meaningful. In order to estimate the effect sizes in the original units of measurement, effect sizes were obtained by modelling the raw, untransformed, cardiac wall thickness measurements. However, the effect sizes for PC1 were based on modelling the mean of the 16 untransformed, cardiac wall thickness measurements.

2.22.8 Haplotype assignment and association analysis

The most probable fully-typed maternal and paternal haplotype pairs for each individual were inferred using Simwalk v2.91 (Sobel and Lange, 1996). This programme uses so-called simulated annealing to estimate the most likely set of fully-typed maternal and paternal haplotypes of the marker loci at each individual in the pedigree. The optimal haplotype configuration were determined in Simwalk v2.91 by running the analysis multiple times using different randomly selected starting points. These haplotypes were then coded, for each individual, as the number of copies 0, 1 or 2. The haplotype-phenotype pairs were modelled with the R function `lmekin`, in exactly the same way as described for genotypes.

Chapter Three

Results

CHAPTER THREE

RESULTS

TABLE OF CONTENTS

RESULTS: PROTEIN INTERACTION STUDY	89
3.1 Yeast two-hybrid analysis of MyBPH.....	89
3.1.1 Sequence analyses of the pGBKT7 bait constructs.....	89
3.1.2 Phenotype test	89
3.1.3 Toxicity test	89
3.1.4 Mating efficiency of GOLD transformed with bait construct.....	90
3.1.5 Y2H screening of pre-transformed cardiac cDNA library	91
3.2 Co-localisation analysis of MyBPH and putative interactors as identified by Y2H analysis	96
3.3 Co-immunoprecipitation (Co-IP) of MyBPH and putative interactors as identified by Y2H analysis	100
3.4 Super resolution microscopy implicates MyBPH and cMyBPC in the process of autophagy	102
3.5 RNAi-mediated MyBPH and cMyBPC knockdowns.....	105
3.5.1 Optimisation of MyBPH and cMyBPC siRNA knockdowns.....	105
3.5.2 Effect of MyBPH and cMyBPC knockdowns on contractility.....	112
RESULTS: MODIFIER STUDY.....	114
3.6 Basic cohort characteristics	114
3.7 Candidate gene selection and SNP prioritisation	116
3.8 Genotyping results	117
3.8.1 KASP assay allelic discrimination.....	117
3.9 Statistical analyses.....	117
3.9.1 Descriptive statistics	117
3.9.2 Linkage disequilibrium assessment.....	119

3.9.3	Principal component analysis	122
3.9.4	Heritability.....	123
3.9.5	Association analyses	124
3.9.5.1	<i>MyBPH</i>	124
3.9.5.2	<i>MYH7</i>	130
3.9.5.3	<i>ACTC1</i>	137
3.9.5.4	<i>UBC9</i>	142

RESULTS: PROTEIN INTERACTION STUDY

3.1 Yeast two-hybrid analysis of MyBPH

3.1.1 Sequence analyses of the pGBKT7 bait constructs

After constructing the pGBKT7-MyBPH bait construct, DNA sequence analysis was performed to ensure that the integrity of the sequence and the reading frame had been maintained. Results revealed that the DNA nucleotide sequence and reading frame had been retained.

3.1.2 Phenotype test

The phenotype of the GOLD and Y187 yeast strains were able to grow on SD-Ura media, but were unable to grow on SD-Ade, SD-Trp, SD-His and SD-Leu. These results confirmed the phenotype of both the GOLD and Y187 yeast strains.

3.1.3 Toxicity test

Growth curves were generated in order to establish whether the MyBPH-pGBKT7 construct was toxic to the GOLD yeast strain (section 2.12.2). The growth curve of the pGBKT7-MyBPH bait construct transformed into GOLD was compared to the growth curve of the non-recombinant pGBKT7 and pGBKT7-53 transformed into GOLD. The linearised growth curve of the pGBKT7-MyBPH bait transformed GOLD strain was similar to the growth curve of the non-recombinant pGBKT7 and pGBKT7-53 transformed GOLD strains, confirming that the bait constructs had no toxic effect on the growth of the GOLD yeast strain (Figure 3.1).

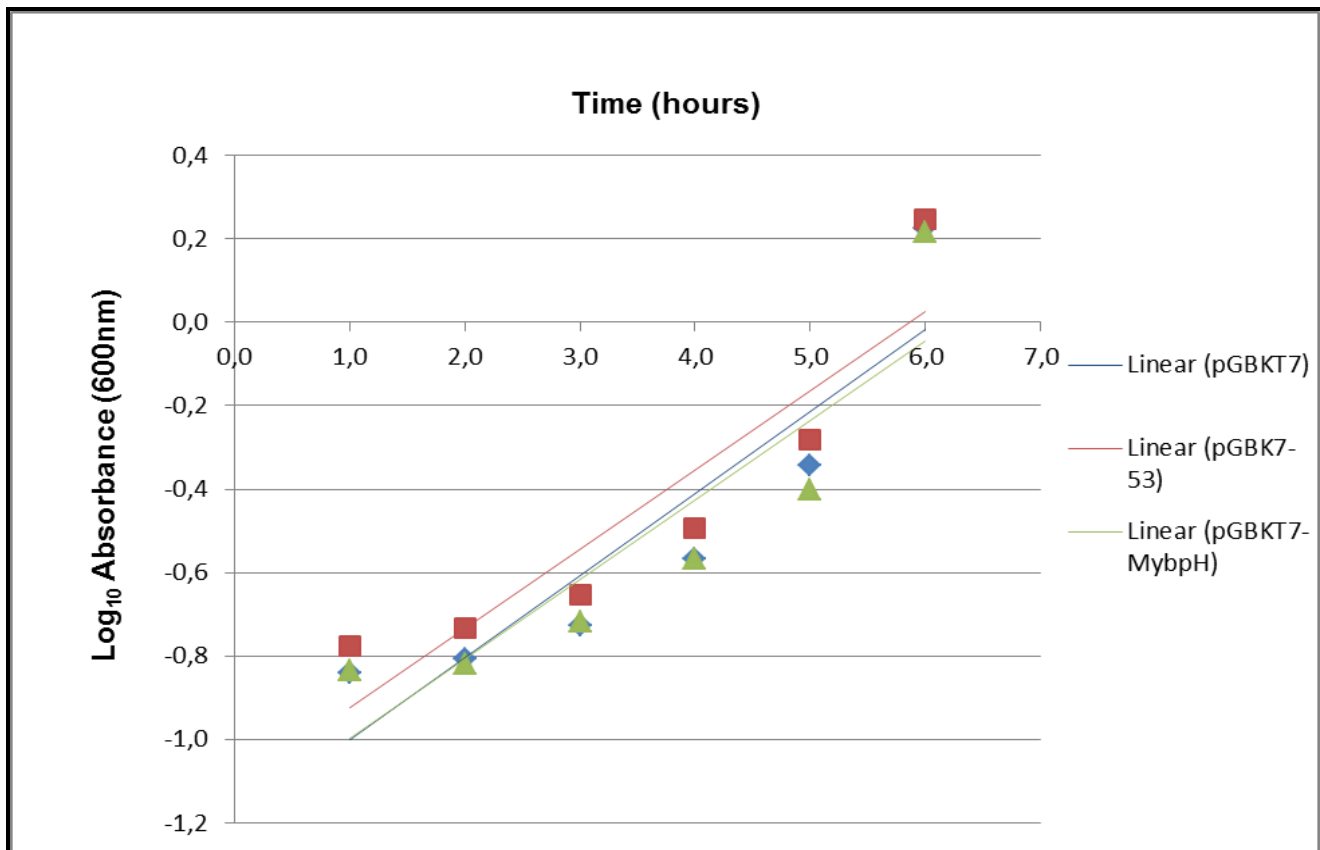


Figure 3.1 Linear growth curves of yeast strain GOLD transformed with non-recombinant pGBKT7, pGBKT7-53 and pGBKT7-MyBPH bait constructs. The growth rate of the pGBKT7-MyBPH transformant were compared to the non-recombinant pGBKT7 and pGBKT7-53, in an attempt to determine if the bait constructs had any toxic effects on the GOLD strain. **Abbreviations:** nm, nanometer; **MyBPH**, myosin binding protein H

3.1.4 Mating efficiency of GOLD transformed with bait construct

To ensure that the mating ability of the GOLD yeast strain was not affected by the pGBKT7-MyBPH transformation, a small scale yeast mating was performed (section 2.12.3). The mating efficiency of the pGBKT7-MyBPH transformed GOLD yeast strain and pTD1.1 transformed Y187 strain was compared to the mating efficiency of pGBKT7-53 and pTD1.1. The calculated mating efficiency was more than the minimum 2% recommended by the manufacturer and we concluded that the pGBKT7-MyBPH bait construct did not affect the mating efficiency (Table 3.1).

Table 3.1 Effect of the pGBKT7-MyBPH bait construct on the GOLD mating efficiency.

Matings	Mating Efficiency (%)
pGBKT7-MyBPH:GOLD x pTD1.1:Y187	>2%
pGBKT7-53:GOLD x pTD1.1:Y187	>2%

3.1.5 Y2H screening of pre-transformed cardiac cDNA library

Using the pGBKT7-MYBPH bait, approximately 6×10^6 cardiac cDNA clones were screened. Four hundred yeast clones were able to activate the *HIS3* reporter gene and were resistant to AbA, as they were able to grow on agar plates containing TDO and AbA (Table 3.2). A further 76 clones were able to activate the *ADE2* reporter gene as was evident by their growth on agar plates containing QDO and AbA (Table 3.2). The X- α -galactosidase assay eliminated a further 64 clones, leaving 12 clones that were subjected to bait-specificity tests via heterologous bait matings. As detailed in Table 3.3, these 12 clones passed the bait specificity tests and were sequenced to reveal the identities of the putative interactors.

DNA sequencing identified three clones encoding cardiac β -myosin heavy chain (MYH7), and three clones encoding the complete mitochondrial genome, together with one clone each encoding γ -filamin (FLNC) transcript variant 2, isoform b, MT-RNR2-like 2 (MTRNR2L2), cardiac α -actin (ACTC1), fas (TNFRSF6)-associated factor 1 (FAF1), fibrillin 1 (FBN1) and ubiquitin-conjugating enzyme E2I (UBE2I) transcript variant 1, also known as SUMO-conjugating enzyme UBC9 (UBC9). Three of the 12 putative interactors, as described in more detail in Table 3.4, were considered to be plausible putative physiological interactors of MyBPH based on their function and cellular localisation as assessed *in silico*.

Table 3.2 Activation of nutritional and colourimetric reporter genes by interaction between MyBPH and prey clones. Below is a representative subset of the scoring of the 400 clones that activated the *HIS3* reporter gene and were resistant to AbA, the 76 clones that activated the *ADE2* reporter gene and the remaining 12 clones that were able to activate the *MEL1* reporter gene.

Activation of nutritional and colourimetric reporter genes by prey-MyBPH interaction			
Clone #	Growth on TDO+AbA (<i>HIS3</i> activation)	Growth on QDO+AbA (<i>ADE2</i> activation)	X- α -galactosidase (colour) + AbA (<i>MEL1</i> activation)
1	+++	+++	++++ (no blue)
2	++++	++++	++++ (no blue)
3	++++	++++	++++ (no blue)
4	++++	++++	++++ (no blue)
5	++++	++++	++++ (no blue)
6	++++	++++	++++ (no blue)
7	++++	++++	++++ (no blue)
8	++++	++++	++++ (no blue)
9	++++	++++	++++ (no blue)
10	++++	++++	++++ (no blue)
11	+	+	+ (no blue)
12	++++	++++	++++ (no blue)
13	++++	++++	++++ (no blue)
15	++++	++++	++++ (no blue)
16	++++	++++	++++ (no blue)
17	++++	++++	++++ (no blue)
18	++++	++++	++++ (no blue)
19	++++	++++	++++ (no blue)
20	++++	++++	++++ (no blue)
21	++++	++++	++++ (no blue)
22	++	++	++ (no blue)
23	++	++	++ (no blue)
25	++++	++++	++++ (no blue)
26	++++	++++	++++ (no blue)
27	++++	++++	++++ (no blue)
28	++++	++++	++++ (no blue)
29	++++	++++	++++ (no blue)
30	++++	++++	++++ (no blue)
31	++++	++++	++++ (no blue)
32	++++	++++	++++ (no blue)
33	++++	++++	++++ (no blue)
34	++++	++++	++++ (no blue)
35	++++	++++	++++ (no blue)
36	++++	++++	++++ (no blue)
37	++++	++++	++++ (no blue)
38	++++	++++	++++ (no blue)

Activation of nutritional and colourimetric reporter genes by prey-MyBPH interaction			
Clone #	Growth on TDO+AbA (<i>HIS3</i> activation)	Growth on QDO+AbA (<i>ADE2</i> activation)	X- α -galactosidase (colour) +AbA (<i>MEL1</i> activation)
39	++++	++++	++++ (no blue)
40	++++	++++	++++ (no blue)
41	++++	++++	++++ (no blue)
42	++++	++++	++++ (no blue)
43	++++	++++	++++ (no blue)
44	++++	++++	++++ (no blue)
45	++++	++++	++++ (no blue)
46	++++	++++	++++ (no blue)
47	++++	++++	++++ (no blue)
48	++++	++++	++++ (no blue)
49	++++	++++	++++ (no blue)
50	++++	++++	++++ (no blue)
51	++++	++++	++++ (no blue)
52	++++	++++	++++ (no blue)
53	++++	++++	++++ (no blue)
54	++++	++++	++++ (no blue)
55	++++	++++	++++ (no blue)
56	++++	++++	++++ (no blue)
57	++++	++++	++++ (no blue)
58	++++	++++	++++ (no blue)
59	++++	++++	++++ (no blue)
60	++++	++++	++++ (no blue)
61	++++	++++	++++ (no blue)
62	++++	++++	++++ (no blue)
63	++++	++++	++++ (no blue)
64	++++	++++	++++ (no blue)
65	++++	++++	++++ (no blue)
66	++	++	++++ (blue)
67	++	++	++++ (blue)
70	++	++	++ (blue)
71	++	+	++++ (light blue)
72	++	++	++++ (light blue)
77	++	++	+++ (light blue)
79	+++	++++	++++ (light blue)
81	++++	++++	++++ (light blue)
83	++	+++	++++ (blue)
84	++	+++	++++ (light blue)
166	++	++	+++ (blue)
396	++	++	++ (blue)

Colonies in blue font activated *HIS3*, *ADE2*, *MEL1* reporter genes. TDO +AbA= agar plates containing AbA and lacking Leu, Trp and His; QDO+AbA=agar plates containing AbA and lacking Leu, Trp, His and Ade. Growth of colonies on plates: ++++=very good, +++=good, ++=weak, +=very weak, -=no growth.

Abbreviations: AbA, Aureobasidin A; *ADE2*, *HIS3* and *MEL1*, yeast two-hybrid reporter genes; MyBPH, myosin binding protein H

Table 3.3 Interaction between MyBPH preys with heterologous baits in specificity tests. The scores of the clones considered as putative interactors are detailed below.

Clone #	pGBKT7-MyBPH	pGBKT7	pGBKT7-53	pGBKT7-WFS1
66	++++	-	-	-
67	++++	-	-	-
70	++++	-	-	-
71	+++	-	-	-
72	++	+	++	+
77	+	-	-	-
79	+	-	-	-
81	++++	-	-	-
83	+++	-	-	-
84	++	-	-	-
166	++++	++	++	-
396	++++	-	-	-

Growth of colonies after 5 to 8 days on QDO+AbA. QDO+AbA=agar plates containing AbA and lacking Leu, Trp, His and Ade. Growth of colonies on plates: ++++=very good, +++=good, ++=weak, +=very weak, -=no growth.

Abbreviations: **MyBPH**, myosin binding protein H; **WFS1**, Wolframin protein; **pGBKT7-53**, yeast two-hybrid control vector; **pGBKT7**, yeast two-hybrid bait vector; **#**, number

Table 3.4 Identification of MyBPH putative interactor clones from Y2H cardiac library screen. Putative MyBPH interactors are arranged according to interactors represented by multiple clones from highest to lowest activity of nutritional and colourimetric reporter genes. Putative interactors represented by a single clone are arranged similarly. Putative interactors highlighted in pink were chosen to verify based on their cellular localisation and physiological role in the cardiac sarcomere.

Interacting Prey Summary					
Genomic hit			In-frame protein hit		
Clone #	Identity	BLASTN Acc # (E-value)	BLASTP Acc # (E-value)	Cellular localisation	Domains
84, 67, 81	<i>Homo sapiens</i> myosin, heavy chain 7, cardiac muscle, beta (MYH7)	NM_000257.2 (0.0)	NP_000248.2 (2e-159)	Cytoplasm; thick filament	IQ/myosin head-like
77, 79, 396	<i>Homo sapiens</i> mitochondrion, complete genome	NC_012920.1 (0.0)	YP_003024026.1 (0.0)	Mitochondrion; membrane	None
66	<i>Homo sapiens</i> filamin C, gamma (FLNC), transcript variant 2, isoform b	NM_001127487.1 (0.0)	NP_001120959.1 (0.0)	Cytoplasm; membrane; cytoskeleton	Calponin homology/actin-binding
83	<i>Homo sapiens</i> MT-RNR2-like 2 (MTRNR2L2)	NM_001190470.1 (3e-65)	NP_001177399.1 (1e-17)	Cytoplasm; secreted	None
166	<i>Homo sapiens</i> , actin, alpha, cardiac muscle 1 (ACTC1)	NM_005159.4 (0.0)	NP_005150.1 (0.0)	Cytoplasm; cytoskeleton	None
72	<i>Homo sapiens</i> fas (TNFRSF6) associated factor 1 (FAF1)	NM_007051.2 (0.0)	NP_008982.1 (0.0)	Nucleus	UBA/UBX
70	<i>Homo sapiens</i> fibrillin 1 (FBN1)	NM_000138.4 (0.0)	NP_00129.3 (0.0)	Extracellular matrix; secreted	TB/EGF-like
71	<i>Homo sapiens</i> ubiquitin-conjugating enzyme E2I, UBE2I (SUMO-conjugating enzyme UBC9), transcript variant 1	NM_003345.3 (0.0)	NP_003336.1 (1e-113)	Nucleus and cytoplasm	None

Abbreviations: Acc #, accession number; #, number; TB, domains within fibrillin 1; EGF-like, epidermal growth factor like; IQ, domain within myosin

3.2 Co-localisation analysis of MyBPH and putative interactors as identified by Y2H analysis

Confocal imaging was used to assess possible interactions of putative interactors identified by Y2H with MyBPH by means of co-localisation analyses. Intracellular localisation of MyBPH and MYH7, ACTC1 and UBC9 in differentiated H9c2 rat cardiomyocytes showed co-localisation of MyBPH and MYH7, MyBPH and ACTC1 and MyBPH and UBC9 to the same three-dimensional sub-cellular space (Figure 3.2, Figure 3.3, Figure 3.4, respectively). Interestingly, peri-nuclear expression of UBC9 was observed (Figure 3.4).

Quantitative analysis of overlapping pixels and intensity using Zeiss Zen 2009 software further confirmed co-localisation of MyBPH and MYH7, ACTC1 and UBC9 in these cells (Table 3.5, Table 3.6 and Table 3.7). Quantification of co-localisation results included using two algorithms; overlap coefficient and Pearson's correlation (correlation R) as described in section 2.16.1. The pixels in quadrant three in the scatter diagram (Figure 3.5 (F), Figure 3.6 (F) and Figure 3.7 (F)) are an indication of the amount of pixels from the channels indicated in (A) and (B) in the figures that share the same location. In each of the three co-localisation experiments the overlap coefficient was higher than 0.9, towards the upper end of the range (0 to 1). An overlap coefficient of 1 would represent perfectly co-localised pixels. The correlation R for each co-localisation analysis was more than -0.06, indicating that it lies within the middle of the range (-1 to 1). A correlation R of 1 would indicate that co-localisation patterns of the two proteins are perfectly similar. Taken together, in each of the co-localisation experiments the overlap coefficient and correlation R indicated that MyBPH colocalised with MYH7 (Table 3.5), ACTC1 (Table 3.6) and UC9 (Table.3.7).

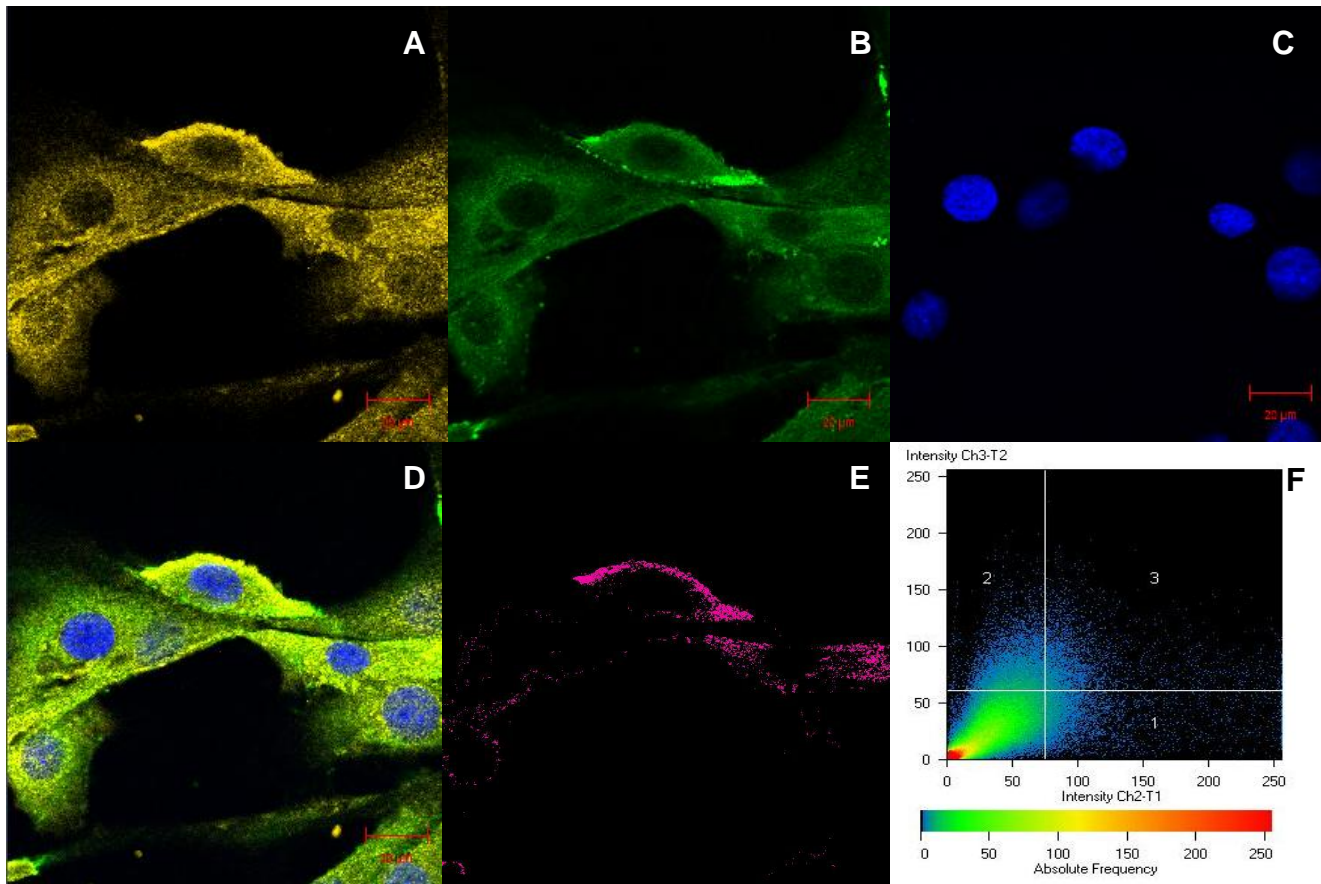


Figure 3.2 Fluorescent imaging and co-localisation analysis of MyBPH and MYH7 in differentiated H9c2 cardiomyocytes. (A) MyBPH labelled with a donkey anti-mouse Cy5 secondary antibody (Yellow). (B) MYH7 labelled with a donkey anti-rabbit Alexa Fluor 488 antibody (Green). (C) Nucleus labelled with Hoechst H-33342 (Blue). (D) Overlay of images A-C. (E) Co-localisation of MyBPH and MYH7 generated from merged images (Pink). (F) Scatter diagram generated by co-localisation analysis with quadrant three representing the degree of co-localisation. Scale bar 20 μ m.

Table 3.5 Quantification of co-localisation for the interaction between MyBPH and MYH7.

Weighted Co-localisation Coefficient Ch2-T1	Weighted Co-localisation Coefficient Ch3-T2	Overlap Coefficient	Correlation R	Correlation R x R
0.2856	0.1870	0.9222	-0.0333	0.0022

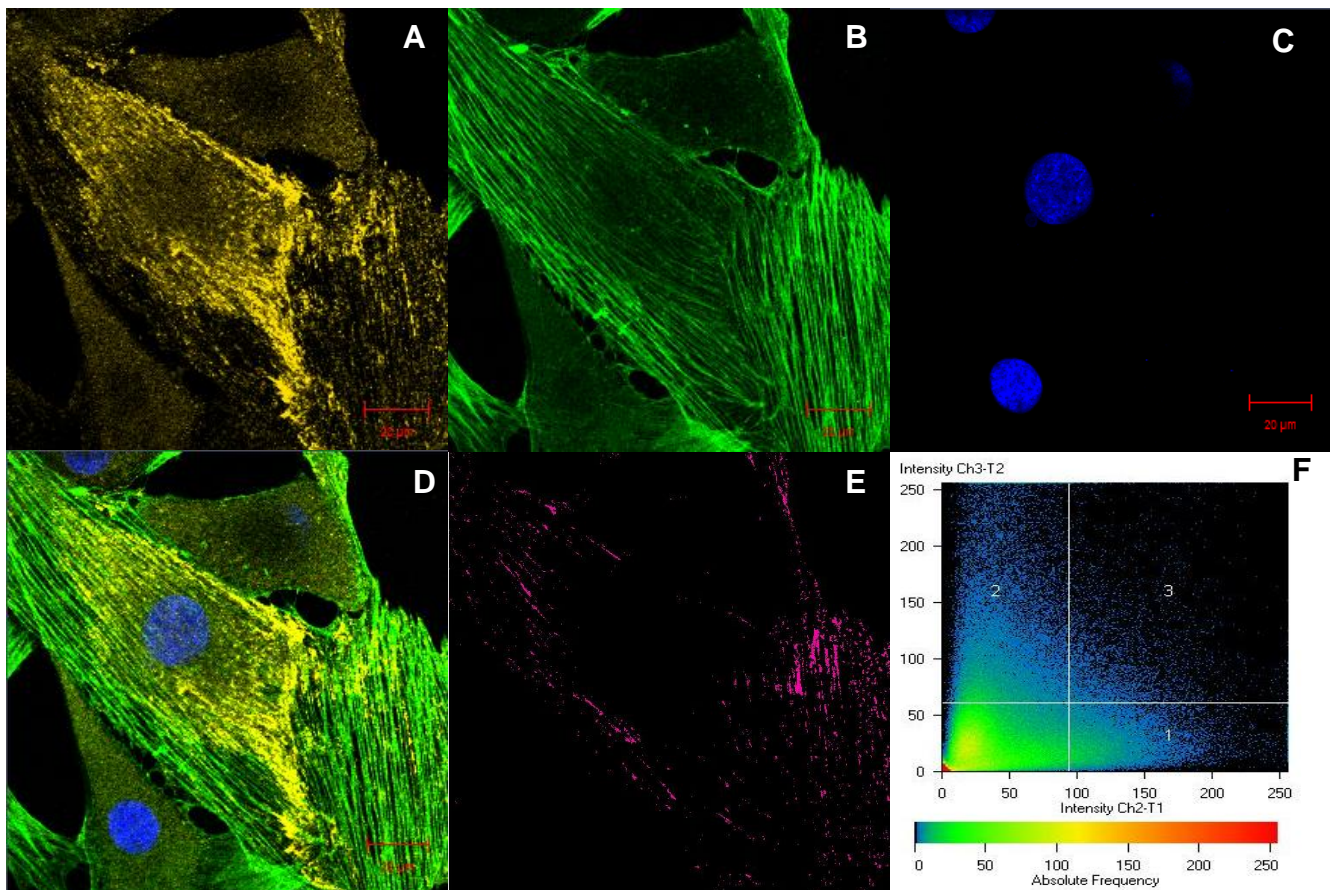


Figure 3.3 Fluorescent imaging and co-localisation analysis of MyBPH and ACTC1 in differentiated H9c2 cardiomyocytes. (A) MyBPH labelled with a donkey anti-mouse Cy5 secondary antibody (Yellow). (B) ACTC1 labelled with a donkey anti-rabbit Alexa Fluor 488 secondary antibody (Green). (C) Nucleus labelled with Hoechst H-33342 (Blue). (D) Overlay of images A-C. (E) Co-localisation of MyBPH and ACTC1 generated from merged images (Pink). (F) Scatter diagram generated by co-localisation analysis with quadrant three representing the degree of co-localisation. Scale bar 20 μ m.

Table 3.6 Quantification of co-localisation for the interaction between MyBPH and ACTC1.

Weighted Co-localisation Coefficient Ch2-T1	Weighted Co-localisation Coefficient Ch3-T2	Overlap Coefficient	Correlation R	Correlation R x R
0.1284	0.2936	0.9125	0.0288	0.0025

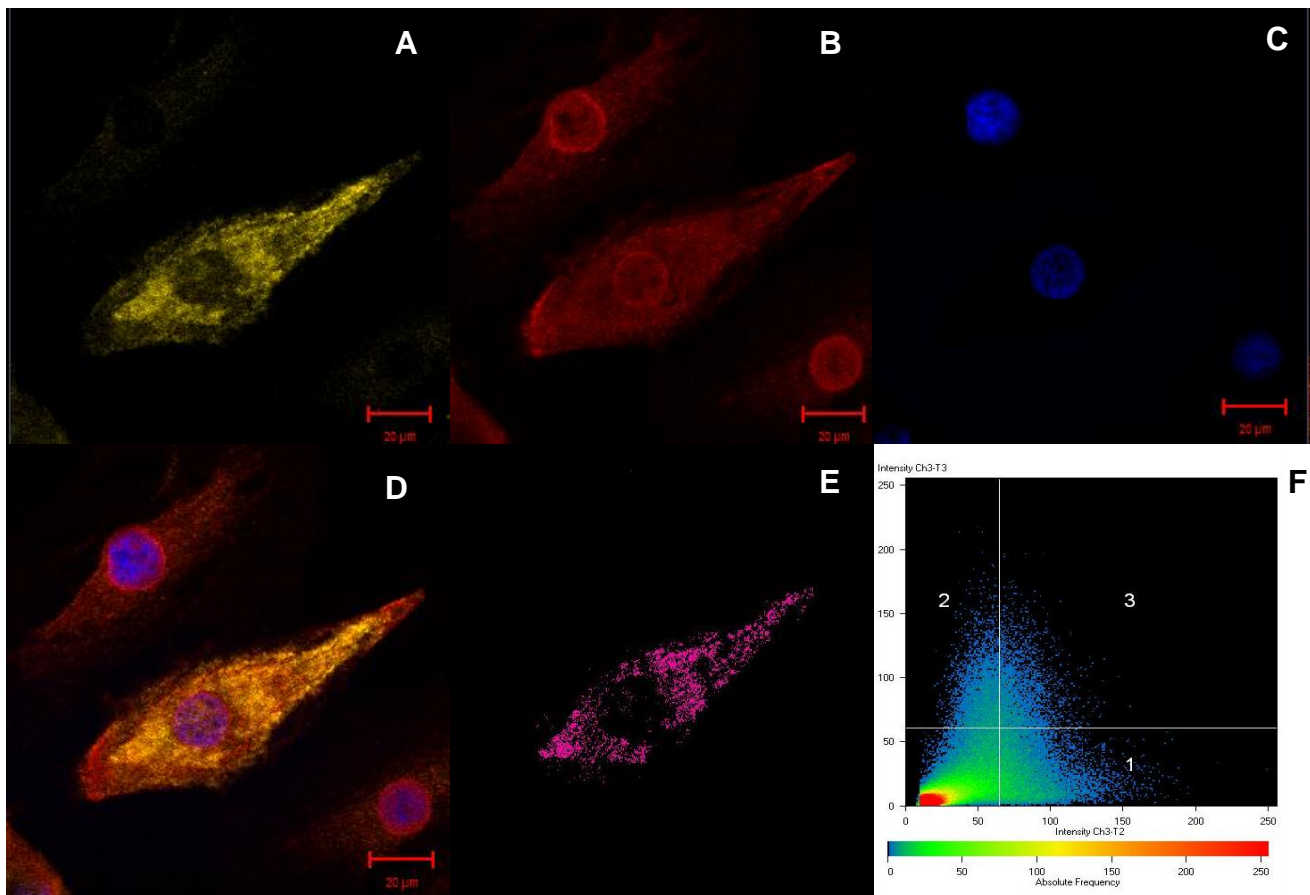


Figure 3.4 Fluorescent imaging and co-localisation analysis of MyBPH and UBC9 in differentiated H9c2 cardiomyocytes. **(A)** MyBPH labelled with a donkey anti-mouse Cy5 secondary antibody (Yellow). **(B)** MYH7 labelled with a donkey anti-goat Cy3 secondary antibody (Red). **(C)** Nucleus labelled with Hoechst H-33342 (Blue). **(D)** Overlay of images A-C. **(E)** Co-localisation of MyBPH and UBC9 generated from merged images (Pink). **(F)** Scatter diagram generated by co-localisation analysis with quadrant three representing the degree of co-localisation. Scale bar 20 μ m.

Table 3.7 Quantification of co-localisation for the interaction between MyBPH and UBC9.

Weighted Co-localisation Coefficient Ch3-T2	Weighted Co-localisation Coefficient Ch3-T3	Overlap Coefficient	Correlation R	Correlation R x R
0.1403	0.3344	0.9500	-0.0542	0.0058

3.3 Co-immunoprecipitation (Co-IP) of MyBPH and putative interactors as identified by Y2H analysis

The interactions of MyBPH with the three putative interactors were further verified in a cellular context in the absence of the GAL4 DNA binding and activating domains by using Co-IP (pull-down assays) analyses in differentiated H9c2 rat cardiomyocytes. Commercial antibodies (section 2.15.2) against endogenous MyBPH, MYH7, ACTC1 and UBC9 were used to detect these proteins in all subsequent pull-down assays.

The results obtained from Co-IP studies show that MyBPH interacts with MYH7, ACTC1 and UBC9 within the context of whole protein lysate from a cell population, without the presence of the GAL4 DNA binding domains continually present in yeast. All negative controls (protein G agarose control and immunoprecipitation with “non-relevant” antibody that served as negative control) were clear in each experiment, suggesting that these results represent direct protein-protein interactions between the relevant proteins.

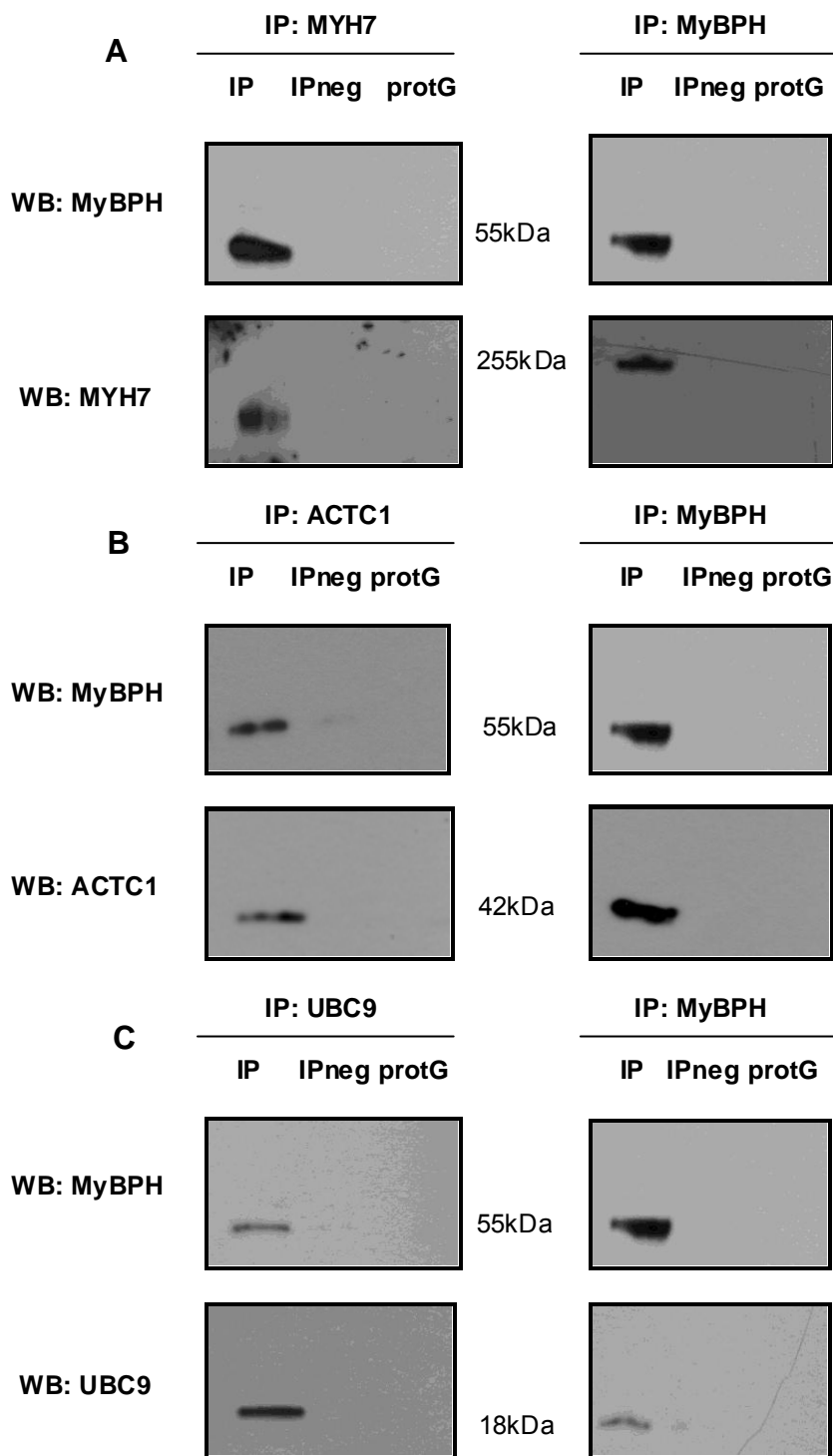


Figure 3.5 Western blots of Co-IP of MyBPH and putative interactors (A) MYH7, (B) ACTC1 and (C) UBC9 in differentiated H9c2 rat cardiomyocytes. Reciprocal Co-IP reactions were performed for each interaction. **Abbreviations:** ACTC1, cardiac α -actin; IP, immunoprecipitation; IPneg, immunoprecipitation using “non-relevant” antibody as negative control; kDa, kilo dalton; MyBPH, myosin binding protein H; MYH7, cardiac β -myosin heavy chain; UBC9, SUMO-conjugating enzyme UBC9; WB, western blot; protG, protein G agarose control

3.4 Super resolution microscopy implicates MyBPH and cMyBPC in the process of autophagy

The observation of small circular structures upon staining of differentiated H9c2 rat cardiomyocytes with anti-MyBPH antibody (Figure 3.6) encouraged further investigation, as the nature of the structures suggested that these were in fact autophagosomes. To confirm this suspicion, super resolution imaging was used to determine whether MyBPH co-localised with LC3b-II, a specific autophagosomal membrane protein (section 2.11.3 and section 2.16.1). Furthermore, since MyBPH and cMyBPC are so similar, the possible co-localisation between LC3b-II and cMyBPC was also investigated.

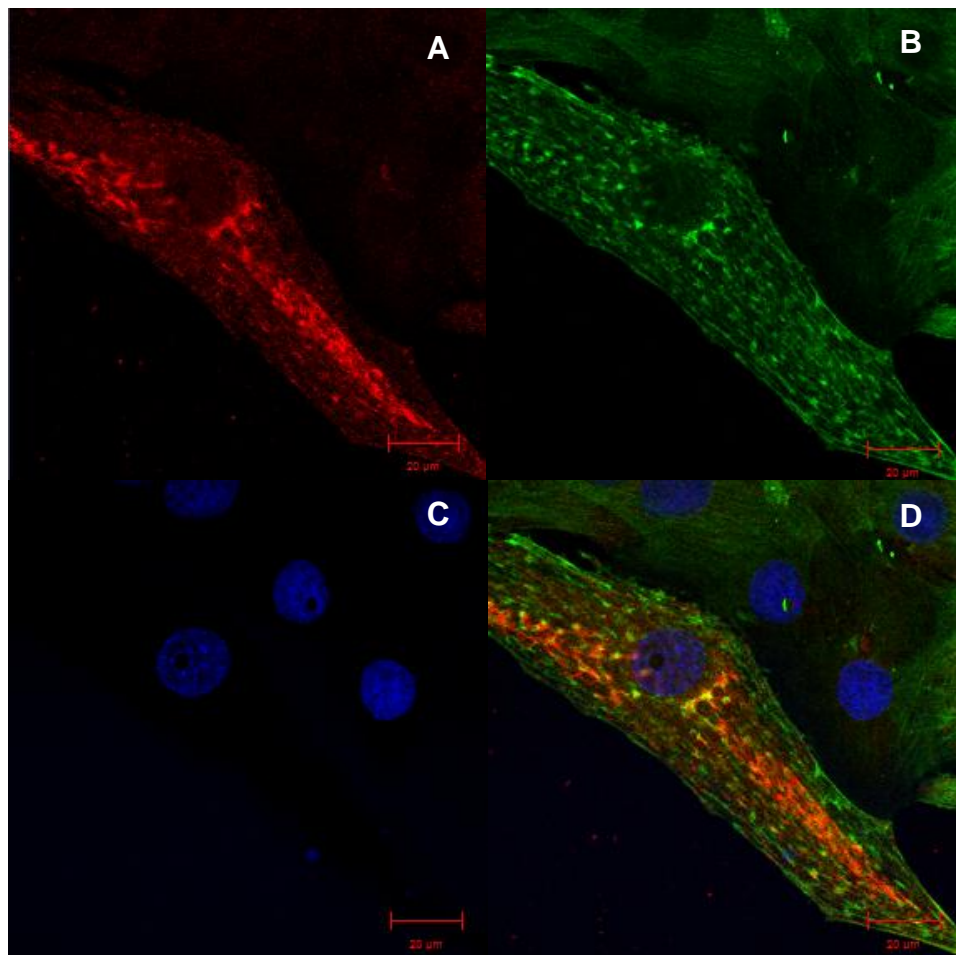


Figure 3.6 Fluorescent imaging of MyBPH and ACTC1 in differentiated H9c2 rat cardiomyocytes. (A) MyBPH labelled with a donkey anti-mouse Cy3 secondary antibody (Red). (B) ACTC1 labelled with a donkey anti-rabbit Alexa Fluor 488 secondary antibody (Green). (C) Nucleus labelled with Hoechst H-33342 (Blue). (D) Overlay of images A-C. Scale bar 20 μm.

Interestingly, MyBPH and cMyBPC co-localised with LC3b-II, suggesting that these proteins may be implicated in the maturation process of autophagosome formation by being recruited to the autophagosomal membrane (Figure 3.7, Figure 3.8).

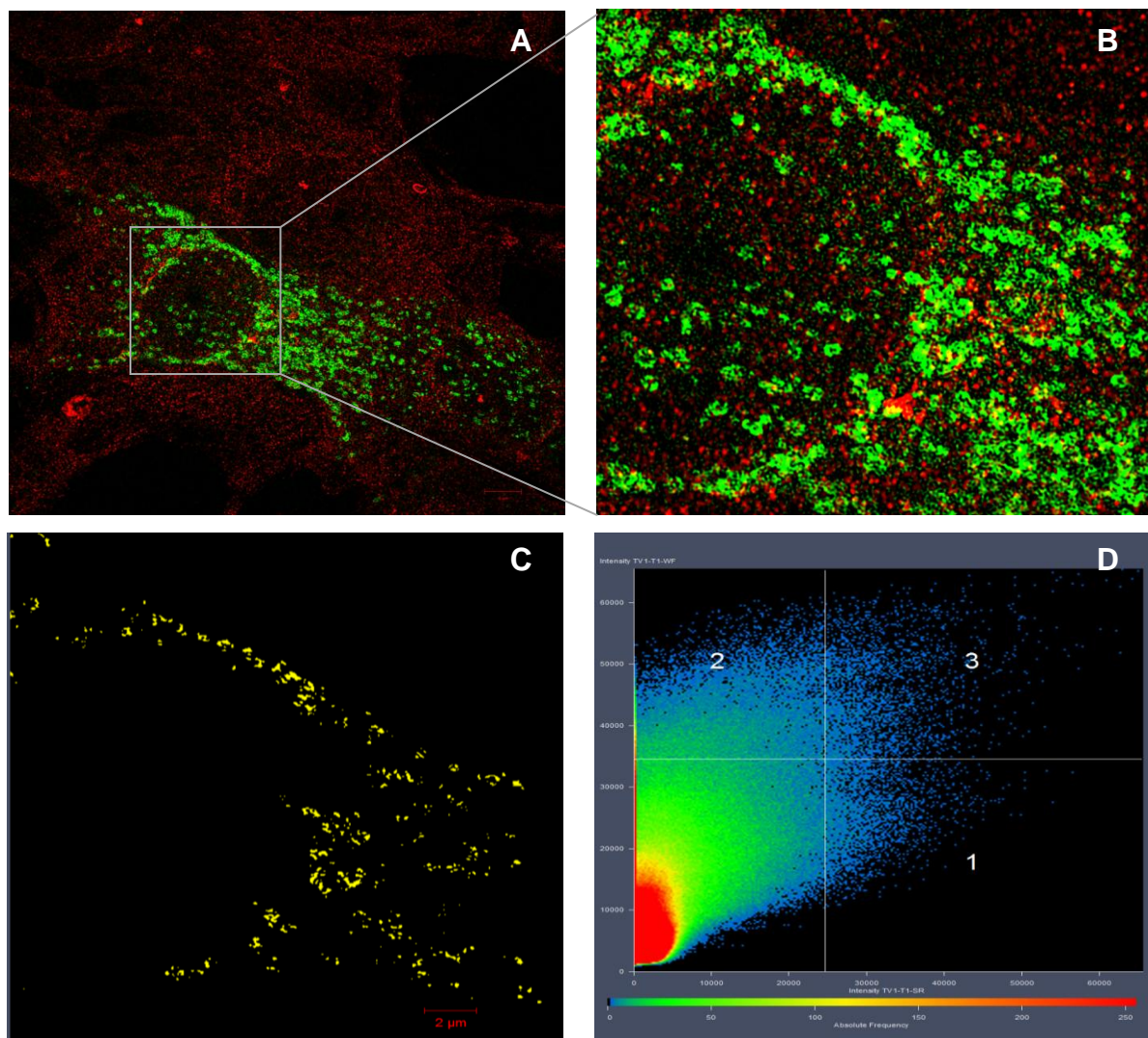


Figure 3.7 Super resolution imaging and co-localisation analysis of MyBPH and LC3b-II_GFP in differentiated H9c2 rat cardiomyocytes. (A) MyBPH labelled with a donkey anti-mouse Cy3 secondary antibody (Red), GFP-tagged LC3b-II (Green). (B, C) Enlarged image. (D) Co-localisation of MyBPH and GFP-tagged LC3b-II generated from merged images (Yellow). Scale bar 10 μ m (A) and 2 μ m (B, C).

Table 3.8 Quantification of co-localisation for the interaction between MyBPH and LC3b-II.

Weighted Co-localisation Coefficient TV1-T1-SR	Weighted Co-localisation Coefficient TV1-T1-WF	Overlap Coefficient	Correlation R	Correlation R x R
0.4820	0.3090	0.0000	0.6600	0.4400

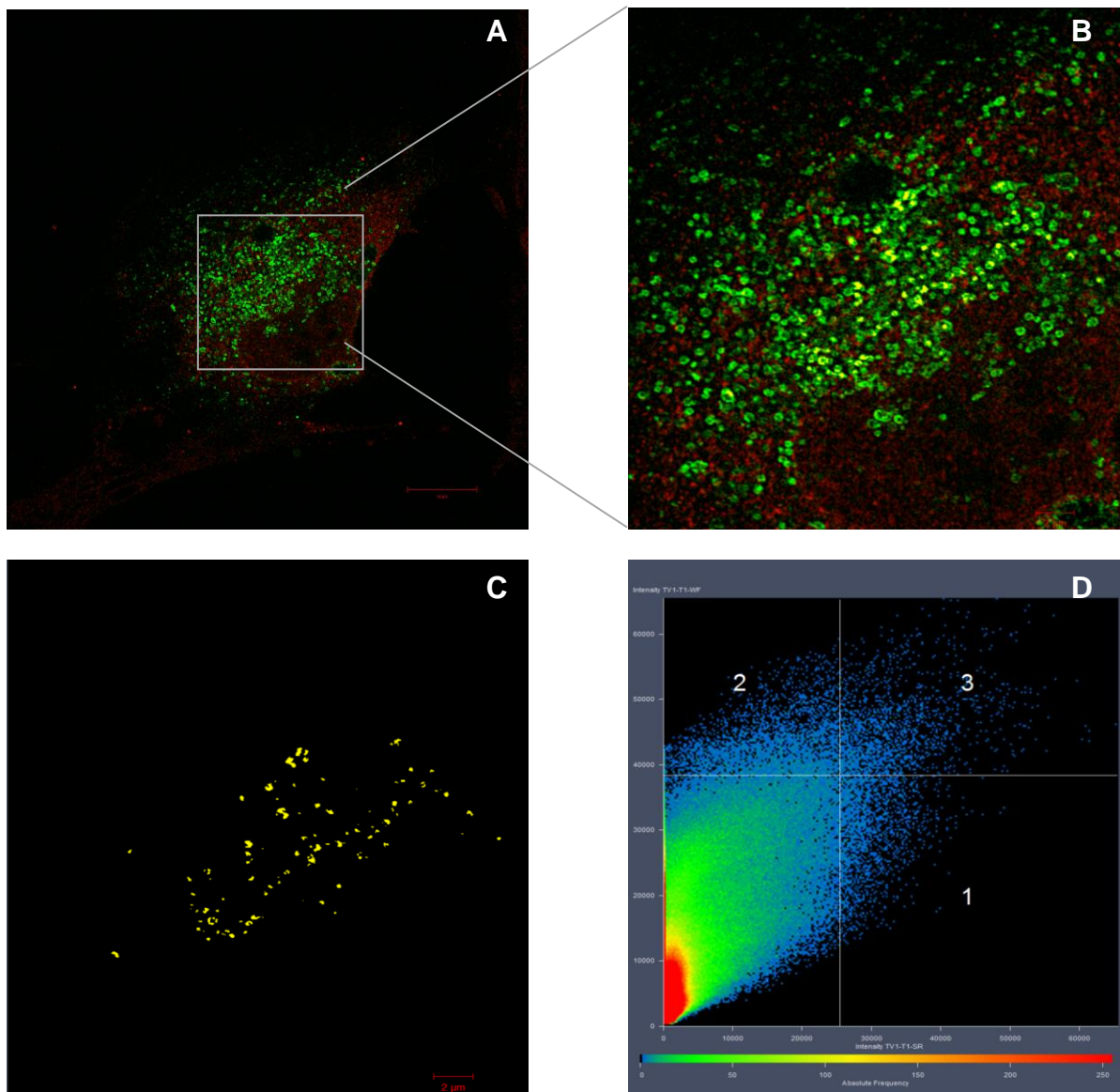


Figure 3.8 Super resolution imaging and co-localisation analysis of cMyBPC and LC3b-II_GFP in differentiated H9c2 rat cardiomyocytes. (A) cMyBPC labelled with a donkey anti-rabbit Cy3 secondary antibody (Red), GFP-tagged LC3b-II (Green). **(B, C)** Enlarged image. **(D)** Co-localisation of MyBPH and GFP-tagged LC3b-II generated from merged images (Yellow). Scale bar 10 μ m (A) and 2 μ m (B, C).

Table 3.9 Quantification of co-localisation for the interaction between cMyBPC and LC3b-II.

Weighted Co-localisation Coefficient TV1-T1-SR	Weighted Co-localisation Coefficient TV1-T1-WF	Overlap Coefficient	Correlation R	Correlation R x R
0.4820	0.3090	0.0000	-0.6600	0.4400

3.5 RNAi-mediated MyBPH and cMyBPC knockdowns

The limited information available on the role that MyBPH plays in the sarcomere, and on its possible role in hypertrophic cardiomyopathy, prompted us to further investigate the function of MyBPH by RNAi-mediated knockdown analysis. Given the sequence homology and similarity in structure between cMyBPC and MyBPH, we proposed that cMyBPC could compensate for the knockdown of MYBPH, and vice versa, and may play critical roles in the structure and functionality of the cardiac sarcomere, and consequently may be involved in HCM pathogenesis.

3.5.1 Optimisation of MyBPH and cMyBPC siRNA knockdowns

Fluorescent imaging confirmed differential expression of MyBPH at three different time points during differentiation of H9c2 rat cardiomyocytes. The expression of MyBPH after 24 hours of differentiation was relatively low (Figure 3.9 A-C) compared to the expression of MyBPH after 5 and 8 days of differentiation (Figure 3.9 D-F and Figure 3.9 G-I). Subsequently, the optimal differentiation time of H9c2 rat cardiomyocytes for knockdown experiments were determined to be 5 or 8 days.

The optimal siRNA concentration and point of differentiation for siRNA-mediated knockdown experiments were determined using Alexa Fluor 488-labelled NSC siRNA. Results indicated that transfecting the cells with 200ng siRNA after 5 days of differentiation were the optimal conditions for the siRNA-mediated knockdown experiment, as markedly more of the Alexa Fluor 488-labelled NSC siRNA was visible upon fluorescent microscope imaging under these conditions (Figure 3.10 A-D).

siRNA-mediated knockdown analyses allowed identification of one of four different siRNAs specific to MyBPH (siRNA type *H1*, *H2*, *H3* and *H4*) (Qiagen, Hilden, Germany), and to cMyBPC (siRNA type *C1*, *C2*, *C3* and *C4*) (Qiagen, Hilden, Germany), *H3* siRNA and *C3* siRNA, respectively, that provided optimal knockdown of MyBPH at 48 hours and cMyBPC at 24 hours after transfection in differentiated H9c2 rat cardiomyocytes. As a result of *H3* siRNA transfection, significantly diminished expression of MyBPH compared to that seen in the NSC was observed ($52.87\% \pm 3.927\%$, $p < 0.05$; Figure 3.11). Similarly, RNAi-mediated knockdown using siRNA *C3* resulted in significantly decreased expression of cMyBPC compared to the NCS ($45.66 \pm 6.110\%$, $p < 0.05$; Figure 3.12). In all subsequent knockdown experiments, siRNAs *H3* and *C3* were used to silence MyBPH and cMyBPC expression.

A significant difference in MyBPH expression was observed between the cells treated with concurrent knockdowns of MyBPH and cMyBPC and the NSC-treated cells ($47.64 \pm 7.779\%$, $p < 0.05$; Figure 13.13). In addition, cMyBPC expression was significantly decreased compared to the expression in the NSC ($40.79 \pm 6.017\%$, $p < 0.05$; Figure 13.14).

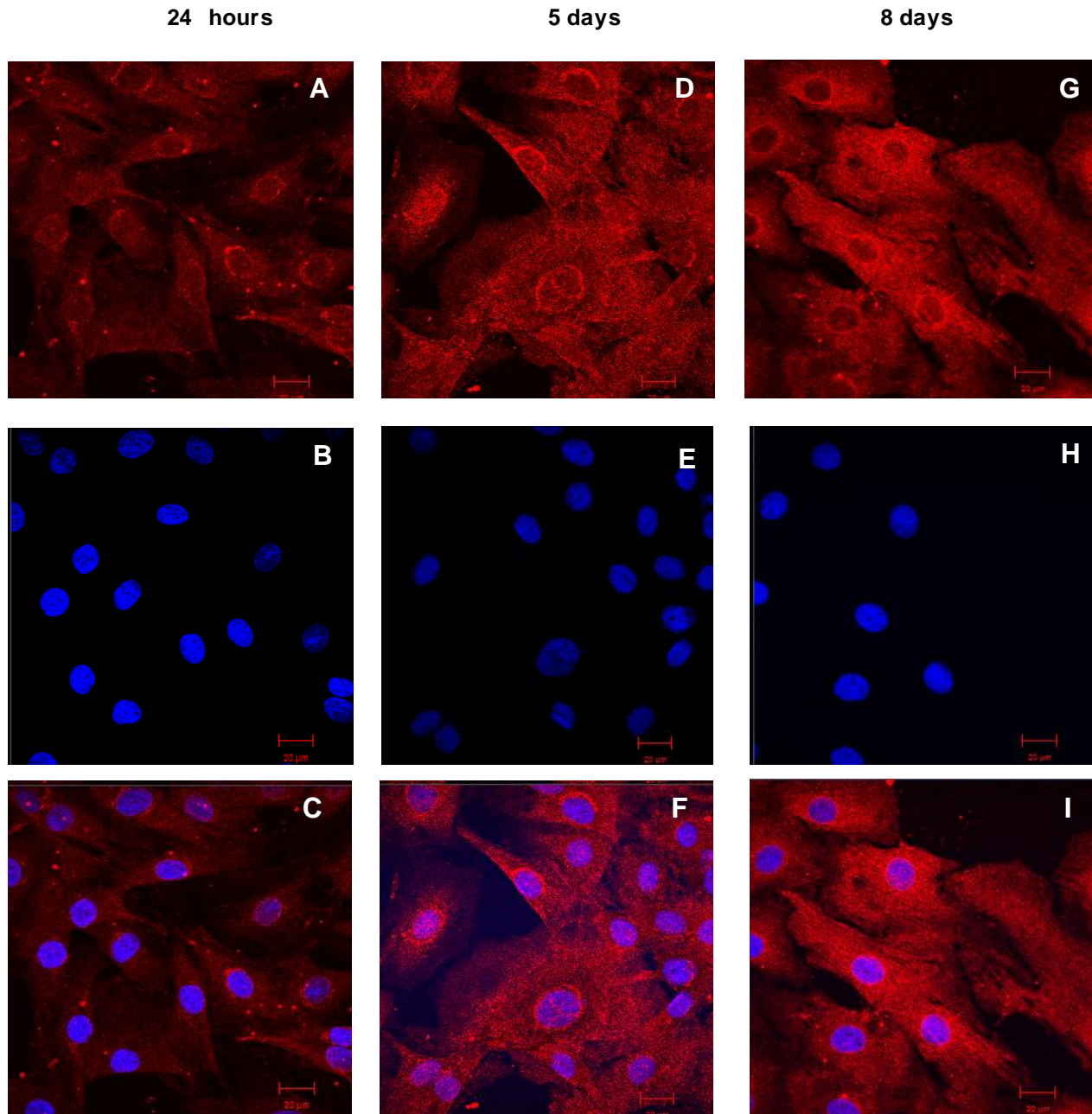


Figure 3.9 Fluorescent imaging of MyBPH in differentiated H9c2 rat cardiomyocytes after 24 hours of differentiation (A-C), after 5 days of differentiation (D-F) and after 8 days of differentiation (G-I). (A, D, G) MyBPH labelled with a donkey anti-mouse Cy3 secondary antibody (Red). (B, E, H) Nucleus labelled with Hoechst H-33342 (Blue). (C, F, I) Overlay images. Scale bar 20 µm.

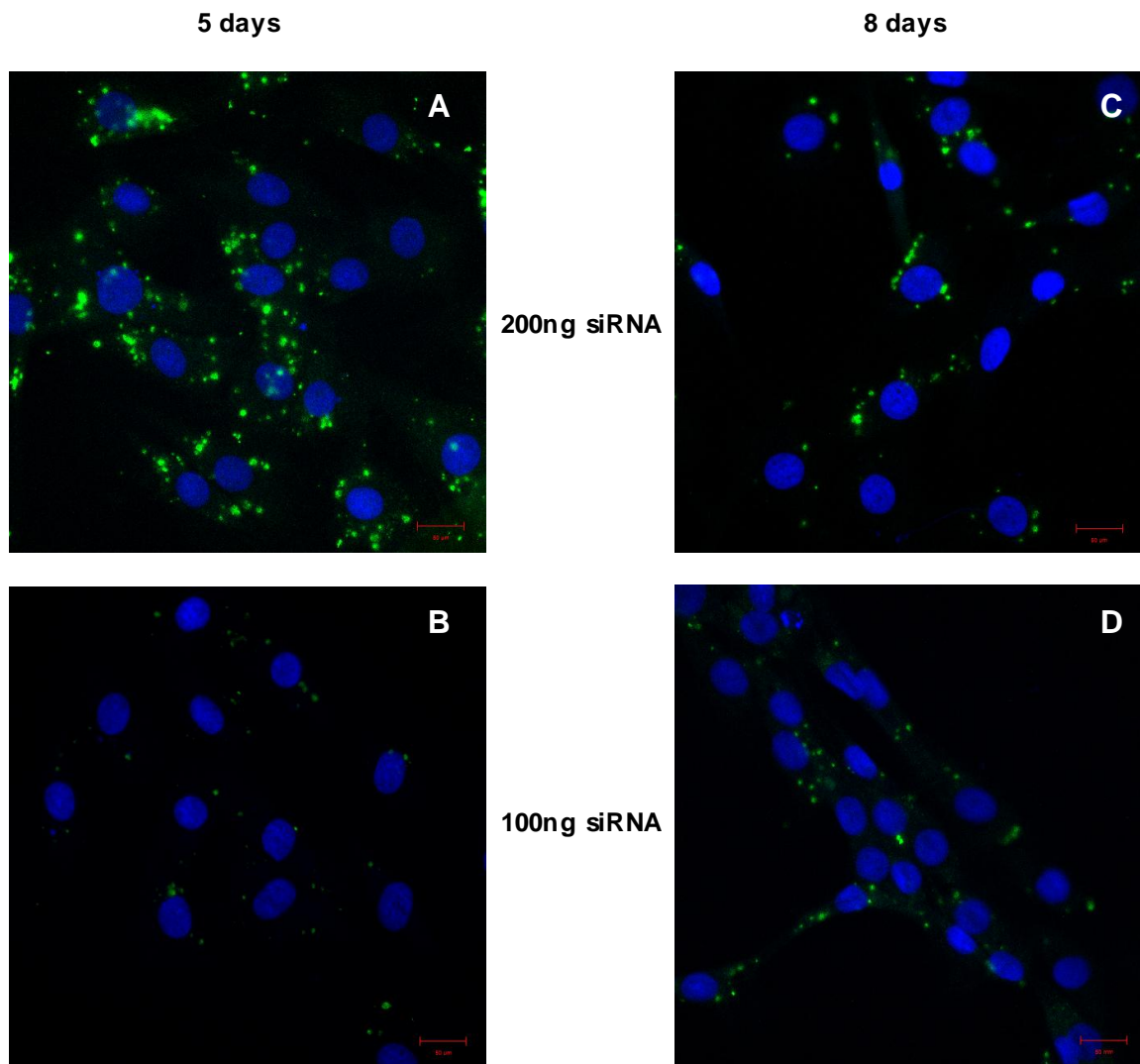


Figure 3.10 Fluorescent imaging of Alexa Fluor 488-labelled NSC siRNA after 24 hours of transfection in H9c2 rat cardiomyocytes that was differentiated for 5 days (A, B) and 8 days (C, D). (A - D) NSC siRNA tagged with Alexa Fluor 488 (Green) and nucleus labelled with Hoechst H-33342 (Blue). Scale bar 50μm. **Abbreviations:** ng, nanogram; siRNA, small interfering RNA

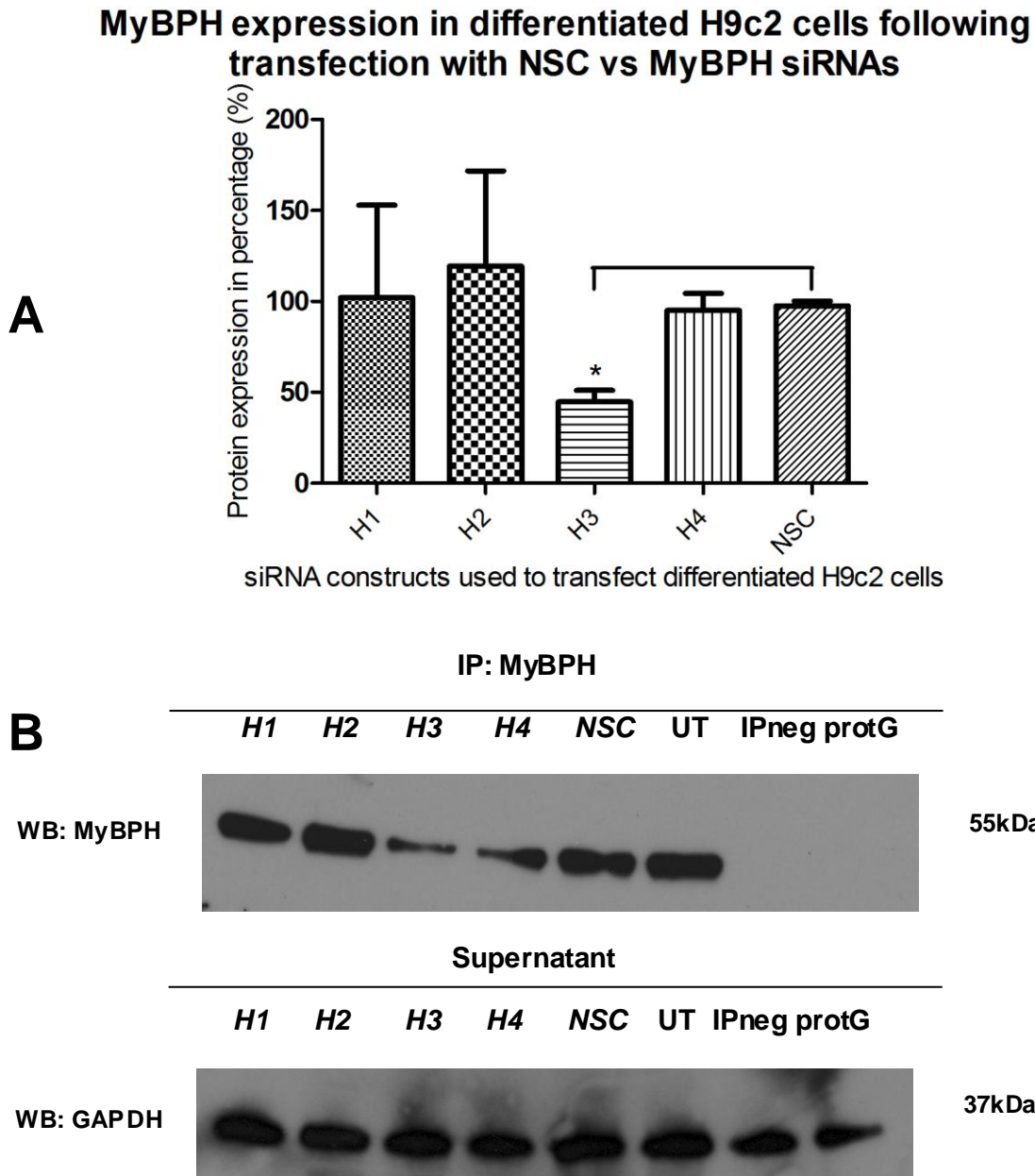
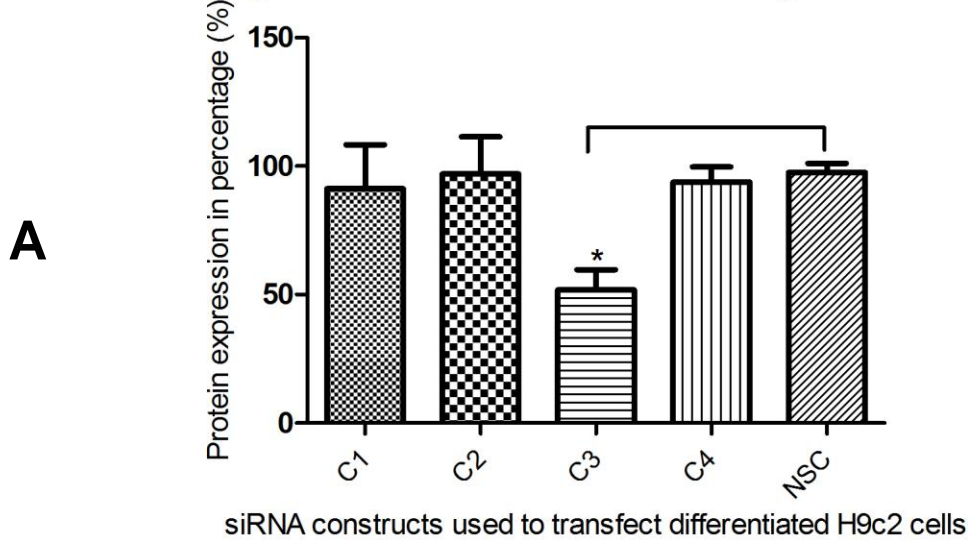


Figure 3.11 Western blotting quantification of MyBPH in differentiated H9c2 rat cardiomyocytes transfected with either a NSC or a particular MyBPH siRNA. The siRNA *H3* resulted in optimal knockdown of MyBPH. Data presented are the mean \pm SEM, representative of three independent experiments, * $p < 0.05$ vs control. **Abbreviations:** GAPDH, glyceraldehyde 3-phosphate dehydrogenase; *H1*, siRNA type H1 specific to MyBPH; *H2*, siRNA type H2 specific to MyBPH; *H3*, siRNA type H3 specific to MyBPH; *H4*, siRNA type H4 specific to MyBPH; IPneg, immunoprecipitation using “non-relevant” antibody as negative control; kDa, kilo dalton; NSC, non-silencing control, MyBPH, myosin binding protein; protG, protein G agarose control; siRNA, small interfering RNA; UT, transfection control; WB, western blot

cMyBPC expression in differentiated H9c2 cells following transfection with NSC vs cMyBPC siRNAs



B

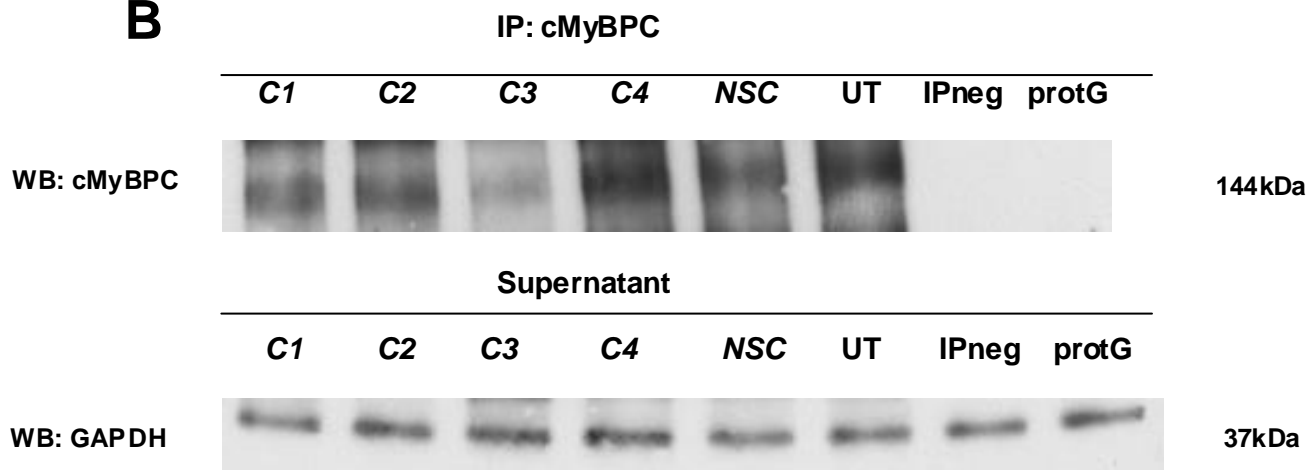


Figure 3.12 Western blotting quantification of cMyBPC in differentiated H9c2 rat cardiomyocytes transfected with either a NSC or a particular cMyBPC siRNA. The siRNA C3 resulted in optimal knockdown of cMyBPC. Data presented are the mean \pm SEM, representative of three independent experiments, * $p < 0.05$ vs control. **Abbreviations:** cMyBPC, cardiac myosin binding protein C; **C1**, siRNA type C1 specific to cMyBPC; **C2**, siRNA type C2 specific to cMyBPC; **C3**, siRNA type C3 specific to cMyBPC; **C4**, siRNA type C4 specific to cMyBPC; **GAPDH**, glyceraldehyde 3-phosphate dehydrogenase; **IPneg**, immunoprecipitation using “non-relevant” antibody as negative control; **NSC**, non-silencing control; **protG**, protein G agarose control; **siRNA**, small interfering RNA; **UT**, transfection control; **WB**, western blot

MyBPH expression in differentiated H9c2 cells following transfection with NSC vs concurrent MyBPH and cMyBPC siRNAs

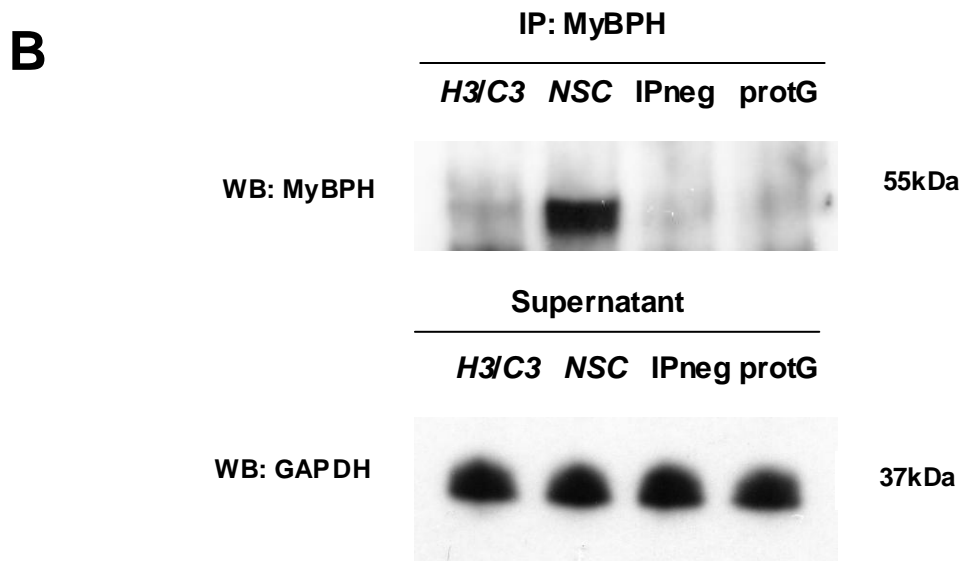
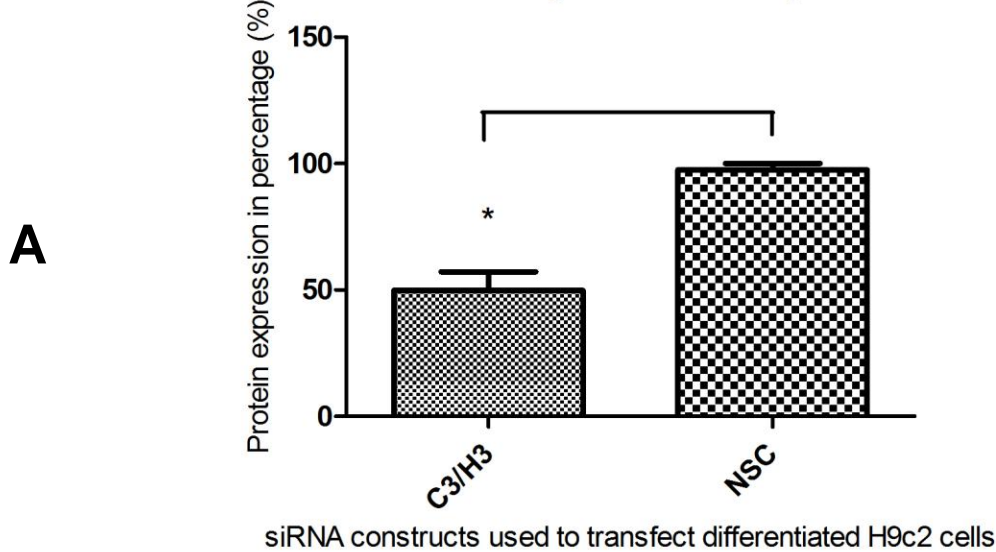
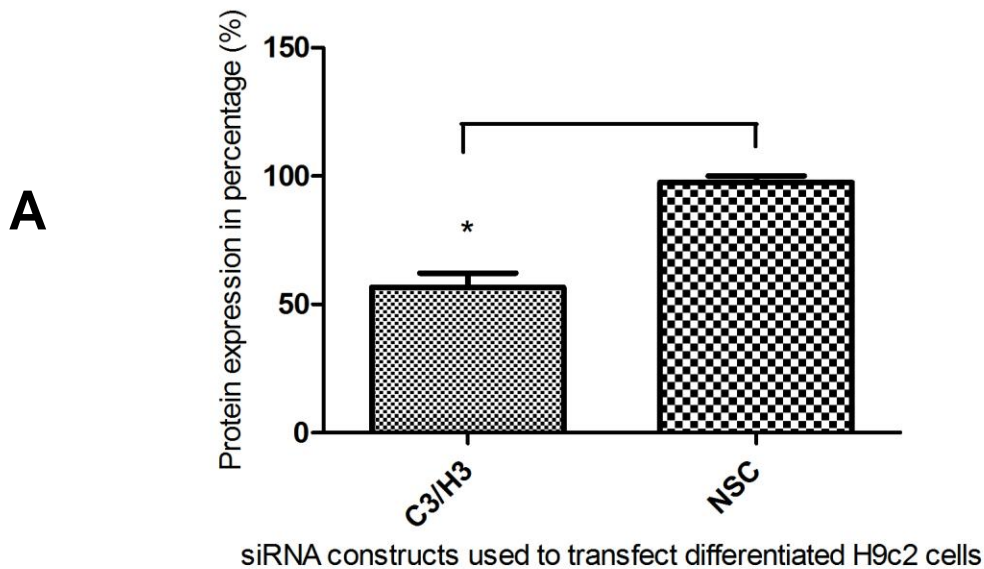


Figure 3.13 Western blotting quantification of MyBPH in differentiated H9c2 rat cardiomyocytes transfected with either a NSC or H3, and C3 MyBPH and cMyBPC siRNAs concurrently. The concurrent transfection of siRNA H3 and C3 resulted in optimal knockdown of MyBPH. Data presented are the mean \pm SEM, representative of three independent experiments, * $p < 0.05$ vs control. **Abbreviations:** cMyBPC, cardiac myosin binding protein C; C3, siRNA type C3 specific to cMyBPC; GAPDH, glyceraldehyde 3-phosphate dehydrogenase; H3, siRNA type H3 specific to MyBPH; IPneg, immunoprecipitation using “non-relevant” antibody as negative control; kDa, kilo dalton; NSC, non-silencing control; MyBPH, myosin binding protein H; protG, protein G agarose control; siRNA, small interfering RNA; UT, transfection control; WB, western blot

cMyBPC expression in differentiated H9c2 cells following transfection with NSC vs concurrent MyBPH and cMyBPC siRNAs



B

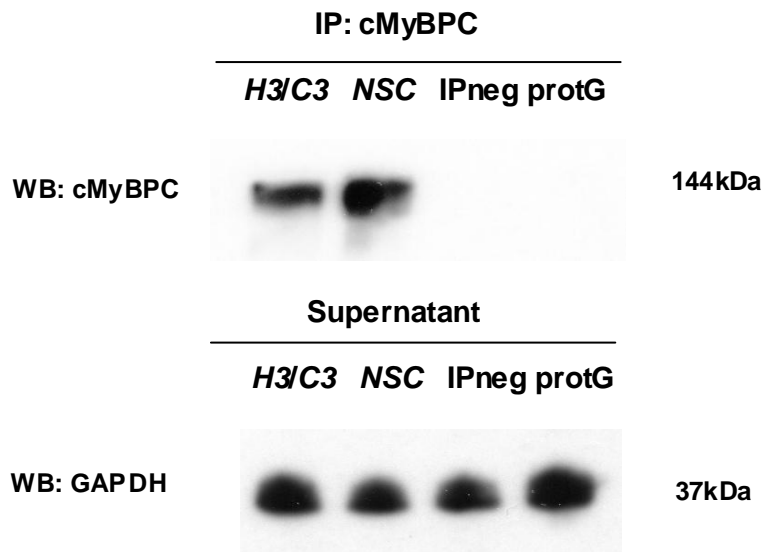
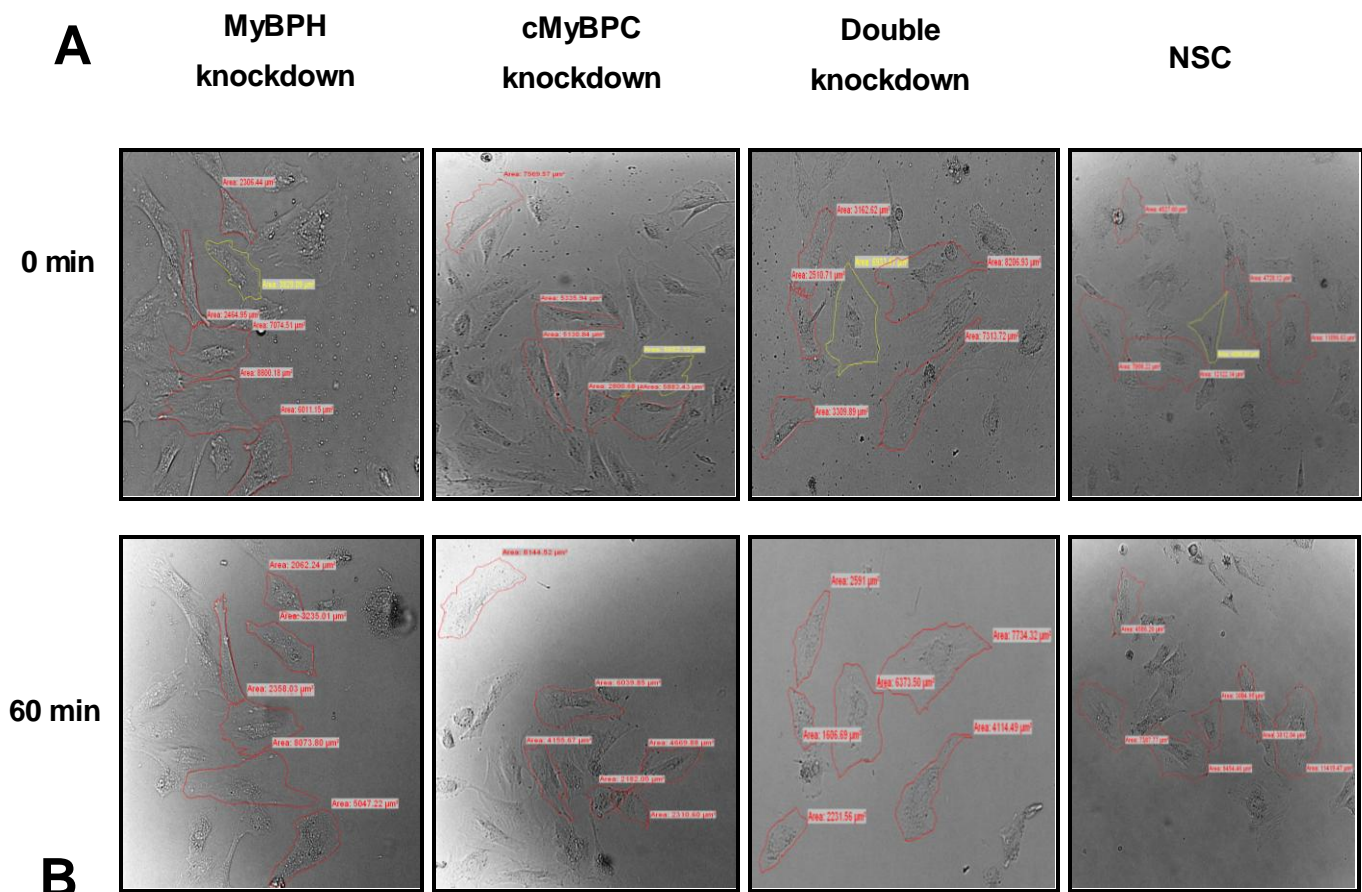


Figure 3.14 Western blotting quantification of cMyBPC in differentiated H9c2 rat cardiomyocytes transfected with either a NSC or H3, and C3 MyBPH and cMyBPC siRNAs concurrently. The concurrent transfection of siRNA H3 and C3 resulted in optimal knockdown of MyBPC. Data presented are the mean \pm SEM, representative of three independent experiments, * $p < 0.05$ vs control. **Abbreviations:** cMyBPC, cardiac myosin binding protein C; C3, siRNA type C3 specific to cMyBPC; GAPDH, glyceraldehyde 3-phosphate dehydrogenase; H3, siRNA type H3 specific to MyBPH; IPneg, immunoprecipitation using “non-relevant” antibody as negative control; MyBPH, myosin binding protein H; NSC, non-silencing control; protG, protein G agarose control; siRNA, small interfering RNA; UT, transfection control; WB, western blot

3.5.2 Effect of MyBPH and cMyBPC knockdowns on contractility

Given that the interactions between MyBPH and two sarcomeric proteins (ACTC1 and MyH7) are known to play crucial roles in regulating cardiac contractility, it was hypothesised that MyBPH itself may be involved in cardiac contractility. To test this hypothesis, the ability of cardiomyocytes to contract efficiently following siRNA-mediated knockdown of MyBPH was assessed. However, because of the sequence homology between MyBPH and cMyBPC, it was decided to assess the effect of the knockdown of both MyBPH and cMyBPC, individually and concurrently (section 2.17) on cardiac contractility. To detect whether differentiated H9c2 rat cardiomyocytes could still contract in the presence of significantly reduced expression of MyBPH and cMyBPC, the percentage planar cell surface area was measured in a live cell contractility assay in response to β -adrenergic stimulation. The β -adrenergic stimulation was necessary to induce contraction of the H9c2 cells. The results in Figure 3.15 represent three individual experiments and the average percentage planar cell surface area of six cells per image.

Results show that the individual knockdown of MyBPH and cMyBPC did not result in significantly different percentage planar cell surface area in response to adrenergic stimulation, compared to the NSC (Figure 3.15). However, interestingly a statistically significant difference in planar cell surface area was observed when both MyBPH and cMyBPC were knocked down concurrently (Figure 3.15) ($51.35 \pm 10.978\%$, $p < 0.05$), when compared to the NSC. These results suggest that these two proteins are both involved in the contractility of cardiomyocytes and that a degree of compensation was achieved when only one of them was knocked down at a time.



Effect of MyBPH and cMyBPC on change in planar cell surface area in response to 0.1 μ M isoproterenol

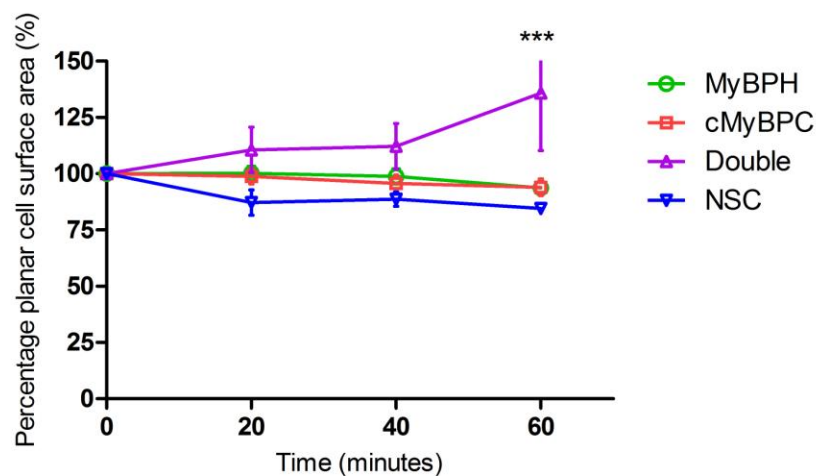


Figure 3.15 Effect of MyBPH and cMyBPC knockdown in differentiated H9c2 rat cardiomyocytes in response to β -adrenergic stimulation. (A) siRNA transfected H9c2 cells before (0 minutes) and after (60 minutes) stimulation by isoproterenol representing the change in planar cell surface area in each group. **(B)** The differences between the four groups as the mean \pm SEM ($n=6$ per group) of three independent experimental repeats. The percentage planar cell surface area differed significantly in the double knockdown group from the NSC (***) ($p < 0.05$). **Abbreviations:** **Double**, knockdown of both cMyBPC and MyBPH; **cMyBPC**, myosin binding protein C; **MyBPH**, myosin binding protein; **NSC**, non-silencing control

RESULTS: MODIFIER STUDY

3.6 Basic cohort characteristics

All 388 study participants included in our study were tested for each of the three South African HCM-causing founder mutations. No individual was found to be compound heterozygous for any of the HCM founder mutations. Furthermore, 256 of the study participants were clinically assessed and the details of the basic characteristics of the cohort are summarised in Table 3.10. Participants are grouped according to their HCM-causing founder mutation carrier status, mutation carrier (MC) and non-carrier (NC).

Table 3.10 Basic characteristics of the study cohort. Individuals are grouped according to the relevant HCM founder mutation and mutation status as either mutation carrier (MC) or non-carrier (NC).

	A797T _{MYH7}		R92W _{TNNT2}		R403W _{MYH7}	
	MC	NC	MC	NC	MC	NC
n	68,0	50,0	48,0	34,0	32,0	24,0
Age	43,0 (26,8-56,8)	41,5 (29,3-53,0)	36,0 (21,0-47,0)	42,0 (25,5-49,0)	36,5 (25,0-46,8)	38,0 (31,3-50,8)
BSA (m²)	1,90 (1,6-2,0)	1,90 (1,7-2,0)	1,7 (1,6-1,8)	1,80 (1,60-1,90)	1,80 (1,7-2,0)	1,95 (1,70-2,05)
SBP (mm Hg)	120,0 (115,0-134,0)	120,0 (110,0-130,0)	115,0 (110,0-130,0)	120,0 (110,0-120,0)	120,0 (115,0-130,0)	120,0 (114,0-143,0)
DBP (mm Hg)	80,0 (70,0-87,0)	80,0 (80,0-89,0)	73,0 (70,0-80,0)	80,0 (70,0-80,0)	80,0 (79,0-80,0)	80,0 (78,0-90,0)
HR (bpm)	68,0 (60,0-75,0)	68,0 (62,0-76,0)	68,0 (61,0-76,0)	67,0 (60,0-73,0)	65,0 (60,0-76,0)	72,0 (65,0-84,0)
LVM (g)	191,0 (135,0-237,0)	135,0 (109,0-159,0)	146,0 (104,0-185,0)	116,0 (100,0-144,0)	170,0 (134,0-205,0)	154,0 (115,0-202,0)
mIVST (mm)	14,5 (11,0-20,9)	10,5 (9,2-11,3)	14,0 (9,6-18,3)	10,0 (8,6-10,9)	13,6 (11,6-16,0)	11,0 (10,2-12,6)
mLVWT (mm)	14,0 (11,0-20,7)	10,5 (9,5-11,3)	13,4 (9,9-18,1)	10,0 (9,2-10,9)	13,6 (11,6-17,8)	11,2 (10,2-12,4)
mPWT (mm)	10,2 (9,1-11,8)	9,0 (8,3-10,0)	10,2 (8,1-11,5)	8,1 (7,5-9,1)	10,1 (9,1-11,5)	9,9 (8,8-10,4)
PC1	2,1 (-0,1-4,9)	-1,3 (-2,5--0,0)	0,9 (-2,6-2,7)	-2,6 (-4,3--1,0)	1,4 (-0,3-2,4)	0,1 (-2,0-1,4)

Abbreviations: **A**, alanine; **bpm**, beats per minute; **BSA**, body surface area; **DBP**, diastolic blood pressure; **g**, gram; **HCM**, hypertrophic cardiomyopathy; **Hg**, mercury; **HR**, heart rate; **LVM**, left ventricular mass; **m²**, per square metre; **MC**, HCM mutation carrier; **mIVST**, maximum interventricular septal thickness; **mLVWT**, maximum left ventricular wall thickness; **mPWT**, maximum posterior wall thickness; **mm**, millimetre; **MYH7**, cardiac β -myosin heavy chain; **NC**, non-carrier; **n**, number of clinically evaluated participants; **PC1**, first principal component; **R**, arginine; **SBP**, systolic blood pressure; **T**, Threonine; **TNNT2**, troponin T gene 2, cardiac; **W**, tryptophan

3.7 Candidate gene selection and SNP prioritisation

Yeast two-hybrid analyses identified three MyBPH-interacting proteins: ACTC1, MYH7 and UBC9. Subsequently, the genes encoding these proteins (*ACTC1*, *MYH7* and *UBC9*), as well as *MYBPH*, were assessed for their potential role as hypertrophy modifiers in the present study. SNPs in each of these genes were selected to achieve 0.5 LDU even spacing throughout the candidate genes and to include all tagSNPs in these genes, in the Central European (CEU) and Yoruba (YRI) populations. Table 3.11 details the 38 SNPs selected for each of the four candidate genes selected and their MAFs for the CEU and YRI populations.

Table 3.11 The SNPs chosen for investigation in this study and their MAF in the CEU and YRI populations.

Candidate Gene	Chromosome Location	SNP ID	Nucleotide Change	MAF*	
				CEU	YRI
<i>MyBPH</i>	1q32.1	rs2642531	G/C	0,208 (C)	0,417 (G)
		rs4950926	G/A	0,343 (A)	0,000 (A)
		rs7545750	T/A	0,044 (A)	0,127 (A)
		rs2250509	C/A	0,100 (A)	0,217 (A)
		rs2791718	C/A	0,158 (A)	0,458 (A)
		rs3737872	T/C	0,415 (C)	0,017 (C)
		rs762625	C/T	0,142 (T)	0,358 (T)
		<i>MYH7</i>	14q11.2	rs12147570	G/T
rs3729833	C/T			0,169 (T)	0,367 (T)
rs765019	T/C			0,108 (C)	0,212 (C)
rs3729832	T/A			0,108 (A)	0,217 (A)
rs7140721	G/A			0,333 (A)	0,192 (G)
rs3729825	C/T			0,167 (C)	0,356 (A)
rs7159367	T/C			0,333 (C)	0,175 (T)
rs10136106	G/A			0,083 (A)	0,342 (A)
rs2277475	A/T			0,333 (T)	0,233 (A)
rs12147533	A/G			0,167 (G)	0,150 (G)
rs743567	T/G			0,325 (C)	0,183 (A)
rs7157087	C/T			0,000 (T)	0,229 (T)
rs7155989	G/A			0,000 (A)	0,102 (A)
rs1951154	G/A			0,308 (A)	0,025 (A)
rs2754163	T/C			0,300 (C)	0,308 (T)
rs3729810	A/G			-	-
rs2239578	A/G			0,442 (G)	0,342 (A)
rs2239577	C/G			0,075 (G)	0,483 (G)
rs17092326	G/A	0,075 (A)	0,367 (A)		

Candidate Gene	Chromosome Location	SNP ID	Nucleotide Change	MAF*	
				CEU	YRI
ACTC1	15q14	rs1370154	C/T	0,258 (T)	0,133 (T)
		rs3729755	C/G	0,276 (G)	0,127 (G)
		rs2070664	T/C	0,500 (T)	0,267 (C)
		rs7165006	C/G	0,086 (G)	0,172 (G)
		rs7166484	G/A	0,448 (G)	0,271 (A)
UBC9	16p13.3	rs2281226	C/A	0,375 (A)	0,317 (C)
		rs11248866	A/G	0,388 (G)	0,254 (A)
		rs9933497	G/A	0,100 (A)	0,033 (A)
		rs8052688	G/C	0,192 (C)	0,450 (C)
		rs761059	G/A	0,398 (A)	-
		rs761060	G/A	0,123 (A)	-
		rs8063	G/A	0,308 (A)	0,375 (G)

*Minor allele indicated in brackets

Abbreviations: **A**, adenine; **ACTC1**, cardiac α -actin; **C**, cytosine; **CEU**, Central European; **G**, guanine; **MAF**, minor allele frequency; **MYH7**, cardiac β -myosin heavy chain; **SNP**, single nucleotide polymorphism; **T**, thymine; **UBC9**, SUMO-conjugating enzyme UBC9; **YRI**, Yoruba

3.8 Genotyping results

3.8.1 KASP assay allelic discrimination

Genotyping was performed by KBioscience (LGC Genomics Ltd., Hertz, UK) and genotypes viewed in SNPviewer2 v3.2.2.16. All 38 SNPs for the four candidate genes were successfully genotyped.

3.9 Statistical analyses

3.9.1 Descriptive statistics

Genotyped frequencies of all 38 SNPs genotyped did not deviate from Hardy-Weinberg equilibrium, since their p-values were >0.01 . Minor allele frequencies from a set of 39 unrelated individuals used in the present study were determined using Haploview v4.2 (Barret et al. 2005) and are included, along with MAFs for the CEU and YRI populations in Table 3.12.

Table 3.12 Cohort-specific descriptives. Hardy-Weinberg equilibrium test p-values and MAF for the SNPs investigated.

Candidate Gene	Chromosome Location	SNP ID	HWE p-value	MAF*		
				Study Cohort	CEU	YRI
<i>MyBPH</i>	1q32.1	rs2642531	1,000	0,220 (C)	0,208 (C)	0,417 (G)
		rs4950926	0,305	0,200 (A)	0,343 (A)	0,000 (A)
		rs7545750	0,187	0,080 (A)	0,044 (A)	0,127 (A)
		rs2250509	0,581	0,180 (A)	0,100 (A)	0,217 (A)
		rs2791718	1,000	0,130 (A)	0,158 (A)	0,458 (A)
		rs3737872	0,231	0,260 (C)	0,415 (C)	0,017 (C)
		rs762625	1,000	0,250 (T)	0,142 (T)	0,358 (T)
<i>MYH7</i>	14q11.2	rs12147570	0,192	0,080 (T)	0,109 (T)	0,125 (T)
		rs3729833	0,328	0,100 (T)	0,169 (T)	0,367 (T)
		rs765019	1,000	0,140 (C)	0,108 (C)	0,212 (C)
		rs3729832	1,000	0,140 (A)	0,108 (A)	0,217 (A)
		rs7140721	1,000	0,260 (A)	0,333 (A)	0,192 (G)
		rs3729825	0,336	0,100 (T)	0,167 (C)	0,356 (A)
		rs7159367	1,000	0,260 (C)	0,333 (C)	0,175 (T)
		rs10136106	1,000	0,100 (A)	0,083 (A)	0,342 (A)
		rs2277475	0,395	0,220 (T)	0,333 (T)	0,233 (A)
		rs12147533	0,255	0,090 (G)	0,167 (G)	0,150 (G)
		rs743567	0,395	0,220 (G)	0,325 (C)	0,183 (A)
		rs7157087	1,000	0,070 (T)	0,000 (T)	0,229 (T)
		rs7155989	1,000	0,050 (A)	0,000 (A)	0,102 (A)
		rs1951154	1,000	0,270 (A)	0,308 (A)	0,025 (A)
		rs2754163	0,449	0,260 (C)	0,300 (C)	0,308 (T)
		rs3729810	1,000	0,150 (G)	-	-
		rs2239578	0,520	0,350 (G)	0,442 (G)	0,342 (A)
rs2239577	1,000	0,100 (G)	0,075 (G)	0,483 (G)		
rs17092326	1,000	0,080 (A)	0,075 (A)	0,367 (A)		

Candidate Gene	Chromosome Location	SNP ID	HWE p-value	Study Cohort	MAF	
					CEU	YRI
<i>ACTC1</i>	15q14	rs1370154	0,282	0,290 (T)	0,258 (T)	0,133 (T)
		rs3729755	0,272	0,300 (G)	0,276 (G)	0,127 (G)
		rs2070664	0,684	0,240 (C)	0,500 (T)	0,267 (C)
		rs7165006	0,095	0,120 (G)	0,086 (G)	0,172 (G)
		rs7166484	0,517	0,380 (A)	0,448 (G)	0,271 (A)
<i>UBC9</i>	14q11.2	rs2281226	0,510	0,390 (A)	0,375 (A)	0,317 (C)
		rs11248866	1,000	0,400 (G)	0,388 (G)	0,254 (A)
		rs9933497	1,000	0,060 (A)	0,100 (A)	0,033 (A)
		rs8052688	1,000	0,180 (C)	0,192 (C)	0,450 (C)
		rs761059	0,723	0,290 (A)	0,398 (A)	-
		rs761060	1,000	0,170 (A)	0,123 (A)	-
		rs8063	1,000	0,270 (A)	0,308 (A)	0,375 (G)

*Minor allele indicated in brackets

Abbreviations: **A**, adenine; **ACTC1**, cardiac α -actin; **C**, cytosine; **CEU**, Central European; **G**, guanine; **HWE**, Hardy-Weinberg equilibrium; **MAF**, minor allele frequency; **MYH7**, cardiac β -myosin heavy chain; **p**, short chromosomal arm; **q**, long chromosomal arm; **SNP**, single nucleotide polymorphism; **T**, thymine; **UBC9**, SUMO-conjugating enzyme UBC9; **YRI**, Yoruba

3.9.2 Linkage disequilibrium assessment

Pair-wise LD was estimated for all SNPs genotyped in this cohort using Haploview v4.2 (Barret et al. 2005). The D' values were obtained from a total of 100 consecutive Haploview runs, to provide the median D' values. Two SNPs are considered to be in complete LD if their D' score is equal to 1, which indicates a complete lack of evidence of recombination between two variants. Refer to section 2.22.2 for more details on LD analyses.

The LD results observed in all four candidate genes are graphically represented in Table 3.13 through to Table 3.16. Complete LD ($D'=1$) was observed for the following SNPs highlighted in red, strong LD, indicated by D' values between 0,60 and 0,99 are highlighted in dark pink, and incomplete LD are indicated by D' values lower than 0,60 and are highlighted in light pink.

Table 3.13 Pair-wise LD structure for *MyBPH*. D' values = 1 are highlighted in red, D' values between 0,60 and 0,99 are highlighted in dark pink and D' values < 0,60 are highlighted in light pink.

<i>MYBPH</i>	rs762625	rs3737872	rs2791718	rs2250509	rs7545750	rs4950926	rs2642531
rs2642531	1	0,23	1	1	1	1	
rs4950926	1	0,92	1	1	1		
rs7545750	1	1	1	1			
rs2250509	1	1	1				
rs2791718	1	1					
rs3737872	1						
rs762625							

Table 3.15 Pair-wise LD structure for *ACTC1*. D' values = 1 are highlighted in red, D' values between 0,60 and 0,99 are highlighted in dark pink and D' values < 0,60 are highlighted in light pink.

<i>ACTC1</i>	rs7166484	rs7165006	rs2070664	rs3729755	rs1370154
rs1370154	1,00	0,62	1,00	1,00	
rs3729755	1,00	0,53	1,00		
rs2070664	0,62	1,00			
rs7165006	1,00				
rs7166484					

Table 3.16 Pair-wise LD structure for *UBC9*. D' values = 1 are highlighted in red, D' values between 0,60 and 0,99 are highlighted in dark pink and D' values < 0,60 are highlighted in light pink.

<i>UBC9</i>	rs8063	rs761060	rs761059	rs8052688	rs9933497	rs11248866	rs2281226
rs2281226	1,00	0,74	0,14	1,00	1,00	1,00	
rs11248866	1,00	0,78	0,13	1,00	1,00		
rs9933497	1,00	0,22	1,00	1,00			
rs8052688	0,53	0,09	0,11				
rs761059	0,45	0,14					
rs761060	0,20						
rs8063							

3.9.3 Principal component analysis

Principal component analysis serves as a measure that best represents the variability in left ventricular wall thickness measurements as a single score, which reflects the weighted average of 16 transformed wall thickness measurements. Approximately 75% of overall variability in hypertrophy is accounted for by the first principal component score, PC1, and Table 3.17 details its weighted composition.

Table 3.17 The PC1 score defined in terms of its weighted composition: the weight of each wall thickness measurement.

Wall Thickness Measurement	Weight Contribution to PC1
pIVS at mitral valve	0,253
aIVS at mitral valve	0,261
AW at mitral valve	0,256
LW at mitral valve	0,249
IW at mitral valve	0,221
PW at mitral valve	0,221
pIVS at papillary muscle	0,262
aIVS at papillary muscle	0,269
AW at papillary muscle	0,267
LW at papillary muscle	0,254
IW at papillary muscle	0,234
PW at papillary muscle	0,238
IVS at apex	0,263
AW at apex	0,259
LW at apex	0,239
PW at apex	0,248

Abbreviations: **aIVS**, anterior interventricular septal thickness; **AW**, anterior wall thickness; **IVS**, interventricular septal thickness; **IW**, inferior wall thickness; **LW**, lateral wall thickness; **PC1**, first principal component; **pIVS**, posterior interventricular septal thickness; **PW**, posterior wall thickness

3.9.4 Heritability

The estimated contributions of environmental and genetic factors to the variability of the five hypertrophy traits, along with the p-values for each of these traits, are detailed in Table 3.18. The five hypertrophy traits indicated a considerable genetic component after adjustment for known hypertrophy covariates.

Table 3.18 The environment and heritability estimates detailed as estimated percentage contribution to trait variance as well as the p-values for heritability.

Hypertrophy Trait	Environmental (%)	Heritability (%)	p-value
LVM	41	59	< 0,0001
mIVST	56	44	< 0,0001
mLVWT	44	55	0,0001
mPWT	44	56	0,0002
PC1	48	52	0,0009

Abbreviations: LVM, left ventricular mass; mIVST, maximal interventricular septum thickness; mLVWT, maximal left ventricular wall thickness; mPWT, maximal posterior wall thickness; PC1, first principal component

3.9.5 Association analyses

The results obtained for the association analyses are described per gene and ordered according to their position on the chromosome. The tables contain exact p-values for additive tests of association, whereas the bar graphs represent $-\log_{10}$ transformed p-values. The dashed red line indicates the p-value significance threshold equal to 0,05. Bars located above this line, therefore, indicate significant p-values (p-values<0,05). Thus, the higher the bar, the lower the p-values. Effect sizes for significant associations are presented in the text. The p-values report the association between allelic variation and hypertrophy traits, independent of hypertrophy cofounders, HCM-founder mutation carrier status and whether a mutation is present.

3.9.5.1 *MyBPH*

The p-values for the association between the *MyBPH* SNPs and hypertrophy traits are graphically represented in Figure 3.16. No statistically significant evidence for association was observed between the *MyBPH* SNPs and the respective hypertrophy traits.

Table 3.19 contains the p-values for the association between *MyBPH* SNPs and hypertrophy traits **within** individual HCM-founder mutation groups. The **rs2250509** had a SNP effect within the A797T_{MYH7} HCM founder mutation group alone, compared to the other groups. This SNP had an effect on PC1 (p=0,016), mVIST (p=0,036), mLVWT (p=0,017) and mPWT (p=0,012). More specifically the A allele was associated with an increase of 4,37mm on the mIVST score, 2,70mm on the mLVWT score, 0,84mm on the mPWT score and 3,5mm on the PC1 score within the A797T_{MYH7} mutation group.

Additionally, the effect of the C allele of **rs3737872** was an increase of 29,4g on the LVM score ($p=0,003$) within the A797T_{MYH7} mutation group. The C allele of **rs762625** was associated with an increase of 1,14mm in mPWT ($p=0,011$) within the A797T_{MYH7} mutation group.

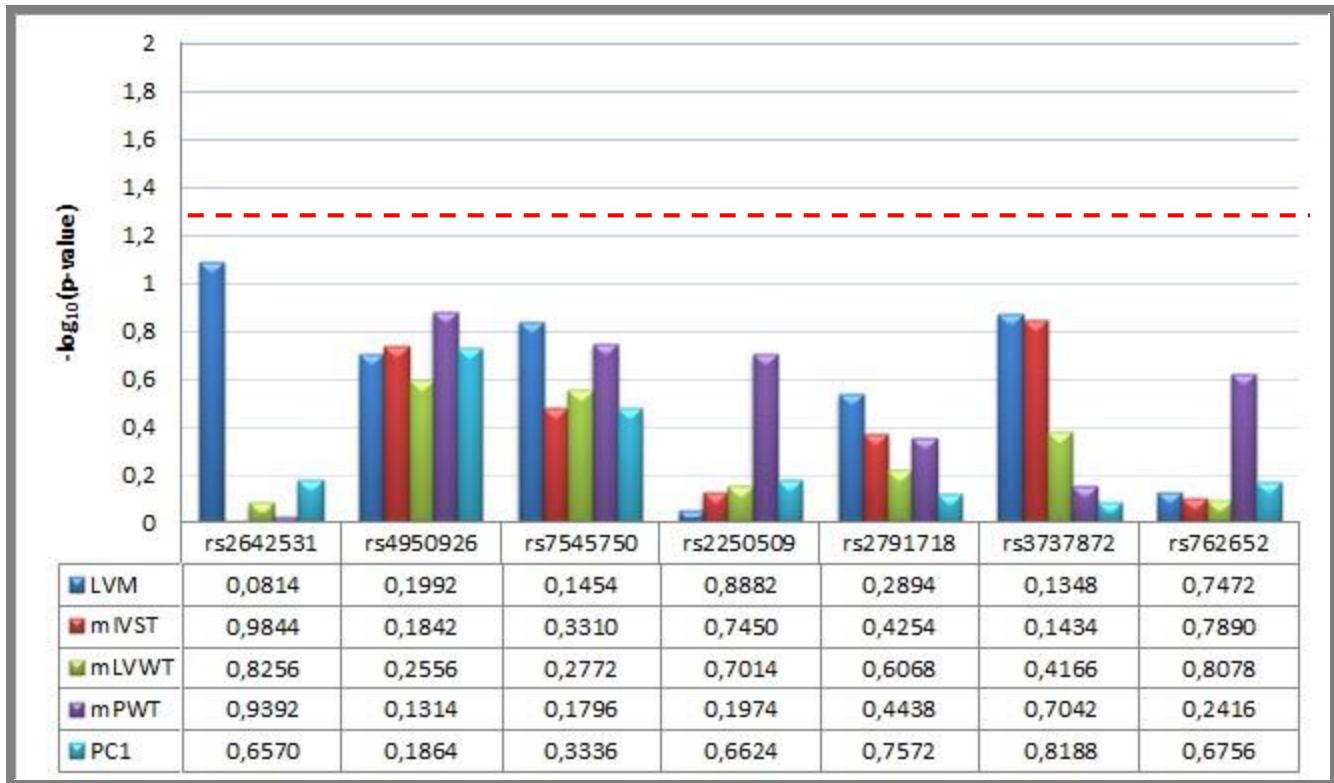


Figure 3.16 The p-values for tests of association between single SNPs in *MyBPH* and individual hypertrophy traits. The bar graph represents $-\log_{10}$ transformed p-values and the data table below indicates the original p-values for additive tests of allelic association. The dashed red line indicates the p-value significance threshold equal to 0,05. Bars located above this line, therefore, indicate significant p-values ($p\text{-values} < 0,05$). Effect sizes for significant associations are indicated in the text. **Abbreviations:** A, alanine; LVM, left ventricular mass; mIVST, maximum interventricular septal thickness; mLVWT, maximum left ventricular wall thickness; mPWT, maximum posterior wall thickness; PC1, first principal component; R, arginine

Table 3.19 The p-values obtained for the analysis of the additive allelic models inside the mutation groups in *MyBPH*, illustrating the allelic effect of the particular variants within these groups. Significant p-values are indicated in bold red font and the corresponding effect sizes are discussed in the text.

SNP ID	LVM			mVIST			mLVWT			mPWT			PC1		
	A797T	R403W	R92W												
rs2642531	0,742	0,198	0,111	0,365	0,840	0,473	0,515	0,958	0,802	0,500	0,388	0,290	0,846	0,680	0,808
rs4950926	0,056	0,540	0,934	0,322	0,275	0,722	0,472	0,242	0,746	0,540	0,278	0,188	0,659	0,186	0,381
rs7545750	0,117	0,747	0,389	0,362	0,928	0,343	0,240	0,747	0,597	0,166	0,824	0,344	0,074	0,659	0,388
rs2250509	0,106	0,744	0,159	0,036	0,732	0,125	0,017	0,666	0,066	0,012	0,131	0,197	0,016	0,788	0,094
rs2791718	0,340	0,451	0,959	0,883	0,712	0,278	0,769	0,614	0,310	0,121	0,841	0,313	0,221	0,787	0,382
rs3737872	0,003	0,888	0,554	0,631	0,321	0,263	0,934	0,303	0,631	0,622	0,860	0,822	0,502	0,275	0,805
rs762625	0,876	0,471	0,954	0,116	0,769	0,535	0,110	0,818	0,417	0,011	0,402	0,397	0,153	0,785	0,454

Abbreviations: **A**, alanine; **LVM**, left ventricular mass; **mVIST**, maximum interventricular septal thickness; **mLVWT**, maximum left ventricular wall thickness; **mPWT**, maximum posterior wall thickness; **MyBPH**, myosin binding protein H; **PC1**, first principal component; **R**, arginine; **SNP**, single nucleotide polymorphism; **T**, threonine; **W**, tryptophan

The p-values for the association between the *MyBPH* haplotypes and hypertrophy traits are graphically represented in Figure 3.17 and demonstrated a statistically significant effect for haplotype **GGTGCTT** in the total cohort. This haplotype is present in 4% of the cohort and the estimated effect was an increase of 26,55g on LVM ($p=0,0326$).

Table 3.20 gives the p-values for the association between *MyBPH* haplotypes and hypertrophy traits **within** HCM-founder mutation groups. Haplotype **CGTACTC**, present at a frequency of 1%, was estimated to increase LVM with 132,07g ($p=0,003$), mIVST with 15,53mm ($p=0,012$), the mLWWT with 15,29mm ($p=0,015$) and the PC1 with 4mm ($p=0,025$) within the A797T_{MYH7} mutation group. Haplotype **CGTGATC**, observed in 12% of the total cohort was associated with a 2.93mm increase in PC1 ($p=0,008$) within the R403W_{MYH7} mutation group. In addition, haplotype **GGTACTT**, observed in 16% of the cohort, was associated with an increase of 2,62mm in mIVST ($p=0,029$), 2,76mm in mLWWT ($p=0,029$) and 1,38mm in PC1 ($p=0,021$) within the A797T_{MYH7} mutation group. Haplotype **GGTGCCC**, observed in 6% of the total cohort, was associated with a 64,88g increase in LVM ($p=0,016$) and a 2,14mm increase in mPWT ($p=0,030$) within mutation group A797T_{MYH7}, whereas this haplotype decreased mIVST with 3,28mm ($p=0,008$), mLWWT with 4,39mm ($p=0,010$) and PC1 with 3,33mm ($p=0,001$) within the R403W_{MYH7} mutation group. Interestingly, haplotype **GGTGCTC** was observed in 19% of the cohort and demonstrated a statistically significant decrease of 20,98g ($p=0,027$) in LVM within the A797T_{MYH7} mutation group. Lastly, even though **GGTGCTT** was present in merely 4% of the cohort, a statistically significant increase of 56,01g in the LVM ($p=0,031$) within the R92W_{TNN2} mutation carrier group was observed.

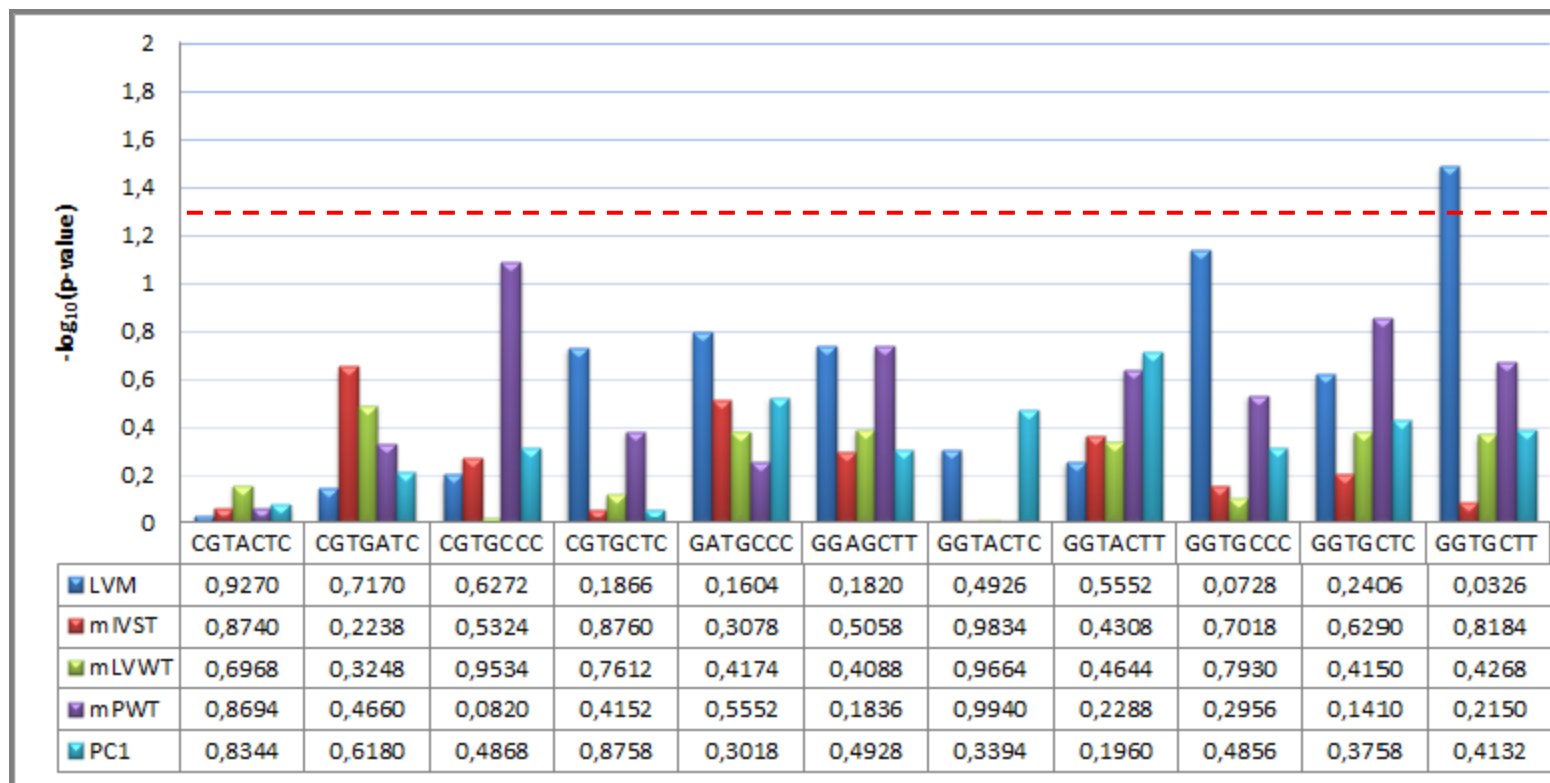


Figure 3.17 The p-values for tests of association between *MYBPH* haplotypes and individual hypertrophy traits. The bar graph represents $-\log_{10}$ transformed p-values and the data table below indicates the original p-values for additive tests of allelic association. The dashed red line indicates the p-value significance threshold equal to 0,05. Bars located above this line, therefore, indicate significant p-values (p -values < 0,05). Effect sizes for significant associations are indicated in the text. **Abbreviations:** LVM, left ventricular mass; mIVST, maximum interventricular septal thickness; mLVWT, maximum left ventricular wall thickness; mPWT, maximum posterior wall thickness; PC1, first principal component; R, arginine

Table 3.20 The p-values obtained for the analysis of the association with *MyBPH* haplotypes within the mutation groups.

Haplotype							Frequency	LVM			mIVST			mLVWT			mPWT			PC1		
rs2642531	rs4950926	rs7545750	rs2250509	rs2791718	rs3737872	rs762625		A797T	R403W	R92W	A797T	R403W	R92W	A797T	R403W	R92W	A797T	R403W	R92W	A797T	R403W	R92W
C	G	T	A	C	T	C	0,01	0,003		0,169	0,012		0,284	0,015		0,399	0,072		0,965	0,025		0,134
C	G	T	G	A	T	C	0,12	0,610	0,794	0,987	0,925	0,143	0,283	0,740	0,087	0,338	0,250	0,579	0,300	0,251	0,008	0,234
C	G	T	G	C	C	C	0,05			0,146			0,944			0,849			0,188			0,235
C	G	T	G	C	T	C	0,03	0,032		0,456	0,310		0,291	0,469		0,403	0,288		0,772	0,062		0,384
G	A	T	G	C	C	C	0,18	0,295	0,676	0,993	0,196	0,626	0,701	0,564	0,635	0,833	0,427	0,564	0,185	0,622	0,555	0,356
G	G	A	G	C	T	T	0,08	0,213	0,987	0,988	0,899	0,750	0,811	0,920	0,839	0,492	0,492	0,804	0,612	0,383	0,482	0,682
G	G	T	A	C	T	C	0,01	0,563	0,166		0,814	0,758		0,956	0,890		0,959	0,340		0,912	0,109	
G	G	T	A	C	T	T	0,16	0,373	0,416	0,339	0,029	0,461	0,156	0,029	0,409	0,085	0,101	0,149	0,941	0,021	0,069	0,147
G	G	T	G	C	C	C	0,06	0,016	0,615	0,797	0,605	0,008	0,780	0,370	0,010	0,656	0,030	0,375	0,629	0,119	0,001	0,989
G	G	T	G	C	T	C	0,19	0,027	0,253	0,718	0,508	0,154	0,684	0,217	0,177	0,689	0,217	0,934	0,344	0,234	0,314	0,903
G	G	T	G	C	T	T	0,04	0,466	0,475	0,031	0,585	0,321	0,415	0,710	0,862	0,109	0,317	0,935	0,294	0,824	0,956	0,079

Abbreviations: A, alanine; LVM, left ventricular mass; mIVST, maximum interventricular septal thickness; mLVWT, maximum left ventricular wall thickness; mPWT, maximum posterior wall thickness; PC1, first principal component; R, arginine; T, threonine; W, tryptophan

* Absence of p-values indicates insufficient statistical power for testing because the unequal distribution of haplotypes in the three HCM mutation groups resulted in very small groups.

3.9.5.2 *MYH7*

Figure 3.18 graphically represents the p-values for the association between the *MYH7* SNPs and hypertrophy traits in the total cohort. A statistically significant effect was observed for the following SNPs: ***rs2147570***, ***rs3729833***, ***rs7140721***, ***rs3729825***, ***rs7159367***, ***rs2277475***, ***rs2147533***, ***rs743567***, ***rs2754163***. The T allele of ***rs2147570*** was associated with a decrease in LVM (21,9g; $p=0,0284$), mIVST (2,94mm; $p=0,0002$), mLWWT (2,93mm; $p=0,0004$), mPWT (0,88mm; $p=0,0030$) and PC1 (1,39mm; $p=0,0032$). The effect of the T allele of ***rs3729833*** was an estimated decrease of 24g in LVM ($p=0,0210$), 2,38mm in mIVST ($p=0,0032$), 2,37mm in mLWWT ($p=0,0072$), 0,86mm in mPWT ($p=0,0222$) and 1,13mm in PC1 ($p=0,0112$). The A allele of ***rs7140721*** was estimated to decrease LVM (13,3g; $p=0,0096$), mIVST (1,10mm; $p=0,0048$) and mLWWT (1,09mm; $p=0,0240$). The T allele of ***rs3729825*** was associated with a decrease of 24,7g in LVM ($p=0,0186$), 2,56mm in mIVST ($p=0,0024$), 2,55mm in mLWWT ($p=0,0048$), 0,87mm in PWT ($p=0,0198$) and 1,16mm in PC1 ($p=0,0098$). The effect of the C allele of ***rs7159367*** was to decrease LVM (12,2g; $p=0,0108$), mIVST (1,00mm; $p=0,0042$) and mLWWT (0,96mm; $p=0,0166$). The T allele of ***rs2277475*** decreased LVM by 15g ($p=0,0078$), mIVST by 1,19mm ($p=0,0066$), mLWWT by 1,23mm ($p=0,0176$) and the PC1 score by 1,31mm in ($p=0,0414$). Furthermore, the effect of the G allele of ***rs2147533*** resulted in decreased mIVST (2,43mm; $p=0,0016$), mLWWT (2,32mm; $p=0,0092$) and PC1 (1,50mm; $p=0,0076$). The G allele of ***rs743567*** was estimated to decrease LVM (15,9g; $p=0,0054$) and mIVST (0,96mm; $p=0,0366$) and the C allele of ***rs2754163*** estimated to decrease LVM with 10,7g ($p=0,0312$).

Table 3.21 details the p-values for the association between *MYH7* SNPs and hypertrophy traits **within** individual HCM founder mutation groups. The ***rs12147570*** SNP had a statistically significant effect within the R92W_{TNNI2} and A797T_{MYH7} mutation groups. The T allele was associated with a decrease of 19,1g in LVM ($p=0,050$), 2,37mm in mIVST ($p=0,019$), 2,22mm in mLWWT ($p=0,024$) and 1,08mm on PC1 score ($p=0,022$) within the R92W_{TNNI2} mutation group. However, the effect of the T allele within the A797T_{MYH7} mutation group was observed to decrease mIVST by 3,47mm ($p=0,010$), mLWWT by 3,49mm ($p=0,031$) and PC1 score by 1,42mm ($p=0,032$). The T allele of ***rs3729833*** was associated with a decrease in mIVST (2,71mm; $p=0,023$) and PC1 score (1,13mm; $p=0,049$) within the A797T_{MYH7} mutation group, compared to the decrease observed in LVM (24,3g; $p=0,021$), mIVST (2,54mm; $p=0,039$), mLWWT (2,44mm; $p=0,045$), mPWT (1,06mm; $p=0,025$) and PC1 (1,31mm; $p=0,007$) within the R92W_{TNNI2} mutation group. The effect of the A allele of ***rs7140721*** was associated with a decrease of 1,44mm in mIVST ($p=0,007$) within the A797T_{MYH7} mutation group. The T allele of ***rs3729825*** was associated with a decrease in all five hypertrophic traits within the R92W_{TNNI2} mutation group; 25,9g in LVM ($p=0,014$), 2,72mm in mIVST ($p=0,030$), 2,56mm in mLWWT ($p=0,039$),

1,08mm in mPWT ($p=0,023$) and 1,31mm in PC1 ($p=0,007$). However, within the A797T_{MYH7} mutation group this allele was only associated with a 2,77mm decrease in mIVST ($p=0,03$). The effect of the C allele of **rs7159367** was to decrease LVM (16,6g; $p=0,029$) within the R92W_{TNNI2} mutation group and mIVST (1,40mm; $p=0,009$) within the A797T_{MYH7} mutation group. A decrease of 20,4g in LVM ($p=0,009$), 1,59mm in mIVST ($p=0,040$), 1,64mm in mLWWT ($p=0,037$), 0,56mm in mPWT and 0,76mm in PC1 score ($p=0,007$) was observed as a statistically significant effect of the T allele of **rs2277475** within the R92W_{TNNI2} mutation group. However, within the A797T_{MYH7} mutation group the T allele of this SNP was associated with a decrease of 1,34mm in mIVST ($p=0,016$). The effect of the G allele of **rs12147533** was associated with a decrease in mIVST (2,34mm; $p=0,024$), in mLWWT (2,23mm; $p=0,030$) and in PC1 (1,08mm; $p=0,023$) within the R92W_{TNNI2} mutation group, whereas within the A797T mutation group, the G allele was associated with a decrease in mIVST (2,99mm; $p=0,012$) and PC1 (1,22mm; $p=0,037$). Additionally, the G allele of **rs743567** was associated with a decrease in LVM (19,6g; $p=0,014$), mIVST (1,50mm; $p=0,047$), mLWWT (1,58mm; $p=0,042$), mPWT (0,60mm; $p=0,025$) and PC1 (0,82mm; $p=0,008$) within the R92W_{TNNI2} mutation group. The G allele of **rs2239577** was significantly associated with PC1 (1.78mm; $p=0,031$) within the R403W_{MYH7} mutation group; however, no GG genotype was observed.

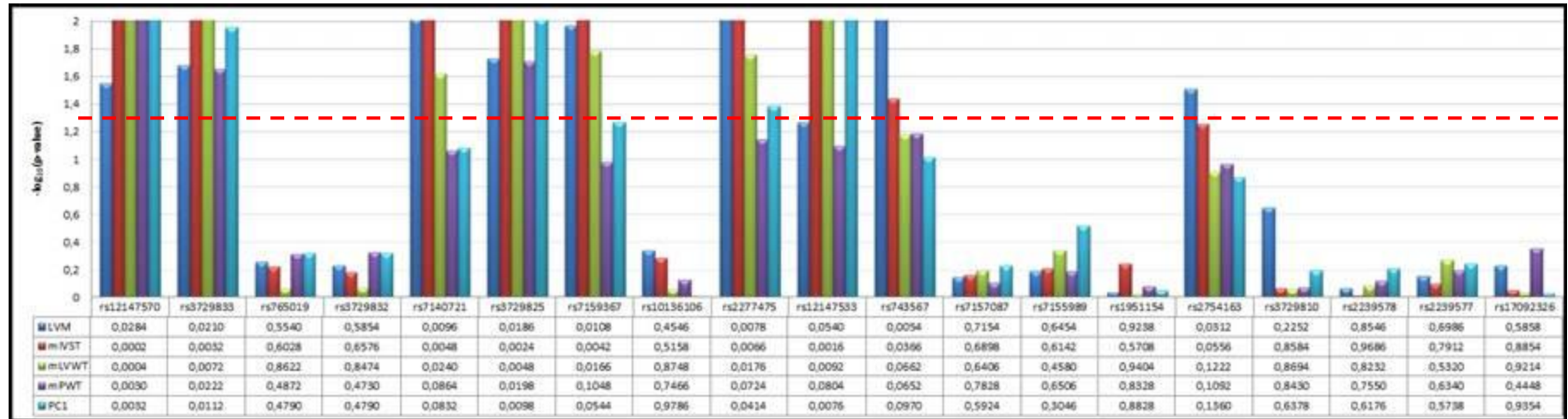


Figure 3.18 The p-values for tests of association between single SNPs in *MYH7* and individual hypertrophy traits. The bar graph represents $-\log_{10}$ transformed p-values and the data table below indicates the original p-values for additive tests of allelic association. The dashed red line indicates the p-value significance threshold equal to 0,05. Bars located above this line, therefore, indicate significant p-values (p-values<0,05). Effect sizes for significant associations are indicated in the text. **Abbreviations:** LVM, left ventricular mass; mIVST, maximum interventricular septal thickness; mLVWT, maximum left ventricular wall thickness; mPWT, maximum posterior wall thickness; PC1, first principal component; R, arginine

Table 3.21 The p-values obtained for the analysis of the additive allelic models inside the mutation groups in *MYH7*, illustrating the differences in allelic effect of the particular variants within these groups. Significant p-values are indicated in bold red font and the corresponding effect sizes are discussed in the text.

SNP ID	LVM			mIVST			mLVWT			mPWT			PC1		
	A797T	R403W	R92W	A797T	R403W	R92W	A797T	R403W	R92W	A797T	R403W	R92W	A797T	R403W	R92W
rs12147570	0,247	0,646	0,050	0,010	0,102	0,019	0,031	0,096	0,024	0,365	0,155	0,083	0,032	0,966	0,022
rs3729833	0,352	0,530	0,021	0,023	0,562	0,039	0,070	0,493	0,045	0,312	0,542	0,025	0,049	0,331	0,007
rs765019	0,537	0,975	0,790	0,175	0,812	0,577	0,584	0,832	0,450	0,705	0,654	0,696	0,937	0,480	0,558
rs3729832	0,565	0,977	0,812	0,191	0,784	0,546	0,600	0,826	0,452	0,677	0,654	0,702	0,937	0,480	0,558
rs7140721	0,161	0,215	0,056	0,007	0,691	0,137	0,069	0,576	0,165	0,361	0,575	0,145	0,079	0,444	0,118
rs3729825	0,441	0,450	0,014	0,030	0,469	0,030	0,066	0,382	0,039	0,336	0,456	0,023	0,055	0,405	0,007
rs7159367	0,163	0,364	0,029	0,009	0,643	0,068	0,082	0,551	0,080	0,362	0,603	0,170	0,084	0,807	0,079
rs10136106	0,331	0,851	0,532	0,124	0,999	0,645	0,439	0,941	0,540	0,873	0,987	0,707	0,546	0,847	0,649
rs2277475	0,276	0,431	0,009	0,016	0,887	0,040	0,101	0,919	0,037	0,468	0,965	0,028	0,109	0,163	0,007
rs12147533	0,229	0,361	0,050	0,012	0,667	0,024	0,062	0,524	0,030	0,227	0,262	0,084	0,037	0,184	0,023
rs743567	0,184	0,422	0,014	0,130	0,846	0,047	0,372	0,983	0,042	0,416	0,860	0,025	0,291	0,147	0,008
rs7157087	0,770	0,643	0,710	0,867	0,395	0,770	0,644	0,483	0,783	0,634	0,289	0,375	0,388	0,318	0,451
rs7155989	0,710	0,873	0,695	0,908	0,751	0,492	0,855	0,683	0,480	0,611	0,324	0,778	0,319	0,590	0,784
rs1951154	0,909	0,842	0,881	0,793	0,925	0,512	0,852	0,981	0,621	0,776	0,740	0,763	0,567	0,589	0,827
rs2754163	0,276	0,436	0,062	0,162	0,501	0,212	0,427	0,490	0,242	0,380	0,605	0,178	0,281	0,966	0,162
rs3729810	0,140	0,986	0,201	0,347	0,555	0,733	0,235	0,369	0,846	0,837	0,449	0,761	0,436	0,905	0,945
rs2239578	0,614	0,804	0,671	0,470	0,765	0,646	0,446	0,946	0,606	0,979	0,395	0,931	0,331	0,437	0,488
rs2239577	0,994	0,717	0,770	0,858	0,295	0,851	0,502	0,424	0,915	0,868	0,262	0,218	0,787	0,031	0,479
rs17092326	0,733	0,660	0,832	0,809	0,566	0,680	0,804	0,632	0,712	0,561	0,352	0,178	0,839	0,095	0,396

Abbreviations: A, alanine; LVM, left ventricular mass; mIVST, maximum interventricular septal thickness; mLVWT, maximum left ventricular wall thickness; mPWT, maximum posterior wall thickness; *MYH7*, cardiac β -myosin heavy chain; PC1, first principal component; R, arginine; SNP, single nucleotide polymorphism; T, threonine; W, tryptophan

The p-values for the association between the *MYH7* haplotypes and hypertrophy traits are graphically represented in Figure 3.19 and demonstrated statistically significant haplotype effects for three haplotypes.

The **GCCAACCATAGCGGCGGCG** haplotype was observed in 3% of the cohort and was associated with a decrease of 19,95g in LVM ($p=0,0284$). Furthermore, the **TTTTATCGTAGCGGCGGGA** haplotype was estimated to effect mPWT with a decrease of 2,52mm ($p=0,007$). The latter mentioned haplotype was only observed in 1% of the total cohort. Additionally, haplotype **TTTTATCGTGGCGGCAACG**, observed in 3% of the cohort, decreased mIVST (2,88mm; $p=0,0228$), mLWWT (2,90mm; $p=0,0358$) and PC1 (1,69mm; $p=0,0286$).

Table 3.22 details the p-values for the association between *MYH7* haplotypes and hypertrophy traits **within** individual HCM-founder mutation groups. Four haplotypes demonstrated a statistically significant association with at least one of the hypertrophy traits. Interestingly, all of these significant associations were observed within the R403W_{*MYH7*} mutation group and not in any of the other two mutation groups. Haplotype **GCCAACCGTAGTAGCAGGA**, observed in 3% of the cohort, was estimated to increase mPWT 1,48mm ($p=0,036$) and PC1 with 2,71mm ($p=0,001$). Haplotype **GCTTGCTGAATCGGTAACG**, observed in 13% of the total cohort, demonstrated to decrease PC1 with 1,62mm ($p=0,007$). Furthermore, a decrease in mIVST with 2,71mm ($p=0,015$) was observed as the effect of haplotype **GCTTGCTGAATCGGTAGCG**, observed at a frequency of 21% in the total cohort. Lastly, haplotype **TTTTATCGTAGCGGCGGGA** demonstrated a decrease in LVM (52,40g; $p=0,022$), mIVST (4,11mm; $p=0,012$), mLWWT (3,39mm; $p=0,012$), mPWT (3,13mm; $p=0,000$) and PC1 score (2,73mm; $p=0,038$). This haplotype was however only observed in 1% of the cohort.

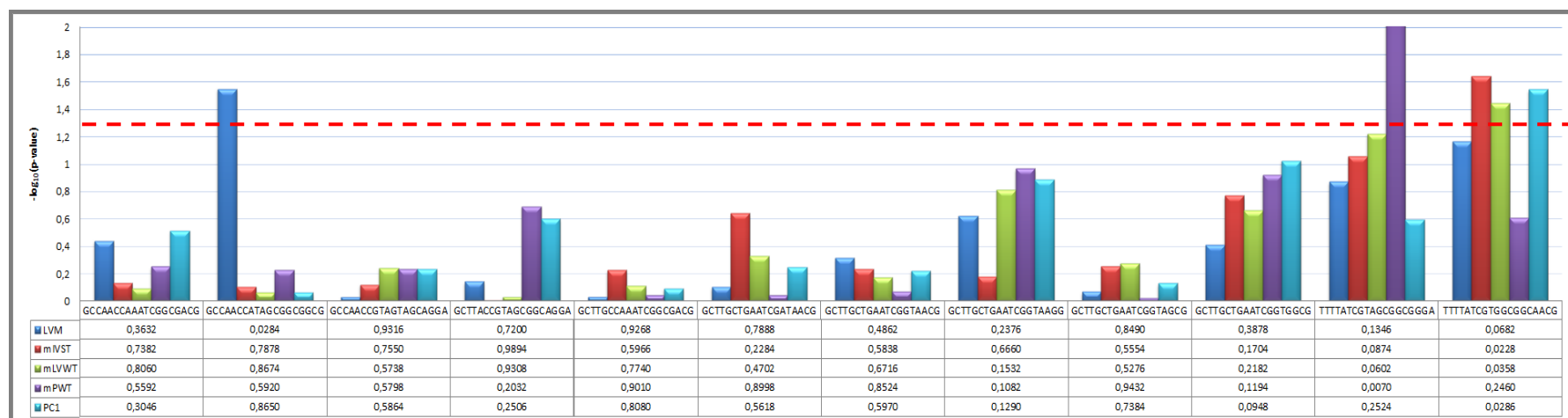


Figure 3.19 The p-values for tests of association between *MYH7* haplotypes and individual hypertrophy traits. The bar graph represents $-\log_{10}$ transformed p-values and the data table below indicates the original p-values for additive tests of allelic association. The dashed red line indicates the p-value significance threshold equal to 0,05. Bars located above this line, therefore, indicate significant p-values (p -values < 0,05). Effect sizes for significant associations are indicated in the text. **Abbreviations:** LVM, left ventricular mass; mIVST, maximum interventricular septal thickness; mLVWT, maximum left ventricular wall thickness; mPWT, maximum posterior wall thickness; PC1, first principal component; R, arginine

Table 3.22 The p-values obtained for the analysis of the association with *MYH7* haplotypes within the mutation groups.

Haplotype														Frequency	LVM			mIVST			mLVWT			mPWT			PC1						
rs12147570	rs3729833	rs765019	rs3729832	rs7140721	rs3729825	rs7159367	rs10136106	rs2277475	rs12147533	rs743567	rs7157087	rs7155989	rs1951154		rs2754163	rs3729810	rs2239578	rs2239577	rs17092326	A79TT	R403W	R92W	A79TT	R403W									
G	C	C	A	A	C	C	A	A	T	A	T	C	G	G	C	G	C	G	0,02	0,894	0,247	0,588	0,869	0,543	0,491	0,654	0,298	0,872	0,132				
G	C	C	A	A	C	C	A	T	A	G	C	G	G	C	G	C	G	0,03	0,104	0,685	0,207	0,494	0,852	0,764	0,698	0,824	0,592	0,938	0,566	0,703	0,765	0,874	0,570
G	C	C	A	A	C	C	G	T	A	G	T	A	G	C	A	G	A	0,03	0,780	0,888	0,771	0,630	0,924	0,941	0,984	0,808	0,951	0,950	0,036	0,171	0,409	0,001	0,789
G	C	T	T	A	C	C	G	T	A	G	C	G	G	C	A	G	A	0,03	0,432	0,897	0,829	0,802	0,857	0,839	0,177	0,944	0,276	0,822					
G	C	T	T	G	C	C	A	A	A	T	C	G	G	C	G	A	C	0,01	0,805	0,216	0,216	0,216	0,195	0,855	0,834								
G	C	T	T	G	C	T	G	A	A	T	C	G	A	T	A	A	C	0,27	0,496	0,771	0,771	0,111	0,883	0,860	0,291	0,538	0,746	0,975	0,636	0,453	0,948	0,125	0,450
G	C	T	T	G	C	T	G	A	A	T	C	G	G	T	A	A	C	0,13	0,257	0,520	0,531	0,269	0,932	0,720	0,336	0,541	0,531	0,380	0,131	0,861	0,616	0,007	0,855
G	C	T	T	G	C	T	G	A	A	T	C	G	G	T	A	A	G	0,01	0,422	0,913	0,466	0,812	0,079	0,804	0,105	0,931	0,105	0,651					
G	C	T	T	G	C	T	G	A	A	T	C	G	G	T	A	G	C	0,21	0,278	0,449	0,987	0,594	0,015	0,371	0,816	0,082	0,411	0,912	0,295	0,235	0,585	0,216	0,391
G	C	T	T	G	C	T	G	A	A	T	C	G	G	T	A	G	C	0,02	0,588	0,222	0,901	0,463	0,764	0,617	0,370	0,706	0,667	0,895	0,236	0,083	0,782	0,167	0,265
T	T	T	T	A	T	C	G	T	A	G	C	G	G	C	G	A	A	0,01	0,022	0,901	0,463	0,764	0,617	0,370	0,706	0,667	0,895	0,236	0,083	0,782	0,167	0,265	
T	T	T	T	A	T	C	G	T	A	G	C	G	G	C	G	A	A	0,03	0,419	0,203	0,071	0,880	0,076	0,989	0,469	0,334	0,100	0,886					

Abbreviations: A, alanine; LVM, left ventricular mass; mIVST, maximum interventricular septal thickness; mLVWT, maximum left ventricular wall thickness; mPWT, maximum posterior wall thickness; PC1, first principal component; R, arginine; T, threonine; W, tryptophan

* Absence of p-values indicates insufficient statistical power for testing because the unequal distribution of haplotypes in the three HCM mutation groups resulted in very small groups.

3.9.5.3 *ACTC1*

Figure 3.20 graphically represents the p-values for the association between the *ACTC1* SNPs and hypertrophy traits in the cohort. A statistically significant effect was observed for SNP **rs2070664**, for which the effect of the C allele was estimated to decrease LVM with 13,1g ($p=0,0056$).

Table 3.23 details the p-values for the association between *ACTC1* SNPs and hypertrophy traits **within** individual HCM founder mutation groups. The C allele of **rs2070664** had a statistically significant effect within the A797T_{MYH7} mutation group and was estimated to decrease LVM with 16,6g ($p=0,026$). Additionally, the G allele of **rs7165006** was statistically significantly associated with an increase of 31,2g in LVM ($p=0,032$), 3,25mm in mIVST ($p=0,050$) and 1,17mm in mPWT ($p=0,035$) within the A797T_{MYH7} mutation group.

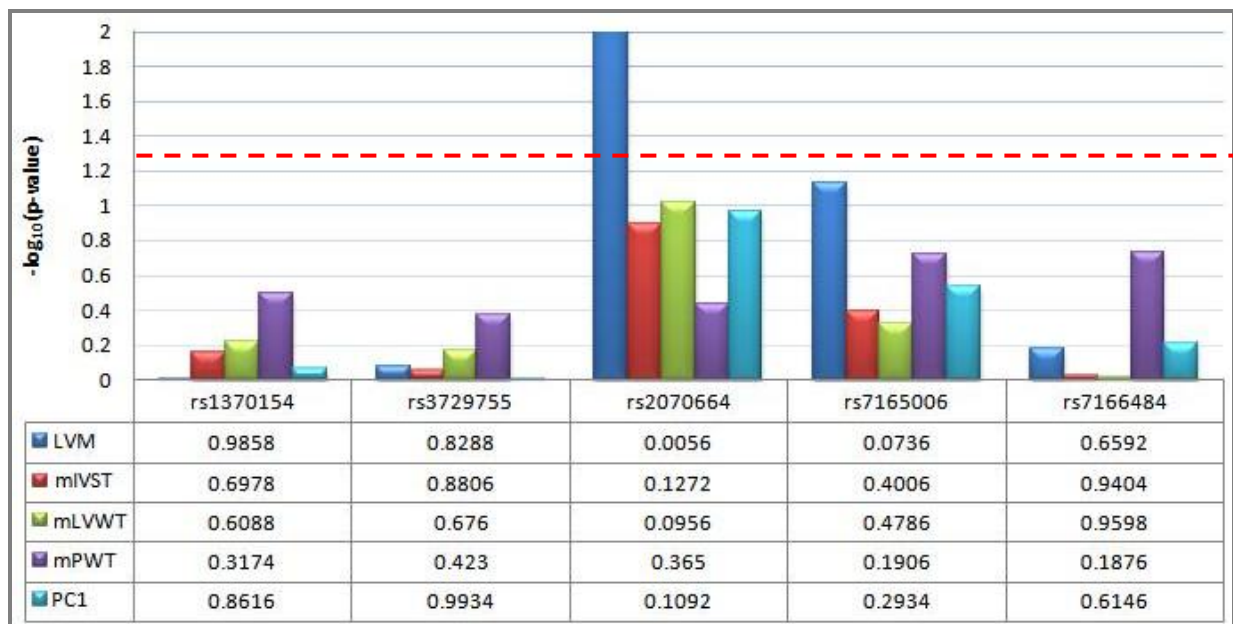


Figure 3.20 The p-values for tests of association between single SNPs in *ACTC1* and individual hypertrophy traits. The bar graph represents $-\log_{10}$ transformed p-values and the data table below indicates the original p-values for additive tests of allelic association. The dashed red line indicates the p-value significance threshold equal to 0,05. Bars located above this line, therefore, indicate significant p-values ($p\text{-values} < 0,05$). Effect sizes for significant associations are indicated in the text. **Abbreviations:** *ACTC1*, cardiac α -actin; **LVM**, left ventricular mass; **mIVST**, maximum interventricular septal thickness; **mLVWT**, maximum left ventricular wall thickness; **mPWT**, maximum posterior wall thickness; **PC1**, first principal component; **R**, arginine

Table 3.23 The p-values obtained for the analysis of the additive allelic models inside the mutation groups in *ACTC1*, illustrating the differences in allelic effect of the particular variants within these groups. Significant p-values are indicated in bold red font and the corresponding effect sizes are discussed in the text.

SNP ID	LVM			mIVST			mLVWT			mPWT			PC1		
	A797T	R403W	R92W	A797T	R403W	R92W	A797T	R403W	R92W	A797T	R403W	R92W	A797T	R403W	R92W
rs1370154	0,642	0,686	0,373	0,735	0,516	0,846	0,876	0,452	0,894	0,934	0,149	0,564	0,940	0,439	0,859
rs3729755	0,707	0,950	0,399	0,767	0,921	0,881	0,830	0,670	0,886	0,930	0,360	0,533	0,918	0,720	0,882
rs2070664	0,026	0,369	0,129	0,060	0,567	0,349	0,109	0,797	0,211	0,295	0,947	0,713	0,273	0,492	0,335
rs7165006	0,032	0,541	0,946	0,050	0,393	0,880	0,088	0,354	0,973	0,035	0,631	0,857	0,246	0,997	0,566
rs7166484	0,708	0,282	0,606	0,937	0,990	0,830	0,901	0,995	0,829	0,206	0,619	0,279	0,935	0,420	0,848

Abbreviations: **A**, alanine; **ACTC1**, cardiac α -actin; **LVM**, left ventricular mass; **mIVST**, maximum interventricular septal thickness; **mLVWT**, maximum left ventricular wall thickness; **mPWT**, maximum posterior wall thickness; **PC1**, first principal component; **R**, arginine; **SNP**, single nucleotide polymorphism; **T**, threonine; **W**, tryptophan

The p-values for the association between the *ACTC1* haplotypes and hypertrophy traits are graphically represented in Figure 3.21 and demonstrated statistically significant haplotype effects for two haplotypes. Haplotype **CCCCA** was associated with a decrease of 16,95g in LVM ($p=0,0356$) and 1,43mm in mLWWT ($p=0,0328$). Conversely, haplotype **CCTGG** caused a significant 35,25g higher LVM ($p=0,0196$). These two haplotypes were observed in the total cohort at a frequency of 18% and 8%, respectively.

Table 3.24 details the p-values for the association between *ACTC1* haplotypes and hypertrophy traits **within** individual HCM-founder mutation groups. Three haplotypes demonstrated a statistically significant association with at least one of the hypertrophy traits. Haplotype **CCCCG** was observed in 10% of the cohort and estimated to increase mPWT 1,69mm ($p=0,039$) within the R92W_{TNNT2} mutation group. In addition, haplotype **CCTCA**, observed in 22% of the cohort, affected the R92W_{TNNT2} mutation group with an estimated increase of 23,39g in LVM ($p=0,004$). Lastly haplotype **CCTGG** was associated with an estimated increase of 44,61g in LVM ($p=0,036$) and 1,75mm in mPWT ($p=0,041$) within the A797T_{MYH7} mutation group.

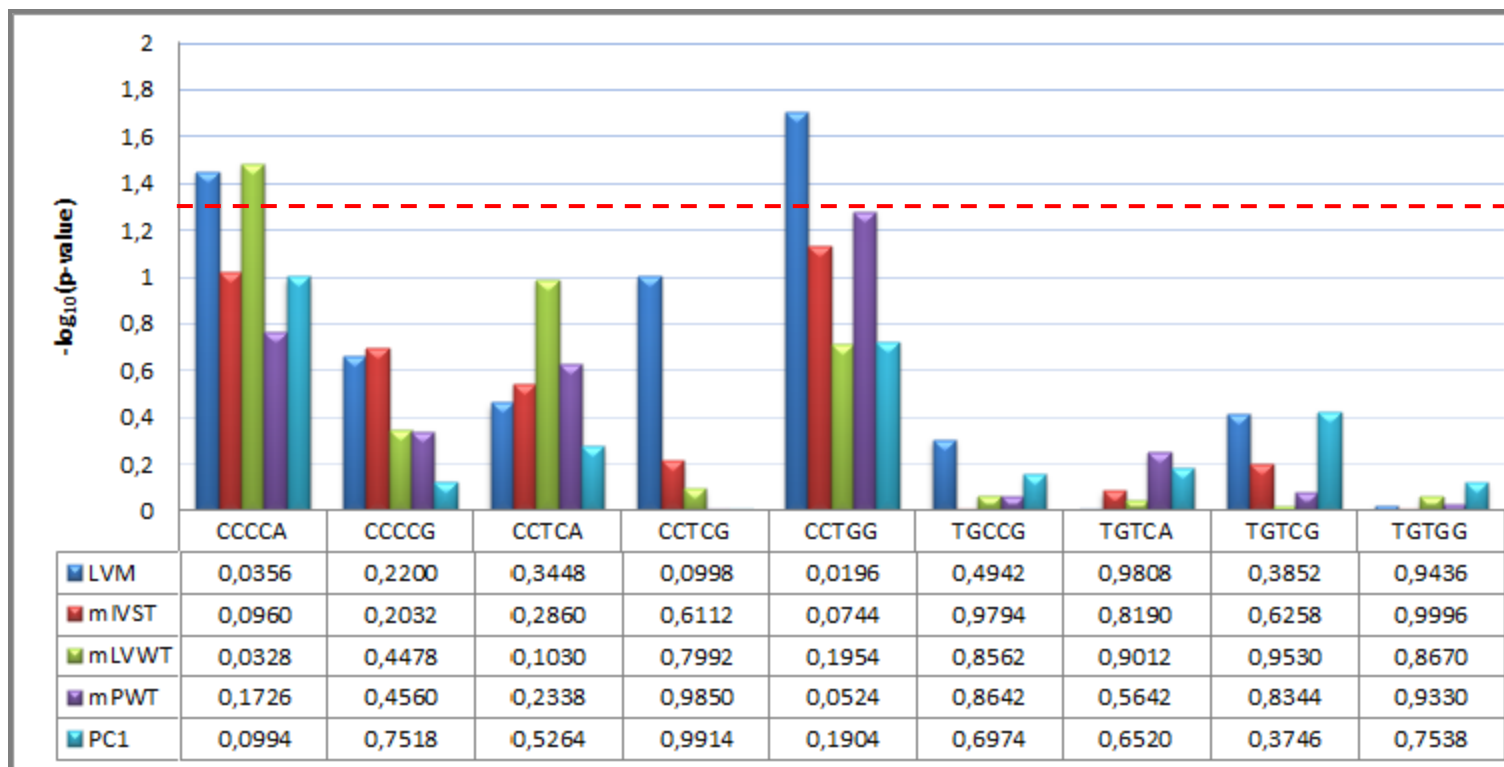


Figure 3.21 The p-values for tests of association between *ACTC1* haplotypes and individual hypertrophy traits. The bar graph represents $-\log_{10}$ transformed p-values and the data table below indicates the original p-values for additive tests of allelic association. The dashed red line indicates the p-value significance threshold equal to 0,05. Bars located above this line, therefore, indicate significant p-values (p-values < 0,05). Effect sizes for significant associations are indicated in the text. **Abbreviations:** **LVM**, left ventricular mass; **mIVST**, maximum interventricular septal thickness; **mLVWT**, maximum left ventricular wall thickness; **mPWT**, maximum posterior wall thickness; **PC1**, first principal component; **R**, arginine

Table 3.24 The p-values obtained for the analysis of the association with *ACTC1* haplotypes within the mutation groups.

Haplotype					Frequency	LVM			mIVST			mLVWT			mPWT			PC1		
rs1370154	rs3729755	rs2070664	rs7165006	rs7166484		A797T	R403W	R92W	A797T	R403W	R92W	A797T	R403W	R92W	A797T	R403W	R92W	A797T	R403W	R92W
C	C	C	C	A	0,18	0,293		0,170	0,601	0,303	0,178		0,097	0,519		0,768	0,341		0,078	
C	C	C	C	G	0,10	0,057		0,905	0,072	0,699	0,182		0,775	0,860		0,039	0,385		0,274	
C	C	T	C	A	0,22	0,761		0,004	0,492	0,114	0,245		0,075	0,553		0,408	0,554		0,240	
C	C	T	C	G	0,09	0,966		0,990	0,638	0,734	0,264		0,731	0,737		0,138	0,479		0,467	
C	C	T	G	G	0,08	0,036		0,962	0,052	0,577	0,111		0,811	0,041		0,968	0,241		0,856	
T	G	C	C	G	0,01	0,324			0,898		0,940			0,942			0,507			
T	G	T	C	A	0,01	0,743			0,790		0,959			0,501			0,440			
T	G	T	C	G	0,30	0,810		0,816	0,926	0,914	0,789		0,802	0,390		0,423	0,414		0,923	
T	G	T	G	G	0,02	0,983			0,994		0,895			0,729			0,720			

Abbreviations: **A**, alanine; **LVM**, left ventricular mass; **mIVST**, maximum interventricular septal thickness; **mLVWT**, maximum left ventricular wall thickness; **mPWT**, maximum posterior wall thickness; **PC1**, first principal component; **R**, arginine; **T**, threonine; **W**, tryptophan

* Absence of p-values indicates insufficient statistical power for testing because the unequal distribution of haplotypes in the three HCM mutation groups resulted in very small groups.

3.9.5.4 *UBC9*

Figure 3.22 graphically represents the p-values for the association between the *UBC9* SNPs and hypertrophy traits in the cohort. The C allele of **rs8052688** was significantly associated with an increase of 1,43mm in mIVST (p=0,0462).

Table 3.25 details the p-values for the association between *UBC9* SNPs and hypertrophy traits **within** individual HCM founder mutation groups. Interestingly, the A allele of **rs761059** was estimated to decrease LVM (26,1g; p=0,016), mIVST (3,08mm; p=0,006), mLWT (3,33mm; p=0,002), mPWT (0,96mm; p=0,002) and PC1 (1,81mm; p=0,004) within the A797T_{MYH7} mutation group. Conversely, since no AA genotype of **rs761060** was observed, the effect of the AG genotype was estimated to cause an increase of 45,2g in LVM (p=0,038), 2,73mm in mIVST and 1,28mm in PC1 (p=0,039) within the A797T_{MYH7} mutation group. Interestingly, the effect of AG within the R403W_{MYH7} mutation group was estimated to decrease mPWT by 0,74mm (p=0,049), whereas, within the R92W_{TNNI2} mutation group, AG was estimated to increase mPWT by 1,00mm (p=0,041). The effect of the A allele of **rs8063** was associated with an increase of 33,5g in LVM (p=0,017) within the A797T_{MYH7} mutation group.

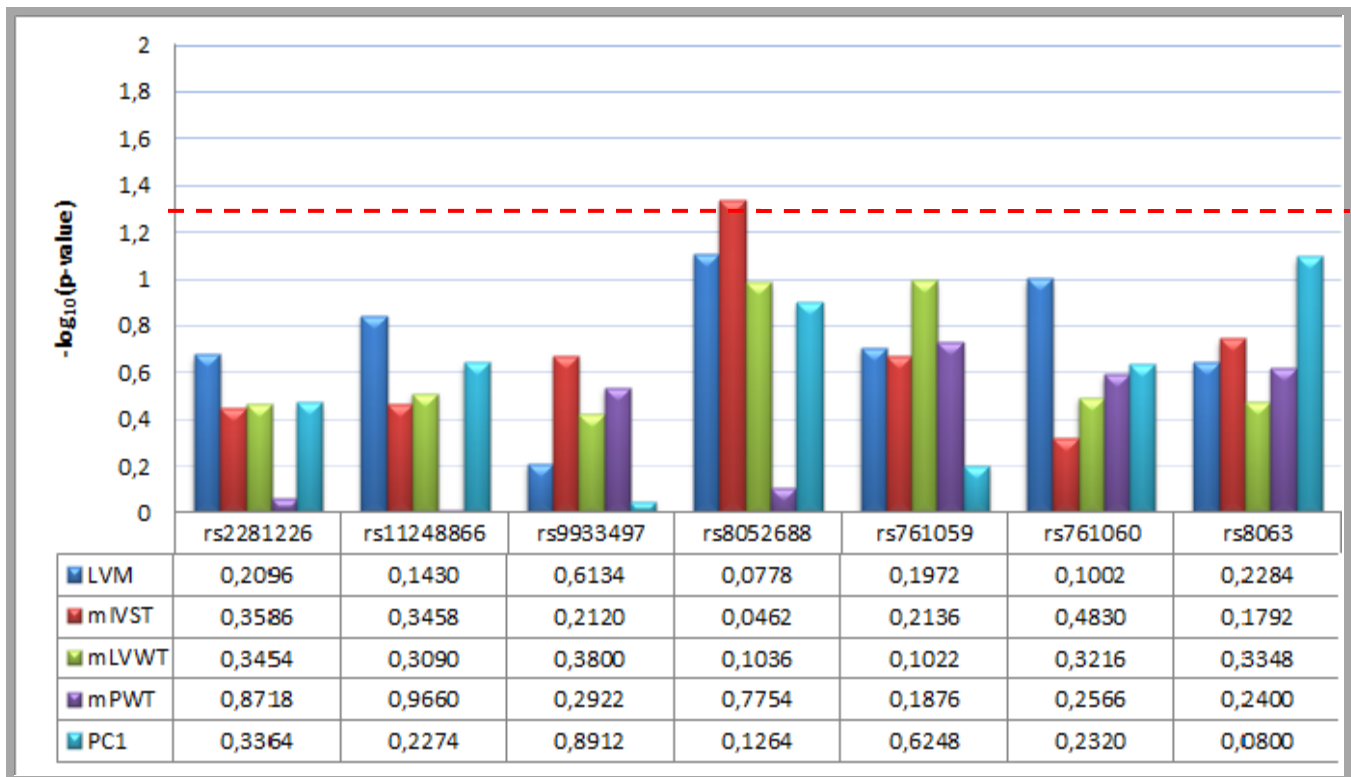


Figure 3.22 The p-values for tests of association between single SNPs in *UBC9* and individual hypertrophy traits. The bar graph represents $-\log_{10}$ transformed p-values and the data table below indicates the original p-values for additive tests of allelic association. The dashed red line indicates the p-value significance threshold equal to 0,05. Bars located above this line, therefore, indicate significant p-values (p -values < 0,05). Effect sizes for significant associations are indicated in the text. **Abbreviations:** LVM, left ventricular mass; mIVST, maximum interventricular septal thickness; mLVWT, maximum left ventricular wall thickness; mPWT, maximum posterior wall thickness; PC1, first principal component; R, arginine; *UBC9*, SUMO-conjugating enzyme UBC9

Table 3.25 The p-values obtained for the analysis of the additive allelic models inside the mutation groups in *UBC9*, illustrating the differences in allelic effect of the particular variants within the se groups. Significant p-values are indicated in bold red font and the corresponding effect sizes are discussed in the text.

SNP ID	LVM			mIVST			mLVWT			mPWT			PC1		
	A797T	R403W	R92W	A797T	R403W	R92W	A797T	R403W	R92W	A797T	R403W	R92W	A797T	R403W	R92W
rs2281226	0,292	0,621	0,112	0,603	0,626	0,114	0,712	0,770	0,115	0,779	0,306	0,704	0,645	0,868	0,298
rs11248866	0,264	0,849	0,241	0,633	0,898	0,201	0,711	0,963	0,162	0,775	0,469	0,765	0,636	0,410	0,376
rs9933497															
rs8052688	0,238	0,738	0,142	0,262	0,602	0,070	0,540	0,625	0,060	0,520	0,597	0,941	0,188	0,925	0,359
rs761059	0,016	0,506	0,986	0,006	0,489	0,116	0,002	0,366	0,199	0,002	0,620	0,446	0,004	0,396	0,133
rs761060	0,003	0,528	0,975	0,038	0,186	0,786	0,093	0,306	0,442	0,064	0,049	0,041	0,039	0,250	0,348
rs8063	0,017	0,907	0,592	0,276	0,656	0,148	0,625	0,820	0,174	0,308	0,555	0,713	0,161	0,334	0,516

Abbreviations: **A**, alanine; **LVM**, left ventricular mass; **mIVST**, maximum interventricular septal thickness; **mLVWT**, maximum left ventricular wall thickness; **mPWT**, maximum posterior wall thickness; **PC1**, first principal component; **R**, arginine; **SNP**, single nucleotide polymorphism; **T**, threonine; **UBC9**, SUMO-conjugating enzyme UBC9; **W**, tryptophan

The p-values for the association between the *UBC9* haplotypes and hypertrophy traits are graphically represented in Figure 3.23 and demonstrated statistically significant effects for four haplotypes. The effect of haplotype **AAGCAGA**, which was observed in 3% of the cohort, was estimated to increase mIVST with 2,79mm ($p=0,0324$). Haplotype **AAGCGAA** was associated with an increase in all five hypertrophy traits measured, although this haplotype was only observed in 3% of the cohort. This haplotype was estimated to cause an increase of 75,79g in LVM ($p=0,0030$), 6,02mm in mIVST ($p=0,0252$), 5,98mm in mLWWT ($p=0,0074$), 1,91mm in mPWT ($p=0,0122$) and 2,27mm in PC1 ($p=0,0168$). Conversely, haplotypes **AAGGAGG** and **CGGGAGG** was estimated to decrease mPWT with 1,43mm ($p=0,0334$) and mLWWT with 1,44mm ($p=0,0312$), respectively. However, haplotype **AAGGAGG** was only observed in 3% of the cohort, compared to haplotype **CGGGAGG**, which was observed in 14% of the cohort.

Table 3.26 details the p-values for the association between *UBC9* haplotypes and hypertrophy traits **within** individual HCM-founder mutation groups. Haplotype **AAGCGAA** was associated with an increase in LVM (132,50g; $p=0,001$), mIVST (11,25mm; $p=0,037$), mLWWT (10,82mm; $p=0,034$), mPWT (3,96mm; $p=0,004$) and PC1 (4,18mm; $p=0,002$) within the A797T_{MYH7} mutation group, whereas the effect observed within the R92W_{MYH7} mutation group was an increase of 2,85mm in mPWT ($p=0,048$). This haplotype, however, was only observed in 3% of the cohort. The effect of haplotype **AAGCGGA**, observed in 6% of the cohort, was estimated to increase mPWT (2,00mm; $p=0,040$) within the R92W_{TNNT2} mutation group and PC1 (4,46mm; $p=0,027$) within the R043W_{MYH7} mutation group. Conversely, haplotype **AAGGAGG**, observed in 3% of the total cohort, was associated with a decrease of 2,85mm in mPWT ($p=0,007$) within the A797T_{MYH7} mutation group. Interestingly, the estimated effect of haplotype **AAGGGAA** was an 83,26g increase in LVM ($p=0,013$) within the A797T_{MYH7} mutation group, in contrast to the estimated decrease of 94,90g in LVM ($p=0,035$) within the R403W_{MYH7} mutation group. However, this haplotype was only observed in 1% of the cohort. Haplotype **AAGGGAG**, observed in 3% of the cohort, demonstrated an association with an estimated decrease in LVM (29,34g; $p=0,015$), mIVST (2,86mm; $p=0,000$), mLWWT (3,97mm; $p=0,000$), mPWT (1,68mm; $p=0,001$) and PC1 (2,86mm; $p=0,000$) within the R403W_{MYH7} mutation group. Haplotype **AAGGGGG** was observed in 10% of the cohort and was estimated to increase PC1 with 1,65mm ($p=0,028$) within the R403W_{MYH7} mutation group. The effect of haplotype **CAGGGAG** was associated with a significant increase in LVM with 105,87g ($p=0,000$), mIVST with 5,09mm ($p=0,005$), mLWWT with 4,26mm ($p=0,0164$), mPWT with 2,23mm ($p=0,006$) and PC1 with 5,74mm ($p=0,005$) within the R403W_{MYH7} mutation group. This haplotype however was only observed in 1% of the cohort. In addition, haplotype **CGGGAGG**, observed in 14% of the cohort, was estimated to decrease LVM with 25,56g ($p=0,014$) and mPWT with 0,83mm ($p=0,030$) within the A797T_{MYH7}

mutation group. Lastly, haplotype **CGGGGG**, observed in 36% of the cohort, was associated with a 11,72mm decrease in PC1 ($p=0,030$) within the R92W_{TNNT2} mutation group.

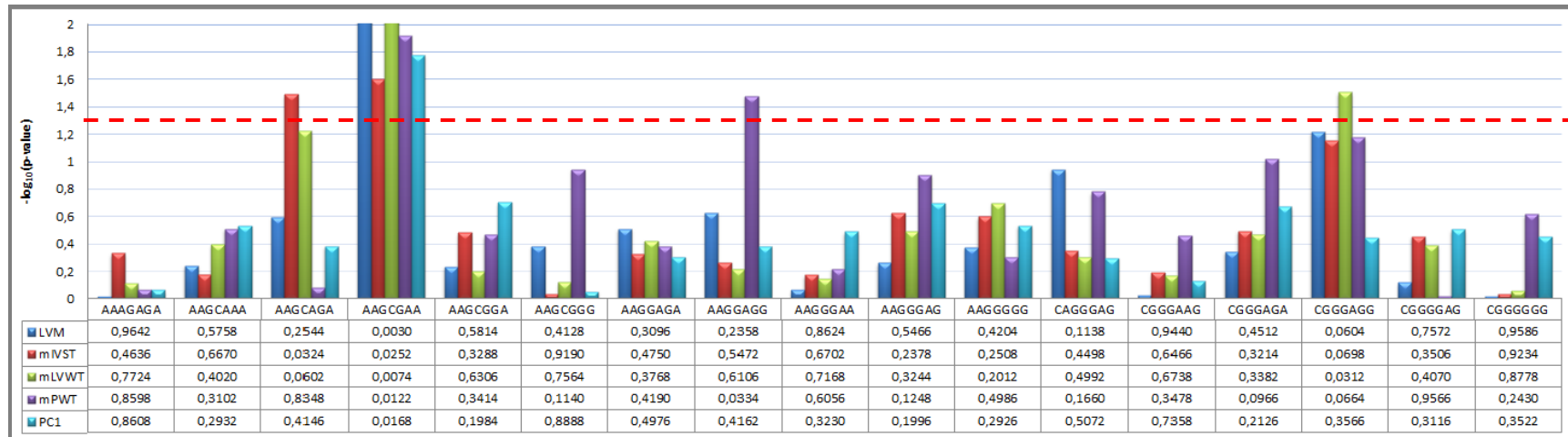


Figure 3.23 The p-values for tests of a association between *UBC9* haplotypes and individual hypertrophy traits. The bar graph represents $-\log_{10}$ transformed p-values and the data table below indicates the original p-values for additive tests of allelic association. The dashed red line indicates the p-value significance threshold equal to 0,05. Bars located above this line, therefore, indicate significant p-values (p-values<0,05). Effect sizes for significant associations are indicated in the text. **Abbreviations:** LVM, left ventricular mass; mIVST, maximum interventricular septal thickness; mLVWT, maximum left ventricular wall thickness; mPWT, maximum posterior wall thickness; PC1, first principal component; R, arginine; *UBC9*, SUMO-conjugating enzyme UBC9

Table 3.26 The p-values obtained for the analysis of the association with *UBC9* haplotypes within the mutation groups.

Haplotype							Frequency	LVM			mIVST			mLVWT			mPWT			PC1		
rs2281226	rs11248866	rs9933497	rs8052688	rs761059	rs761060	rs8063		A797T	R403W	R92W	A797T	R403W	R92W									
A	A	A	G	A	G	A	0,02	0,972			0,874			0,815			0,979			0,840		
A	A	G	C	A	A	A	0,03	0,382			0,363			0,238			0,192			0,240		
A	A	G	C	A	G	A	0,03			0,169		0,078			0,103			0,704			0,429	
A	A	G	C	G	A	A	0,03	0,001	0,857	0,304	0,037	0,437	0,782	0,034	0,493	0,220	0,004	0,102	0,048	0,002	0,249	0,403
A	A	G	C	G	G	A	0,06	0,743	0,353	0,636	0,306	0,196	0,829	0,606	0,157	0,904	0,620	0,128	0,040	0,464	0,027	0,325
A	A	G	C	G	G	G	0,03	0,322	0,643	0,948	0,397	0,268	0,506	0,174	0,162	0,601	0,583	0,095	0,205	0,688	0,227	0,933
A	A	G	G	A	G	A	0,02	0,194	0,604	0,174	0,212	0,341	0,872	0,152	0,258	0,981	0,077	0,549	0,677	0,168	0,666	0,994
A	A	G	G	A	G	G	0,03	0,064	0,470	0,510	0,527	0,113	0,222	0,809	0,174	0,133	0,007	0,416	0,057	0,313	0,154	0,170
A	A	G	G	G	A	A	0,01	0,013	0,035		0,734	0,414		0,758			0,693			0,382		
A	A	G	G	G	A	G	0,03		0,015	0,218		0,000	0,280		0,000	0,246		0,001	0,683		0,000	0,352
A	A	G	G	G	G	G	0,10	0,500	0,517	0,229	0,905	0,189	0,765	0,614	0,063	0,998	0,202	0,794	0,767	0,992	0,028	0,528
C	A	G	G	G	A	G	0,01		0,000	0,666		0,005	0,971		0,016	0,848		0,006	0,617		0,005	0,693
C	G	G	G	A	A	G	0,01			0,827			0,744			0,732			0,204			0,745
C	G	G	G	A	G	A	0,01		0,633	0,970		0,966	0,194		0,957	0,189		0,138	0,934		0,200	0,371
C	G	G	G	A	G	G	0,14	0,014	0,899	0,836	0,109	0,217	0,962	0,121	0,112	0,815	0,030	0,129	0,309	0,120	0,445	0,344
C	G	G	G	G	A	G	0,03	0,399		0,789	0,082		0,501	0,081		0,420	0,960		0,758	0,117		0,820
C	G	G	G	G	G	G	0,36	0,576	0,480	0,236	0,593	0,404	0,092	0,722	0,441	0,099	0,145	0,956	0,829	0,515	0,075	0,030

Abbreviations: A, alanine; LVM, left ventricular mass; mIVST, maximum interventricular septal thickness; mLVWT, maximum left ventricular wall thickness; mPWT, maximum posterior wall thickness; PC1, first principal component; R, arginine; T, threonine; W, tryptophan

* Absence of p-values indicates insufficient statistical power for testing because the unequal distribution of haplotypes in the three HCM mutation groups resulted in very small groups.

Chapter Four

Discussion

CHAPTER FOUR

DISCUSSION

TABLE OF CONTENTS

DISCUSSION: PROTEIN INTERACTION STUDY.....	152
4.1 Yeast two-hybrid analyses to identify interactors of MyBPH.....	152
4.1.1 Preys excluded from this study.....	153
a) Non-relevant protein function	153
b) Incompatible cellular compartments.....	154
4.1.2 MyBPH binds proteins involved in cardiac contractility.....	154
a) Myosin.....	154
b) Cardiac actin.....	156
4.1.3 MyBPH binds a SUMO-conjugating enzyme	157
4.2 MyBPH and cMyBPC are implicated in the autophagic pathway.....	158
4.3 MyBPH and cMyBPC play an essential part in contractility	160
4.4 Implications for MyBPH in cardiac sarcomere.....	163
4.5 Limitations of interaction studies	165
4.5.1 Yeast two-hybrid	165
4.5.2 H9c2 cardiomyocyte cell line	166
4.5.3 Co-localisation.....	166
DISCUSSION: MYBPH AND INTERACTORS AS MODIFIERS OF HYPERTROPHY	168
4.6 Caveats in association analyses.....	168
4.6.1 Population stratification.....	168
4.6.2 Phenotypic definition and distribution	169
4.6.3 Linkage disequilibrium	171
4.6.4 Marker selection.....	172
4.6.5 Genotyping approach.....	174

4.6.6	Power	174
4.6.7	Confounders	175
4.6.8	Multiple testing	176
4.7	Use of haplotypes in association studies	177
4.8	Heritability	178
4.9	Association analyses results	179
4.9.1	Myosin binding protein H (<i>MyBPH</i>)	179
4.9.2	Myosin (<i>MYH7</i>)	181
4.9.3	Cardiac actin (<i>ACTC1</i>)	183
4.9.4	SUMO-conjugating enzyme UBC9 (<i>UBC9</i>)	185
4.10	Closing thoughts and future direction	188
4.11	Conclusion	189

DISCUSSION: PROTEIN INTERACTION STUDY

MyBPC3, the gene encoding cMyBPC, is one of the most frequently mutated genes in HCM and genes encoding protein interactors of cMyBPC have previously been investigated as potential HCM modifier genes. Previous investigations conducted in our laboratory to elucidate the functions of cMyBPC have identified several novel cMyBPC interactors through a succession of Y2H analyses. These studies have shed much light on cMyBPC function and possible mechanisms by which mutations in MYBPC3 cause HCM.

Much of the current research had focused on cMyBPC, while very little is known about the functions and molecular mechanisms of MyBPH. Given the sequence homology and similarity in structure between cMyBPC and MyBPH, and since both proteins are known to bind myosin (Alyonycheva et al., 1997b), we proposed that MyBPH may also play a crucial role in the cardiac sarcomere and possibly in HCM pathogenesis.

In the present study, the Y2H approach was used to identify interactors of MyBPH. MyBPH was used as bait protein to screen a cardiac cDNA library for putative interactors of MyBPH. These putative interactors were prioritised according to their function and location within the cell, before selected putative interactors were verified. Furthermore, the role of MyBPH in the context of the sarcomere was investigated using a siRNA-mediated approach and a contractility assay.

In the present study one of the main findings was the lack of response in cardiac contractility with individual knockdown of MyBPH and cMyBPC upon β -adrenergic stimulation; this could be the result of partial functional compensation between cMyBPC and MyBPH. More specifically, concurrent knockdowns of MyBPH and cMyBPC resulted in reduced contractility upon β -adrenergic stimulation, indicating that the absence of this functional compensation between cMyBPC and MyBPH was detrimental to contractility. Our results thus suggested that both cMyBPC and MyBPH are essential for cardiac contraction.

4.1 Yeast two-hybrid analyses to identify interactors of MyBPH

In the present study, a total of 12 clones were able to activate three reporter genes and proved to be resistant to the antibiotic, Aureobasidin A (AbA), in Y2H analyses. Based on bioinformatic analyses and extensive literature research, putative interactors of MyBPH were prioritised for further verification and analyses. Interestingly, three MYH7 clones and three full mitochondrial clones were pulled out

using MyBPH in Y2H analyses, and all other identified putative interactors were represented by only a single clone.

4.1.1 Preys excluded from this study

Proteins were excluded from further study for the following reasons:

a) Non-relevant protein function

Of particular interest in the present study were proteins that could possibly be involved in pathways and processes that underlie the aetiology of HCM. Although a very recent study found an association between variants in *MTRNR2L2* and HCM (Hagen et al., 2013), at the time of our analyses, this protein had not previously been implicated in HCM, or in any processes or functions known to underlie the disease pathogenesis. This protein was therefore excluded as a putative interactor from further analyses in the present study. However, since this protein has previously been implicated in HCM, it would be worth investigating the interaction of this protein with MyBPH in future studies.

FLNC was also excluded from any further analysis based on the fact that it has been identified in almost every Y2H screen from past studies in our laboratory, suggesting that this protein acts as a “sticky” protein. It is unclear whether this promiscuity of FLNC is biologically relevant or if it is a result of an artefact of assays that use highly expressed proteins.

Additionally, the putative MyBPH interactor, FAF1, is the product of *PARK10*, which has been associated with late onset Parkinson’s disease (PD) (Hicks et al., 2002). A more recent study has implicated FAF1 in the pathogenesis of PD (Betarbet et al., 2008). Although this protein has previously been implicated in apoptosis (Chu et al., 1995) and is thought to mediate cell death, it has not been implicated in the development of hypertrophy or any obvious processes underlying the pathogenesis of HCM and was therefore excluded as putative interactor from further analyses. However, previous observations of MyBPH in the peri-nucleus and nucleus (Welikson and Fischman, 2002) and the nuclear location of FAF1 make an interaction with MyBPH very plausible, thus this putative interaction should be investigated in future in order to gain a more comprehensive understanding of MyBPH in the cardiomyocytes.

b) Incompatible cellular compartments

It is reasonable to assume that proteins localised in separate sub-cellular compartments *in vivo* will in all probability not interact. Therefore, all proteins that were not localised to the same compartment to where MyBPH is localised (cytosolic, peri-nuclear and nuclear) were excluded. In the present study, preys that exclusively localised to the mitochondria, or that were secreted into the extracellular matrix, such as FBN1, and proteins encoding the complete mitochondrial genome were excluded from further analyses. We thus hypothesised that since the localisations of these preys do not coincide with the sarcomeric C-zone localisation of MyBPH (cytosolic, peri-nuclear or nuclear), they would most likely not be able to interact with MyBPH.

4.1.2 MyBPH binds proteins involved in cardiac contractility

In cardiac muscle cells actin and myosin filaments, together with a larger number of scaffolding and regulatory proteins, are arranged into contractile units known as sarcomeres (section 1.2.1). The tight regulation of the formation of these sarcomeres, as well as the regulation of muscle contraction, is dependent on a complex network of protein-protein interactions (Ababou et al., 2007). In the present study, interactions of MyBPH with the contractile proteins myosin and actin were identified and verified.

Cardiac actin and myosin have both shown to be involved in contraction of the sarcomere (Gautel et al., 1995b; Levine et al., 2001; Skwarek-Maruszewska et al., 2009; Weisberg and Winegrad, 1996, 1998) and information regarding proteins that interact with these two proteins could contribute to the ever-growing knowledge about their role in cardiac contractility.

a) Myosin

Identifying MYH7 as a putative interactor of MyBPH in the current study by using the Y2H system confirmed a previously validated interaction between these two proteins (Alyonycheva et al., 1997b; Okagaki et al., 1993). Furthermore, these results proved the reliability and the efficacy of the Y2H system as a tool to identify putative interactors of MyBPH.

Sarcomeric myosin was observed to form clusters of spindle-shaped filament aggregates in the cytoplasm of COS cells expressing myosin but not MyBPH or cMyBPC (Moncman et al., 1993; Rindt et al., 1993; Seiler et al., 1996; Straceski et al., 1994; Vikstrom et al., 1993). However, myosin

formed long peri-nuclear cable-like structures in COS cells expressing GFP-tagged MyBPH and cMyBPC (Welikson and Fischman, 2002). Furthermore, domains C10 and H4 in cMyBPC and MyBPH respectively proved to be critical to induce myosin cable formation (Welikson and Fischman, 2002).

A study by Welikson and Fischman confirmed that MyBPH and myosin co-localised in a non-muscle COS cell system (Welikson and Fischman, 2002). However, co-localisation of these two proteins has not, to our knowledge, previously been investigated in cardiomyocytes. In fact, the interactions of MyBPH and cMyBPC with myosin investigated in COS cells were investigated in the absence of other sarcomeric proteins since COS cells do not contain sarcomeres (Moncman et al., 1993; Vikstrom et al., 1993). In the present study we showed that MyBPH and myosin co-localised to the same cellular region in differentiated H9c2 rat cardiomyocytes (section 3.2).

Not only did MyBPH and myosin co-localise in the present study, but the Co-IP analysis confirmed a physical interaction of MyBPH with myosin in differentiated H9c2 cardiomyocytes. The functional relevance of MyBPH interacting with myosin could be explained by the well-established interaction of the C-terminal of cMyBPC with myosin and titin (Freiburg and Gautel, 1996; Gilbert et al., 1999; Miyamoto et al., 1999; Okagaki et al., 1993). The interaction of cMyBPC with myosin is considered to be constitutive and it is crucial for the correct incorporation of cMyBPC into the thick filament (Koretz, 1979). Additionally, domains C6 to C10 of cMyBPC were demonstrated to be essential for the correct incorporation of cMyBPC into the A-band of the sarcomere (Gilbert et al., 1996, 1999). Moreover, this interaction is thought to play a role in the stability and stiffness of the thick filament (Nyland et al., 2009). We hypothesise that since MyBPH has strong homology to the C-terminal of cMyBPC (domains C6-C10), the interaction of MyBPH and myosin may have a similar function to that of the interaction of cMyBPC with myosin, i.e. the incorporation of MyBPH into the A-band of the sarcomere and the stabilisation and organisation of the thick filament.

Interestingly, despite the co-localisation of MyBPH with myosin in the peri-nuclear cables in COS cells (Welikson and Fischman, 2002), we observed co-localisation of these two proteins in the cytoplasm and membrane of the differentiated H9c2 cardiomyocytes (section 3.2). The difference in cell types, as well as the fact that the H9c2 cells were in a process of differentiating into myotubes, could explain the discrepancy in localisation of myosin and MyBPH in the current study. Furthermore, we postulate that the localisation of myosin and MyBPH to the membrane of differentiated cardiomyocytes, could be the

result of its structural and stabilising role and the organisation of the cardiomyotubes to form the thick filament.

b) Cardiac actin

In the normal adult myocardium, α -cardiac and α -skeletal actins are co-expressed and represent the majority of the actin isoforms in the thin filament of cardiomyocyte contractile units (Vandekerckhove et al., 1986). The α -cardiac isoform proved to be the dominant isoform present in a 20-week-old foetal heart that essentially exhibits all the morphological characteristics of adult hearts. Furthermore, this cardiac actin isoform proved to be expressed uniformly in these hearts (Suurmeijer et al., 2003).

A study by Skwarek-Maruszewska and colleagues demonstrated that contractility is essential for the accurate organisation of actin filaments during sarcomere maturation. For this reason, cardiomyocyte maturation is associated with an increase in the regular organisation of sarcomeric actin filaments and contractility-induced actin dynamics may thus play an essential role in depolymerisation of non-productive actin filaments during this process (Skwarek-Maruszewska et al., 2009). Interestingly, MyBPH has recently been implicated in cardiac actin organisation in non-muscle cells, since pulmonary adenocarcinoma (NC1-H441) cells treated with MyBPH-specific siRNA proved to contain more triton-insoluble filamentous actin (F-actin) (TIF) pools compared to control cells (Hosono et al., 2011). Triton-insoluble F-actin forms a three-dimensional cross-linked meshwork of actin filaments that include stress fibres (Watts and Howard, 1992) and associates with filamin A, α -actinin and tropomyosin. MyBPH was also found to inhibit Rho kinase 1 (ROCK1) through direct interaction, which in turn negatively regulates actomyosin organisation. These results suggest that MyBPH is involved in the regulation of cell shape, motility, invasion and metastasis in non-muscle cells (Hosono et al., 2011). In accordance with these results, we propose that in the present study, the interaction of actin with MyBPH could play a similar role in regulating the organisation of the sarcomeric actin filaments in differentiated cardiomyocytes.

MyBPH is structurally homologous to the C-terminal half of cMyBPC (domains FnIII-IgI-FnIII-IgI), but lacks the upstream regulatory region. The C-terminal domains (C5-C10) of cMyBPC have previously been shown to bind actin (Rybakova et al., 2011), resulting in the inhibition of actin-tropomyosin activity (Colson et al., 2012a). It is therefore possible that the interaction of MyBPH with actin identified (section 3.3) in the present study, could have a similar effect on actin dynamics to the interaction of cMyBPC with actin.

4.1.3 MyBPH binds a SUMO-conjugating enzyme

UBC9 is a unique SUMO-conjugating enzyme that is known to play a vital role in the sumoylation pathway (section 1.2.4.1). A previous study by Nacerddine and colleagues demonstrated that a targeted germ line mutation of mouse SUMO-specific UBC9 abolished the SUMO-conjugating pathway and that this affected nuclear functioning, which resulted in early embryonic lethality and caused severe defects in cell proliferation (Nacerddine et al., 2005). It is thus evident that UBC9 is a particularly critical component in the sumoylation process and could consequently be crucial for the maintenance of normal cardiomyocyte activities. In the present study a novel interaction between MyBPH and UBC9 was identified by Y2H, and subsequently verified by three-dimensional co-localisation and Co-IP analysis.

The co-localisation of UBC9 with MyBPH (section 3.2) in the present study provided convincing evidence for peri-nuclear localisation of UBC9. This is in accordance with that which was expected, since UBC9 has previously shown to be involved in several activities including DNA-binding (Pan et al., 2009; Tateishi et al., 2009), chromatin remodelling (Baek, 2006) and nuclear-cytoplasmic trafficking (Zhu et al., 2009). Interestingly, occasional peri-nuclear and nuclear localisation of MyBPH was observed in the present study, confirming results from a previous study (Welikson and Fischman, 2002).

Interestingly, findings from a recent article by Chase and co-workers proposed that sarcomeric proteins, tropomyosin and troponin are localised to the nucleus in striated muscle cells (Chase et al., 2013). Furthermore, they proposed the role of sumoylation in modifying the nuclear localisation and function of tropomyosin and troponin. Additionally, HCM-causing mutations, p.Glu192Lys and p.Glu62Gln, were predicted to alter the localisation of α -tropomyosin to the nucleus and the p.Ile172Thr mutation in the α -tropomyosin gene was predicted to alter sumoylation of this gene. It is thus possible that the interaction of MyBPH with UBC9 could aid in the trafficking of MyBPH to and from the nucleus. We therefore postulate that modifications in the interaction of MyBPH with UBC9 could alter normal nuclear structure, function and trafficking, which would influence the localisation and functioning of both MyBPH and UBC9 in cardiomyocytes. Studies have shown that both actin and myosin, in addition to being localised to the sarcomere, are also found in the nucleus, where they are involved in key functions, including transcriptional regulation and chromatin remodelling (De Lanerolle and Serebryanny, 2011; Grummt, 2006; Miralles and Visa, 2006). The

interaction of MyBPH with ACTC1, MYH7 and UBC9 could thus further implicate MyBPH in functions such as chromatin remodelling. Actin binding proteins have previously been shown to localise to the nucleus where they play critical roles in gene regulation (Baarlink et al., 2013; Nacerddine et al., 2005), it is thus possible that this may also be the case for MyBPH.

Epigenetic activation and silencing of genes is critical for cell survival. Several factors involved in chromatin remodelling proved to be modulated by the SUMO pathway and are important in cardiac development. For example, although the SUMO modification of histone deacetylases 1 and 2 has not yet been determined, it has been suggested that they are involved in regulating cardiac morphogenesis, growth and contractility (Montgomery et al., 2007). It is thus likely that altered sumoylation of these proteins during either embryonic cardiac development or the maintenance of postnatal heart function would promote abnormal gene expression. Altered gene expression could subsequently lead to dysfunctional chromatin remodelling and/or impaired cardiac structural formation. The dysfunctional regulation of several chromatin regulators has been associated with the development, regulation and stimulation of cardiac hypertrophy (Bartha et al., 2009; Gusterson et al., 2003; Vega et al., 2004; Yanazume et al., 2003; Zhang et al., 2011). It is therefore likely that the novel interaction of UBC9 with MyBPH could play a vital role in the normal functioning of sumoylation, and subsequently, chromatin remodelling, cardiac structural formation and development of hypertrophy.

UBC9 has also previously been implicated in muscle development. In previous independent investigations, UBC9 proved to be critical for the formation of myotubes in C2C12 cells (Nacerddine et al., 2005) and in muscle development in *Caenorhabditis elegans* (Nacerddine et al., 2005; Roy Chowdhuri et al., 2006). Therefore, the interaction of MyBPH with UBC9 could indicate that these proteins cooperatively play a role in the formation and maintenance of the structure of cardiac cells.

4.2 MyBPH and cMyBPC are implicated in the autophagic pathway

The observation of small circular structures upon staining of differentiated H9c2 rat cardiomyocytes with anti-MyBPH antibody in this study compelled further investigation into elucidating the cause for this specific expression and whether these structures could be autophagosomes. The co-localisation of MyBPH and cMyBPC with the autophagosomal protein LC3b-II to the membrane of the autophagosome strongly suggested that both these proteins are involved in autophagy. Although the main degradation system for sarcomeric proteins is thought to be the UPS, several studies suggest

that the autophagy-lysosome pathway (ALP) and UPS may function in concert to regulate the turnover of proteins (Zheng and Wang, 2010; Zheng et al., 2009). Additionally, truncated cMyBPC mutants have been associated with an impaired UPS system and the lysosome-inhibitor bafilomycin A1 was shown to increase the level of truncated cMyBPC after gene transfer in cardiomyocytes (Sarikas et al., 2005), implicating autophagy in the degradation of cMyBPC and suggesting that the turnover of cMyBPC indeed relies on the autophagic system. The extent to which this occurs can be quantified by using bafilomycin A1 at saturating concentrations and assessing the fold-change of the cMyBPC protein.

Interestingly, we did not observe co-localisation of MyBPH and cMyBPC with LC3b-II in all the autophagosomal structures. We thus postulate that these proteins may not only be processed in the autophagosome, but could be involved in the maturation process of the autophagosomal membranes, being recruited or targeted to the membrane only at very specific periods during maturation and membrane formation. Occasionally we observed peri-nuclear localisation of both MyBPH and cMyBPC proteins, similar to what has been seen in previous studies (Welikson and Fischman, 2002). This observation supported the suggestion that both MyBPH and cMyBPC could be targeted to the membrane of autophagosomes, as several studies have shown that autophagosomes are, at least in part, derived from the ER, although mitochondrial and golgi-based, as well as de novo synthesis, have been postulated (Arstila and Trump, 1968; Dunn, 1990; Ericsson, 1969; Fujita et al., 2008b; Hayashi-Nishino et al., 2009; Ylä-Anttila et al., 2009). It is thus possible that both MyBPH and cMyBPC are involved in the maturation and elongation of the membranes of autophagosomes, explaining the reason for observing co-localisation with LC3b-II in only some of the autophagosomes.

Another interesting observation from the present study was that both MyBPH and cMyBPC seemed to be involved in autophagy under basal conditions. This observation is in agreement with results from previous studies showing that constitutive autophagy under basal conditions serve as a homeostatic mechanism for maintaining normal cardiac structure and function (Nakai et al., 2007). In a recent study, Schlossarek and colleagues observed that a defective ALP is the underlying mechanism in genetically engineered mice with cardiac hypertrophy (Schlossarek et al., 2012). In their study, these investigators generated a homozygous cMyBPC KI mouse which expressed a known HCM-causing mutant cMyBPC, as well as homozygous cMyBPC KO mouse that expressed no cMyBPC (both of which exhibited significant cardiac hypertrophy) and showed that while both these mutant mice were able to activate autophagy, their autophagy responses were impaired (Schlossarek et al. 2012). The observation of impaired autophagy in the cMyBPC KO mice is

particularly interesting as it suggests that cMyBPC may be critical for the function of ALP. In addition to the indication that cMyBPC, and potentially MyBPH, relies on autophagy for protein turnover, we propose that cMyBPC and MyBPH could play a structural and functional role in autophagy, given that both cMyBPC and MyBPH localised to the membrane of the autophagosomes (section 3.4). Protein turnover by autophagy is thought to involve fusion of the outer membrane of the autophagosome with a vacuole or lysosome and in doing so exposes the inner autophagosome membrane and its luminal content to the degradation machinery of the vacuole or lysosome (Mizushima, 2011). However, the localisation of these proteins to the membrane of autophagosomes substantiates the implication of cMyBPC and MyBPH in the function and structure of the autophagosome membrane. Further findings from the study by Schlossarek and co-workers suggested that the impairment in autophagy in both the cMyBPC KI and KO mice is a result of a blockade of the fusion between autophagosomes and lysosomes. Therefore, it could be hypothesised that cMyBPC may play a role in the fusion of autophagosomes and lysosomes. Given the structural similarities between cMyBPC and MyBPH, it is thus possible that MyBPH may also be involved in this fusion process. Interestingly, although impaired autophagic activity was observed in cMyBPC KO mice, autophagy was not completely abolished (Schlossarek et al., 2012). These results suggest that other proteins, such as MyBPH, may partially compensate for the loss of cMyBPC in these mice, similar to the compensation we had observed in contractility.

4.3 MyBPH and cMyBPC play an essential part in contractility

The interactions of MyBPH with actin and myosin identified in the present study prompted the investigation into whether MyBPH is involved in cardiac contractility. By using targeted siRNA knockdown of both MyBPH and cMyBPC, individually and concurrently, the present study confirmed the results of previous investigations that cMyBPC acts as a modulator or regulator during cardiac contractility (De Lange et al., 2012; Gautel et al., 1995b; Harris et al., 2002; Stöhr et al., 2013; Weisberg and Winegrad, 1996). Additionally, our data suggested that both MyBPH and cMyBPC are essential for cardiac contractility and that these two proteins may work in concert to regulate cardiac contractility, at least under conditions of β -adrenergic stimulation.

It is well known that MyBPH and cMyBPC appear to function in the assembly and registration of thick filaments during myofibrillogenesis (Winegrad, 1999). Moreover, several studies have shown that phosphorylation of cMyBPC plays an essential role in regulating movement of the myosin head and

contraction of the myofilament (Gautel et al., 1995b; Levine et al., 2001; Weisberg and Winegrad, 1996, 1998).

Cardiac MyBPC is one of several sarcomeric proteins (phospholamban and troponin I) that is phosphorylated following β -adrenergic stimulation by cAMP-dependent protein kinase A (PKA) (Garvey et al., 1988; Hartzell and Titus, 1982). In the present study, the differentiated H9c2 cells were treated with isoproterenol to mimic a state of β -adrenergic phosphorylation. Phosphorylation of cMyBPC by PKA in cardiac muscle is thought to abolish the interaction of the myosin sub-fragment S2 for binding to cMyBPC (Ababou et al., 2008), and consequently myosin cross-bridges are in closer proximity to potentially interact with actin (Shaffer et al., 2009). Furthermore, the degree of phosphorylation of cMyBPC is thought to regulate the interactions between myosin and actin in the thick and thin filaments, respectively (Levine et al., 2001; McClellan et al., 2001). It is therefore hypothesised that in response to cMyBPC phosphorylation, the probability of myosin-actin cross-bridge formation would increase (Colson et al., 2008, 2010, 2012b; Hofmann et al., 1991; Weisberg and Winegrad, 1996). Therefore, the predicted effect is thought to result in an increased production of force and accelerate contractile kinetics, which would contribute to the dynamic capacity of the heart to respond to an increased demand for cardiac output.

Cardiac MyBPC KO mice have been used as a model to study the effect of phosphorylation of cMyBPC by PKA, as the complete loss of cMyBPC is expected to mimic the function of fully phosphorylated cMyBPC, inhibiting its effects upon contractility. Interestingly, many of these studies have observed a decrease in cardiac contractility (Brickson et al., 2007; Carrier et al., 2004; De Lange et al., 2012; Harris et al., 2002; Tong et al., 2008), although several other studies have observed contrasting results, since many predict an acceleration in contractile kinetics (Harris et al., 2002; Korte et al., 2003; Stelzer et al., 2006a, 2006b, 2006c, 2007; Tong et al., 2008) and others a deceleration (Carrier et al., 2004; Pohlmann et al., 2007). It is thought that the discrepancy in the results from these studies could be due to the marked hypertrophic remodelling that occurs in KO cMyBPC hearts (De Lange et al., 2012).

Our findings that the planar cell surface area of differentiated H9c2 rat cardiomyocytes with either reduced cMyBPC or MyBPH expression was not significantly changed upon β -adrenergic stimulation contradicts previous suggestions that cMyBPC KO mice exhibited decreased contractility (Brickson et al., 2007; Carrier et al., 2004; De Lange et al., 2012; Harris et al., 2002;

Tong et al., 2008). Interestingly, cMyBPC normally functions as a “brake” on cross-bridge kinetics by potentially stabilising the power stroke state or by functioning as an internal cross-bridge load (Hofmann et al., 1991; Palmer et al., 2004). Beta-adrenergic stimulation by PKA phosphorylation is thus thought to reverse the inhibitory effect of cMyBPC and increase cross-bridge kinetics, since PKA phosphorylation and the loss of cMyBPC have similar effects to increase cardiac contractility (Stelzer et al., 2006a, 2006b, 2006c, 2007).

The lack in contractile response that we observed with reduced expression of cMyBPC upon β -adrenergic stimulation could thus be explained by the fact that the functional cMyBPC remaining after the individual knockdown of cMyBPC was enough for the cardiomyocytes to function normally, or that MyBPH compensated for cMyBPC to some degree in response to β -adrenergic stimulation. Interestingly, a previous study suggested that the up-regulation of another myosin-binding protein could possibly be the reason that the sarcomere pattern in cMyBPC KO mice appear normal, although these hearts developed hypertrophy (Harris et al., 2002). Results of the present study indicated that MyBPH may be that protein.

Furthermore, our results show that although individual knockdown of cMyBPC and MyBPH did not have a significant effect on planar cell surface area, concurrent knockdowns of both proteins significantly increased the planar cell surface area, suggesting decreased contractility in response to β -adrenergic stimulation. This is in accordance with our expectation that reduced expression of cMyBPC should decrease contractile responses upon phosphorylation, which was based on observations from several previous studies (Brickson et al., 2007; Carrier et al., 2004; De Lange et al., 2012; Harris et al., 2002; Tong et al., 2008). We hypothesise that the discrepancy in results from the individual knockdown of cMyBPC and the concurrent knockdown may be explained by the lack of sufficient MyBPH in the concurrent knockdown group to compensate for the loss of cMyBPC. Cardiac MyBPC was therefore not available to continue its normal role by suppressing force generation and stabilising the power-stroke step of the cross-bridge cycle.

Evidence suggests that cMyBPC and its phosphorylation status are critical to the regulation of cardiac function. It has been well established that mutations of cMyBPC are most frequent causes of familial hypertrophic cardiomyopathy (Richard et al., 2003; Van Driest et al., 2005b). Furthermore, reduced phosphorylation of cMyBPC in humans has been associated with heart failure (El-Armouche et al., 2007) and atrial fibrillation (El-Armouche et al., 2006), known clinical features of

hypertrophic cardiomyopathy. A recent study by Tong and colleagues observed marked systolic dysfunction as a result of decreased phosphorylation in a mouse model lacking three cMyBPC phosphorylation sites in the absence of β -adrenergic stimulation (Tong et al., 2008). In the presence of β -adrenergic stimulation, cMyBPC could not be phosphorylated and the mutant mouse model exhibited blunted contractile reserve. Similarly, in our study the limited expression of both cMyBPC and MyBPH in the concurrent knockdown group may impair the ability of cMyBPC to be phosphorylated, thus resulting in impaired contractile function.

Results from our knockdown and contractility analyses suggests that PKA phosphorylation of cMyBPC accelerates cross-bridge kinetics, but that the reduced expression of cMyBPC and MyBPH leads to reduced contraction of differentiated H9c2 rat cardiomyocytes. From these results we thus postulate that both MyBPH and cMyBPC are essential for cardiac contraction.

4.4 Implications for MyBPH in cardiac sarcomere

In the present study Y2H analyses identified 12 putative protein interactors with various protein functions and localisations in the sarcomere. Myosin was the only identified putative interactor that has previously been documented and the others were all novel. It is plausible that cardiac dysfunction could be the result of altered pathways of which the identified protein interactions form part of. Considering that approximately 60% of HCM patients are identified with disease-causing mutations (Ramaraj, 2008), leaving the cause of HCM in 40% of HCM patients unresolved, putative interactors of proteins such as MyBPH serve as good candidate genes for investigating HCM-causing and HCM modifier effects.

The interaction of MyBPH with myosin is well defined (Alyonycheva et al., 1997b; Okagaki et al., 1993) and in our study we used Y2H and Co-IP and western blotting to confirm this interaction. The protein domain H4 is a known myosin-interacting domain, which supports the hypothesis that MyBPH is embedded in the thick filament at its C-terminal side, stabilising the thick filament similar to the interaction of myosin with cMyBPC (Nyland et al., 2009).

Despite the identification of the novel interaction of actin with MyBPH, the question remains which domain of MyBPH would interact with actin. If we consider the similarities between MyBPH and cMyBPC, it is reasonable to speculate that domains H1-H4 of MyBPH could interact with actin, as a

recent study by Rybakova and colleagues suggested that cMyBPC domains C6-C10, corresponding to MyBPH domains H1-H4, bind actin (Rybakova et al., 2011). If we propose that MyBPH domain H4 is embedded in the thick filament, domain H1 would be most likely reach the thin filament for interacting with actin. However, we do not exclude the possibility that any of the other MyBPH domains could interact with actin.

Results from the present study also implicated MyBPH in autophagy for the first time. Despite the fact that autophagy has been shown to be involved in the degradation of cMyBPC (Sarikas et al., 2005), neither cMyBPC nor MyBPH have previously been shown to co-localise with LC3b-II to the membrane of autophagosomes. To the best of our knowledge, the present study is the first to show an association of cMyBPC and MyBPH with autophagosome membrane formation and elongation, since co-localisation with LC3b-II to the autophagosome membranes were observed in only some of the autophagosomes at very specific periods during maturation and membrane formation. However, sequential ATG5 knockdown experiments are suggested to dissect the exact role of these proteins in the autophagic pathway, by assessing the potential change in cMyBPC and MyBPH on western blots and their localisation.

Interestingly, despite the absence of phosphorylation sites, such as those present in the N-terminal region of cMyBPC, MyBPH has been proven to affect the phosphorylation state of proteins involved in regulating actin dynamics in the cytoskeleton in non-muscle cells (Maekawa et al., 1999; Yoshioka, 2003). Additionally, Hosono and colleagues observed that MyBPH affects the phosphorylation state of LIM domain kinase 1 (LIMK1), likely to be a component of an intracellular signalling pathway, and cofilin 1, an intracellular actin modulating protein (Hosono et al., 2011). It could thus be hypothesised that although MyBPH does not contain any phosphorylation sites, it could play a role in regulating phosphorylation by interacting with proteins that are themselves involved in regulating phosphorylation.

Furthermore, in addition to postulating that both MyBPH and cMyBPC are essential for cardiac contractility, we propose that MyBPH can functionally compensate for cMyBPC to some degree, and vice versa. Compensation for a reduction or loss of cMyBPC or MyBPH would minimise the effect of the alterations or dysfunctions caused by mutations in these proteins. Most mutations found in cMyBPC result in either a disrupted reading frame or a stop codon and are therefore expected to produce truncated cMyBPC (Carrier et al., 1997). We postulate that the mild and late onset HCM

phenotype (Charron et al., 1998), that is associated with cMyBPC mutations could be because MyBPH can partially compensate for the loss of cMyBPC, resulting in a less severe phenotype.

4.5 Limitations of interaction studies

4.5.1 Yeast two-hybrid

The Y2H technique is a powerful, cost-effective assay that is methodically simple and has a high throughput capacity, making it a very popular tool for identifying protein-protein interactions in yeast cells (Fields and Song, 1989). Yeast is used as host to identify or investigate mammalian protein-protein interactions and serves as a true cellular environment (Brückner et al., 2009), since this *in vivo* technique is more similar to higher eukaryotic systems than systems that investigate interactions within a bacterial host (Van Criekeing and Beyaert, 1999).

However, several limitations are associated with this technique. Firstly, Y2H is associated with a high false negative rate and the number of interactions is thus largely underestimated. Secondly, certain interactions, such as interactions with membrane proteins, cannot be detected due to the localisation of the bait and prey protein in the yeast nucleus. Furthermore, interactions that require post-translational modifications, such as glycosylation and phosphorylation cannot be detected, unless the enzymes responsible for their modification happen to be present in the yeast cells, which is not always the case (Cusick et al., 2005). Transient interactions are also mostly not identified using Y2H analyses.

Another limitation of Y2H is the high false positive detection rate, as many identified interactions are not plausible physiological interactions. Technical false positives can be eliminated by specificity tests and heterologous matings. However, “sticky” proteins or incorrectly folded proteins are often identified as putative interactors. For example, in our study we identified FLNC, which is considered a “sticky” protein and were therefore not selected for further investigation (section 4.1.1).

For the above-mentioned reasons, it is therefore important to validate putative interaction identified by the Y2H assay using independent assays. In the present study we used co-localisation assays to determine whether the proteins in the identified interaction are located in the same sub-cellular region in a mammalian cell-based system to ensure that the interactions can take place in a more

physiologically relevant environment. Furthermore, interactions were verified by using both co-localisation and Co-IP assays in a relevant cell system.

4.5.2 H9c2 cardiomyocyte cell line

The survival of primary rat neonatal cardiomyocytes are approximately 5-8 days (personal communication, Prof B Huisamen) and since we needed to differentiate the cardiomyocytes for five to eight days before we could perform co-localisation or siRNA knockdown experiments, we had to consider that these cells would not be viable for the duration of the experiment.

We therefore selected the myoblast cell line H9c2, which is derived from embryonic rat heart. This cell line has been used as an *in vitro* model for both skeletal and cardiac muscles as the cells show electrophysiological and biochemical properties of both skeletal and cardiac tissues (Kimes and Brandt, 1976; Sardao et al., 2007).

Although H9c2 cells lack the ability to beat, they show many similarities to primary cardiomyocytes and have therefore previously been used for investigating molecular and cellular processes involved in myocardial hypertrophy, apoptosis, differentiation and toxicology (Koekemoer et al., 2009; Pereira et al., 2011; Watkins et al., 2011). Furthermore, H9c2 cells have ability to divide, compared with terminally differentiated cardiomyocytes, and many studies have used the H9c2 cardiomyocyte cell line as an animal-free alternative (Kimes and Brandt, 1976; Koekemoer et al., 2009). The above-mentioned studies suggest that cardiomyocyte cell lines are a valid *in vitro* system for examining key aspects of cardiomyocyte hypertrophy.

4.5.3 Co-localisation

Detecting endogenous proteins require specific, high quality primary antibodies that were raised against the protein of interest; often such antibodies are not commercially available or the quality or specificity of the available antibodies are very low. Often endogenous proteins cannot be detected if the protein components of the identified protein complex are not expressed in the available cell lines. However, in the present study, high quality primary antibodies were available and all proteins of interest could be detected in differentiated H9c2 rat cardiomyocytes.

It is important to bear in mind that although this technique can determine whether two proteins are localised to the same subcellular space, it gives no direct information about whether they physically

interact. Results from this technique can only aid in confirming the interaction between two proteins and needs to be used in combination with other verification techniques such as Förster resonance energy transfer (FRET) analysis or Co-IP assays. For FRET analyses, the resolution of light microscopy (approximately 200nm) is brought down to 2-10nm, as only then is FRET able to occur. This indicates protein-protein interaction on the nano-scale, as opposed to their mere proximity to one another based on co-localisation analysis. However, FRET analyses suffer from various drawbacks, including autofluorescence, detector noise, optical noise and photobleaching. Additionally, spectral bleedthrough or contributions of donor and acceptor fluorescence emission into the FRET channel is a major problem (Sekar, 2003). For this reasons, we selected Co-IP analyses for verifying protein interactions in the present study.

To obtain quantitative co-localisation information in the present study, quantitative 3D co-localisation was estimated by using Pearons's coefficient and an overlap coefficient. The manner in which these parameters quantify the level of co-localisation between two proteins has been associated with some drawbacks. Although Pearson's coefficient is not sensitive to the intensity of the background or the overlapping pixels, it is difficult to interpret. Furthermore, it does not provide any information about the individual fluorescent channels. The overlap coefficient is easier to interpret and is also not sensitive to the intensity of overlapping pixels. However, it is very sensitive to background and also provides no information about individual channels. Despite these disadvantages, using a combination of the two co-localisation quantification parameters to determine the co-localisation between two proteins of interest in the present study, provided more robust quantitative analyses.

DISCUSSION: MYBPH AND INTERACTORS AS MODIFIERS OF HYPERTROPHY

HCM has been viewed as a model in which to study the causal molecular factors underlying isolated cardiac hypertrophy. In addition to the variability in phenotype between patients harbouring different HCM-causing mutations, there is also a great deal of phenotypic variability among individuals harbouring the same causal mutation, suggesting that the phenotype can be modified by other genetic factors (Marian, 2002). These modifier genes are known to affect the severity of the phenotype, although they are neither necessary nor sufficient to cause the phenotype observed (Alcalai et al., 2008). Individual modifier genes that contribute to the variability of hypertrophy seen in HCM are largely unknown and the identification of such modifier genes could shed some light on the disease etiology and pathology underlying HCM.

In the present study, in addition to *MyBPH*, the genes encoding binding partners of MyBPH identified in the interaction studies (MYH7, ACTC1 and UBC9; sections 3.1 to 3.5) were assessed as candidate hypertrophy modifying genes contributing to the variability in disease phenotype in patients suffering from HCM. From the results obtained we have identified multiple associations of single variants and haplotypes with hypertrophy traits within the total study cohort, as well as within the three different HCM founder mutation groups. The results from the present study therefore suggest that some of these variants and haplotypes could contribute to cardiac hypertrophy, affecting the severity of HCM.

4.6 Caveats in association analyses

There are particular factors that concern association studies in general and these basic caveats affect the reproducibility of these studies. It is thus important to take these basic concerns into consideration to ensure the accuracy of the results in these types of studies. For this reason, we aim to address these concerns and caveats, with particular emphasis on identifying hypertrophy modifiers in HCM.

4.6.1 Population stratification

Undetected population structure could lead to the identification of spurious associations between specific genotypes and hypertrophy traits (Cardon and Palmer, 2003; Clayton et al., 2005; Cooper et al., 2008; Ioannidis et al., 2001; Koller et al., 2004). Population stratification is therefore considered a confounding variable that affects the association between a variant and disease trait (Colhoun et al., 2003).

A population that consists of two or more sub-populations, for which their allele frequency and disease risk is different, contribute to population stratification (Colhoun et al., 2003). It is therefore important to consider the structure of the population in designing an association study, especially if the allele frequencies and disease risk are very different amongst the sub-populations. In the present study the cohort consisted of sub-populations from different ethnic origins, viz., Caucasian and Mixed Ancestry. The latter population is known to have originated from an admixture of Khoi San, Dutch and Black African individuals (Loubser et al., 1999).

In complex association studies, such as the present study, we expected small to modest effect sizes, which could be confounded by population stratification. Additionally, considering the population structure of the cohort in the present study, we did correct for the confounding effect underlying population stratification to ensure the observation of true effects of specific genotypes on hypertrophy traits. There are several methods to correct for the confounding effects of population substructure. The genomic control (GC) method entails adjusting for a single factor that summarises the average effect of confounding (Devlin and Roeder, 1999). Another approach is to adjust for estimated ancestries (Pritchard et al., 2000) or ancestry-related principal components (Price et al., 2006). Both these methods are dependent on genotypes of a larger number of markers. To address confounding due to family structure, cryptic relatedness and population stratification, we applied a specialised mixed effects model that was also able to incorporate fixed and random effects (Price et al., 2010). In the present study, fixed effects included self-reported ethnicity to control for population stratification and random effects included individual-specific random effects (kinship coefficients measure relatedness) and family random effects, allowing for testing associations within and between families, all of which would also help to adjust for population structure (Price et al., 2010). These models ensure the maximum statistical power of the study.

4.6.2 Phenotypic definition and distribution

Accurate phenotypic classification and definition of patients is critical for the optimal design of association studies, as inaccuracies could affect the statistical power and reproducibility of an association study, consequently leading to spurious associations and effects. To minimise the chance of spurious associations the study design should consider the most appropriate methods for phenotypic classification and relevant statistical analyses.

Heritability is dependent on the accuracy of the phenotypic classification and definition. Inaccurate phenotypic classification of specific hypertrophy traits, such as described in the present association study, could therefore affect the strength of the study. Furthermore it is suggested that for association studies, quantitative measures should be easy to measure in a large cohort and should show high heritability (Newton-Cheh and Hirschhorn, 2005).

The phenotypic classification for HCM is particularly challenging as the cardiac phenotype of HCM is extremely heterogeneous and previous studies have shown that the clinical presentations vary greatly between individuals, even in individuals harbouring the same disease-causing mutation (Thierfelder et al., 1994). This is especially true since cardiac hypertrophy in HCM is usually asymmetrical and patients with HCM rarely exhibit concentric hypertrophy (Elliott et al., 2000; Roberts and Sigwart, 2001). Therefore, using one measurement to indicate the extent and distribution of hypertrophy in a HCM cohort would not be accurate. In the present study we therefore measured a number of quantitative traits to describe hypertrophy (section 2.18.1). One of the major advantages of investigating quantitative data (provided by measurements as described above), compared to information about the disease state (qualitative data), is that it enables a more accurate and comprehensive diagnosis of the disease (Newton-Cheh and Hirschhorn, 2005). This is especially important since HCM is a complicated disease that requires interpretation and the discretion of the treating cardiologist to make a diagnosis.

Since one single measurement is not sufficient to give a true representation of hypertrophy seen in any given individual in our cohort, we addressed this concern by using composite scores. The composite score, PC1, best describes the variability in the 16 wall thickness measurements at three levels in the heart measured in the present study. However, we do recognise that there are other composite scores that have been used in other association studies, such as the Wigle score (Wigle et al., 1985) and the Maron-Spirito score (Spirito and Maron, 1990). The Maron-Spirito score is a quantitative measure of the sum of the maximum wall thickness obtained from four left ventricular segments at mitral and papillary muscle levels of the heart. However, considering the variability in extent and distribution of LVH in HCM patients, this score is not suitable for accurately describing hypertrophy in HCM patients. Furthermore, this score will not incorporate LVH that is restricted to the apex in a less frequent form of HCM. Moreover, the semi-quantitative measure of the Wigle score is potentially open for subjective interpretation by the clinician, since it consists of a number of subjective scores added together to obtain a general impression of the extent of hypertrophy. In the present study, the composite score, PC1, offered a more accurate evaluation of the overall LVH since it

provided a weighted sum of wall thickness measurements of the combination of all 16 measurements, spread throughout the left ventricle.

The distribution of hypertrophy in mLWWT, mPWT and mIVST was measured using 2D and M-mode echocardiography, while echocardiography was used to measure LVM. The most commonly studied phenotype in HCM is LVM, as determined by echocardiography and it provides a more comprehensive measure of the extent of hypertrophy than that of a single wall thickness measurement. The extent and distribution of LVH in HCM is, however, extremely variable and asymmetric, as mentioned earlier, while echocardiographically determined LVM is derived from geometric assumptions. Therefore, echocardiographically determined LVM may be an inaccurate measure of total LVH in the context of HCM. The echocardiography measurements were taken by a single cardiologist. It is important to note that echocardiography is not as sensitive and reproducible as measurements ascertained by cardiac magnetic resonance imaging (cMRI) (Bauml and Underwood, 2010). However, for the design of the present association study echocardiography was not only more cost effective, but it was also readily available.

Due to the heterogeneity observed in the phenotype of HCM, the distribution of trait values are not normally distributed. Any deviation from the normal distribution of trait values affect the outcome of the analysis, since statistical models for association analysis of quantitative traits assume normal distribution of trait values (Diao and Lin, 2006; Lange et al., 2002). Therefore, in the present study, trait values were transformed to approximate normality (Pilia et al., 2006).

4.6.3 Linkage disequilibrium

Linkage disequilibrium (LD) is the non-random association of alleles at two or more loci, suggesting that the genotypes at these loci are not independent. It is important to bear in mind that even if seemingly non-functional variants show a significant association with a disease trait, the possibility exists that these variants could be in LD with other functional variants that could contribute to the risk of developing hypertrophy.

Genetic association between a variant and a specific disease trait indicates association with a specific region on the chromosome. The size of this region is dependent on the measure of LD in the particular ethnic population, since LD differs across populations of different ethnic origin (Conrad et al., 2006;

Gabriel et al., 2002; Hinds et al., 2005). Interestingly, the observed LD in Caucasian populations is known to be higher than the LD in African populations (Henn et al., 2011; Reich et al., 2001; Shifman et al., 2003). Variation in LD between populations is mainly affected by factors such as genetic drift, ethnic diversity and recent population admixture and inbreeding, which is considered population specific (Shifman et al., 2003).

Some other factors that underlie the variability in LD include recombinant patterns, gene conversion and natural selection, which are considered specific to particular genomic regions (Ardlie et al., 2002). It is thus expected that the variability of LD through the genome and that of markers in the region investigated might show variable patterns of LD, reflecting their history and selection. It is therefore possible that markers closely located to a functional variant could show more or less LD than markers located further away, although it is not currently possible to predict which of these variants will be in strongest LD with an adjacent functional variant (Cardon and Bell, 2001). Despite the concerns in variability of LD between populations of different ethnicity, we cannot ignore LD in association studies, such as the present study, since it can inflate false positive rates (Schaid et al., 2002).

It is, therefore, important to be familiar with the LD structure of the particular population under investigation. Ideally, one would use an LD map constructed from LD information from the particular population group under investigation. The cohort in our study consisted of mixed populations, including individuals from Caucasian and Mixed Ancestry. However, comprehensive LD maps are not available for all ethnic populations and at the time of marker selection, no specific LD map was available for either of our population groups. In the absence of such a specific map for our population, we used LD information from both the HapMap CEU and YRI populations as proxy for our population for marker selection purposes (section 4.6.4).

4.6.4 Marker selection

One of the major challenges researchers face in designing association studies is selecting appropriate polymorphic markers for genotyping since it is difficult to select a suitable set of markers that would allow for cost-effective genotyping. Fortunately, the development of high throughput genotyping technologies provides us with financially feasible methods to genotype more variants simultaneously, ensuring time-efficient and high quality results. The pattern of alleles of multiple markers is usually better able to predict the alleles at a loci that has not been genotyped, therefore simultaneous analysis of multiple markers improve the power of association studies (De Bakker et al., 2005).

It is not feasible to genotype all available markers in genes of interest, since not all markers are informative and genotyping such a large number of markers would not be cost effective. Additionally, the allele frequencies of markers are known to be different between population groups (Bamshad, 2005; Frazer et al., 2009; Ioannidis et al., 2004; Jorde and Wooding, 2004). For these reasons it is important to prioritise markers for genotyping, which requires selecting markers that would provide an association study with the highest possible statistical power at a reasonable cost. There are a number of proposed strategies for marker selection, one of which includes the selection of markers based on LD. This method is based on selecting SNPs according to their LD and makes use of metric LD maps, expressed in LD units (LDU). Linkage disequilibrium units define a metric coordinate system where the distances between SNPs are additive and these distances are directly proportional to the degree of LD between them (De La Vega et al., 2006). Furthermore, LDU maps provide greater power when compared to the centi-Morgan/kb maps. Therefore, these maps serve as a powerful tool for disease gene association mapping using LD.

Another proposed method to select markers for association studies is by selecting haplotype-tagging SNPs. This method takes into consideration that markers indicating high LD are often inherited together on a chromosomal segment. These segments contain a limited number of haplotypes that are found in the population, therefore it is possible to select a small subset of markers that distinguish or “tag” the common haplotypes previously found in a gene or locus in a given population. This method eliminates the necessity for a large number of markers to cover the region, which allows for a more cost effective study, with good statistical power (De La Vega et al., 2005a). In addition, previous studies have shown that a small number of haplotype tagging SNPs is necessary to capture most of the haplotype structure in high LD regions of the human genome (Johnson et al., 2001; Patil et al., 2001; Stram, 2004).

It is important to note that low MAF have previously been associated with reduced reliability of results in association studies (Donahue and Allen, 2005). It is therefore customary to select markers with a relatively high MAF (≥ 0.05), especially in association studies in small cohorts. Previous studies have associated markers selected based on the LDU maps and high MAF with increased statistical power and the ability to detect a true association (Weiss and Clark, 2002; Zhang and Sun, 2005; Zhang et al., 2002).

In the present study, SNPbrowser™ v4.1 software was used to select markers for association analyses (De La Vega et al., 2006). SNPbrowser is a freely available software tool that contains detailed information on millions of validated SNPs. The SNP collection includes more than a million genome-wide distributed SNPs genotyped by the International HapMap Project (International HapMap Consortium, 2003), which include gene and SNP annotations (De La Vega, 2007). Furthermore, it contains 160 000 intragenic SNPs that have previously been validated in four populations using TaqMan genotyping assays (De La Vega et al., 2002, 2005b) This software thus provided us with a comprehensive set of data to ensure the selection of an appropriate set of markers for an association study with results of high quality and power.

A combination of the two methods discussed above, together with a MAF frequency cut off of 5% was used to select an appropriate set of markers in the present study. As mentioned in section 4.6.3, we selected our markers based on information from LD maps, with LDU serving as guide, from HapMap CEU and YRI populations. In addition, all the remaining haplotype tagging SNPs that were not selected using the LDU approach were also included in the association study.

4.6.5 Genotyping approach

The PCR-based KASP™ genotyping assays proved to be a more efficient and cost-effective method than the PCR-based methods previously used to genotype the current cohort in our laboratory. PCR-based KASP™ genotyping assays are homogeneous, fluorescence (FRET)-based assays that enable accurate bi-allelic discrimination of known SNPs and insertion/deletions. The main advantage of KASP assays are that they require no labelling of target-specific primers or probes, giving it a clear cost advantage. Furthermore, genotyping clustering relative to most other PCR-based genotyping methods display marked improvement. Several of the samples genotyped in the current HCM cohort were collected years ago and the remaining DNA for some patients were very limited; however, the minimal DNA required for genotyping using these assays (0.1-10ng, based on genome size) allowed genotyping of more variants per individual.

4.6.6 Power

The statistical power of an association study refers to the probability that the result of a statistical test reflects a true association between a genetic variant and a phenotypic trait (Cardon and Bell, 2001; Gordon and Finch, 2005). Besides the genetic effect size, the power of a study is dependent on

several factors, which include marker allele frequency, the accuracy of phenotypic and genotypic classification and the number of confounding variables for which adjustments were made (Cardon and Bell, 2001; Colhoun et al., 2003; Gordon and Finch, 2005). The power of a study also depends on the number of individuals in the study group and how closely related they are, especially if an inherited trait is being investigated. The results from studies with relatively small study groups should thus be interpreted with caution. It is therefore important that the power of the study is taken into account in designing, and interpreting results from, an association study.

Currently, there are no statistical methods available to calculate the power of a study that includes extended families, such as the cohort in the present study. The number of individuals of the HCM cohort genotyped in this study is considered modest, however this is to be expected since HCM is estimated to affect one in every 500 individuals (as mentioned in section 1.1.1) (Maron et al., 1995). Additionally, taking into account that the laboratory where the work for the current study was undertaken serves as the reference laboratory for screening patients for HCM founder mutations in South Africa (as mentioned in section 1.1.4), the HCM cohort used in this study was the maximum study size available, and larger than any HCM-cohort with known genotypes used in a modifier study reported to date. We included all available family members of 27 HCM founder families, which is also one of the largest cohorts of individuals carrying a limited number of founder mutations.

4.6.7 Confounders

A confounder is a factor that is linked to the disease and the particular disease traits under investigation. Confounders are often the reason for spurious associations identified between a variant and a disease trait (Campbell and Rudan, 2002; Cordell and Clayton, 2005). It is therefore important to control for confounding effects to isolate the effect of a particular trait or disease. This could be addressed by structuring the cohort with regards to the distribution of known confounding variables. This was not an option in our study; therefore, in the current study, statistical models were used to adjust for known hypertrophy confounders. Adjusting for confounding variables are directly related to the reproducibility of an association study (Cardon and Palmer, 2003). An important factor in designing an association study, involves taking into consideration confounding variables. It is thus important to consider the underlying etiology of the disease when identifying confounders to adjust for.

The confounding variables for which adjustments were made in this study were age (Fleg and Strait, 2012; Lasky-Su et al., 2008), sex (Maass et al., 2004; Okin et al., 2000), BSA/HR

(Saba et al., 2001), mean arterial pressure (Roman et al., 2010), presence of hypertension (Kraja et al., 2011; Levy et al., 1990b; Puntmann et al., 2010; Sipola et al., 2011) and ethnicity (Okin et al., 2000). Additionally, since the HCM cohort genotyped in this study is one of the largest cohorts of individuals carrying the same founder mutations, the three HCM founder mutations (A797T_{MYH7}, R403W_{MYH7} and R92W_{TNNI2}) were adjusted for confounding hypertrophy.

4.6.8 Multiple testing

Multiple testing is associated with an increased probability of obtaining a significant association by chance (type 1 error). This is because when multiple hypothesis tests are performed in a study, there is a risk of increasing the chance of falsely claiming an association when there is in fact none. Currently, there are several methods to correct for type 1 error (false positives), of which Bonferroni adjustment is probably used most often. This approach is a particularly conservative method of stringent corrections and it assumes that all performed tests are independent; therefore, it involves multiplying each p-value with the number of tests performed. It is thus possible that associations between specific genotypes and disease traits could be missed due to stringency of the correction. In the present study the measured hypertrophy traits were derived from the same 16 wall thickness measurements (section 2.18.1) and since we observed some degree of LD between variants associated with the measured hypertrophy traits we could not assume, as Bonferroni method requires, that these variants are independent. Furthermore, since we do not have any prior information on the probability of the involvement of the variants in disease, the application of Bayesian methods for correcting for multiple testing was inappropriate (Campbell and Rudan, 2002; Thomas and Clayton, 2004). We therefore did not correct for multiple testing in the present study.

Currently there is no appropriate statistical method to adjust for multiple testing in studies with cohorts of extended family pedigrees and complex phenotypes such as the one used in the present study. It is thus possible that true biological effects could remain undetected if initial explorative studies are subjected to excessively stringent corrections for multiple testing. However, the replication of association studies remains critical, since false positive and negative results remain a possibility (Ioannidis et al., 2001). That said, since we considered our association study explorative and “hypothesis generating”, as opposed to “hypothesis driven”, we did not employ correction for multiple testing and consider these results a contribution to the understanding of the underlying etiology of HCM.

4.7 Use of haplotypes in association studies

The use of haplotypes in association analyses not only adds complexity to the study, but also increases the statistical power of the study, since haplotypes consider the compound effects of individual variants (Clark, 2004; Liu et al., 2008). This has been shown to be true for both family-based and population-based association studies (Akey et al., 2001; Bader, 2001; Botstein and Risch, 2003; Clark, 2004; Li and Jiang, 2005; Martin et al., 2000; Morris and Kaplan, 2002; Zaykin et al., 2002; Zhang et al., 2002).

For optimal design and interpretation of association studies, it is necessary to understand the structure of haplotypes in the human genome. Haplotypes are the particular combination of alleles (at multiple loci) observed in a population (Gabriel et al., 2002). Additionally, haplotypes are used to capture the inter-dependence of markers and are used to better understand LD patterns across the human genome (Ardlie et al., 2002; Liu et al., 2008; Weiss and Clark, 2002).

Haplotypes are considered a popular approach to complex disease mapping for several reasons. Firstly, there is a higher chance that haplotypes consisting of two or more markers would indicate LD with a disease mutation, than an individual marker (Garner and Slatkin, 2003). Secondly, haplotypes can be tested for association with a specific disease trait to serve as an indirect association with un-typed causal variants (Newton-Cheh and Hirschhorn, 2005). Furthermore, both haplotypes and tagging SNPs are proposed to be able to capture the associations of un-typed marker combinations. Interestingly, it is suggested that tagging SNPs could capture more un-typed variants efficiently, compared to haplotypes. However, in the present study there were no detailed LD maps available for our populations and consequently the selection of tagging SNPs was made using the HapMap YRI and CEU population LD maps. It is thus important to bear in mind that some information might have been lost in following this approach, as LD structures are known to be different between populations. Thirdly, haplotypes consisting of marker alleles that were associated with weak individual effects could be associated with stronger combined effects (Newton-Cheh and Hirschhorn, 2005). It is thus possible that although no significant effect is observed for individual markers, the compound effect of these markers could significantly affect the disease phenotype.

Haplotypes in coding regions have the ability to affect protein folding and function. For instance if several nucleotide changes occur in the coding regions of a gene without independently affecting the protein function, the combined effect of these variants could have a significant effect on the functioning

of the protein (Clark, 2004; Schaid, 2004). This is especially interesting since the present association study was preceded by a protein interaction study in which the proteins encoding the candidate genes investigated in the present association study were proven to interact with MyBPH. Despite genotyping very few coding variants and the incorporation of only a few of these coding variants into haplotypes, haplotypes with sufficiently high frequency in the cohort have previously been associated with altered protein function in humans (Clark et al., 1998; Fung and Gottesman, 2009; Hollox et al., 2001; Tavtigian et al., 2001). As described by Fung and Gottesman, a common haplotype, consisting of three mutations Gly412Gly, Ala893Ser and Ile1145Ile in the multidrug resistance (*MDR1*) gene, is suggested to play a role in drug response and disease susceptibility (Fung and Gottesman, 2009). Additionally, they propose a possible molecular mechanism of action by ribosome stalling that can change protein structure and function by altering protein folding.

In the present study the most likely pair of haplotypes for each individual was inferred using Simwalk (Sobel and Lange, 1996). This software programme has proven to be efficient in handling large datasets consisting of extended pedigrees and incorporating data that includes a certain proportion of missing information (Sobel and Lange, 1996). This software programme was therefore suitable for inferring haplotypes from our genotyping data, since our cohort consisted of extended pedigrees of which some information was missing.

4.8 Heritability

Heritability (h^2) refers to the estimated percentage contribution of genetic factors to the variability of a specific measured trait or disease. For association analyses it is critical to know which proportion of the variability observed in the quantitative measures investigated is attributable to genetic, and which to environmental factors. If the observed variability in quantitative measurements cannot be explained by a significant contribution of genetic factors, there would be no reason to continue with a genetic association study. Subsequently, the variability observed in disease phenotype, would then be ascribed to environmental factors, since there would be no significant genetic component underlying the observed variability.

The proportion of heritability of a specific trait is dependent on the effect of a number of modifier loci, especially in complex diseases (Manolio et al., 2009). However, these modifier loci explain only a modest proportion of the heritability underlying a specific trait. In the present study, the percentage contribution of genetic components to the variability of each measured trait was significant ($p < 0.001$)

(section 3.9.4). The heritability value of 59% estimated for LVM ($p < 0.0001$) was in agreement with findings from a previous study by Swan and colleagues, since they observed that 53% of the variation in LVM could be explained by genetic components ($p = 0.006$), after correcting for age, sex, blood pressure and weight (Swan et al., 2003).

4.9 Association analyses results

4.9.1 Myosin binding protein H (*MyBPH*)

The *MyBPH* SNPs rs2250509, rs3737872 and rs762625 each revealed a significant association with hypertrophy traits in only the $A797T_{MYH7}$ mutation group. However, no significant association between these variants and any of the measured hypertrophy traits were observed in the total cohort. The results suggest that the SNP effects could be diluted in the larger total cohort and that these variants could, however, act as modifiers of HCM when present with the $A797T_{MYH7}$ founder mutation. The C allele of rs2250509 was associated with increases in all but one of the hypertrophy traits (4.37mm in mIVST, 2.70mm in mLWWT, 0.84mm in mPWT and 3.5mm in the PC1 score), the T allele of rs762625 was associated with a 1.14mm increase in mPWT and, interestingly, the T allele of rs3737872 exhibited a significant increase of 29.4g in LVM.

Despite the absence of single SNP effects in the total cohort, we identified a significant association between haplotype GGTGCTT and an increase of 25.55g in LVM in the total cohort. This could be due to the fact that the variants act together to markedly affect hypertrophy development, while the individual effects were too weak to detect. Furthermore haplotype effects were observed in all three mutation groups, although the single variant associations were found only in the presence of the $A797T_{MYH7}$ mutation, further suggesting that the observed haplotype effects are owing to allelic interactions. Four of these haplotypes were observed at low frequency (Table 3.20) in the different mutation groups, while haplotypes GGTACTT and GGTGCTC were observed in the presence of the $A797T_{MYH7}$ HCM founder mutation at a frequency of 16% and 19%, respectively. Interestingly, these two haplotypes were associated with converse effects. Haplotype GGTACTT resulted in a marked increase of 2.62mm in mIVST, 2.76mm in mLWWT and 1.38mm in PC1 and haplotype GGTGCTC in a marked decrease of 20.98g in LVM. Additionally, a significant association between haplotype CGTGATC and a marked increase of 2.93mm in PC1 was found in the presence of the $R403W_{MYH7}$ mutation. This haplotype was observed at a frequency of 12% in the total cohort. These results suggest that the haplotype effects are dependent on the presence of the HCM founder mutation. The functional effect of this haplotype could be ascribed to the effect of functional variant with which it is in

LD that could be affected by the functional effect of the HCM-causing gene (or the effect of the HCM-causing mutation) or the functional effect of the modifying protein.

LD evaluation revealed that the three significantly associated variants (rs2250509, rs3737872 and rs762625) were in LD ($D'=1$) (Table 3.13). However, each of these variants affected different hypertrophy traits, all within the same A797T_{MYH7} mutation group. It is important to note that LD as indicated by D' is an estimate value as defined in section 2.22.2 and it is therefore possible that these variants are not necessarily in complete LD.

The rs762625 variant is positioned in the 5'UTR of *MyBPH*. *In silico* analysis was performed to determine the potential effect of this variant on transcriptional activity of *MyBPH*. The SNPInspector, within the Genomatix software suite v2.5 (<http://www.genomatix.de/>), evaluations revealed that the C allele abolished a transcription factor binding site for the transcription factor HAND2 (Cartharius et al., 2005). Interestingly, a recent study identified this transcription factor as one of four transcription factors, (GATA binding protein 4 (GATA4), HAND2, T-box5 (Tbx5) and myocardin) and two microRNAs (miRNA) (MiR-1 and MiR-133) that activated cardiac marker expression in neonatal and adult human fibroblasts (Nam et al., 2013). In the study by Nam and colleagues, human foreskin fibroblasts were cultured for four to 11 weeks in the presence of these transcription factors and miRNAs, and they managed to reprogramme the fibroblasts to form cells with sarcomere-like structures with calcium transients. Interestingly, a small subset of these cells were able to contract (Nam et al., 2013). Additionally, the activation of tropomyosin was found to be inhibited in the absence of HAND2 whereas, upon the removal of each of the remaining transcription factors, none of them affected the activity of tropomyosin. The authors speculated that the remaining reprogramming factors (GATA4, Tbx5, myocardin, MiR-1 and MiR-133) were functioning redundantly to complement the reprogramming activity of HAND2 in the activation of tropomyosin expression in human foreskin fibroblasts. The abolishment of the putative transcription factor binding site for HAND2 caused by the C allele of rs762625 could therefore result in altered binding of HAND2. This could subsequently affect tropomyosin activity and expression, which is essential for normal cardiac functioning. Interestingly, altered tropomyosin expression caused by mutations in the gene encoding tropomyosin has previously been associated with the pathogenesis of HCM (Prabhakar et al., 2001, 2003).

The SNPs rs2250509 and rs3737872, significantly associated with hypertrophy traits in the A797T_{MYH7} mutation group, are positioned intronically. *In silico* analyses were performed using software

programmes NetGene2 (<http://www.cbs.dtu.dk/services/NetGene2/>) and ASSP (<http://wangcomputing.com/assp/index.html>) to determine their potential effect on mRNA splicing. However, these variants did not indicate any differences in recognition of splice site motifs (Brunak et al., 1991; Hebsgaard et al., 1996). Despite no variation in predicted splice site recognition, the significant effects of these particular variants could be ascribed to that of unknown functional variants in LD with rs2250509 and rs3737872.

4.9.2 Myosin (*MYH7*)

The SNPs rs2147570, rs3729833, 7140721, rs3729825, rs7159367, rs2277475, rs2147533 and rs743567 were found to have a protective effect since their significant effects were shown to decrease various hypertrophy traits in the total cohort and in the presence of the R92W_{MYH7} and A797T_{MYH7} mutations. It is thus possible that the protective effect of these variants is dependent on the presence of the R92W_{MYH7} and A797T_{MYH7} mutations and that the effects are strong enough to observe in the total cohort. One other variant, rs2754163, was found to have a protective effect within the total cohort. The C allele of rs2754163 was found to decrease LVM by 10.7g, however this effect was not observed in any of the three mutation groups. It is possible that although the p-values for LVM in the A797T_{MYH7} (p=0.276), R403W_{MYH7} (p=0.436) and R92W_{TNNI2} (p=0.06) mutation groups were not significant, the larger size of the total cohort increased the power sufficiently to enable us to detect a significant association with LVM.

The GCCAACCATAGCGGCGGCG haplotype was shown to decrease LVM by 19.95g. This effect reflected the single SNP effects observed in the total cohort; i.e. the alleles of the single SNPs associated with a decrease in LVM were also present in the haplotype. This result is thus a reflection of the combined effects of the single SNP effects. However, the effects of haplotypes TTTTATCGTAGCGGCGGGA to decrease mPWT with 2.52mm and TTTTATCGTGGCGGCAACG to decrease PC1 with 1.69mm, mIVST with 2.88mm and mLWWT with 2.90mm in the total cohort, did not reflect the single SNP effect observed in the total cohort. Both these haplotypes had relatively large effects (Table 3.22). This result is consistent with the general trend observed in the contribution of genetic variation to complex phenotypes, where rarer variants are associated with larger effects compared to more common variants (Frazer et al., 2009). Furthermore, the significant effects of these haplotypes could thus be ascribed to allelic interactions of variants in the haplotype with each other or with other variants with which they are in LD.

Despite the observation of significant single SNP effects in all three mutation groups, significant haplotype effects were observed in the presence of the R403W_{MYH7} mutation, but not in the presence of the A797T_{MYH7} and R92W_{MYH7} mutations, suggesting that the observed haplotype effects are owing to allelic interactions. Interestingly, although the effect of the single variants and haplotypes observed in the three mutation groups were considered protective, the effect of haplotype GCCAACCGTAGTAGCAGGA was to increase mPWT with 1.48mm and PC1 with 2.71mm in the presence of the R403W_{MYH7} mutation. Not only could the effect of this haplotype be ascribed to allelic interactions, but it further suggests that this haplotype could act as a modifier in the presence of the R403W_{MYH7} mutation.

Significant associations were also identified between two common haplotypes and hypertrophy traits in the presence of the R403W_{MYH7} HCM founder mutation. Haplotype GCTTGCTGAATCGGTAACG was observed at a frequency of 13% and resulted in a significant decrease of 1.62mm in PC1 and haplotype GCTTGCTGAATCGGTAGCG, observed at a frequency of 21%, resulted in a significant decrease of 2.71mm in mIVST. Furthermore, these two haplotypes differ with respect to allele A and G of rs2239578 (underlined), neither of which were found to be significantly associated with any hypertrophy trait. Despite the fact that this variant is a tagging SNP, it was in low LD (D') with other variants significantly associated with hypertrophy traits. This result could be a reflection of the high LD observed in this large gene, or the fact that this particular variant is in LD with other functional variants not typed in the present study. All the variants associated with a significant effect, excluding rs2239577, in either the total cohort or within the mutation groups, were in LD with each other ($D'=1$). LD evaluations for SNP rs2239577 revealed LD ($D'>0.8$) with only rs2147570, rs3729833, rs3729825 and rs2147533 (Table 3.14).

The SNPs rs3729833, rs7140721, rs3729825, rs7159367, rs2277475, rs2147533, rs743567, rs2754163 and rs2239577 are positioned in the intronic region of *MYH7*. *In silico* analysis was performed to determine the potential effect of the associated alleles of each of these intronic variants on mRNA splicing of *MYH7*. NetGene2 (<http://www.cbs.dtu.dk/services/NetGene2/>) and ASSP (<http://wangcomputing.com/assp/index.html>) evaluations revealed that the C allele of rs7159367 resulted in an additional splice acceptor site (Brunak et al., 1991; Hebsgaard et al., 1996). The presence of an additional acceptor site could result in additional intronic sequences being incorporated in the mRNA. This could subsequently disrupt the splicing of the succeeding exon or it could shift the coding frame of the remaining exons. Additionally, NetGene2 predicted that the G allele of SNPs rs743567 abolished a donor splice site and the C allele of rs2754163 abolished an acceptor splice

site. The abolishment of an acceptor or donor site could result in aberrant splicing by skipping the splicing of an exon. The loss of the coding sequence could affect protein structure, function and expression. Interestingly, ASSP evaluations did not confirm the NetGene2 predictions which highlight the fact that these programmes merely provide predictions and it is therefore important that these results should be validated experimentally.

Micro RNAs (miRNAs) are single-stranded RNA species approximately 22 nucleotides long that form part of a large class of small, noncoding RNAs. miRNAs target mRNAs based on sequence complementarity mostly in the 3' UTRs (Zhang et al., 2007). We therefore used the SNP function Predictor software tool within the SNPinfo Web Server (<http://snpinfo.niehs.nih.gov/snpinfo/snpfunc.htm>) to perform *in silico* evaluations to determine if the SNP rs12147570, positioned in the 3'UTR region of the *MYH7* gene, could affect the binding of miRNAs to the mRNA of *MYH7*. *In silico* evaluations revealed no differences in miRNA binding sites between the T allele and the G allele that could affect the binding of miRNA sequences to the *MYH7* gene. In the case of perfect complementarity between the miRNA and target mRNA, the target RNA is degraded. In the absence of perfect complementarity, the target is not cleaved but is deadenylated, which leads to decapping and subsequent exonucleolytic digestion or translational repression (through a different mechanism at each translational step, namely initiation, elongation and termination) (Kuss and Chen, 2008).

To our knowledge, no association with hypertrophy or any functional role has been ascribed to any of the variants or haplotypes in the *MYH7* gene that were significantly associated with hypertrophy traits in our cohort. A few recent studies have, however, identified rs3729833 and rs12147570, rs3729825, rs7159367 and rs2277475 in an Egyptian patient with restrictive cardiomyopathy (Pinto et al., 2011) and rs3729833 in a Portuguese cohort with HCM (Santos et al., 2012) while screening for HCM-causing mutations. However, these studies did not find any significant association of any of these variants with HCM.

4.9.3 Cardiac actin (*ACTC1*)

In the present study, the C allele of SNP rs2070664 was found to have a protective effect, since it resulted in a significant decrease of 13.1g and 16.6g in LVM in the total cohort and in the A797T_{*MYH7*} mutation group, respectively. Conversely, the G allele of SNP rs7165006 was significantly associated with an increase of 31.2g in LVM, 3.25mm in mIVST and 1.17mm in mPWT within the A797T_{*MYH7*}

mutation group. LD evaluation revealed that these two SNPs were in perfect LD ($D'=1$) with each other (Table 3.15). These results suggest that the effects of rs7165006 are diluted or masked within the total cohort and that both these variants could act as modifiers of HCM in the presence of the A797T_{MYH7} mutation. Furthermore, it is possible that the effect of the G allele of SNP rs7165006 is dependent on the A797T_{MYH7} mutation. It may be that this SNP is in LD with a functional variant which could be affected by the functional effect of the HCM-causing gene (or the effect of the HCM-causing mutation) or the functional effect of the modifying protein.

The protective effect of haplotype CCCCA to decrease LVM with 16.95g and mLWWT with 1.43mm in the total cohort only partly reflects the effect of the C allele of SNP rs2070664 observed in the total cohort. Despite identifying a significant association between haplotype CCTGG and an increase of 35.25g in LVM in the total cohort, none of the alleles of the variants comprising this haplotype were associated with a similar effect in the total cohort. It is thus possible that the observed haplotype effects are the result of allelic interactions.

A significant association of haplotype CCTGG with increased LVM (44.61g) and mPWT (1.75mm) in the presence of the A797T_{MYH7} mutation correlated with significant effects of the G allele of SNP rs7165006, which is associated with a 31.2g increase in LVM and a 1.17mm increase in mPWT. These results suggest that the effect of this particular haplotype is a reflection of the effect of the G allele of SNP rs7165006.

Haplotypes CCCCG and CCTCA were associated with a significant increase of 1.69mm in mPWT and 23.39g in LVM within the R92W_{MYH7} group, respectively. These haplotype effects do not reflect single SNP effects within the mutation groups, since no single SNP in any of these two haplotypes were associated with any hypertrophy traits in the presence of the R92W_{MYH7} mutation. There are two possible reasons for this observation. Firstly, it may be that the effects of the single SNPs are too weak to detect, but that the interaction between these variants result in a significant combined effect and, secondly, it is possible that the effects of both these haplotypes are dependent on the presence of the R92W_{MYH7} mutation.

The rs2070664 and rs7165006 variants are positioned in the intronic region of *ACTC1* and were therefore subjected to *in silico* evaluation, however NetGene2

(<http://www.cbs.dtu.dk/services/NetGene2/>) and ASSP (<http://wangcomputing.com/assp/index.html>) evaluations did not predict any differences in recognition of splice sites (Brunak et al., 1991; Hebsgaard et al., 1996). The significant effects of these two variants could be due to unknown functional effects, since neither of these two variants have previously been characterised functionally or implicated in disease pathogenesis. Alternatively the effect could be ascribed to that of unknown functional variants in LD with rs2070664 and rs7165006.

4.9.4 SUMO-conjugating enzyme UBC9 (*UBC9*)

A significant association between the C allele of the *UBC9* SNP rs8052688 and an increase of 1.43mm in mIVST in the total cohort; however, this allele had no significant effect within the mutation groups. The AG genotype of SNP rs761060 demonstrated different effects in the three different mutation groups as it resulted in a 45.2g increase in LVM, a 2.73mm increase in mIVST and an 1.28mm increase in PC1 in the A797T_{MYH7} mutation group, a 0.74mm decrease in mPWT in the R403W_{MYH7} mutation group and a 1.00mm increase in mPWT in the R92W_{TNNI2} mutation group. The effect of the AG genotype could thus be dependent on the causal mutation with which it occurs, suggesting that the modifying effect of the AG genotype of this SNP is dependent on the HCM founder mutation with which it occurs. Interestingly, the rs761059 and rs8063 variants each revealed a significant effect only in the presence of the A797T_{MYH7} mutation. It is possible that the effects of these variants are diluted in the larger total cohort or that these variants could only modify the HCM phenotype in the presence of the A797T_{MYH7} mutation. Additionally, none of the variants found to have a significant effect in the total cohort or the mutation groups were in LD with each other ($D' < 0.6$) (Table 3.16).

Four haplotypes were found to be significantly associated with hypertrophy traits within the total cohort, of which the effects of haplotypes AAGCAGA and AAGCGAA reflected the effects of the C allele of SNP rs8052688 observed in the total cohort. However, haplotype AAGCAGA resulted in an increase of 2.79mm in mIVST and haplotype AAGCGAA resulted in an increase of 75.79g in LVM, 6.02mm in mIVST, 1.91mm in mPWT, 5.98mm in mLWWT and 2.27mm in PC1 while the C allele of rs8052688 only had an effect on mIVST, by increasing it with 1.43mm. The frequency of both these haplotypes was 3%, which is consistent with the general trend seen in the effect of genetic variation on complex phenotypes, where rare variants are associated with larger effects.

Intriguingly, the significant association of haplotype AAGGAGG with a decrease of 1.43mm in mPWT, and CGGGAGG with a decrease of 1.44mm in mLWWT in the total cohort did not reflect the single SNP effects observed within the total cohort. It is thus possible that the effects of the single variants were too weak to be detected, but that their combined effects have a significant effect on the disease phenotype. In the presence of the A797T_{MYH7} mutation, the AAGGAGG haplotype was significantly associated with a decrease of 2.85mm in mPWT and haplotype CGGGAGG with a decrease of 0.83mm in mPWT and 25.56g in LVM. Of particular interest is the fact that these two haplotypes shared the A allele of SNP rs761059 (underlined in the above haplotype), which was significantly associated with a decrease of 26.1g in LVM, 3.08mm in mIVST, 3.33mm in mLWWT, 0.96mm in mPWT and 1.81 in PC1 in the presence of the A797T_{MYH7} mutation. Collectively, these results suggest that these two haplotypes could have a protective effect in the presence of the A797T_{MYH7} mutation.

Haplotype analyses revealed one common haplotype, CGGGGGG, and a large range of low frequency haplotypes, as evident from Table 3.26. The effects of these haplotypes were markedly different in the presence of the three HCM founder mutations and only partly reflected the effects of the single SNPs observed within the mutation groups, suggesting that the effects of these haplotypes could be due to allelic interactions. For instance, haplotype AAGCGAA was significantly associated with an increase of 132.50g in LVM, 11.25mm in mIVST, 10.82mm in mLWWT, 3.96mm in mPWT and 4.18mm in PC1 in the presence of the A797T_{MYH7} mutation and was associated with an increase of 2.85mm in mPWT in the presence of the R92W_{TNNI2} mutation. However, this haplotype was only present at a frequency of 3%. On the other hand, haplotype AAGGGAA was found in the presence of different HCM founder mutations, since this haplotype resulted in an increase of 83.26g in LVM in the presence of the A797T_{MYH7} mutation and a decrease of 94.90g in the presence of the R403W_{MYH7} mutation. However, this haplotype was observed at a frequency of only 1% in the total cohort. Taken together, the large effects of these low frequency haplotypes are consistent with the current theory that rarer variants exert greater effects in complex phenotypes.

Interestingly, none of the alleles in haplotype CGGGGGG were individually, significantly associated with any hypertrophy traits in the total cohort or any of the three mutation groups. This particular haplotype was found to have a protective effect by decreasing PC1 by 11.72mm in the presence of the R92W_{TNNI2} HCM founder mutation. Furthermore, this haplotype was observed at a relatively high frequency of 36% in the total cohort. These results suggest that the significant haplotype effect observed may be ascribed to allelic interactions among variants present in the haplotype or variants with which they are in LD.

The SNPs rs8052688, rs761059 and rs761060 are positioned in the intronic region of *UBC9* and SNP rs8063 is positioned in the 3'UTR region. *In silico* evaluations using NetGene2 (<http://www.cbs.dtu.dk/services/NetGene2/>) and ASSP (<http://wangcomputing.com/assp/index.html>) revealed some rather interesting results (Brunak et al., 1991; Hebsgaard et al., 1996). ASSP evaluation of rs8052688 found that the C allele resulted in an additional acceptor splice site. Furthermore, NetGene2 found that the A allele of rs761059 resulted in an additional acceptor splice site. Additionally, both ASSP and NetGene2 evaluations found that the A allele of rs761060 resulted in an additional splice acceptor site. These results indicate that the additional acceptor sites, predicted as a possible result of these variants, could be retained in the mRNA sequence and may consequently disrupt splicing.

In silico evaluation of rs8063, using the SNP function Predictor software tool within the SNPinfo Web Server (<http://snpinfo.niehs.nih.gov/snpinfo/snpfunc.htm>), revealed several miRNA binding sites that could affect the binding of miRNA sequences to the *UBC9* gene. The A allele is predicted to create an additional binding site for the miRNA hsa-miR-1236, while abolishing hsa-miR-500 and hsa-miR-1237 binding sites. The binding of a miRNA to the 3'UTR of the *UBC9* mRNA could cause translational repression and/or mRNA degradation, while the loss of miRNA binding sites could result in the up-regulated gene expression. These miRNAs have, to date, not been associated with any cardiac disease. However, changes in miRNA expression levels have been associated with cardiac stress and development of cardiac hypertrophy (Sayed et al., 2007). It is thus possible that these specific miRNAs could thus serve as a biomarker for HCM, since the specific expression patterns and biostability of miRNAs allow for their detection in human plasma and serum and miRNAs have been suggested as relevant markers for heart failure (Gilad et al., 2008; Van Empel et al., 2012).

None of the SNPs demonstrating a significant effect have functionally been characterised and although SNPs rs8052688 and rs8063 have previously been associated with an increased risk of developing mild cognitive impairment of the amnesic type in young women (Cacabelos et al., 2012) and SNP rs761059 have been associated with Alzheimer's disease (Ahn et al., 2009), none of these SNPs have been associated with HCM.

4.10 Closing thoughts and future direction

While several novel MyBPH-interacting proteins have been identified in the present study, it is important that future investigations are conducted in order to verify the putative interactions of MyBPH with FLNC, MTRNL2L2, FAF1 and fibrillin 1 (FBN1). The results from the current study provide a good platform for further investigations into the role of MyBPH and each of the identified putative MyBPH-interactors in the structure and function of the sarcomere, including the mechanisms underlying hypertrophy in HCM.

Interestingly, previous findings observed impaired autophagic activity in cMyBPC KO mice, although autophagy was not completely abolished (Schlossarek et al., 2012). These results suggest that other proteins may partially compensate for the loss of cMyBPC in these mice. We therefore postulate that since MyPBH could compensate for the partial loss of cMyBPC, as was found in the contractility assay (section 3.5.2), it may also be able to compensate for the loss of cMyBPC with respect to autophagy. Therefore, future studies should investigate the change in autophagic activity after individual and concurrent knockdowns of MyBPH and cMyBPC to confirm whether these two proteins compensate for each other to some extent, and what the effect of the loss of cMyBPC and MyBPH would have on autophagy under basal conditions. If autophagosome accumulation is shown to increase during these conditions, these proteins are indeed required for autophagy.

It has been well established that mutations of cMyBPC are the most frequent causes of familial hypertrophic cardiomyopathy (Richard et al., 2003; Van Driest et al., 2005b). Given the similarity in terms of its location, structure and function within the sarcomere to the MyBPH protein, mutation screening of the *MyBPH* gene for HCM-disease causing mutations in South African probands should be included in future studies.

From previous studies it is known that the H4 domain in the C-terminal of MyBPH interacts with light meromyosin (LMM)-binding sites within myosin (section 1.4.2.1). The present study confirms previous findings that MyBPH interact with MYH7 (Alyonycheva et al., 1997b; Okagaki et al., 1993). However we did not confirm which MyBPH domains interacted with myosin. Although the A797T_{MYH7} and R403W_{MYH7} HCM founder mutations are located within the head domain of myosin, which have not shown to interact with MyBPH before, it would be interesting to investigate whether these two mutations would affect the interaction of myosin with MyBPH.

It is important to note that since the association study served as a basis for continuing studies, the current association study would need to be replicated to confirm the results. Additionally, the results from the association analyses warrant further investigation to establish the functional role of the identified modifying single variants and haplotypes in the sarcomere. For instance, since the rs8063 variant in the *UBC9* gene was predicted to create a binding site for the hsa-miR-1236 miRNA and to abolish the binding sites for the hsa-miR-500 and has-miR-1237 miRNAs; it would be interesting to investigate whether these alterations in miRNA-binding would affect translational repression and/or gene expression. Co-transfecting H9c2 cells with a luciferase expression vector containing the rs8063 variant, and each of the three different miRNAs, would allow for detecting differences in luciferase signal, which would be an indication of activation of gene expression. The binding of a miRNA to *UBC9* would, in theory, reduce the expression of *UBC9*, resulting in decreased luciferase signal.

4.11 Conclusion

In the present study we identified 12 putative interactors of MyBPH, of which interactions with MYH7, ACTC1 and UBC9 were confirmed using co-localisation and Co-IP analyses. These interactions expand our knowledge about the interactome of MyBPH and its possible function within the cardiac sarcomere. Furthermore, the results of the present study ascribe novel functions to MyBPH. We show that MyBPH and cMyBPC are involved autophagy and that in combination with cMyBPC, MyBPH plays a critical role in sarcomere contraction. Additionally, these results confirmed that MyBPH could compensate for cMyBPC and vice versa, further confirming that both these proteins are required for efficient sarcomere contraction. Results from association analyses suggest that single variants and haplotypes of *MyBPH*, and the genes encoding the binding partners of MyBPH, could play a role as modifiers of LVH in the context of HCM, contributing to the severity of the disease phenotype. The results from the interaction and association studies therefore provide a platform for future studies which could improve our knowledge of the role these proteins play in the sarcomere, which could possibly contribute to improved risk profiles and management of HCM patients.

APPENDIX I
SOLUTIONS AND BUFFERS

1. DNA EXTRACTION SOLUTIONS**Cell lysis buffer**

Sucrose	0.32M
Triton X-100	1%
MgCl ₂	5mM
Tris-HCl	10mM

Add ddH₂O to a final volume of 1L

3M Sodium acetate

Sodium acetate	40.81g
ddH ₂ O	50ml

Adjust pH to 5.2 with glacial acetic acid and adjust volume to 100ml with ddH₂O

Na-EDTA solution

NaCl	18.75ml of 4mM stock solution
EDTA	250ml of 100mM stock solution

Mix well

TE-buffer (10x stock solution)

TrisOH	0.1M (pH 8.00)
EDTA	0.01M (pH 8.00)
H ₂ O	150ml

Mix well

Phenol/chloroform

Phenol (saturated with 1x TE) 50ml

Chloroform 48ml

8-hydroxyquinone 2ml

Mix well, store at 4°C

Chloroform/octanol (24:1)

Chloroform 96ml

Octanol 4ml

Mix well, store at 4°C

2. ELECTROPHORESIS STOCK SOLUTIONS**SB buffer (20X stock)**

Di-sodium tetraborate decahydrate 38.137g/mol

Add ddH₂O to a final volume of 1L

10X SDS-PAGE running buffer

Tris base 30g

Glycine 144g

10% SDS 100ml

Add ddH₂O to a final volume of 1L

1X SDS-PAGE running buffer

1X SDS-PAGE running buffer 100ml

Add ddH₂O to a final volume of 1L

3. LOADING DYES

Cressol

Cressol red solution	10mg in 1ml ddH ₂ O
Sucrose solution	3.4g sucrose in 9.8ml ddH ₂ O

Add 200µl Cressol red solution to 10ml of sucrose solution

Ethidium bromide

Ethidium bromide	500mg
ddH ₂ O	50ml

4. GELS

1% agarose gel

Agarose	1g
SB buffer (1X)	100ml

Microwave for 1 minute on maximum power and add 5µl ethidium bromide (10mg/ml) when temperature of approximately 55°C is reached

5. Co-IP REAGENTS

TBST (pH 7.6)

NaCl	8g
1M Tris-HCl (pH 7.6)	20ml
Tween 20	1ml

Add ddH₂O to a final volume of 1L. Adjust pH to 7.6 and store solution at room temperature

6. WESTERN BLOT REAGENTS

Phosphate buffer saline (PBS)

PBS tablet 1 tablet

Add ddH₂O to final volume of 200ml.

Dissolve tablet and store solution at 4°C

Passive cell lysis buffer

EDTA 0.5M

NaVO₄ 1M

Nappi 1M

HEPES 1M

NaCl 5M

Triton X-100 1%

Add ddH₂O to a final volume of 200ml and store at 4°C. Prior to use, add 1mM PMSF and dissolve protein inhibitor tablet (1 tablet/20ml working solution)

7. YEAST TRANSFORMATION REAGENTS

1M LiAc

LiAc 5.1g

Add ddH₂O to final volume of 50ml

100mM LiAc

1M LiAc 5ml

Add ddH₂O to final volume of 50ml

50% PEG 4000

PEG 4000 25g

Add ddH₂O to final volume of 50ml

8. YEAST PLASMID PURIFICATION SOLUTIONS**Yeast lysis buffer**

SDS	1%
Triton X-100	2%
NaCl	100mM
Tris, pH 8	10mM
EDTA, pH 8	1mM

9. YEAST MEDIA**YPDA media**

Difco peptone	10g
Yeast extract	10g
Glucose	10g
L-adenine hemisulphate (0.2% stock solution)	7.5ml

Add ddH₂O to a final volume of 500ml. Autoclave at 121°C for 15 minutes

2X YPDA media

Difco peptone	12g
Yeast extract	6g
Glucose	12g
L-adenine hemisulphate(0.2% stock solution)	9ml

Add ddH₂O to a final volume of 500ml. Autoclave at 121°C for 15 minutes

0.5X YPDA media

Difco peptone	2g
Yeast extract	1g
Glucose	2g
L-adenine hemisulphate(0.2% stock solution)	1.5ml

Add ddH₂O to a final volume of 200ml. Autoclave at 121°C for 15 minutes

YPDA agar plates

Difco peptone	10g
Yeast extract	10g
Bacto agar	10g
Glucose	10g
L-adenine hemisulphate (2.0% stock solution)	7.5ml

Add ddH₂O to a final volume of 500ml and autoclave at 121°C for 15 minutes. Allow to cool to a temperature of approximately 55°C, prior to pouring approximately 20, 90mm plates. These plates were then allowed to set for 2 to 5 hours and stored at room temperature for up to 3 weeks

SD-Trp media

Glucose	12g
Yeast nitrogen base without amino acids	4g
SD-Trp amino acid supplement	0.4g

Add ddH₂O to a final volume of 600ml and adjust pH to 5.8 and autoclave at 121°C for 15 minutes

SD-Trp agar plates

Glucose	12g
Yeast nitrogen base without amino acids	4g
Bacto agar	12g
SD-Trp amino acid supplement	0.4g

Add ddH₂O to a final volume of 600ml. Adjust pH to 5.8 and autoclave at 121°C for 15 minutes. Allow to cool to a temperature of approximately 55°C, prior to pouring approximately 20, 90mm plates. These plates were then allowed to set for 2 to 5 hours and stored at room temperature for up to 3 weeks

SD-Leu media

Glucose	12g
Yeast nitrogen base without amino acids	4g
SD-Leu amino acid supplement	0.4g

Add ddH₂O to a final volume of 600ml and adjust pH to 5.8 and autoclave at 121°C for 15 minutes

SD-Leu agar plates

Glucose	12g
Yeast nitrogen base without amino acids	4g
Bacto agar	12g
SD-Leu amino acid supplement	0.4g

Add ddH₂O to a final volume of 600ml. Adjust pH to 5.8 and autoclave at 121°C for 15 minutes. Allow to cool to a temperature of approximately 55°C, prior to pouring approximately 20, 90mm plates. These plates were then allowed to set for 2 to 5 hours and stored at room temperature for up to 3 weeks

SD-Trp-Leu media

Glucose	12g
Yeast nitrogen base without amino acids	4g
SD-Trp-Leu amino acid supplement	0.4g

Add ddH₂O to a final volume of 600ml and adjust pH to 5.8 and autoclave at 121°C for 15 minutes

SD-Trp-Leu agar plates

Glucose	12g
Yeast nitrogen base without amino acids	4g
Bacto agar	12g
SD-Trp-Leu amino acid supplement	0.4g

Add ddH₂O to a final volume of 600ml. Adjust pH to 5.8 and autoclave at 121°C for 15 minutes. Allow to cool to a temperature of approximately 55°C, prior to pouring approximately 20, 90mm plates. These plates were then allowed to set for 2 to 5 hours and stored at room temperature for up to 3 weeks

TDO media

Glucose	12g
Yeast nitrogen base without amino acids	4g
SD-Trp-Leu-His amino acid supplement	0.4g

Add ddH₂O to a final volume of 600ml and adjust pH to 5.8 and autoclave at 121°C for 15 minutes

TDO agar plates

Glucose	12g
Yeast nitrogen base without amino acids	4g
Bacto agar	12g
SD-Trp-Leu-His amino acid supplement	0.4g

Add ddH₂O to a final volume of 600ml. Adjust pH to 5.8 and autoclave at 121°C for 15 minutes. Allow to cool to a temperature of approximately 55°C, prior to pouring approximately 20, 90mm plates. These plates were then allowed to set for 2 to 5 hours and stored at room temperature for up to 3 weeks

QDO media

Glucose	12g
Yeast nitrogen base without amino acids	4g
SD-Trp-Leu-His-Ade amino acid supplement	0.4g

Add ddH₂O to a final volume of 600ml and adjust pH to 5.8 and autoclave at 121°C for 15 minutes

QDO agar plates

Glucose	12g
Yeast nitrogen base without amino acids	4g
Bacto agar	12g
SD-Trp-Leu-His-Ade amino acid supplement	0.4g

Add ddH₂O to a final volume of 600ml. Adjust pH to 5.8 and autoclave at 121°C for 15 minutes. Allow to cool to a temperature of approximately 55°C, prior to pouring approximately 20, 90mm plates. These plates were then allowed to set for 2 to 5 hours and stored at room temperature for up to 3 weeks

SD-Ura agar plates

Glucose	12g
Yeast nitrogen base without amino acids	4g
Bacto agar	12g
SD-Ura	0.4g

Add ddH₂O to a final volume of 600ml. Adjust pH to 5.8 and autoclave at 121°C for 15 minutes. Allow to cool to a temperature of approximately 55°C, prior to pouring approximately 20, 90mm plates. These plates were then allowed to set for 2 to 5 hours and stored at room temperature for up to 3 weeks

SD-His agar plates

Glucose	12g
Yeast nitrogen base without amino acids	4g
Bacto agar	12g
SD-His	0.4g

Add ddH₂O to a final volume of 600ml. Adjust pH to 5.8 and autoclave at 121°C for 15 minutes. Allow to cool to a temperature of approximately 55°C, prior to pouring approximately 20, 90mm plates. These plates were then allowed to set for 2-5 hours and stored at room temperature for up to three weeks

SD-Ade agar plates

Glucose	12g
Yeast nitrogen base without amino acids	4g
Bacto agar	12g
SD-Ade	0.4g

Add ddH₂O to a final volume of 600ml. Adjust pH to 5.8 and autoclave at 121°C for 15 minutes. Allow to cool to a temperature of approximately 55°C, prior to pouring approximately 20, 90mm plates. These plates were then allowed to set for 2 to 5 hours and stored at room temperature for up to 3 weeks

Aureobasidin A stock solution (500µg/ml)

Aureobasidin A	1mg
----------------	-----

Dissolve in 2ml absolute ethanol. Store at 4°C

Aureobasidin A working solution (125ng/ml)

Aureobasidin A stock solution	150µl
-------------------------------	-------

Add to 600ml dropout agar media after cooled to temperature of approximately 55 °C, prior to pouring approximately 20, 90mm plates. These plates were then allowed to set for 2 to 5 hours and stored at room temperature for up to 3 weeks

X-α-galactosidase stock solution (20mg/ml)

X-α-galactosidase	20mg
-------------------	------

Dimethylformamide	1ml
-------------------	-----

Prepare a 20mg/ml stock. Store at -20°C in the dark

X-α-galactosidase Working Solution (5mg/ml)

Add 1.2ml of X-α-galactosidase stock solution to 600ml dropout agar media after cooled to temperature of approximately 55 °C, prior to pouring approximately 20, 90mm plates. These plates were then allowed to set for 2 to 5 hours and stored at room temperature for up to 3 weeks

10. SOLUTIONS FOR THE ESTABLISHMENT OF BACTERIAL COMPETENT CELLS**CAP buffer**

CaCl ₂	2.21g
-------------------	-------

Glycerol	37.5ml
----------	--------

PIPES	0.76g
-------	-------

Add ddH₂O to final volume of 250ml. Adjust pH to 7.0 and store at 4°C

11. BACTERIAL MEDIA

LB media

Bacto tryptone	5g
Yeast extract	2.5g
NaCl	5g
Bacto agar	8g

Add ddH₂O to final volume of 500ml. Autoclave and add appropriate antibiotic (Ampicillin 25mg/l, Kanamycin 5mg/l or ZeocinTM 10mg/l) to the media when cooled to temperature of approximately 55°C is reached, prior to pouring approximately 20, 90mm plates. These plates were then allowed to set for 2 to 5 hours and stored at room temperature for up to 3 weeks

12. EUKARIOTIC CELL CULTURE MEDIA

Complete growth media

DMEM (4.5g/L glucose, with L-glutamine)	178ml
Foetal calf serum (heat inactivated)	20ml
Penicillin/Streptomycin	2ml

Serum-free media

DMEM (4.5g/L glucose, with L-glutamine)	196ml
Pre-warm to 37°C before use	

Differentiating growth media

DMEM (4.5g/L glucose, with L-glutamine)	196ml
Horse serum	2ml
Penicillin/Streptomycin	2ml
Pre-warm to 37°C before use	

13. CO-LOCALISATION REAGENTS

Mowiol

Glycerol	30g
Mowiol 4-88	12.0g

Add ddH₂O to final volume of 30.0ml. Heat for 1 hour at 55°C, Centrifuge at 5000g for 15 minutes to remove undissolved particles. Aliquot supernatant in 2ml tubes, store at -20°C. Prior to use, freshly add <0.01g n-propylgallate as anti-fade, heat for 1 hour at 55°C. Centrifuge at 5000rpm for 5 minutes to remove undissolved particles, remove supernatant as mounting media. Store in dark at 4°C for 3 to 4 weeks

APPENDIX II**CALCULATING YEAST MATING EFFICIENCIES (Calculations based on Clontech Manual)**

Count number of colonies on all plates with 30-300 colonies after 4 days.

$$\text{\#colony forming units (cfu/ml)} = \frac{\text{cfu} \times 1000\mu\text{l/ml}}{\text{Volume plated } (\mu\text{l}) \times \text{dilution factor}}$$

1. Number of cfu/ml on SD-Trp plates = viability of bait partner
2. Number of cfu/ml on SD-Leu plates = viability of prey library
3. Number of cfu/ml on SD-Trp-Leu plates = viability of diploids
4. Lowest number of cfu/ml of SD-Trp or SD-Leu plates indicate limiting partner

$$5. \text{ Mating efficiency (\% diploids)} = \frac{\text{\#cfu/ml of diploids} \times 100}{\text{\#cfu/ml of limiting partner}}$$

LIBRARY TITRE

Count number of colonies on all plates with 30-300 colonies after 4 days.

$$\text{\#cfu/ml} = \frac{\text{\#colonies}}{\text{plating volume (ml)} \times \text{dilution factor}}$$

$$\text{\# colonies clones screened} = \text{\# cfu/ml} \times \text{final resuspension volume}$$

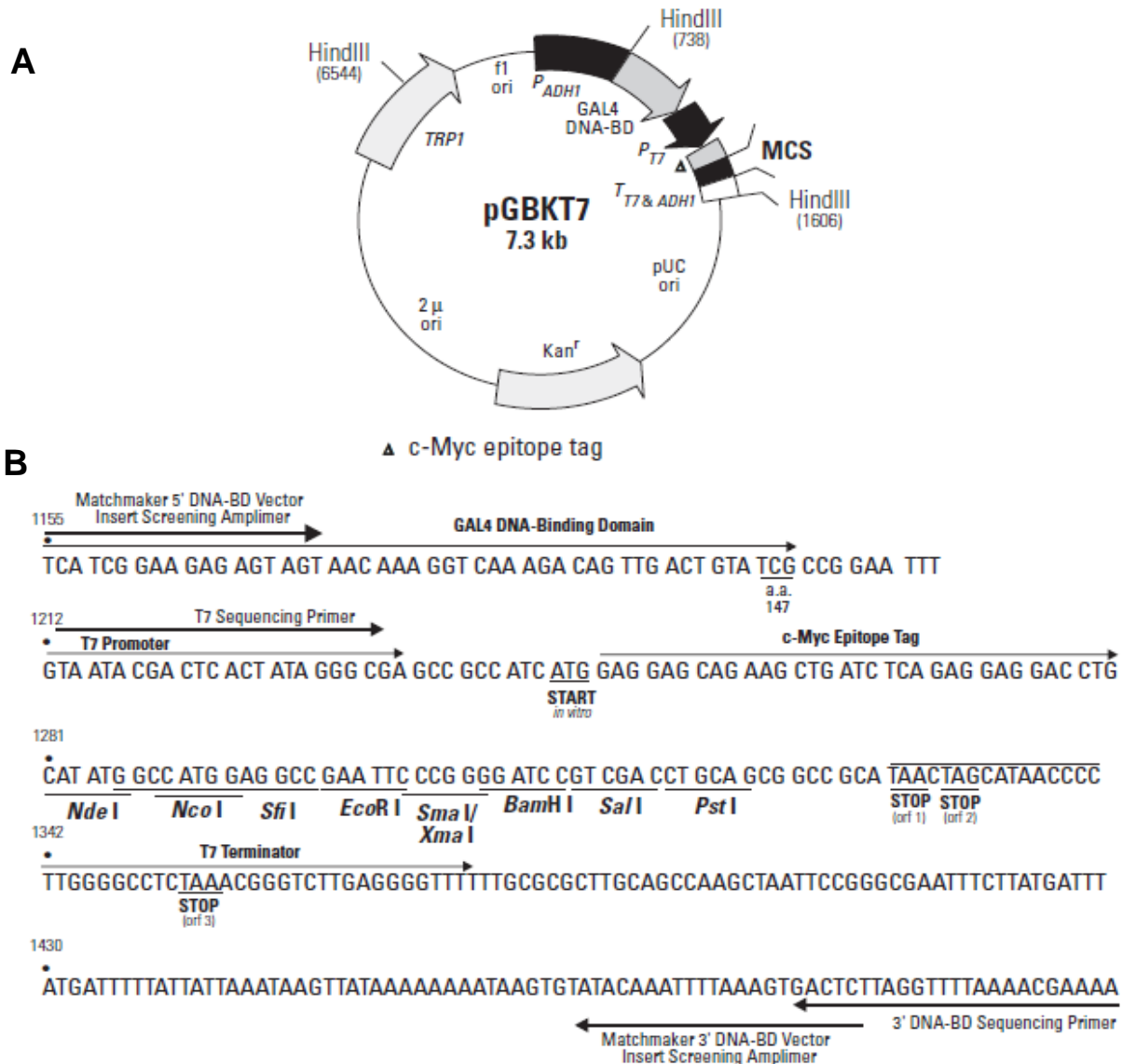
HAEMOCYTOMETRIC CELL COUNT

A cell count using a Neubauer haemocytometer (Superior, Berlin, Germany), was required to determine the titre of bait cultures used in the library mating experiments, as well as to determine the concentration of the H9c2 cells used in the co-localisation and contractility assays. Prior to counting, both the surface of the chamber and the glass cover-slip was cleaned with alcohol. The glass cover slip was then placed over the counting surface; a dilution of (1:100) of the sample prepared an aliquot of 10 μ l was placed into the V-shaped wells. Once the area under the coverslip filled with the sample through capillary action, the counting chamber was subsequently placed on a microscope (Nikon Corporation, Tokyo, Japan) stage and the counting area was brought into focus under low magnification. The number of cells in the large central quadrant of the haemocytometer were counted and this value was used to calculate the number of cells per millilitre using the following formula:

Number of cells/ml – number of cells x dilution factor x 10⁴ (a constant used because of the depth of the haemocytometer is 0.1mm)

APPENDIX III

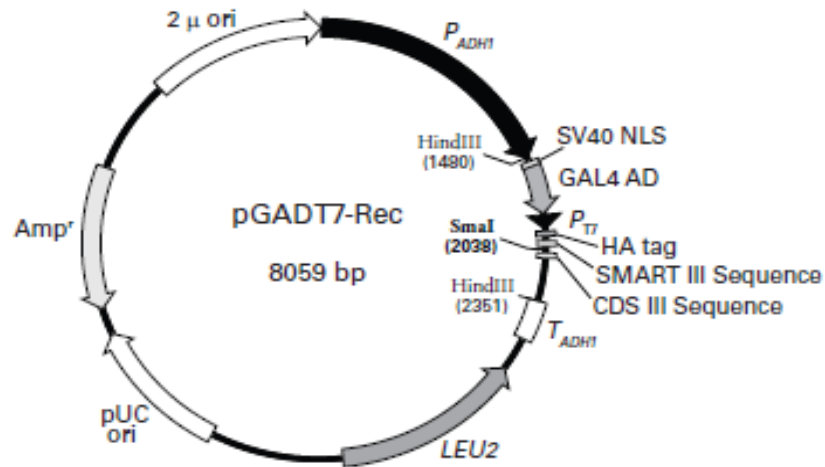
VECTORS



Restriction map and Multiple Cloning Site (MCS) of pGBKT7 Y2H vector. (A) The positions of the Kanamycin resistance gene (*Kan^r*), the trypsin (*TRP1*) nutritional marker for selection in yeast, GAL4 DNA binding domain coding sequences, f1 bacteriophage and pUC origins of replication, the truncated *S.cerevisiae ADH1* promoter sequence (*P_{ADH1}*) and the MCS. **(B)** The nucleotide sequence of the pGBKT7 MCS. The sequence indicated the positions of all the unique restriction enzyme recognition sequences, stop codons in the T7 termination sequence, GAL4 DNA binding domain coding sequence, T7 promoter sequence, c-Myc epitope tag, position of screening and sequencing primers.

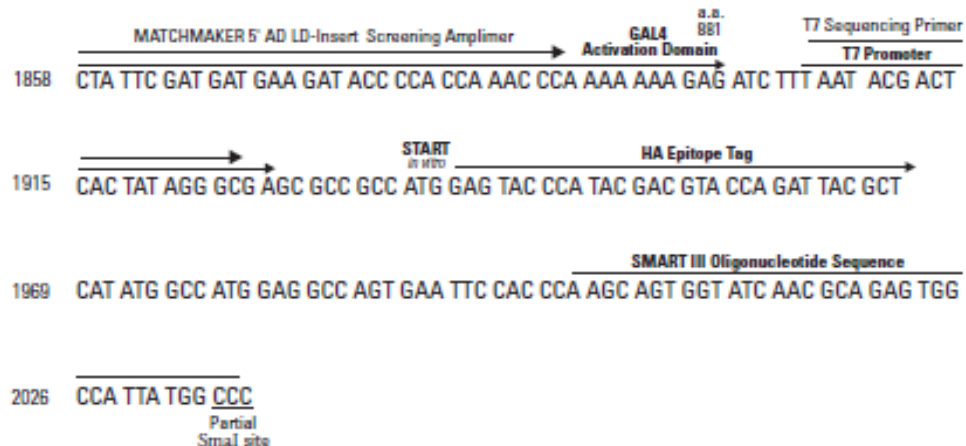
(Adapted from pGBKT7 vector information datasheet, Clontech Laboratories, Inc., Palo Alto, California, USA).

A

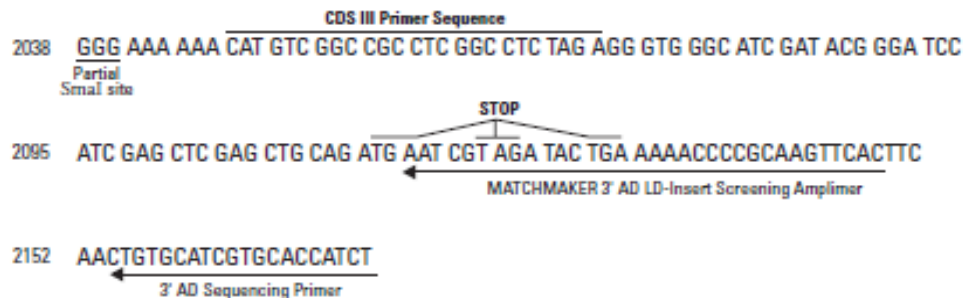


B

SMART™ III terminus



CDS III terminus



Restriction map and Multiple Cloning Site (MCS) of pGADT7-Rec Y2H prey vector. (A) Shows the positions of unique restriction enzyme sites indicated in bold font as well as the positions of the Ampicillin resistance gene (*Amp^r*), the leucine (*LEU2*) nutritional marker, GAL4 DNA activating domain

coding sequence, 2 μ and pUC plasmid origin of replication, the *S.cerevisiae ADH1* promoter, *S.cerevisiae ADH1* termination sequence, the hemagglutinin (HA) epitope tag and the MCS. **(B)** The nucleotide sequence of the pGADT7-Rec SMARTTM terminus and CDS III terminus. The position of restriction enzyme sites, stop codons, GAL4 DNA activating domain coding sequence, HA epitope tag and the positions of the T7 sequencing and 3'AD sequencing primer sequences, position of Matchmaker 5'AD and 3'AD LD-insert screening amplimer sequences. (Adapted from pACT2 vector information datasheet, Clontech Laboratories, Inc., Palo Alto, California, USA).

REFERENCES

Electronic references

Alternative splice site predictor (ASSP) website: <http://wangcomputing.com/assp/index.html>

Cardiogenomics sarcomere protein gene mutation database:

<http://genepath.med.harvard.edu/~seidman/cg3/>

Clontech™ Matchmaker™ vector handbook: www.clontech.com

Ensemble database: www.ensembl.org

Genbank database: www.ncbi.nlm.nih.gov/Entrez

Genomatix software suite v2.5: <http://www.genomatix.de/>

Graphpad Prism software version 5.03: www.graphpad.com

Integrated DNA Technologies Software, Primer Quest: <http://www.idtdna.com>

Kinship2 function: Pedigree functions, R package v1.5.0: <http://CRAN.R-project.org/package=kinship2>

lmeKin function, coxme: Mixed Effects Cox Models, R package v2.2-3: <http://CRAN.R-project.org/package=coxme>

Max Planck Institute of Immunobiology and Epigenetics' website:

<http://www3.ie-freiburg.mpg.de/research-groups/epigenetics/pichler/regulation-of-sumoylation-by-its-sole-e2-enzyme-ubc9/>

Molecular mechanisms of muscle contraction, downloaded from the Flashcard Machine website:

<http://www.flashcardmachine.com/hosmolecular-mechanisms-ofmusclecontractionlecture16.html>

National Centre for Biotechnology Information (NCBI) Basic Local Alignment Search Tool (BLAST):

<http://www.ncbi.nlm.nih.gov/BLAST/>

National Centre for Biotechnology Information (NCBI) Entrez Nucleotides Database:

<http://www.ncbi.nlm.nih.gov/nucleotide/>

National Centre for Biotechnology Information (NCBI) Entrez Protein Database:

<http://blast.ncbi.nlm.nih.gov/protein/>

NetGene2 website: <http://www.cbs.dtu.dk/services/NetGene2/>

SNP function Predictor software tool, within the SNPinfo Web Server:

<http://snpinfonia.nih.gov/snpinfonia/snpfunc.htm>

Yale School of Medicine website: http://www.med.yale.edu/.../aortic_regurgitation.html

Zeiss Zen 2011 Lite software package, downloaded from the Carl Zeiss website:

http://microscopy.zeiss.com/microscopy/en_de/downloads/zen.html

Ababou, A., Gautel, M., and Pfuhl, M. (2007). Dissecting the N-terminal myosin binding site of human cardiac myosin-binding protein C. Structure and myosin binding of domain C2. *J. Biol. Chem.* 282, 9204–9215.

Ababou, A., Rostkova, E., Mistry, S., Le Masurier, C., Gautel, M., and Pfuhl, M. (2008). Myosin binding protein C positioned to play a key role in regulation of muscle contraction: structure and interactions of domain C1. *J. Mol. Biol.* 384, 615–630.

Abecasis, G.R., Cardon, L.R., and Cookson, W.O. (2000). A general test of association for quantitative traits in nuclear families. *Am. J. Hum. Genet.* 66, 279–292.

Abegaz, B. (1990). The impact of echocardiography in the diagnosis of hypertrophic cardiomyopathy. *East AfrMedJ* 67, 556–567.

Ahn, K., Song, J.H., Kim, D.K., Park, M.H., Jo, S.A., and Koh, Y.H. (2009). Ubc9 gene polymorphisms and late-onset Alzheimer's disease in the Korean population: a genetic association study. *Neurosci. Lett.* 465, 272–275.

Akey, J., Jin, L., and Xiong, M. (2001). Haplotypes vs single marker linkage disequilibrium tests: what do we gain? *Eur. J. Hum. Genet. EJHG* 9, 291–300.

Alcalai, R., Seidman, J.G., and Seidman, C.E. (2008). Genetic basis of hypertrophic cardiomyopathy: from bench to the clinics. *J. Cardiovasc. Electrophysiol.* 19, 104–110.

Al-Khayat, H.A., Morris, E.P., and Squire, J.M. (2009). The 7-stranded structure of relaxed scallop muscle myosin filaments: support for a common head configuration in myosin-regulated muscles. *J. Struct. Biol.* 166, 183–194.

Alonso-Montes, C., Naves-Diaz, M., Fernandez-Martin, J.L., Rodriguez-Reguero, J., Moris, C., Coto, E., Cannata-Andia, J.B., and Rodriguez, I. (2012). New polymorphisms in human MEF2C gene as potential modifier of hypertrophic cardiomyopathy. *Mol. Biol. Rep.* 39, 8777–8785.

Alyonycheva, T., Cohen-Gould, L., Siewert, C., Fischman, D.A., and Mikawa, T. (1997a). Skeletal muscle-specific myosin binding protein-H is expressed in Purkinje fibers of the cardiac conduction system. *Circ. Res.* 80, 665–672.

- Alyonycheva, T.N., Mikawa, T., Reinach, F.C., and Fischman, D.A. (1997b). Isoform-specific interaction of the myosin-binding proteins (MyBPs) with skeletal and cardiac myosin is a property of the C-terminal immunoglobulin domain. *J. Biol. Chem.* 272, 20866–20872.
- Amoah, A.G., and Kallen, C. (2000). Aetiology of heart failure as seen from a National Cardiac Referral Centre in Africa. *Cardiology* 93, 11–18.
- Andersen, P.S., Hedley, P.L., Page, S.P., Syrris, P., Moolman-Smook, J.C., McKenna, W.J., Elliott, P.M., and Christiansen, M. (2012). A novel Myosin essential light chain mutation causes hypertrophic cardiomyopathy with late onset and low expressivity. *Biochem. Res. Int.* 2012, 685108.
- Ardlie, K.G., Kruglyak, L., and Seielstad, M. (2002). Patterns of linkage disequilibrium in the human genome. *Nat. Rev. Genet.* 3, 299–309.
- Arstila, A.U., and Trump, B.F. (1968). Studies on cellular autophagocytosis. The formation of autophagic vacuoles in the liver after glucagon administration. *Am. J. Pathol.* 53, 687–733.
- Arya, R., Kedar, V., Hwang, J.R., McDonough, H., Li, H.-H., Taylor, J., and Patterson, C. (2004). Muscle ring finger protein-1 inhibits PKC $\{\epsilon\}$ activation and prevents cardiomyocyte hypertrophy. *J. Cell Biol.* 167, 1147–1159.
- Asumda, F.Z., and Chase, P.B. (2012). Nuclear cardiac troponin and tropomyosin are expressed early in cardiac differentiation of rat mesenchymal stem cells. *Differ. Res. Biol. Divers.* 83, 106–115.
- Au, Y. (2004). The muscle ultrastructure: a structural perspective of the sarcomere. *Cell. Mol. Life Sci. CMLS* 61, 3016–3033.
- Axe, E.L., Walker, S.A., Manifava, M., Chandra, P., Roderick, H.L., Habermann, A., Griffiths, G., and Ktistakis, N.T. (2008). Autophagosome formation from membrane compartments enriched in phosphatidylinositol 3-phosphate and dynamically connected to the endoplasmic reticulum. *J. Cell Biol.* 182, 685–701.
- Baarlink, C., Wang, H., and Grosse, R. (2013). Nuclear Actin Network Assembly by Formins Regulates the SRF Coactivator MAL. *Science* 340, 864–867.
- Bader, J.S. (2001). The relative power of SNPs and haplotype as genetic markers for association tests. *Pharmacogenomics* 2, 11–24.
- Baek, S.H. (2006). A novel link between SUMO modification and cancer metastasis. *Cell Cycle Georget. Tex* 5, 1492–1495.
- Bahrudin, U., Morisaki, H., Morisaki, T., Ninomiya, H., Higaki, K., Nanba, E., Igawa, O., Takashima, S., Mizuta, E., Miake, J., et al. (2008). Ubiquitin-proteasome system impairment caused by a missense

- cardiac myosin-binding protein C mutation and associated with cardiac dysfunction in hypertrophic cardiomyopathy. *J. Mol. Biol.* 384, 896–907.
- Bahrudin, U., Morikawa, K., Takeuchi, A., Kurata, Y., Miake, J., Mizuta, E., Adachi, K., Higaki, K., Yamamoto, Y., Shirayoshi, Y., et al. (2011). Impairment of ubiquitin-proteasome system by E334K cMyBPC modifies channel proteins, leading to electrophysiological dysfunction. *J. Mol. Biol.* 413, 857–878.
- Bamshad, M. (2005). Genetic influences on health: does race matter? *JAMA J. Am. Med. Assoc.* 294, 937–946.
- Bang, M.-L., Li, X., Littlefield, R., Bremner, S., Thor, A., Knowlton, K.U., Lieber, R.L., and Chen, J. (2006). Nebulin-deficient mice exhibit shorter thin filament lengths and reduced contractile function in skeletal muscle. *J. Cell Biol.* 173, 905–916.
- Barki-Harrington, L., and Rockman, H.A. (2003). Sensing heart stress. *Nat. Med.* 9, 19–20.
- Barrett, J.C., Fry, B., Maller, J., and Daly, M.J. (2005). Haploview: analysis and visualization of LD and haplotype maps. *Bioinforma. Oxf. Engl.* 21, 263–265.
- Bartel, S., Karczewski, P., and Krause, E.G. (1993). Protein phosphorylation and cardiac function: cholinergic-adrenergic interaction. *Cardiovasc. Res.* 27, 1948–1953.
- Bartha, E., Solti, I., Kereskai, L., Lantos, J., Plozer, E., Magyar, K., Szabados, E., Kálai, T., Hideg, K., Halmosi, R., et al. (2009). PARP inhibition delays transition of hypertensive cardiopathy to heart failure in spontaneously hypertensive rats. *Cardiovasc. Res.* 83, 501–510.
- Bauml, M.A., and Underwood, D.A. (2010). Left ventricular hypertrophy: an overlooked cardiovascular risk factor. *Cleve. Clin. J. Med.* 77, 381–387.
- Bennett, P., Craig, R., Starr, R., and Offer, G. (1986). The ultrastructural location of C-protein, X-protein and H-protein in rabbit muscle. *J. Muscle Res. Cell Motil.* 7, 550–567.
- Bergink, S., and Jentsch, S. (2009). Principles of ubiquitin and SUMO modifications in DNA repair. *Nature* 458, 461–467.
- Bergmann, O., Bhardwaj, R.D., Bernard, S., Zdunek, S., Barnabé-Heider, F., Walsh, S., Zupicich, J., Alkass, K., Buchholz, B.A., Druid, H., et al. (2009). Evidence for cardiomyocyte renewal in humans. *Science* 324, 98–102.
- Bergmann, O., Zdunek, S., Alkass, K., Druid, H., Bernard, S., and Frisén, J. (2011). Identification of cardiomyocyte nuclei and assessment of ploidy for the analysis of cell turnover. *Exp. Cell Res.* 317, 188–194.

- Betarbet, R., Anderson, L.R., Gearing, M., Hodges, T.R., Fritz, J.J., Lah, J.J., and Levey, A.I. (2008). Fas-associated factor 1 and Parkinson's disease. *Neurobiol. Dis.* 31, 309–315.
- Blair, E. (2001). Mutations in the gamma2 subunit of AMP-activated protein kinase cause familial hypertrophic cardiomyopathy: evidence for the central role of energy compromise in disease pathogenesis. *Hum. Mol. Genet.* 10, 1215–1220.
- Blommaart, E.F., Krause, U., Schellens, J.P., Vreeling-Sindelárová, H., and Meijer, A.J. (1997). The phosphatidylinositol 3-kinase inhibitors wortmannin and LY294002 inhibit autophagy in isolated rat hepatocytes. *Eur. J. Biochem. FEBS* 243, 240–246.
- Bodine, S.C., Latres, E., Baumhueter, S., Lai, V.K., Nunez, L., Clarke, B.A., Poueymirou, W.T., Panaro, F.J., Na, E., Dharmarajan, K., et al. (2001). Identification of ubiquitin ligases required for skeletal muscle atrophy. *Science* 294, 1704–1708.
- Bos, J.M., Poley, R.N., Ny, M., Tester, D.J., Xu, X., Vatta, M., Towbin, J.A., Gersh, B.J., Ommen, S.R., and Ackerman, M.J. (2006). Genotype-phenotype relationships involving hypertrophic cardiomyopathy-associated mutations in titin, muscle LIM protein, and telethonin. *Mol. Genet. Metab.* 88, 78–85.
- Bos, J.M., Towbin, J.A., and Ackerman, M.J. (2009). Diagnostic, Prognostic, and Therapeutic Implications of Genetic Testing for Hypertrophic Cardiomyopathy. *J. Am. Coll. Cardiol.* 54, 201–211.
- Botstein, D., and Risch, N. (2003). Discovering genotypes underlying human phenotypes: past successes for mendelian disease, future approaches for complex disease. *Nat. Genet.* 33 *Suppl*, 228–237.
- Brickson, S., Fitzsimons, D.P., Pereira, L., Hacker, T., Valdivia, H., and Moss, R.L. (2007). In vivo left ventricular functional capacity is compromised in cMyBP-C null mice. *Am. J. Physiol. Heart Circ. Physiol.* 292, H1747–1754.
- Bristow, M.R. (1998). Why does the myocardium fail? Insights from basic science. *Lancet* 352 *Suppl* 1, S18–14.
- Brodde, O.E., and Michel, M.C. (1999). Adrenergic and muscarinic receptors in the human heart. *Pharmacol. Rev.* 51, 651–690.
- Brückner, A., Polge, C., Lentze, N., Auerbach, D., and Schlattner, U. (2009). Yeast Two-Hybrid, a Powerful Tool for Systems Biology. *Int. J. Mol. Sci.* 10, 2763–2788.
- Brunak, S., Engelbrecht, J., and Knudsen, S. (1991). Prediction of human mRNA donor and acceptor sites from the DNA sequence. *J. Mol. Biol.* 220, 49–65.

- Bukowska, A., Lendeckel, U., Bode-Böger, S.M., and Goette, A. (2012). Physiologic and pathophysiologic role of calpain: implications for the occurrence of atrial fibrillation. *Cardiovasc. Ther.* 30, e115–127.
- Cacabelos, R., Martínez, R., Fernández-Novoa, L., Carril, J.C., Lombardi, V., Carrera, I., Corzo, L., Tellado, I., Leszek, J., McKay, A., et al. (2012). Genomics of Dementia: APOE- and CYP2D6-Related Pharmacogenetics. *Int. J. Alzheimers Dis.* 2012, 1–37.
- Cadete, V.J.J., Arcand, S.A., Lin, H.-B., and Sawicki, G. (2013). Synergistic protection of MLC 1 against cardiac ischemia/reperfusion-induced degradation: a novel therapeutic concept for the future. *Future Med. Chem.* 5, 389–398.
- Caldwell, J.E., Heiss, S.G., Mermall, V., and Cooper, J.A. (1989). Effects of CapZ, an actin capping protein of muscle, on the polymerization of actin. *Biochemistry (Mosc.)* 28, 8506–8514.
- Campbell, H., and Rudan, I. (2002). Interpretation of genetic association studies in complex disease. *Pharmacogenomics J.* 2, 349–360.
- Carafoli, E., and Molinari, M. (1998). Calpain: a protease in search of a function? *Biochem. Biophys. Res. Commun.* 247, 193–203.
- Cardon, L.R., and Bell, J.I. (2001). Association study designs for complex diseases. *Nat. Rev. Genet.* 2, 91–99.
- Cardon, L.R., and Palmer, L.J. (2003). Population stratification and spurious allelic association. *Lancet* 361, 598–604.
- Carniel, E., Taylor, M.R., Sinagra, G., Di, L.A., Ku, L., Fain, P.R., Boucek, M.M., Cavanaugh, J., Miodic, S., Slavov, D., et al. (2005). Alpha-myosin heavy chain: a sarcomeric gene associated with dilated and hypertrophic phenotypes of cardiomyopathy. *Circulation* 112, 54–59.
- Carrier, L., Bonne, G., Bährend, E., Yu, B., Richard, P., Niel, F., Hainque, B., Cruaud, C., Gary, F., Labeit, S., et al. (1997). Organization and sequence of human cardiac myosin binding protein C gene (MYBPC3) and identification of mutations predicted to produce truncated proteins in familial hypertrophic cardiomyopathy. *Circ. Res.* 80, 427–434.
- Carrier, L., Knöll, R., Vignier, N., Keller, D.I., Bausero, P., Prudhon, B., Isnard, R., Ambrosine, M.-L., Fiszman, M., Ross, J., Jr, et al. (2004). Asymmetric septal hypertrophy in heterozygous cMyBP-C null mice. *Cardiovasc. Res.* 63, 293–304.
- Carstens, N., Van der Merwe, L., Revera, M., Heradien, M., Goosen, A., Brink, P.A., and Moolman-Smook, J.C. (2011). Genetic variation in angiotensin II type 2 receptor gene influences extent of left

- ventricular hypertrophy in hypertrophic cardiomyopathy independent of blood pressure. *J. Renin-Angiotensin-Aldosterone Syst. JRAAS* 12, 274–280.
- Cartharius, K., Frech, K., Grote, K., Klocke, B., Haltmeier, M., Klingenhoff, A., Frisch, M., Bayerlein, M., and Werner, T. (2005). MatInspector and beyond: promoter analysis based on transcription factor binding sites. *Bioinforma. Oxf. Engl.* 21, 2933–2942.
- Centner, T., Yano, J., Kimura, E., McElhinny, A.S., Pelin, K., Witt, C.C., Bang, M.L., Trombitas, K., Granzier, H., Gregorio, C.C., et al. (2001). Identification of muscle specific ring finger proteins as potential regulators of the titin kinase domain. *J. Mol. Biol.* 306, 717–726.
- Charron, P., Dubourg, O., Desnos, M., Bennaceur, M., Carrier, L., Camproux, A.-C., Isnard, R., Hagege, A., Langlard, J.M., Bonne, G., et al. (1998). Clinical Features and Prognostic Implications of Familial Hypertrophic Cardiomyopathy Related to the Cardiac Myosin-Binding Protein C Gene. *Circulation* 97, 2230–2236.
- Chase, P.B., Szczypinski, M.P., and Soto, E.P. (2013). Nuclear tropomyosin and troponin in striated muscle: new roles in a new locale? *J. Muscle Res. Cell Motil.* 34, 275–284.
- Chen, J.-S., Lee, H.-S., Jin, J.-S., Chen, A., Lin, S.-H., Ka, S.-M., and Lin, Y.-F. (2004). Attenuation of mouse mesangial cell contractility by high glucose and mannitol: involvement of protein kinase C and focal adhesion kinase. *J. Biomed. Sci.* 11, 142–151.
- Chen, Z.-C., Yu, B.-C., Chen, L.-J., Cheng, K.-C., Lin, H.J., and Cheng, J.-T. (2011). Characterization of the mechanisms of the increase in PPAR δ expression induced by digoxin in the heart using the H9c2 cell line: Mechanism of increased PPAR δ expression by digoxin. *Br. J. Pharmacol.* 163, 390–398.
- Chien, K.R. (1999). Stress pathways and heart failure. *Cell* 98, 555–558.
- Chiu, C., Tebo, M., Ingles, J., Yeates, L., Arthur, J.W., Lind, J.M., and Semsarian, C. (2007). Genetic screening of calcium regulation genes in familial hypertrophic cardiomyopathy. *J. Mol. Cell. Cardiol.* 43, 337–343.
- Chu, K., Niu, X., and Williams, L.T. (1995). A Fas-associated protein factor, FAF1, potentiates Fas-mediated apoptosis. *Proc. Natl. Acad. Sci. U. S. A.* 92, 11894–11898.
- Civantos Calzada, B., and Aleixandre de Artiñano, A. (2001). Alpha-adrenoceptor subtypes. *Pharmacol. Res. Off. J. Ital. Pharmacol. Soc.* 44, 195–208.
- Clark, A.G. (2004). The role of haplotypes in candidate gene studies. *Genet. Epidemiol.* 27, 321–333.

- Clark, A.G., Weiss, K.M., Nickerson, D.A., Taylor, S.L., Buchanan, A., Stengård, J., Salomaa, V., Vartiainen, E., Perola, M., Boerwinkle, E., et al. (1998). Haplotype structure and population genetic inferences from nucleotide-sequence variation in human lipoprotein lipase. *Am. J. Hum. Genet.* 63, 595–612.
- Clayton, D.G., Walker, N.M., Smyth, D.J., Pask, R., Cooper, J.D., Maier, L.M., Smink, L.J., Lam, A.C., Ovington, N.R., Stevens, H.E., et al. (2005). Population structure, differential bias and genomic control in a large-scale, case-control association study. *Nat. Genet.* 37, 1243–1246.
- Colhoun, H.M., McKeigue, P.M., and Davey Smith, G. (2003). Problems of reporting genetic associations with complex outcomes. *Lancet* 361, 865–872.
- Collins, A., Lau, W., and De La Vega, F.M. (2004). Mapping genes for common diseases: the case for genetic (LD) maps. *Hum. Hered.* 58, 2–9.
- Colson, B.A., Bekyarova, T., Locher, M.R., Fitzsimons, D.P., Irving, T.C., and Moss, R.L. (2008). Protein kinase A-mediated phosphorylation of cMyBP-C increases proximity of myosin heads to actin in resting myocardium. *Circ. Res.* 103, 244–251.
- Colson, B.A., Locher, M.R., Bekyarova, T., Patel, J.R., Fitzsimons, D.P., Irving, T.C., and Moss, R.L. (2010). Differential roles of regulatory light chain and myosin binding protein-C phosphorylations in the modulation of cardiac force development. *J. Physiol.* 588, 981–993.
- Colson, B.A., Rybakova, I.N., Prochniewicz, E., Moss, R.L., and Thomas, D.D. (2012a). Cardiac myosin binding protein-C restricts intrafilament torsional dynamics of actin in a phosphorylation-dependent manner. *Proc. Natl. Acad. Sci.* 109, 20437–20442.
- Colson, B.A., Patel, J.R., Chen, P.P., Bekyarova, T., Abdalla, M.I., Tong, C.W., Fitzsimons, D.P., Irving, T.C., and Moss, R.L. (2012b). Myosin binding protein-C phosphorylation is the principal mediator of protein kinase A effects on thick filament structure in myocardium. *J. Mol. Cell. Cardiol.* 53, 609–616.
- Conrad, D.F., Jakobsson, M., Coop, G., Wen, X., Wall, J.D., Rosenberg, N.A., and Pritchard, J.K. (2006). A worldwide survey of haplotype variation and linkage disequilibrium in the human genome. *Nat. Genet.* 38, 1251–1260.
- Cooper, R.S., Tayo, B., and Zhu, X. (2008). Genome-wide association studies: implications for multiethnic samples. *Hum. Mol. Genet.* 17, R151–155.
- Cordell, H.J., and Clayton, D.G. (2005). Genetic association studies. *Lancet* 366, 1121–1131.

- Corfield, V.A., Moolman, J.C., Martell, R., and Brink, P.A. (1993). Polymerase chain reaction-based detection of MN blood group-specific sequences in the human genome. *Transfusion (Paris)* 33, 119–124.
- Craig, R.W., and Pedron, R. (2004). Molecular structure of the sarcomere. In *Myology*, A.C. Engel, and C. Franzini-Armstrong, ed. (New York: McGraw Hill Companies, Inc.), pp. 128-166.
- Crocini, C., Arimura, T., Reischmann, S., Eder, A., Braren, I., Hansen, A., Eschenhagen, T., Kimura, A., and Carrier, L. (2013). Impact of ANKRD1 mutations associated with hypertrophic cardiomyopathy on contraction parameters of engineered heart tissue. *Basic Res. Cardiol.* 108, 349.
- Cusick, M.E., Klitgord, N., Vidal, M., and Hill, D.E. (2005). Interactome: gateway into systems biology. *Hum. Mol. Genet.* 14 Spec No. 2, R171–181.
- Dämmrich, J., and Pfeifer, U. (1983). Cardiac hypertrophy in rats after supra-avalvular aortic constriction. II. Inhibition of cellular autophagy in hypertrophying cardiomyocytes. *Virchows Arch. B Cell Pathol. Incl. Mol. Pathol.* 43, 287–307.
- Davis, J.S. (1988). Interaction of C-protein with pH 8.0 synthetic thick filaments prepared from the myosin of vertebrate skeletal muscle. *J. Muscle Res. Cell Motil.* 9, 174–183.
- Davis, J.S., Hassanzadeh, S., Winitzky, S., Lin, H., Satorius, C., Vemuri, R., Aletras, A.H., Wen, H., and Epstein, N.D. (2001). The overall pattern of cardiac contraction depends on a spatial gradient of myosin regulatory light chain phosphorylation. *Cell* 107, 631–641.
- Day, S.M. (2013). The ubiquitin proteasome system in human cardiomyopathies and heart failure. *Am. J. Physiol. Heart Circ. Physiol.* 304, H1283–1293.
- Dayton, W.R., and Schollmeyer, J.V. (1981). Immunocytochemical localization of a calcium-activated protease in skeletal muscle cells. *Exp. Cell Res.* 136, 423–433.
- De Bakker, P.I.W., Yelensky, R., Pe'er, I., Gabriel, S.B., Daly, M.J., and Altshuler, D. (2005). Efficiency and power in genetic association studies. *Nat. Genet.* 37, 1217–1223.
- Decker, R.S., and Wildenthal, K. (1980). Lysosomal alterations in hypoxic and reoxygenated hearts. I. Ultrastructural and cytochemical changes. *Am. J. Pathol.* 98, 425–444.
- De Lanerolle, P., and Serebryanny, L. (2011). Nuclear actin and myosins: life without filaments. *Nat. Cell Biol.* 13, 1282–1288.
- De Lange, W.J., Grimes, A.C., Hegge, L.F., and Ralphe, J.C. (2012). Ablation of cardiac myosin-binding protein-C accelerates contractile kinetics in engineered cardiac tissue. *J. Gen. Physiol.* 141, 73–84.

- De La Vega, F.M. (2007). Selecting single-nucleotide polymorphisms for association studies with SNPbrowser software. *Methods Mol. Biol. Clifton NJ* 376, 177–193.
- De La Vega, F.M., Dailey, D., Ziegler, J., Williams, J., Madden, D., and Gilbert, D.A. (2002). New generation pharmacogenomic tools: a SNP linkage disequilibrium Map, validated SNP assay resource, and high-throughput instrumentation system for large-scale genetic studies. *BioTechniques Suppl*, 48–50, 52, 54.
- De La Vega, F.M., Gordon, D., Su, X., Scafe, C., Isaac, H., Gilbert, D.A., and Spier, E.G. (2005a). Power and sample size calculations for genetic case/control studies using gene-centric SNP maps: application to human chromosomes 6, 21, and 22 in three populations. *Hum. Hered.* 60, 43–60.
- De La Vega, F.M., Isaac, H., Collins, A., Scafe, C.R., Halldórsson, B.V., Su, X., Lippert, R.A., Wang, Y., Laig-Webster, M., Koehler, R.T., et al. (2005b). The linkage disequilibrium maps of three human chromosomes across four populations reflect their demographic history and a common underlying recombination pattern. *Genome Res.* 15, 454–462.
- De La Vega, F.M., Isaac, H.I., and Scafe, C.R. (2006). A tool for selecting SNPs for association studies based on observed linkage disequilibrium patterns. *Pac. Symp. Biocomput. Pac. Symp. Biocomput.* 487–498.
- Devereux, R.B., and Roman, M.J. (1993). Inter-relationships between hypertension, left ventricular hypertrophy and coronary heart disease. *J. Hypertens. Suppl. Off. J. Int. Soc. Hypertens.* 11, S3–9.
- Devlin, B., and Roeder, K. (1999). Genomic control for association studies. *Biometrics* 55, 997–1004.
- Diao, G., and Lin, D.Y. (2006). Improving the power of association tests for quantitative traits in family studies. *Genet. Epidemiol.* 30, 301–313.
- Dice, J.F. (2007). Chaperone-mediated autophagy. *Autophagy* 3, 295–299.
- Dlugosz, A.A., Antin, P.B., Nachmias, V.T., and Holtzer, H. (1984). The relationship between stress fiber-like structures and nascent myofibrils in cultured cardiac myocytes. *J. Cell Biol.* 99, 2268–2278.
- Docherty, J.R. (2010). Subtypes of functional alpha1-adrenoceptor. *Cell. Mol. Life Sci. CMLS* 67, 405–417.
- Donahue, M.P., and Allen, A.S. (2005). Genetic association studies in cardiology. *Am. Heart J.* 149, 964–970.
- Dorval, V., and Fraser, P.E. (2007). SUMO on the road to neurodegeneration. *Biochim. Biophys. Acta* 1773, 694–706.

- Du, A., Sanger, J.M., and Sanger, J.W. (2008). Cardiac myofibrillogenesis inside intact embryonic hearts. *Dev. Biol.* 318, 236–246.
- Dunn, W.A., Jr (1990). Studies on the mechanisms of autophagy: formation of the autophagic vacuole. *J. Cell Biol.* 110, 1923–1933.
- Dunn, K.W., Kamocka, M.M., and McDonald, J.H. (2011). A practical guide to evaluating colocalization in biological microscopy. *Am. J. Physiol. - Cell Physiol.* 300, C723–C742.
- Einheber, S., and Fischman, D.A. (1990). Isolation and characterization of a cDNA clone encoding avian skeletal muscle C-protein: an intracellular member of the immunoglobulin superfamily. *Proc. Natl. Acad. Sci. U. S. A.* 87, 2157–2161.
- El-Armouche, A., Boknik, P., Eschenhagen, T., Carrier, L., Knaut, M., Ravens, U., and Dobrev, D. (2006). Molecular determinants of altered Ca²⁺ handling in human chronic atrial fibrillation. *Circulation* 114, 670–680.
- El-Armouche, A., Pohlmann, L., Schlossarek, S., Starbatty, J., Yeh, Y.-H., Nattel, S., Dobrev, D., Eschenhagen, T., and Carrier, L. (2007). Decreased phosphorylation levels of cardiac myosin-binding protein-C in human and experimental heart failure. *J. Mol. Cell. Cardiol.* 43, 223–229.
- Elliott, P., Andersson, B., Arbustini, E., Bilinska, Z., Cecchi, F., Charron, P., Dubourg, O., Kühn, U., Maisch, B., McKenna, W.J., et al. (2008). Classification of the cardiomyopathies: a position statement from the European Society Of Cardiology Working Group on Myocardial and Pericardial Diseases. *Eur. Heart J.* 29, 270–276.
- Elliott, P.M., Poloniecki, J., Dickie, S., Sharma, S., Monserrat, L., Varnava, A., Mahon, N.G., and McKenna, W.J. (2000). Sudden death in hypertrophic cardiomyopathy: identification of high risk patients. *J. Am. Coll. Cardiol.* 36, 2212–2218.
- Engelhardt, S. (2001). Early impairment of calcium handling and altered expression of junctin in hearts of mice overexpressing the b1-adrenergic receptor. *FASEB J.* 15, 2718–2720.
- Ericsson, J.L. (1969). Studies on induced cellular autophagy. I. Electron microscopy of cells with in vivo labelled lysosomes. *Exp. Cell Res.* 55, 95–106.
- Esposito, G. (2002). Genetic Alterations That Inhibit In Vivo Pressure-Overload Hypertrophy Prevent Cardiac Dysfunction Despite Increased Wall Stress. *Circulation* 105, 85–92.
- Fabiato, A. (1983). Calcium-induced release of calcium from the cardiac sarcoplasmic reticulum. *Am. J. Physiol.* 245, C1–14.

- Fan, W., Nassiri, A., and Zhong, Q. (2011). Autophagosome targeting and membrane curvature sensing by Barkor/Atg14(L). *Proc. Natl. Acad. Sci. U. S. A.* 108, 7769–7774.
- Fields, S., and Song, O. (1989). A novel genetic system to detect protein-protein interactions. *Nature* 340, 245–246.
- Fielitz, J., Kim, M.-S., Shelton, J.M., Latif, S., Spencer, J.A., Glass, D.J., Richardson, J.A., Bassel-Duby, R., and Olson, E.N. (2007). Myosin accumulation and striated muscle myopathy result from the loss of muscle RING finger 1 and 3. *J. Clin. Invest.* 117, 2486–2495.
- Flashman, E., Redwood, C., Moolman-Smook, J., and Watkins, H. (2004). Cardiac myosin binding protein C: its role in physiology and disease. *Circ.Res.* 94, 1279–1289.
- Flashman, E., Korkie, L., Watkins, H., Redwood, C., and Moolman-Smook, J.C. (2008). Support for a trimeric collar of myosin binding protein C in cardiac and fast skeletal muscle, but not in slow skeletal muscle. *FEBS Lett.* 582, 434–438.
- Flavigny, J., Richard, P., Isnard, R., Carrier, L., Charron, P., Bonne, G., Forissier, J.F., Desnos, M., Dubourg, O., Komajda, M., et al. (1998). Identification of two novel mutations in the ventricular regulatory myosin light chain gene (MYL2) associated with familial and classical forms of hypertrophic cardiomyopathy. *J. Mol. Med. Berl. Ger.* 76, 208–214.
- Flavigny, J., Souchet, M., Sébillon, P., Berrebi-Bertrand, I., Hainque, B., Mallet, A., Bril, A., Schwartz, K., and Carrier, L. (1999). COOH-terminal truncated cardiac myosin-binding protein C mutants resulting from familial hypertrophic cardiomyopathy mutations exhibit altered expression and/or incorporation in fetal rat cardiomyocytes. *J. Mol. Biol.* 294, 443–456.
- Fleg, J.L., and Strait, J. (2012). Age-associated changes in cardiovascular structure and function: a fertile milieu for future disease. *Heart Fail. Rev.* 17, 545–554.
- Franklin, S., Zhang, M.J., Chen, H., Paulsson, A.K., Mitchell-Jordan, S.A., Li, Y., Ping, P., and Vondriska, T.M. (2011). Specialized compartments of cardiac nuclei exhibit distinct proteomic anatomy. *Mol. Cell. Proteomics MCP* 10, M110.000703.
- Frazer, K.A., Murray, S.S., Schork, N.J., and Topol, E.J. (2009). Human genetic variation and its contribution to complex traits. *Nat. Rev. Genet.* 10, 241–251.
- Freiburg, A., and Gautel, M. (1996). A molecular map of the interactions between titin and myosin-binding protein C. Implications for sarcomeric assembly in familial hypertrophic cardiomyopathy. *Eur. J. Biochem. FEBS* 235, 317–323.
- Frey, N., and Olson, E.N. (2003). Cardiac hypertrophy: the good, the bad, and the ugly. *Annu. Rev. Physiol.* 65, 45–79.

- Fujita, N., Itoh, T., Omori, H., Fukuda, M., Noda, T., and Yoshimori, T. (2008a). The Atg16L complex specifies the site of LC3 lipidation for membrane biogenesis in autophagy. *Mol. Biol. Cell* 19, 2092–2100.
- Fujita, N., Hayashi-Nishino, M., Fukumoto, H., Omori, H., Yamamoto, A., Noda, T., and Yoshimori, T. (2008b). An Atg4B mutant hampers the lipidation of LC3 paralogues and causes defects in autophagosome closure. *Mol. Biol. Cell* 19, 4651–4659.
- Funderburk, S.F., Wang, Q.J., and Yue, Z. (2010). The Beclin 1-VPS34 complex—at the crossroads of autophagy and beyond. *Trends Cell Biol.* 20, 355–362.
- Fung, K.L., and Gottesman, M.M. (2009). A synonymous polymorphism in a common MDR1 (ABCB1) haplotype shapes protein function. *Biochim. Biophys. Acta* 1794, 860–871.
- Fürst, D.O., Vinkemeier, U., and Weber, K. (1992). Mammalian skeletal muscle C-protein: purification from bovine muscle, binding to titin and the characterization of a full-length human cDNA. *J. Cell Sci.* 102 (Pt 4), 769–778.
- Gabriel, S.B., Schaffner, S.F., Nguyen, H., Moore, J.M., Roy, J., Blumenstiel, B., Higgins, J., DeFelice, M., Lochner, A., Faggart, M., et al. (2002). The structure of haplotype blocks in the human genome. *Science* 296, 2225–2229.
- Galvez, A.S., Diwan, A., Odley, A.M., Hahn, H.S., Osinska, H., Melendez, J.G., Robbins, J., Lynch, R.A., Marreez, Y., and Dorn, G.W., 2nd (2007). Cardiomyocyte degeneration with calpain deficiency reveals a critical role in protein homeostasis. *Circ. Res.* 100, 1071–1078.
- Gao, W.D., Atar, D., Liu, Y., Perez, N.G., Murphy, A.M., and Marban, E. (1997). Role of troponin I proteolysis in the pathogenesis of stunned myocardium. *Circ. Res.* 80, 393–399.
- Garner, C., and Slatkin, M. (2003). On selecting markers for association studies: patterns of linkage disequilibrium between two and three diallelic loci. *Genet. Epidemiol.* 24, 57–67.
- Garvey, J.L., Kranias, E.G., and Solaro, R.J. (1988). Phosphorylation of C-protein, troponin I and phospholamban in isolated rabbit hearts. *Biochem. J.* 249, 709–714.
- Gautel, M., Zuffardi, O., Freiburg, A., and Labeit, S. (1995a). Phosphorylation switches specific for the cardiac isoform of myosin binding protein-C: a modulator of cardiac contraction? *EMBO J.* 14, 1952–1960.
- Gautel, M., Castiglione Morelli, M.A., Pfuhl, M., Motta, A., and Pastore, A. (1995b). A calmodulin-binding sequence in the C-terminus of human cardiac titin kinase. *Eur. J. Biochem. FEBS* 230, 752–759.

- Geiss-Friedlander, R., and Melchior, F. (2007). Concepts in sumoylation: a decade on. *Nat. Rev. Mol. Cell Biol.* 8, 947–956.
- Geisterfer-Lowrance, A.A., Kass, S., Tanigawa, G., Vosberg, H.P., McKenna, W., Seidman, C.E., and Seidman, J.G. (1990). A molecular basis for familial hypertrophic cardiomyopathy: a beta cardiac myosin heavy chain gene missense mutation. *Cell* 62, 999–1006.
- Gerhardstein, B.L., Puri, T.S., Chien, A.J., and Hosey, M.M. (1999). Identification of the sites phosphorylated by cyclic AMP-dependent protein kinase on the beta 2 subunit of L-type voltage-dependent calcium channels. *Biochemistry (Mosc.)* 38, 10361–10370.
- Gilad, S., Meiri, E., Yogev, Y., Benjamin, S., Lebanony, D., Yerushalmi, N., Benjamin, H., Kushnir, M., Cholak, H., Melamed, N., et al. (2008). Serum microRNAs are promising novel biomarkers. *PLoS One* 3, e3148.
- Gilbert, R., Kelly, M.G., Mikawa, T., and Fischman, D.A. (1996). The carboxyl terminus of myosin binding protein C (MyBP-C, C-protein) specifies incorporation into the A-band of striated muscle. *J. Cell Sci.* 109 (Pt 1), 101–111.
- Gilbert, R., Cohen, J.A., Pardo, S., Basu, A., and Fischman, D.A. (1999). Identification of the A-band localization domain of myosin binding proteins C and H (MyBP-C, MyBP-H) in skeletal muscle. *J. Cell Sci.* 112 (Pt 1), 69–79.
- Girolami, F., Olivetto, I., Passerini, I., Zachara, E., Nistri, S., Re, F., Fantini, S., Baldini, K., Torricelli, F., and Cecchi, F. (2006). A molecular screening strategy based on beta-myosin heavy chain, cardiac myosin binding protein C and troponin T genes in Italian patients with hypertrophic cardiomyopathy. *J. Cardiovasc. Med. (Hagerstown.)* 7, 601–607.
- Goldberg, A.L. (2003). Protein degradation and protection against misfolded or damaged proteins. *Nature* 426, 895–899.
- Goll, D.E., Thompson, V.F., Li, H., Wei, W., and Cong, J. (2003). The calpain system. *Physiol. Rev.* 83, 731–801.
- Gomes, M.D., Lecker, S.H., Jagoe, R.T., Navon, A., and Goldberg, A.L. (2001). Atrogin-1, a muscle-specific F-box protein highly expressed during muscle atrophy. *Proc. Natl. Acad. Sci. U. S. A.* 98, 14440–14445.
- Gordon, D., and Finch, S.J. (2005). Factors affecting statistical power in the detection of genetic association. *J. Clin. Invest.* 115, 1408–1418.
- Gregorio, C.C., and Antin, P.B. (2000). To the heart of myofibril assembly. *Trends Cell Biol.* 10, 355–362.

- Grossman, W., Jones, D., and McLaurin, L.P. (1975). Wall stress and patterns of hypertrophy in the human left ventricle. *J. Clin. Invest.* 56, 56–64.
- Gruen, M., Prinz, H., and Gautel, M. (1999). cAPK-phosphorylation controls the interaction of the regulatory domain of cardiac myosin binding protein C with myosin-S2 in an on-off fashion. *FEBS Lett.* 453, 254–259.
- Grummt, I. (2006). Actin and myosin as transcription factors. *Curr. Opin. Genet. Dev.* 16, 191–196.
- Gustafsson, A.B., and Gottlieb, R.A. (2003). Mechanisms of apoptosis in the heart. *J. Clin. Immunol.* 23, 447–459.
- Gusterson, R.J., Jazrawi, E., Adcock, I.M., and Latchman, D.S. (2003). The transcriptional co-activators CREB-binding protein (CBP) and p300 play a critical role in cardiac hypertrophy that is dependent on their histone acetyltransferase activity. *J. Biol. Chem.* 278, 6838–6847.
- Hagen, C.M., Aidt, F.H., Hedley, P.L., Jensen, M.K., Havndrup, O., Kanters, J.K., Moolman-Smook, J.C., Larsen, S.O., Bundgaard, H., and Christiansen, M. (2013). Mitochondrial haplogroups modify the risk of developing hypertrophic cardiomyopathy in a danish population. *PLoS One* 8, e71904.
- Haglund, K., Di Fiore, P.P., and Dikic, I. (2003). Distinct monoubiquitin signals in receptor endocytosis. *Trends Biochem. Sci.* 28, 598–603.
- Haider, A.W., Larson, M.G., Benjamin, E.J., and Levy, D. (1998). Increased left ventricular mass and hypertrophy are associated with increased risk for sudden death. *J. Am. Coll. Cardiol.* 32, 1454–1459.
- Hall, T.A. (1999). BioEdit: a user-friendly biological sequence alignment editor and analysis program for Windows 95/98/NT. *Nucleic Acids Symp. Ser.* 41, 95–98.
- Hamacher-Brady, A., Brady, N.R., and Gottlieb, R.A. (2006). The interplay between pro-death and pro-survival signaling pathways in myocardial ischemia/reperfusion injury: apoptosis meets autophagy. *Cardiovasc. Drugs Ther. Spons. Int. Soc. Cardiovasc. Pharmacother.* 20, 445–462.
- Hamacher-Brady, A., Brady, N.R., Logue, S.E., Sayen, M.R., Jinno, M., Kirshenbaum, L.A., Gottlieb, R.A., and Gustafsson, A.B. (2007). Response to myocardial ischemia/reperfusion injury involves Bnip3 and autophagy. *Cell Death Differ.* 14, 146–157.
- Hariharan, N., Ikeda, Y., Hong, C., Alcendor, R.R., Usui, S., Gao, S., Maejima, Y., and Sadoshima, J. (2013). Autophagy Plays an Essential Role in Mediating Regression of Hypertrophy during Unloading of the Heart. *PLoS ONE* 8, e51632.
- Harris, S.P. (2004). Binding of Myosin Binding Protein-C to Myosin Subfragment S2 Affects Contractility Independent of a Tether Mechanism. *Circ. Res.* 95, 930–936.

- Harris, S.P., Bartley, C.R., Hacker, T.A., McDonald, K.S., Douglas, P.S., Greaser, M.L., Powers, P.A., and Moss, R.L. (2002). Hypertrophic cardiomyopathy in cardiac myosin binding protein-C knockout mice. *Circ. Res.* 90, 594–601.
- Hartzell, H.C., and Titus, L. (1982). Effects of cholinergic and adrenergic agonists on phosphorylation of a 165,000-dalton myofibrillar protein in intact cardiac muscle. *J. Biol. Chem.* 257, 2111–2120.
- Hayashi, T., Seki, M., Maeda, D., Wang, W., Kawabe, Y., Seki, T., Saitoh, H., Fukagawa, T., Yagi, H., and Enomoto, T. (2002). Ubc9 is essential for viability of higher eukaryotic cells. *Exp. Cell Res.* 280, 212–221.
- Hayashi, T., Arimura, T., Ueda, K., Shibata, H., Hohda, S., Takahashi, M., Hori, H., Koga, Y., Oka, N., Imaizumi, T., et al. (2004). Identification and functional analysis of a caveolin-3 mutation associated with familial hypertrophic cardiomyopathy. *Biochem. Biophys. Res. Commun.* 313, 178–184.
- Hayashi-Nishino, M., Fujita, N., Noda, T., Yamaguchi, A., Yoshimori, T., and Yamamoto, A. (2009). A subdomain of the endoplasmic reticulum forms a cradle for autophagosome formation. *Nat. Cell Biol.* 11, 1433–1437.
- Hayashi-Nishino, M., Fujita, N., Noda, T., Yamaguchi, A., Yoshimori, T., and Yamamoto, A. (2010). Electron tomography reveals the endoplasmic reticulum as a membrane source for autophagosome formation. *Autophagy* 6, 301–303.
- Hebsgaard, S.M., Korning, P.G., Tolstrup, N., Engelbrecht, J., Rouzé, P., and Brunak, S. (1996). Splice site prediction in Arabidopsis thaliana pre-mRNA by combining local and global sequence information. *Nucleic Acids Res.* 24, 3439–3452.
- Hedhli, N., Pelat, M., and Depre, C. (2005). Protein turnover in cardiac cell growth and survival. *Cardiovasc. Res.* 68, 186–196.
- Henn, B.M., Gignoux, C.R., Jobin, M., Granka, J.M., Macpherson, J.M., Kidd, J.M., Rodríguez-Botigué, L., Ramachandran, S., Hon, L., Brisbin, A., et al. (2011). Hunter-gatherer genomic diversity suggests a southern African origin for modern humans. *Proc. Natl. Acad. Sci. U. S. A.* 108, 5154–5162.
- Herron, T.J. (2006). Activation of Myocardial Contraction by the N-Terminal Domains of Myosin Binding Protein-C. *Circ. Res.* 98, 1290–1298.
- Hershberger, R.E., Lindenfeld, J., Mestroni, L., Seidman, C.E., Taylor, M.R.G., Towbin, J.A., and Heart Failure Society of America (2009). Genetic evaluation of cardiomyopathy--a Heart Failure Society of America practice guideline. *J. Card. Fail.* 15, 83–97.

- Hicks, A.A., Pétursson, H., Jónsson, T., Stefánsson, H., Jóhannsdóttir, H.S., Sainz, J., Frigge, M.L., Kong, A., Gulcher, J.R., Stefánsson, K., et al. (2002). A susceptibility gene for late-onset idiopathic Parkinson's disease. *Ann. Neurol.* 52, 549–555.
- Hilgarth, R.S., Murphy, L.A., Skaggs, H.S., Wilkerson, D.C., Xing, H., and Sarge, K.D. (2004). Regulation and function of SUMO modification. *J. Biol. Chem.* 279, 53899–53902.
- Hinds, D.A., Stuve, L.L., Nilsen, G.B., Halperin, E., Eskin, E., Ballinger, D.G., Frazer, K.A., and Cox, D.R. (2005). Whole-genome patterns of common DNA variation in three human populations. *Science* 307, 1072–1079.
- Ho, C.Y. (2010). Genetics and Clinical Destiny: Improving Care in Hypertrophic Cardiomyopathy. *Circulation* 122, 2430–2440.
- Ho, C.Y., and Seidman, C.E. (2006). A contemporary approach to hypertrophic cardiomyopathy. *Circulation* 113, e858–862.
- Ho, K.K., Anderson, K.M., Kannel, W.B., Grossman, W., and Levy, D. (1993). Survival after the onset of congestive heart failure in Framingham Heart Study subjects. *Circulation* 88, 107–115.
- Hoegge, C., Pfander, B., Moldovan, G.-L., Pyrowolakis, G., and Jentsch, S. (2002). RAD6-dependent DNA repair is linked to modification of PCNA by ubiquitin and SUMO. *Nature* 419, 135–141.
- Hofmann, P.A., Hartzell, H.C., and Moss, R.L. (1991). Alterations in Ca²⁺ sensitive tension due to partial extraction of C-protein from rat skinned cardiac myocytes and rabbit skeletal muscle fibers. *J. Gen. Physiol.* 97, 1141–1163.
- Hollox, E.J., Poulter, M., Zvarik, M., Ferak, V., Krause, A., Jenkins, T., Saha, N., Kozlov, A.I., and Swallow, D.M. (2001). Lactase haplotype diversity in the Old World. *Am. J. Hum. Genet.* 68, 160–172.
- Hosokawa, N., Hara, T., Kaizuka, T., Kishi, C., Takamura, A., Miura, Y., Iemura, S., Natsume, T., Takehana, K., Yamada, N., et al. (2009). Nutrient-dependent mTORC1 association with the ULK1-Atg13-FIP200 complex required for autophagy. *Mol. Biol. Cell* 20, 1981–1991.
- Hosono, Y., Yamaguchi, T., Mizutani, E., Yanagisawa, K., Arima, C., Tomida, S., Shimada, Y., Hiraoka, M., Kato, S., Yokoi, K., et al. (2011). MYBPH, a transcriptional target of TTF-1, inhibits ROCK1, and reduces cell motility and metastasis. *EMBO J.* 31, 481–493.
- Howarth, J.W., Ramisetty, S., Nolan, K., Sadayappan, S., and Rosevear, P.R. (2012). Structural insight into unique cardiac myosin-binding protein-C motif: a partially folded domain. *J. Biol. Chem.* 287, 8254–8262.

- Huang, Y., and Wang, K.K. (2001). The calpain family and human disease. *Trends Mol. Med.* 7, 355–362.
- Huxley, A.F., and Niedergerke, R. (1954). Structural Changes in Muscle During Contraction: Interference Microscopy of Living Muscle Fibres. *Nature* 173, 971–973.
- Ichimura, Y., Imamura, Y., Emoto, K., Umeda, M., Noda, T., and Ohsumi, Y. (2004). In vivo and in vitro reconstitution of Atg8 conjugation essential for autophagy. *J. Biol. Chem.* 279, 40584–40592.
- Imamura, T., McDermott, P.J., Kent, R.L., Nagatsu, M., Cooper, G., and Carabello, B.A. (1994). Acute changes in myosin heavy chain synthesis rate in pressure versus volume overload. *Circ. Res.* 75, 418–425.
- International HapMap Consortium (2003). The International HapMap Project. *Nature* 426, 789–796.
- Ioannidis, J.P., Ntzani, E.E., Trikalinos, T.A., and Contopoulos-Ioannidis, D.G. (2001). Replication validity of genetic association studies. *Nat. Genet.* 29, 306–309.
- Ioannidis, J.P.A., Ntzani, E.E., and Trikalinos, T.A. (2004). “Racial” differences in genetic effects for complex diseases. *Nat. Genet.* 36, 1312–1318.
- Jarvik, G.P. (2003). Paraoxonase Activity, But Not Haplotype Utilizing the Linkage Disequilibrium Structure, Predicts Vascular Disease. *Arterioscler. Thromb. Vasc. Biol.* 23, 1465–1471.
- Jeffries, C.M., Whitten, A.E., Harris, S.P., and Trehwella, J. (2008). Small-angle X-ray scattering reveals the N-terminal domain organization of cardiac myosin binding protein C. *J. Mol. Biol.* 377, 1186–1199.
- Johnson, E.S., and Blobel, G. (1997). Ubc9p is the conjugating enzyme for the ubiquitin-like protein Smt3p. *J. Biol. Chem.* 272, 26799–26802.
- Johnson, E.S., and Gupta, A.A. (2001). An E3-like factor that promotes SUMO conjugation to the yeast septins. *Cell* 106, 735–744.
- Johnson, E.S., Schwienhorst, I., Dohmen, R.J., and Blobel, G. (1997). The ubiquitin-like protein Smt3p is activated for conjugation to other proteins by an Aos1p/Uba2p heterodimer. *EMBO J.* 16, 5509–5519.
- Johnson, G.C., Esposito, L., Barratt, B.J., Smith, A.N., Heward, J., Di Genova, G., Ueda, H., Cordell, H.J., Eaves, I.A., Dudbridge, F., et al. (2001). Haplotype tagging for the identification of common disease genes. *Nat. Genet.* 29, 233–237.

- Jones, D., Crowe, E., Stevens, T.A., and Candido, E.P.M. (2002). Functional and phylogenetic analysis of the ubiquitylation system in *Caenorhabditis elegans*: ubiquitin-conjugating enzymes, ubiquitin-activating enzymes, and ubiquitin-like proteins. *Genome Biol.* 3, RESEARCH0002.
- Jorde, L.B., and Wooding, S.P. (2004). Genetic variation, classification and “race.” *Nat. Genet.* 36, S28–33.
- Jung, C.H., Jun, C.B., Ro, S.-H., Kim, Y.-M., Otto, N.M., Cao, J., Kundu, M., and Kim, D.-H. (2009). ULK-Atg13-FIP200 complexes mediate mTOR signaling to the autophagy machinery. *Mol. Biol. Cell* 20, 1992–2003.
- Kabeya, Y., Mizushima, N., Ueno, T., Yamamoto, A., Kirisako, T., Noda, T., Kominami, E., Ohsumi, Y., and Yoshimori, T. (2000). LC3, a mammalian homologue of yeast Apg8p, is localized in autophagosome membranes after processing. *EMBO J.* 19, 5720–5728.
- Kagey, M.H., Melhuish, T.A., and Wotton, D. (2003). The polycomb protein Pc2 is a SUMO E3. *Cell* 113, 127–137.
- Karibe, A., Tobacman, L.S., Strand, J., Butters, C., Back, N., Bachinski, L.L., Arai, A.E., Ortiz, A., Roberts, R., Homsher, E., et al. (2001). Hypertrophic cardiomyopathy caused by a novel alpha-tropomyosin mutation (V95A) is associated with mild cardiac phenotype, abnormal calcium binding to troponin, abnormal myosin cycling, and poor prognosis. *Circulation* 103, 65–71.
- Kataoka, A., Hemmer, C., and Chase, P.B. (2007). Computational simulation of hypertrophic cardiomyopathy mutations in troponin I: influence of increased myofilament calcium sensitivity on isometric force, ATPase and $[Ca^{2+}]_i$. *J. Biomech.* 40, 2044–2052.
- Ke, L., Qi, X.Y., Dijkhuis, A.-J., Chartier, D., Nattel, S., Henning, R.H., Kampinga, H.H., and Brundel, B.J.J.M. (2008). Calpain mediates cardiac troponin degradation and contractile dysfunction in atrial fibrillation. *J. Mol. Cell. Cardiol.* 45, 685–693.
- Kensler, R.W., Shaffer, J.F., and Harris, S.P. (2011). Binding of the N-terminal fragment C0-C2 of cardiac MyBP-C to cardiac F-actin. *J. Struct. Biol.* 174, 44–51.
- Keren, A., Syrris, P., and McKenna, W.J. (2008). Hypertrophic cardiomyopathy: the genetic determinants of clinical disease expression. *Nat. Clin. Pract. Cardiovasc. Med.* 5, 158–168.
- Kim, I., Rodriguez-Enriquez, S., and Lemasters, J.J. (2007). Selective degradation of mitochondria by mitophagy. *Arch. Biochem. Biophys.* 462, 245–253.
- Kim, J., Kundu, M., Viollet, B., and Guan, K.-L. (2011). AMPK and mTOR regulate autophagy through direct phosphorylation of Ulk1. *Nat. Cell Biol.* 13, 132–141.

- Kimes, B.W. and Brandt, B.L. (1976). Properties of a clonal muscle cell line from rat heart. *Exp. Cell. Res.* 98, 367-381.
- Klionsky, D.J., and Emr, S.D. (2000). Autophagy as a regulated pathway of cellular degradation. *Science* 290, 1717–1721.
- Koekemoer, A.L., Chong, N.W., Goodall, A.H., Samani, N.J. (2009). Myocyte stress 1 plays an important role in cellular hypertrophy and protection against apoptosis. *FEBS Lett.* 583, 2964-2967.
- Koller, D.L., Peacock, M., Lai, D., Foroud, T., and Econs, M.J. (2004). False positive rates in association studies as a function of degree of stratification. *J. Bone Miner. Res. Off. J. Am. Soc. Bone Miner. Res.* 19, 1291–1295.
- Koretz, J.F. (1979). Effects of C-protein on synthetic myosin filament structure. *Biophys. J.* 27, 433–446.
- Koretz, J.F., Irving, T.C., and Wang, K. (1993). Filamentous aggregates of native titin and binding of C-protein and AMP-deaminase. *Arch. Biochem. Biophys.* 304, 305–309.
- Korte, F.S., McDonald, K.S., Harris, S.P., and Moss, R.L. (2003). Loaded shortening, power output, and rate of force redevelopment are increased with knockout of cardiac myosin binding protein-C. *Circ. Res.* 93, 752–758.
- Kraja, A.T., Hunt, S.C., Rao, D.C., Dávila-Román, V.G., Arnett, D.K., and Province, M.A. (2011). Genetics of hypertension and cardiovascular disease and their interconnected pathways: lessons from large studies. *Curr. Hypertens. Rep.* 13, 46–54.
- Kulikovskaya, I., McClellan, G., Flavigny, J., Carrier, L., and Winegrad, S. (2003). Effect of MyBP-C binding to actin on contractility in heart muscle. *J. Gen. Physiol.* 122, 761–774.
- Kumamoto, T., Kleese, W.C., Cong, J.Y., Goll, D.E., Pierce, P.R., and Allen, R.E. (1992). Localization of the Ca(2+)-dependent proteinases and their inhibitor in normal, fasted, and denervated rat skeletal muscle. *Anat. Rec.* 232, 60–77.
- Kunst, G., Kress, K.R., Gruen, M., Uttenweiler, D., Gautel, M., and Fink, R.H. (2000). Myosin binding protein C, a phosphorylation-dependent force regulator in muscle that controls the attachment of myosin heads by its interaction with myosin S2. *Circ. Res.* 86, 51–58.
- Kunz, J.B. (2003). Determination of Four Sequential Stages during Microautophagy in Vitro. *J. Biol. Chem.* 279, 9987–9996.
- Kuo, T.-Y., Lau, W., and Collins, A.R. (2007). LDMAP: the construction of high-resolution linkage disequilibrium maps of the human genome. *Methods Mol. Biol. Clifton NJ* 376, 47–57.

- Kurosawa, M. (1994). Phosphorylation and dephosphorylation of protein in regulating cellular function. *J. Pharmacol. Toxicol. Methods* 31, 135–139.
- Kuss, A.W., and Chen, W. (2008). MicroRNAs in brain function and disease. *Curr. Neurol. Neurosci. Rep.* 8, 190–197.
- Labeit, S., and Kolmerer, B. (1995). Titins: Giant Proteins in Charge of Muscle Ultrastructure and Elasticity. *Science* 270, 293–296.
- Labeit, S., Gautel, M., Lakey, A., and Trinick, J. (1992). Towards a molecular understanding of titin. *EMBO J.* 11, 1711–1716.
- Landstrom, A.P., Weisleder, N., Bataalden, K.B., Bos, J.M., Tester, D.J., Ommen, S.R., Wehrens, X.H., Claycomb, W.C., Ko, J.K., Hwang, M., et al. (2007). Mutations in JPH2-encoded junctophilin-2 associated with hypertrophic cardiomyopathy in humans. *JMolCell Cardiol* 42, 1026–1035.
- Landstrom, A.P., Parvatiyar, M.S., Pinto, J.R., Marquardt, M.L., Bos, J.M., Tester, D.J., Ommen, S.R., Potter, J.D., and Ackerman, M.J. (2008). Molecular and functional characterization of novel hypertrophic cardiomyopathy susceptibility mutations in TNNC1-encoded troponin C. *J. Mol. Cell. Cardiol.* 45, 281–288.
- Landstrom, A.P., Adekola, B.A., Bos, J.M., Ommen, S.R., and Ackerman, M.J. (2011). PLN-encoded phospholamban mutation in a large cohort of hypertrophic cardiomyopathy cases: summary of the literature and implications for genetic testing. *Am. Heart J.* 161, 165–171.
- Lange, C., DeMeo, D.L., and Laird, N.M. (2002). Power and design considerations for a general class of family-based association tests: quantitative traits. *Am. J. Hum. Genet.* 71, 1330–1341.
- Lasky-Su, J., Lyon, H.N., Emilsson, V., Heid, I.M., Molony, C., Raby, B.A., Lazarus, R., Klanderma, B., Soto-Quiros, M.E., Avila, L., et al. (2008). On the replication of genetic associations: timing can be everything! *Am. J. Hum. Genet.* 82, 849–858.
- Lechin, M., Quiñones, M.A., Omran, A., Hill, R., Yu, Q.T., Rakowski, H., Wigle, D., Liew, C.C., Sole, M., and Roberts, R. (1995). Angiotensin-I converting enzyme genotypes and left ventricular hypertrophy in patients with hypertrophic cardiomyopathy. *Circulation* 92, 1808–1812.
- Letavernier, E., Zafrani, L., Perez, J., Letavernier, B., Haymann, J.-P., and Baud, L. (2012). The role of calpains in myocardial remodelling and heart failure. *Cardiovasc. Res.* 96, 38–45.
- Levine, B., and Klionsky, D.J. (2004). Development by self-digestion: molecular mechanisms and biological functions of autophagy. *Dev. Cell* 6, 463–477.
- Levine, B., and Kroemer, G. (2008). Autophagy in the Pathogenesis of Disease. *Cell* 132, 27–42.

- Levine, B., and Yuan, J. (2005). Autophagy in cell death: an innocent convict? *J. Clin. Invest.* 115, 2679–2688.
- Levine, R., Weisberg, A., Kulikovskaya, I., McClellan, G., and Winegrad, S. (2001). Multiple structures of thick filaments in resting cardiac muscle and their influence on cross-bridge interactions. *Biophys. J.* 81, 1070–1082.
- Levy, D., Labib, S.B., Anderson, K.M., Christiansen, J.C., Kannel, W.B., and Castelli, W.P. (1990a). Determinants of sensitivity and specificity of electrocardiographic criteria for left ventricular hypertrophy. *Circulation* 81, 815–820.
- Levy, D., Garrison, R.J., Savage, D.D., Kannel, W.B., and Castelli, W.P. (1990b). Prognostic implications of echocardiographically determined left ventricular mass in the Framingham Heart Study. *N. Engl. J. Med.* 322, 1561–1566.
- Lewis, B.S., Armstrong, T.G., Mitha, A.S., Gotsman, M.S. (1973). Hypertrophic obstructive cardiomyopathy in the South African Bantu. *S. Afr. Med. J.* 34, 599-604.
- Li, J., and Jiang, T. (2005). Haplotype-based linkage disequilibrium mapping via direct data mining. *Bioinforma. Oxf. Engl.* 21, 4384–4393.
- Li, S.J., and Hochstrasser, M. (1999). A new protease required for cell-cycle progression in yeast. *Nature* 398, 246–251.
- Lin, B., Govindan, S., Lee, K., Zhao, P., Han, R., Runte, K.E., Craig, R., Palmer, B.M., and Sadayappan, S. (2013). Cardiac Myosin Binding Protein-C Plays No Regulatory Role in Skeletal Muscle Structure and Function. *PLoS ONE* 8, e69671.
- Lindemann, J.P., Jones, L.R., Hathaway, D.R., Henry, B.G., and Watanabe, A.M. (1983). beta-Adrenergic stimulation of phospholamban phosphorylation and Ca²⁺-ATPase activity in guinea pig ventricles. *J. Biol. Chem.* 258, 464–471.
- Liu, N., Zhang, K., and Zhao, H. (2008). Haplotype-association analysis. *Adv. Genet.* 60, 335–405.
- Lohse, M.J. (2003). What Is the Role of β -Adrenergic Signaling in Heart Failure? *Circ. Res.* 93, 896–906.
- Lorell, B.H., and Carabello, B.A. (2000). Left ventricular hypertrophy: pathogenesis, detection, and prognosis. *Circulation* 102, 470–479.
- Loubser, O., Marais, A.D., Kotze, M.J., Godenir, N., Thiart, R., Scholtz, C.L., de Villiers, J.N., Hillermann, R., Firth, J.C., Weich, H.F., et al. (1999). Founder mutations in the LDL receptor gene

- contribute significantly to the familial hypercholesterolemia phenotype in the indigenous South African population of mixed ancestry. *Clin. Genet.* 55, 340–345.
- Lu, Y., Kwan, A.H., Trewhella, J., and Jeffries, C.M. (2011). The C0C1 fragment of human cardiac myosin binding protein C has common binding determinants for both actin and myosin. *J. Mol. Biol.* 413, 908–913.
- Luther, P.K., Bennett, P.M., Knupp, C., Craig, R., Padrón, R., Harris, S.P., Patel, J., and Moss, R.L. (2008). Understanding the organisation and role of myosin binding protein C in normal striated muscle by comparison with MyBP-C knockout cardiac muscle. *J. Mol. Biol.* 384, 60–72.
- Maass, A.H., Ikeda, K., Oberdorf-Maass, S., Maier, S.K.G., and Leinwand, L.A. (2004). Hypertrophy, fibrosis, and sudden cardiac death in response to pathological stimuli in mice with mutations in cardiac troponin T. *Circulation* 110, 2102–2109.
- Maekawa, M., Ishizaki, T., Boku, S., Watanabe, N., Fujita, A., Iwamatsu, A., Obinata, T., Ohashi, K., Mizuno, K., and Narumiya, S. (1999). Signaling from Rho to the actin cytoskeleton through protein kinases ROCK and LIM-kinase. *Science* 285, 895–898.
- Maiuri, M.C., Zalckvar, E., Kimchi, A., and Kroemer, G. (2007). Self-eating and self-killing: crosstalk between autophagy and apoptosis. *Nat. Rev. Mol. Cell Biol.* 8, 741–752.
- Maniatis, N., Collins, A., Gibson, J., Zhang, W., Tapper, W., and Morton, N.E. (2004). Positional cloning by linkage disequilibrium. *Am. J. Hum. Genet.* 74, 846–855.
- Manolio, T.A., Collins, F.S., Cox, N.J., Goldstein, D.B., Hindorf, L.A., Hunter, D.J., McCarthy, M.I., Ramos, E.M., Cardon, L.R., Chakravarti, A., et al. (2009). Finding the missing heritability of complex diseases. *Nature* 461, 747–753.
- Marian, A.J. (2002). Modifier genes for hypertrophic cardiomyopathy. *Curr. Opin. Cardiol.* 17, 242–252.
- Marian, A.J. (2008). Genetic determinants of cardiac hypertrophy. *Curr. Opin. Cardiol.* 23, 199–205.
- Marian, A.J. (2010). Update on hypertrophic cardiomyopathy. *TexHeart InstJ* 37, 322–323.
- Marian, A.J., and Roberts, R. (2001). The molecular genetic basis for hypertrophic cardiomyopathy. *J. Mol. Cell. Cardiol.* 33, 655–670.
- Marian, A.J., Yu, Q.T., Workman, R., Greve, G., and Roberts, R. (1993). Angiotensin-converting enzyme polymorphism in hypertrophic cardiomyopathy and sudden cardiac death. *Lancet* 342, 1085–1086.

- Marian, A.J., Salek, L., and Lutucuta, S. (2001). Molecular genetics and pathogenesis of hypertrophic cardiomyopathy. *Minerva Med.* 92, 435–451.
- Marin, T.M., Keith, K., Davies, B., Conner, D.A., Guha, P., Kalaitzidis, D., Wu, X., Lauriol, J., Wang, B., Bauer, M., et al. (2011). Rapamycin reverses hypertrophic cardiomyopathy in a mouse model of LEOPARD syndrome-associated PTPN11 mutation. *J. Clin. Invest.* 121, 1026–1043.
- Maron, B.J. (1993). Hypertrophic cardiomyopathy. *Curr.Probl.Cardiol.* 18, 639–704.
- Maron, B.J., Anan, T.J., and Roberts, W.C. (1981). Quantitative analysis of the distribution of cardiac muscle cell disorganization in the left ventricular wall of patients with hypertrophic cardiomyopathy. *Circulation* 63, 882–894.
- Maron, B.J., Epstein, S.E., and Roberts, W.C. (1986). Causes of sudden death in competitive athletes. *J. Am. Coll. Cardiol.* 7, 204–214.
- Maron, B.J., Gardin, J.M., Flack, J.M., Gidding, S.S., Kurosaki, T.T., and Bild, D.E. (1995). Prevalence of hypertrophic cardiomyopathy in a general population of young adults. Echocardiographic analysis of 4111 subjects in the CARDIA Study. Coronary Artery Risk Development in (Young) Adults. *Circulation* 92, 785–789.
- Martin, A.F. (1981). Turnover of cardiac troponin subunits. Kinetic evidence for a precursor pool of troponin-I. *J. Biol. Chem.* 256, 964–968.
- Martin, E.R., Lai, E.H., Gilbert, J.R., Rogala, A.R., Afshari, A.J., Riley, J., Finch, K.L., Stevens, J.F., Livak, K.J., Slotterbeck, B.D., et al. (2000). SNPing away at complex diseases: analysis of single-nucleotide polymorphisms around APOE in Alzheimer disease. *Am. J. Hum. Genet.* 67, 383–394.
- Marx, S.O., Reiken, S., Hisamatsu, Y., Jayaraman, T., Burkhoff, D., Rosemblit, N., and Marks, A.R. (2000). PKA phosphorylation dissociates FKBP12.6 from the calcium release channel (ryanodine receptor): defective regulation in failing hearts. *Cell* 101, 365–376.
- Mathew, J., Sleight, P., Lonn, E., Johnstone, D., Pogue, J., Yi, Q., Bosch, J., Sussex, B., Probstfield, J., Yusuf, S., et al. (2001). Reduction of cardiovascular risk by regression of electrocardiographic markers of left ventricular hypertrophy by the angiotensin-converting enzyme inhibitor ramipril. *Circulation* 104, 1615–1621.
- Matsui, Y., Takagi, H., Qu, X., Abdellatif, M., Sakoda, H., Asano, T., Levine, B., and Sadoshima, J. (2007). Distinct roles of autophagy in the heart during ischemia and reperfusion: roles of AMP-activated protein kinase and Beclin 1 in mediating autophagy. *Circ. Res.* 100, 914–922.

- Matsunaga, K., Morita, E., Saitoh, T., Akira, S., Ktistakis, N.T., Izumi, T., Noda, T., and Yoshimori, T. (2010). Autophagy requires endoplasmic reticulum targeting of the PI3-kinase complex via Atg14L. *J. Cell Biol.* *190*, 511–521.
- McClellan, G., Kulikovskaya, I., and Winegrad, S. (2001). Changes in cardiac contractility related to calcium-mediated changes in phosphorylation of myosin-binding protein C. *Biophys. J.* *81*, 1083–1092.
- McDermott, P.J., Baicu, C.F., Wahl, S.R., Van Laer, A.O., and Zile, M.R. (2012). In vivo measurements of the contributions of protein synthesis and protein degradation in regulating cardiac pressure overload hypertrophy in the mouse. *Mol. Cell. Biochem.* *367*, 205–213.
- McElhinny, A.S. (2004). Muscle-specific RING finger-2 (MURF-2) is important for microtubule, intermediate filament and sarcomeric M-line maintenance in striated muscle development. *J. Cell Sci.* *117*, 3175–3188.
- McLenachan, J.M., Henderson, E., Morris, K.I., and Dargie, H.J. (1987). Ventricular arrhythmias in patients with hypertensive left ventricular hypertrophy. *N. Engl. J. Med.* *317*, 787–792.
- McMullen, J.R. (2004). Inhibition of mTOR Signaling With Rapamycin Regresses Established Cardiac Hypertrophy Induced by Pressure Overload. *Circulation* *109*, 3050–3055.
- McNally, E.M. (2002). Beta-myosin heavy chain gene mutations in familial hypertrophic cardiomyopathy: the usual suspect? *Circ. Res.* *90*, 246–247.
- Miralles, F., and Visa, N. (2006). Actin in transcription and transcription regulation. *Curr. Opin. Cell Biol.* *18*, 261–266.
- Miyamoto, C.A., Fischman, D.A., and Reinach, F.C. (1999). The interface between MyBP-C and myosin: site-directed mutagenesis of the CX myosin-binding domain of MyBP-C. *J. Muscle Res. Cell Motil.* *20*, 703–715.
- Mizushima, N. (2011). Autophagy in protein and organelle turnover. *Cold Spring Harb. Symp. Quant. Biol.* *76*, 397–402.
- Moncman, C.L., Rindt, H., Robbins, J., and Winkelmann, D.A. (1993). Segregated assembly of muscle myosin expressed in nonmuscle cells. *Mol. Biol. Cell* *4*, 1051–1067.
- Montgomery, R.L., Davis, C.A., Potthoff, M.J., Haberland, M., Fielitz, J., Qi, X., Hill, J.A., Richardson, J.A., and Olson, E.N. (2007). Histone deacetylases 1 and 2 redundantly regulate cardiac morphogenesis, growth, and contractility. *Genes Dev.* *21*, 1790–1802.

- Moolman, J.C., Brink, P.A., and Corfield, V.A. (1993). Identification of a new missense mutation at Arg403, a CpG mutation hotspot, in exon 13 of the beta-myosin heavy chain gene in hypertrophic cardiomyopathy. *Hum. Mol. Genet.* 2, 1731–1732.
- Moolman, J.C., Brink, P.A., and Corfield, V.A. (1995). Identification of a novel Ala797Thr mutation in exon 21 of the beta-myosin heavy chain gene in hypertrophic cardiomyopathy. *Hum. Mutat.* 6, 197–198.
- Moolman, J.C., Corfield, V.A., Posen, B., Ngumbela, K., Seidman, C., Brink, P.A., and Watkins, H. (1997). Sudden death due to troponin T mutations. *J. Am. Coll. Cardiol.* 29, 549–555.
- Moolman-Smook, J., Flashman, E., De Lange, W., Li, Z., Corfield, V., Redwood, C., and Watkins, H. (2002). Identification of novel interactions between domains of Myosin binding protein-C that are modulated by hypertrophic cardiomyopathy missense mutations. *Circ. Res.* 91, 704–711.
- Moolman-Smook, J.C., De Lange, W.J., Bruwer, E.C., Brink, P.A., and Corfield, V.A. (1999). The origins of hypertrophic cardiomyopathy-causing mutations in two South African subpopulations: a unique profile of both independent and founder events. *Am. J. Hum. Genet.* 65, 1308–1320.
- Moolman-Smook, J.C., Mayosi, B.M., Brink, P.A., and Corfield, V.A. (2003). Molecular genetics of cardiomyopathy: changing times, shifting paradigms. *Cardiovasc. J. South Afr. Off. J. South. Afr. Card. Soc. South Afr. Soc. Card. Pr.* 14, 145–155.
- Moos, C., Offer, G., Starr, R., and Bennett, P. (1975). Interaction of C-protein with myosin, myosin rod and light meromyosin. *J. Mol. Biol.* 97, 1–9.
- Moos, C., Mason, C.M., Besterman, J.M., Feng, I.N., and Dubin, J.H. (1978). The binding of skeletal muscle C-protein to F-actin, and its relation to the interaction of actin with myosin subfragment-1. *J. Mol. Biol.* 124, 571–586.
- Morimoto, S. (2007). Sarcomeric proteins and inherited cardiomyopathies. *Cardiovasc. Res.* 77, 659–666.
- Morris, R.W., and Kaplan, N.L. (2002). On the advantage of haplotype analysis in the presence of multiple disease susceptibility alleles. *Genet. Epidemiol.* 23, 221–233.
- Mun, J.Y., Gulick, J., Robbins, J., Woodhead, J., Lehman, W., and Craig, R. (2011). Electron microscopy and 3D reconstruction of F-actin decorated with cardiac myosin-binding protein C (cMyBP-C). *J. Mol. Biol.* 410, 214–225.
- Nacerddine, K., Lehembre, F., Bhaumik, M., Artus, J., Cohen-Tannoudji, M., Babinet, C., Pandolfi, P.P., and Dejean, A. (2005). The SUMO pathway is essential for nuclear integrity and chromosome segregation in mice. *Dev. Cell* 9, 769–779.

- Nakai, A., Yamaguchi, O., Takeda, T., Higuchi, Y., Hikoso, S., Taniike, M., Omiya, S., Mizote, I., Matsumura, Y., Asahi, M., et al. (2007). The role of autophagy in cardiomyocytes in the basal state and in response to hemodynamic stress. *Nat. Med.* 13, 619–624.
- Nam, Y.-J., Song, K., Luo, X., Daniel, E., Lambeth, K., West, K., Hill, J.A., DiMaio, J.M., Baker, L.A., Bassel-Duby, R., et al. (2013). Reprogramming of human fibroblasts toward a cardiac fate. *Proc. Natl. Acad. Sci.* 110, 5588–5593.
- Neitzel, H. (1986). A routine method for the establishment of permanent growing lymphoblastoid cell lines. *Hum. Genet.* 73, 320–326.
- Newton-Cheh, C., and Hirschhorn, J.N. (2005). Genetic association studies of complex traits: design and analysis issues. *Mutat. Res.* 573, 54–69.
- Niimura, H., Bachinski, L.L., Sangwatanaroj, S., Watkins, H., Chudley, A.E., McKenna, W., Kristinsson, A., Roberts, R., Sole, M., Maron, B.J., et al. (1998). Mutations in the gene for cardiac myosin-binding protein C and late-onset familial hypertrophic cardiomyopathy. *N. Engl. J. Med.* 338, 1248–1257.
- Niimura, H., Patton, K.K., McKenna, W.J., Soultis, J., Maron, B.J., Seidman, J.G., and Seidman, C.E. (2002). Sarcomere protein gene mutations in hypertrophic cardiomyopathy of the elderly. *Circulation* 105, 446–451.
- Nishida, K., Kyoji, S., Yamaguchi, O., Sadoshima, J., and Otsu, K. (2009). The role of autophagy in the heart. *Cell Death Differ.* 16, 31–38.
- Nishino, I., Fu, J., Tanji, K., Yamada, T., Shimojo, S., Koori, T., Mora, M., Riggs, J.E., Oh, S.J., Koga, Y., et al. (2000). Primary LAMP-2 deficiency causes X-linked vacuolar cardiomyopathy and myopathy (Danon disease). *Nature* 406, 906–910.
- Nyland, L.R., Palmer, B.M., Chen, Z., Maughan, D.W., Seidman, C.E., Seidman, J.G., Kreplak, L., and Vigoreaux, J.O. (2009). Cardiac Myosin Binding Protein-C Is Essential for Thick-Filament Stability and Flexural Rigidity. *Biophys. J.* 96, 3273–3280.
- Offer, G., Moos, C., and Starr, R. (1973). A new protein of the thick filaments of vertebrate skeletal myofibrils. Extractions, purification and characterization. *J. Mol. Biol.* 74, 653–676.
- Okagaki, T., Weber, F.E., Fischman, D.A., Vaughan, K.T., Mikawa, T., and Reinach, F.C. (1993). The major myosin-binding domain of skeletal muscle MyBP-C (C protein) resides in the COOH-terminal, immunoglobulin C2 motif. *J. Cell Biol.* 123, 619–626.
- Okin, P.M., Devereux, R.B., Jern, S., Kjeldsen, S.E., Julius, S., and Dahlöf, B. (2000). Baseline characteristics in relation to electrocardiographic left ventricular hypertrophy in hypertensive patients:

- the Losartan intervention for endpoint reduction (LIFE) in hypertension study. The Life Study Investigators. *Hypertension* 36, 766–773.
- Ord, J.M., Wakeland, J.R., Crie, J.S., and Wildenthal, K. (1983). Mechanisms of degradation of myofibrillar and nonmyofibrillar protein in heart. *Adv. Myocardiol.* 4, 195–199.
- Orlova, A., Galkin, V.E., Jeffries, C.M.J., Egelman, E.H., and Trewhella, J. (2011). The N-terminal domains of myosin binding protein C can bind polymorphically to F-actin. *J. Mol. Biol.* 412, 379–386.
- Osio, A., Tan, L., Chen, S.N., Lombardi, R., Nagueh, S.F., Shete, S., Roberts, R., Willerson, J.T., and Marian, A.J. (2007). Myozenin 2 is a novel gene for human hypertrophic cardiomyopathy. *Circ. Res.* 100, 766–768.
- Palmer, B.M., Georgakopoulos, D., Janssen, P.M., Wang, Y., Alpert, N.R., Belardi, D.F., Harris, S.P., Moss, R.L., Burgon, P.G., Seidman, C.E., et al. (2004). Role of cardiac myosin binding protein C in sustaining left ventricular systolic stiffening. *Circ. Res.* 94, 1249–1255.
- Pan, M.-R., Chang, T.-M., Chang, H.-C., Su, J.-L., Wang, H.-W., and Hung, W.-C. (2009). Sumoylation of Prox1 controls its ability to induce VEGFR3 expression and lymphatic phenotypes in endothelial cells. *J. Cell Sci.* 122, 3358–3364.
- Papageorgopoulos, C., Caldwell, K., Schweingrubber, H., Neese, R.A., Shackleton, C.H.L., and Hellerstein, M. (2002). Measuring synthesis rates of muscle creatine kinase and myosin with stable isotopes and mass spectrometry. *Anal. Biochem.* 309, 1–10.
- Pappas, C.T., Bhattacharya, N., Cooper, J.A., and Gregorio, C.C. (2008). Nebulin Interacts with CapZ and Regulates Thin Filament Architecture within the Z-Disc. *Mol. Biol. Cell* 19, 1837–1847.
- Patil, N., Berno, A.J., Hinds, D.A., Barrett, W.A., Doshi, J.M., Hacker, C.R., Kautzer, C.R., Lee, D.H., Marjoribanks, C., McDonough, D.P., et al. (2001). Blocks of limited haplotype diversity revealed by high-resolution scanning of human chromosome 21. *Science* 294, 1719–1723.
- Pauws, E., and Stanier, P. (2007). FGF signalling and SUMO modification: new players in the aetiology of cleft lip and/or palate. *Trends Genet.* TIG 23, 631–640.
- Pepe, F.A., Ashton, F.T., Street, C., and Weisel, J. (1986). The myosin filament. X. Observation of nine subfilaments in transverse sections. *Tissue Cell* 18, 499–508.
- Pereira, S., Ramalho-Santos, J., Branco, A., Sardao, V., Oliveira, P., Carvalho, R. (2011). Metabolic remodeling during H9c2 myoblast differentiation: relevance for in vitro toxicity studies. *Cardiovasc. Toxicol.* 11, 180-190.

- Pfeifer, U., Föhr, J., Wilhelm, W., and Dämmrich, J. (1987). Short-term inhibition of cardiac cellular autophagy by isoproterenol. *J. Mol. Cell. Cardiol.* 19, 1179–1184.
- Pichler, A., Gast, A., Seeler, J.S., Dejean, A., and Melchior, F. (2002). The nucleoporin RanBP2 has SUMO1 E3 ligase activity. *Cell* 108, 109–120.
- Pilia, G., Chen, W.-M., Scuteri, A., Orrú, M., Albai, G., Dei, M., Lai, S., Usala, G., Lai, M., Loi, P., et al. (2006). Heritability of cardiovascular and personality traits in 6,148 Sardinians. *PLoS Genet.* 2, e132.
- Pinto, J.R., Yang, S.W., Hitz, M.-P., Parvatiyar, M.S., Jones, M.A., Liang, J., Kokta, V., Talajic, M., Tremblay, N., Jaeggi, M., et al. (2011). Fetal cardiac troponin isoforms rescue the increased Ca²⁺ sensitivity produced by a novel double deletion in cardiac troponin T linked to restrictive cardiomyopathy: a clinical, genetic, and functional approach. *J. Biol. Chem.* 286, 20901–20912.
- Piston, D.W., and Kremers, G.-J. (2007). Fluorescent protein FRET: the good, the bad and the ugly. *Trends Biochem. Sci.* 32, 407–414.
- Pittman, A.M. (2005). Linkage disequilibrium fine mapping and haplotype association analysis of the tau gene in progressive supranuclear palsy and corticobasal degeneration. *J. Med. Genet.* 42, 837–846.
- Pohlmann, L., Kröger, I., Vignier, N., Schlossarek, S., Krämer, E., Coirault, C., Sultan, K.R., El-Armouche, A., Winegrad, S., Eschenhagen, T., et al. (2007). Cardiac myosin-binding protein C is required for complete relaxation in intact myocytes. *Circ. Res.* 101, 928–938.
- Pönicke, K., Schlüter, K.D., Heinroth-Hoffmann, I., Seyfarth, T., Goldberg, M., Osten, B., Piper, H.M., and Brodde, O.E. (2001). Noradrenaline-induced increase in protein synthesis in adult rat cardiomyocytes: involvement of only alpha1A-adrenoceptors. *Naunyn. Schmiedebergs Arch. Pharmacol.* 364, 444–453.
- Posen, B.M., Moolman, J.C., Corfield, V.A., and Brink, P.A. (1995). Clinical and prognostic evaluation of familial hypertrophic cardiomyopathy in two South African families with different cardiac beta myosin heavy chain gene mutations. *Br. Heart J.* 74, 40–46.
- Powell, S.R. (2006). The ubiquitin-proteasome system in cardiac physiology and pathology. *Am. J. Physiol. Heart Circ. Physiol.* 291, H1–H19.
- Prabhakar, R., Boivin, G.P., Grupp, I.L., Hoit, B., Arteaga, G., Solaro, R.J., and Wieczorek, D.F. (2001). A familial hypertrophic cardiomyopathy alpha-tropomyosin mutation causes severe cardiac hypertrophy and death in mice. *J. Mol. Cell. Cardiol.* 33, 1815–1828.

- Prabhakar, R., Petrashevskaya, N., Schwartz, A., Aronow, B., Boivin, G.P., Molkenin, J.D., and Wieczorek, D.F. (2003). A mouse model of familial hypertrophic cardiomyopathy caused by an α -tropomyosin mutation. *Mol. Cell. Biochem.* 251, 33–42.
- Predmore, J.M., Wang, P., Davis, F., Bartolone, S., Westfall, M.V., Dyke, D.B., Pagani, F., Powell, S.R., and Day, S.M. (2010). Ubiquitin Proteasome Dysfunction in Human Hypertrophic and Dilated Cardiomyopathies. *Circulation* 121, 997–1004.
- Price, A.L., Patterson, N.J., Plenge, R.M., Weinblatt, M.E., Shadick, N.A., and Reich, D. (2006). Principal components analysis corrects for stratification in genome-wide association studies. *Nat. Genet.* 38, 904–909.
- Price, A.L., Zaitlen, N.A., Reich, D., and Patterson, N. (2010). New approaches to population stratification in genome-wide association studies. *Nat. Rev. Genet.* 11, 459–463.
- Pritchard, J.K., Stephens, M., and Donnelly, P. (2000). Inference of population structure using multilocus genotype data. *Genetics* 155, 945–959.
- Puntmann, V.O., Jahnke, C., Gebker, R., Schnackenburg, B., Fox, K.F., Fleck, E., and Paetsch, I. (2010). Usefulness of magnetic resonance imaging to distinguish hypertensive and hypertrophic cardiomyopathy. *Am. J. Cardiol.* 106, 1016–1022.
- Ramaraj, R. (2008). Hypertrophic cardiomyopathy: etiology, diagnosis, and treatment. *Cardiol. Rev.* 16, 172–180.
- Rapundalo, S.T., Solaro, R.J., and Kranias, E.G. (1989). Inotropic responses to isoproterenol and phosphodiesterase inhibitors in intact guinea pig hearts: comparison of cyclic AMP levels and phosphorylation of sarcoplasmic reticulum and myofibrillar proteins. *Circ. Res.* 64, 104–111.
- Razumova, M.V., Shaffer, J.F., Tu, A.-Y., Flint, G.V., Regnier, M., and Harris, S.P. (2006). Effects of the N-terminal domains of myosin binding protein-C in an in vitro motility assay: Evidence for long-lived cross-bridges. *J. Biol. Chem.* 281, 35846–35854.
- Reich, D.E., Cargill, M., Bolk, S., Ireland, J., Sabeti, P.C., Richter, D.J., Lavery, T., Kouyoumjian, R., Farhadian, S.F., Ward, R., et al. (2001). Linkage disequilibrium in the human genome. *Nature* 411, 199–204.
- Revera, M., van der, M.L., Heradien, M., Goosen, A., Corfield, V.A., Brink, P.A., and Moolman-Smook, J.C. (2008). Troponin T and beta-myosin mutations have distinct cardiac functional effects in hypertrophic cardiomyopathy patients without hypertrophy. *Cardiovasc.Res.* 77, 687–694.
- Rhee, D., Sanger, J.M., and Sanger, J.W. (1994). The premyofibril: evidence for its role in myofibrillogenesis. *Cell Motil. Cytoskeleton* 28, 1–24.

- Richard, P., Charron, P., Carrier, L., Ledeuil, C., Cheav, T., Pichereau, C., Benaiche, A., Isnard, R., Dubourg, O., Burban, M., et al. (2003). Hypertrophic cardiomyopathy: distribution of disease genes, spectrum of mutations, and implications for a molecular diagnosis strategy. *Circulation* 107, 2227–2232.
- Rindt, H., Bauer, B.J., and Robbins, J. (1993). In vitro production of enzymatically active myosin heavy chain. *J. Muscle Res. Cell Motil.* 14, 26–34.
- Roberts, R., and Sigwart, U. (2001). New Concepts in Hypertrophic Cardiomyopathies, Part II. *Circulation* 104, 2249–2252.
- Rodríguez, J.E., Schisler, J.C., Patterson, C., and Willis, M.S. (2009). Seek and destroy: the ubiquitin--proteasome system in cardiac disease. *Curr. Hypertens. Rep.* 11, 396–405.
- Roman, M.J., Okin, P.M., Kizer, J.R., Lee, E.T., Howard, B.V., and Devereux, R.B. (2010). Relations of central and brachial blood pressure to left ventricular hypertrophy and geometry: the Strong Heart Study. *J. Hypertens.* 28, 384–388.
- Roy Chowdhuri, S., Crum, T., Woollard, A., Aslam, S., and Okkema, P.G. (2006). The T-box factor TBX-2 and the SUMO conjugating enzyme UBC-9 are required for ABA-derived pharyngeal muscle in *C. elegans*. *Dev. Biol.* 295, 664–677.
- Rybakova, I.N., Greaser, M.L., and Moss, R.L. (2011). Myosin binding protein C interaction with actin: characterization and mapping of the binding site. *J. Biol. Chem.* 286, 2008–2016.
- Saba, M.M., Ibrahim, M.M., and Rizk, H.H. (2001). Gender and the relationship between resting heart rate and left ventricular geometry. *J. Hypertens.* 19, 367–373.
- Sachdev, S., Bruhn, L., Sieber, H., Pichler, A., Melchior, F., and Grosschedl, R. (2001). PIASy, a nuclear matrix-associated SUMO E3 ligase, represses LEF1 activity by sequestration into nuclear bodies. *Genes Dev.* 15, 3088–3103.
- Sadayappan, S., Osinska, H., Klevitsky, R., Lorenz, J.N., Sargent, M., Molkentin, J.D., Seidman, C.E., Seidman, J.G., Robbins, J. (2006). Cardiac myosin binding protein C phosphorylation is cardioprotective. *Proc. Natl. Acad. Sci. U.S.A.* 103, 16918–16923.
- Saido, T.C., Sorimachi, H., and Suzuki, K. (1994). Calpain: new perspectives in molecular diversity and physiological-pathological involvement. *FASEB J. Off. Publ. Fed. Am. Soc. Exp. Biol.* 8, 814–822.
- Sanger, J.W., Kang, S., Siebrands, C.C., Freeman, N., Du, A., Wang, J., Stout, A.L., and Sanger, J.M. (2005). How to build a myofibril. *J. Muscle Res. Cell Motil.* 26, 343–354.

- Santos, S., Marques, V., Pires, M., Silveira, L., Oliveira, H., Lança, V., Brito, D., Madeira, H., Esteves, J.F., Freitas, A., et al. (2012). High resolution melting: improvements in the genetic diagnosis of hypertrophic cardiomyopathy in a Portuguese cohort. *BMC Med. Genet.* 13, 17.
- Sardao, V., Oliveira, P., Holy, J., Oliveira, C., Wallace, K. (2007). Vital imaging of H9c2 myoblasts exposed to tert-butylhydroperoxide-characterization of morphological features of cell death. *BMC Cell. Biol.* 8, 11.
- Sarikas, A., Carrier, L., Schenke, C., Doll, D., Flavigny, J., Lindenberg, K.S., Eschenhagen, T., and Zolk, O. (2005). Impairment of the ubiquitin-proteasome system by truncated cardiac myosin binding protein C mutants. *Cardiovasc. Res.* 66, 33–44.
- Sayed, D., Hong, C., Chen, I.-Y., Lypowy, J., and Abdellatif, M. (2007). MicroRNAs play an essential role in the development of cardiac hypertrophy. *Circ. Res.* 100, 416–424.
- Schaid, D.J. (2004). Evaluating associations of haplotypes with traits. *Genet. Epidemiol.* 27, 348–364.
- Schaid, D.J., Rowland, C.M., Tines, D.E., Jacobson, R.M., and Poland, G.A. (2002). Score tests for association between traits and haplotypes when linkage phase is ambiguous. *Am. J. Hum. Genet.* 70, 425–434.
- Schiller, N.B., Shah, P.M., Crawford, M., DeMaria, A., Devereux, R., Feigenbaum, H., Gutgesell, H., Reichek, N., Sahn, D., and Schnittger, I. (1989). Recommendations for quantitation of the left ventricle by two-dimensional echocardiography. American Society of Echocardiography Committee on Standards, Subcommittee on Quantitation of Two-Dimensional Echocardiograms. *J. Am. Soc. Echocardiogr. Off. Publ. Am. Soc. Echocardiogr.* 2, 358–367.
- Schlossarek, S., Englmann, D.R., Sultan, K.R., Sauer, M., Eschenhagen, T., and Carrier, L. (2012). Defective proteolytic systems in Mybpc3-targeted mice with cardiac hypertrophy. *Basic Res. Cardiol.* 107, 235.
- Schoen, F.J. (2008). Hypertrophic cardiomyopathy. In Robbins' pathologic basis of disease, F.J. Schoen, ed. (Philadelphia: WB Saunders Co.), pp. 582-583.
- Schultheiss, T., Lin, Z.X., Lu, M.H., Murray, J., Fischman, D.A., Weber, K., Masaki, T., Imamura, M., and Holtzer, H. (1990). Differential distribution of subsets of myofibrillar proteins in cardiac nonstriated and striated myofibrils. *J. Cell Biol.* 110, 1159–1172.
- Seeley, M., Huang, W., Chen, Z., Wolff, W.O., Lin, X., and Xu, X. (2007). Depletion of zebrafish titin reduces cardiac contractility by disrupting the assembly of Z-discs and A-bands. *Circ. Res.* 100, 238–245.

- Seidman, C.E., and Seidman, J.G. (2011). Identifying sarcomere gene mutations in hypertrophic cardiomyopathy: a personal history. *Circ. Res.* 108, 743–750.
- Seidman, J.G., and Seidman, C. (2001). The genetic basis for cardiomyopathy: from mutation identification to mechanistic paradigms. *Cell* 104, 557–567.
- Seiler, S.H., Fischman, D.A., and Leinwand, L.A. (1996). Modulation of myosin filament organization by C-protein family members. *Mol. Biol. Cell* 7, 113–127.
- Sekar, R.B. (2003). Fluorescence resonance energy transfer (FRET) microscopy imaging of live cell protein localizations. *J. Cell Biol.* 160, 629–633.
- Seufert, W., Futcher, B., and Jentsch, S. (1995). Role of a ubiquitin-conjugating enzyme in degradation of S- and M-phase cyclins. *Nature* 373, 78–81.
- Shaffer, J.F., Kensler, R.W., and Harris, S.P. (2009). The Myosin-binding Protein C Motif Binds to F-actin in a Phosphorylation-sensitive Manner. *J. Biol. Chem.* 284, 12318–12327.
- Shifman, S., Kuypers, J., Kokoris, M., Yakir, B., and Darvasi, A. (2003). Linkage disequilibrium patterns of the human genome across populations. *Hum. Mol. Genet.* 12, 771–776.
- Shimizu, S., Kanaseki, T., Mizushima, N., Mizuta, T., Arakawa-Kobayashi, S., Thompson, C.B., and Tsujimoto, Y. (2004). Role of Bcl-2 family proteins in a non-apoptotic programmed cell death dependent on autophagy genes. *Nat. Cell Biol.* 6, 1221–1228.
- Shimomura, H., Terasaki, F., Hayashi, T., Kitaura, Y., Isomura, T., and Suma, H. (2001). Autophagic degeneration as a possible mechanism of myocardial cell death in dilated cardiomyopathy. *Jpn. Circ. J.* 65, 965–968.
- Shioi, T. (2003). Rapamycin Attenuates Load-Induced Cardiac Hypertrophy in Mice. *Circulation* 107, 1664–1670.
- Simmerman, H.K., and Jones, L.R. (1998). Phospholamban: protein structure, mechanism of action, and role in cardiac function. *Physiol. Rev.* 78, 921–947.
- Singh, R.B., Dandekar, S.P., Elimban, V., Gupta, S.K., and Dhalla, N.S. (2004). Role of proteases in the pathophysiology of cardiac disease. *Mol. Cell. Biochem.* 263, 241–256.
- Sipola, P., Magga, J., Husso, M., Jääskeläinen, P., Peuhkurinen, K., and Kuusisto, J. (2011). Cardiac MRI assessed left ventricular hypertrophy in differentiating hypertensive heart disease from hypertrophic cardiomyopathy attributable to a sarcomeric gene mutation. *Eur. Radiol.* 21, 1383–1389.
- Skwarek-Maruszewska, A., Hotulainen, P., Mattila, P.K., and Lappalainen, P. (2009). Contractility-dependent actin dynamics in cardiomyocyte sarcomeres. *J. Cell Sci.* 122, 2119–2126.

- Sobel, E., and Lange, K. (1996). Descent graphs in pedigree analysis: applications to haplotyping, location scores, and marker-sharing statistics. *Am. J. Hum. Genet.* 58, 1323–1337.
- Sohn, R.L., Vikstrom, K.L., Strauss, M., Cohen, C., Szent-Gyorgyi, A.G., and Leinwand, L.A. (1997). A 29 residue region of the sarcomeric myosin rod is necessary for filament formation. *J. Mol. Biol.* 266, 317–330.
- Solaro, R.J., Moir, A.J., and Perry, S.V. (1976). Phosphorylation of troponin I and the inotropic effect of adrenaline in the perfused rabbit heart. *Nature* 262, 615–617.
- Song, T., Li, G., Jing, G., Jiao, X., Shi, J., Zhang, B., Wang, L., Ye, X., and Cao, F. (2008). SUMO1 polymorphisms are associated with non-syndromic cleft lip with or without cleft palate. *Biochem. Biophys. Res. Commun.* 377, 1265–1268.
- Sorimachi, H., and Suzuki, K. (2001). The structure of calpain. *J. Biochem. (Tokyo)* 129, 653–664.
- Sorimachi, H., Ishiura, S., and Suzuki, K. (1997). Structure and physiological function of calpains. *Biochem. J.* 328 (Pt 3), 721–732.
- Soteriou, A., Gamage, M., and Trinick, J. (1993). A survey of interactions made by the giant protein titin. *J. Cell Sci.* 104 (Pt 1), 119–123.
- Sparrow, J.C., and Schöck, F. (2009). The initial steps of myofibril assembly: integrins pave the way. *Nat. Rev. Mol. Cell Biol.* 10, 293–298.
- Spencer, J.A., Eliazer, S., Ilaria, R.L., Richardson, J.A., and Olson, E.N. (2000). Regulation of Microtubule Dynamics and Myogenic Differentiation by Murf, a Striated Muscle Ring-Finger Protein. *J. Cell Biol.* 150, 771–784.
- Sperelakis, N., Xiong, Z., Haddad, G., and Masuda, H. (1994). Regulation of slow calcium channels of myocardial cells and vascular smooth muscle cells by cyclic nucleotides and phosphorylation. *Mol. Cell. Biochem.* 140, 103–117.
- Spirito, P., and Maron, B.J. (1990). Relation between extent of left ventricular hypertrophy and occurrence of sudden cardiac death in hypertrophic cardiomyopathy. *J. Am. Coll. Cardiol.* 15, 1521–1526.
- Squire, J.M., Luther, P.K., and Knupp, C. (2003). Structural evidence for the interaction of C-protein (MyBP-C) with actin and sequence identification of a possible actin-binding domain. *J. Mol. Biol.* 331, 713–724.
- Squire, J.M., Al-khayat, H.A., Knupp, C., and Luther, P.K. (2005). Molecular Architecture in Muscle Contractile Assemblies. In *Advances in Protein Chemistry*, (Elsevier), pp. 17–87.

- Starr, R., Almond, R., and Offer, G. (1985). Location of C-protein, H-protein and X-protein in rabbit skeletal muscle fibre types. *J. Muscle Res. Cell Motil.* 6, 227–256.
- Stelzer, J.E., Dunning, S.B., and Moss, R.L. (2006a). Ablation of cardiac myosin-binding protein-C accelerates stretch activation in murine skinned myocardium. *Circ. Res.* 98, 1212–1218.
- Stelzer, J.E., Fitzsimons, D.P., and Moss, R.L. (2006b). Ablation of myosin-binding protein-C accelerates force development in mouse myocardium. *Biophys. J.* 90, 4119–4127.
- Stelzer, J.E., Patel, J.R., and Moss, R.L. (2006c). Protein kinase A-mediated acceleration of the stretch activation response in murine skinned myocardium is eliminated by ablation of cMyBP-C. *Circ. Res.* 99, 884–890.
- Stelzer, J.E., Patel, J.R., Walker, J.W., and Moss, R.L. (2007). Differential roles of cardiac myosin-binding protein C and cardiac troponin I in the myofibrillar force responses to protein kinase A phosphorylation. *Circ. Res.* 101, 503–511.
- Stöhr, A., Friedrich, F.W., Flenner, F., Geertz, B., Eder, A., Schaaf, S., Hirt, M.N., Uebeler, J., Schlossarek, S., Carrier, L., et al. (2013). Contractile abnormalities and altered drug response in engineered heart tissue from Mybpc3-targeted knock-in mice. *J. Mol. Cell. Cardiol.*
- Straceski, A.J., Geisterfer-Lowrance, A., Seidman, C.E., Seidman, J.G., and Leinwand, L.A. (1994). Functional analysis of myosin missense mutations in familial hypertrophic cardiomyopathy. *Proc. Natl. Acad. Sci. U. S. A.* 91, 589–593.
- Stram, D.O. (2004). Tag SNP selection for association studies. *Genet. Epidemiol.* 27, 365–374.
- Sulakhe, P.V., and Vo, X.T. (1995). Regulation of phospholamban and troponin-I phosphorylation in the intact rat cardiomyocytes by adrenergic and cholinergic stimuli: roles of cyclic nucleotides, calcium, protein kinases and phosphatases and depolarization. *Mol. Cell. Biochem.* 149-150, 103–126.
- Suurmeijer, A.J., Clement, S., Francesconi, A., Bocchi, L., Angelini, A., Van Veldhuisen, D.J., Spagnoli, L.G., Gabbiani, G., and Orlandi, A. (2003). α -Actin isoform distribution in normal and failing human heart: a morphological, morphometric, and biochemical study. *J. Pathol.* 199, 387–397.
- Suzuki, K., Kubota, Y., Sekito, T., and Ohsumi, Y. (2007). Hierarchy of Atg proteins in pre-autophagosomal structure organization. *Genes Cells Devoted Mol. Cell. Mech.* 12, 209–218.
- Swan, L., Birnie, D.H., Padmanabhan, S., Inglis, G., Connell, J.M.C., and Hillis, W.S. (2003). The genetic determination of left ventricular mass in healthy adults. *Eur. Heart J.* 24, 577–582.

- Tanaka, Y., Guhde, G., Suter, A., Eskelinen, E.L., Hartmann, D., Lüllmann-Rauch, R., Janssen, P.M., Blanz, J., von Figura, K., and Saftig, P. (2000). Accumulation of autophagic vacuoles and cardiomyopathy in LAMP-2-deficient mice. *Nature* 406, 902–906.
- Tanida, I., Ueno, T., and Kominami, E. (2004a). LC3 conjugation system in mammalian autophagy. *Int. J. Biochem. Cell Biol.* 36, 2503–2518.
- Tanida, I., Sou, Y., Ezaki, J., Minematsu-Ikeguchi, N., Ueno, T., and Kominami, E. (2004b). HsAtg4B/HsApg4B/autophagin-1 cleaves the carboxyl termini of three human Atg8 homologues and delipidates microtubule-associated protein light chain 3- and GABAA receptor-associated protein-phospholipid conjugates. *J. Biol. Chem.* 279, 36268–36276.
- Tateishi, Y., Ariyoshi, M., Igarashi, R., Hara, H., Mizuguchi, K., Seto, A., Nakai, A., Kokubo, T., Tochio, H., and Shirakawa, M. (2009). Molecular basis for SUMOylation-dependent regulation of DNA binding activity of heat shock factor 2. *J. Biol. Chem.* 284, 2435–2447.
- Tavtigian, S.V., Simard, J., Teng, D.H., Abtin, V., Baumgard, M., Beck, A., Camp, N.J., Carillo, A.R., Chen, Y., Dayananth, P., et al. (2001). A candidate prostate cancer susceptibility gene at chromosome 17p. *Nat. Genet.* 27, 172–180.
- Thierfelder, L., Watkins, H., MacRae, C., Lamas, R., McKenna, W., Vosberg, H.P., Seidman, J.G., and Seidman, C.E. (1994). Alpha-tropomyosin and cardiac troponin T mutations cause familial hypertrophic cardiomyopathy: a disease of the sarcomere. *Cell* 77, 701–712.
- Thomas, D.C., and Clayton, D.G. (2004). Betting odds and genetic associations. *J. Natl. Cancer Inst.* 96, 421–423.
- Tong, C.W., Stelzer, J.E., Greaser, M.L., Powers, P.A., and Moss, R.L. (2008). Acceleration of crossbridge kinetics by protein kinase A phosphorylation of cardiac myosin binding protein C modulates cardiac function. *Circ. Res.* 103, 974–982.
- Ueno, T., and Takahashi, K. (2009). A cathepsin L-specific inhibitor preferentially inhibits degradation of autophagosomal LC3 and GABARAP in HeLa and Huh-7 cells. *Autophagy* 5, 878–879.
- Van Criekinge, W., and Beyaert, R. (1999). Yeast Two-Hybrid: State of the Art. *Biol. Proced. Online* 2, 1–38.
- Vandekerckhove, J., Bugaisky, G., and Buckingham, M. (1986). Simultaneous expression of skeletal muscle and heart actin proteins in various striated muscle tissues and cells. A quantitative determination of the two actin isoforms. *J. Biol. Chem.* 261, 1838–1843.
- Van der Merwe, L., Cloete, R., Revera, M., Heradien, M., Goosen, A., Corfield, V.A., Brink, P.A., and Moolman-Smook, J.C. (2008). Genetic variation in angiotensin-converting enzyme 2 gene is

- associated with extent of left ventricular hypertrophy in hypertrophic cardiomyopathy. *Hum. Genet.* 124, 57–61.
- Van Driest, S.L., Ommen, S.R., Tajik, A.J., Gersh, B.J., and Ackerman, M.J. (2005a). Yield of genetic testing in hypertrophic cardiomyopathy. *Mayo ClinProc* 80, 739–744.
- Van Driest, S.L., Ommen, S.R., Tajik, A.J., Gersh, B.J., and Ackerman, M.J. (2005b). Sarcomeric genotyping in hypertrophic cardiomyopathy. *Mayo Clin. Proc. Mayo Clin.* 80, 463–469.
- Van Driest, S.L., Vasile, V.C., Ommen, S.R., Will, M.L., Tajik, A.J., Gersh, B.J., and Ackerman, M.J. (2004). Myosin binding protein C mutations and compound heterozygosity in hypertrophic cardiomyopathy. *J. Am. Coll. Cardiol.* 44, 1903–1910.
- Van Empel, V.P.M., De Windt, L.J., and da Costa Martins, P.A. (2012). Circulating miRNAs: reflecting or affecting cardiovascular disease? *Curr. Hypertens. Rep.* 14, 498–509.
- Varnava, A.M., Elliott, P.M., Mahon, N., Davies, M.J., and McKenna, W.J. (2001). Relation between myocyte disarray and outcome in hypertrophic cardiomyopathy. *Am. J. Cardiol.* 88, 275–279.
- Vaughan, K.T., Weber, F.E., Ried, T., Ward, D.C., Reinach, F.C., and Fischman, D.A. (1993a). Human myosin-binding protein H (MyBP-H): complete primary sequence, genomic organization, and chromosomal localization. *Genomics* 16, 34–40.
- Vaughan, K.T., Weber, F.E., Einheber, S., and Fischman, D.A. (1993b). Molecular cloning of chicken myosin-binding protein (MyBP) H (86-kDa protein) reveals extensive homology with MyBP-C (C-protein) with conserved immunoglobulin C2 and fibronectin type III motifs. *J. Biol. Chem.* 268, 3670–3676.
- Vega, R.B., Harrison, B.C., Meadows, E., Roberts, C.R., Papst, P.J., Olson, E.N., and McKinsey, T.A. (2004). Protein kinases C and D mediate agonist-dependent cardiac hypertrophy through nuclear export of histone deacetylase 5. *Mol. Cell. Biol.* 24, 8374–8385.
- Verdecchia, P., Porcellati, C., Reboldi, G., Gattobigio, R., Borgioni, C., Pearson, T.A., and Ambrosio, G. (2001). Left ventricular hypertrophy as an independent predictor of acute cerebrovascular events in essential hypertension. *Circulation* 104, 2039–2044.
- Vignier, N., Schlossarek, S., Fraysse, B., Mearini, G., Krämer, E., Pointu, H., Mougnot, N., Guiard, J., Reimer, R., Hohenberg, H., et al. (2009). Nonsense-mediated mRNA decay and ubiquitin-proteasome system regulate cardiac myosin-binding protein C mutant levels in cardiomyopathic mice. *Circ. Res.* 105, 239–248.

- Vikstrom, K.L., Rovner, A.S., Saez, C.G., Bravo-Zehnder, M., Straceski, A.J., and Leinwand, L.A. (1993). Sarcomeric myosin heavy chain expressed in nonmuscle cells forms thick filaments in the presence of substoichiometric amounts of light chains. *Cell Motil. Cytoskeleton* 26, 192–204.
- Wang, J., and Schwartz, R.J. (2010). Sumoylation and regulation of cardiac gene expression. *Circ. Res.* 107, 19–29.
- Wang, K., and Williamson, C.L. (1980). Identification of an N2 line protein of striated muscle. *Proc. Natl. Acad. Sci. U. S. A.* 77, 3254–3258.
- Wang, J., Sanger, J.M., and Sanger, J.W. (2005). Differential effects of Latrunculin-A on myofibrils in cultures of skeletal muscle cells: insights into mechanisms of myofibrillogenesis. *Cell Motil. Cytoskeleton* 62, 35–47.
- Wang, L., Seidman, J.G., and Seidman, C.E. (2010). Narrative review: harnessing molecular genetics for the diagnosis and management of hypertrophic cardiomyopathy. *Ann. Intern. Med.* 152, 513–520, W181.
- Watkins, H., McKenna, W.J., Thierfelder, L., Suk, H.J., Anan, R., O'Donoghue, A., Spirito, P., Matsumori, A., Moravec, C.S., and Seidman, J.G. (1995). Mutations in the genes for cardiac troponin T and alpha-tropomyosin in hypertrophic cardiomyopathy. *N. Engl. J. Med.* 332, 1058–1064.
- Watkins, S.J., Borthwick, G.M., Arthur, H.M. (2011). The H9c2 cell line and primary neonatal cardiomyocyte cells show similar hypertrophic responses in vitro. *In vitro Cell. Dev. Biol. Animal* 47, 125-131.
- Watts, R.G., and Howard, T.H. (1992). Evidence for a gelsolin-rich, labile F-actin pool in human polymorphonuclear leukocytes. *Cell Motil. Cytoskeleton* 21, 25–37.
- Weidberg, H., Shvets, E., Shpilka, T., Shimron, F., Shinder, V., and Elazar, Z. (2010). LC3 and GATE-16/GABARAP subfamilies are both essential yet act differently in autophagosome biogenesis. *EMBO J.* 29, 1792–1802.
- Weisberg, A., and Winegrad, S. (1996). Alteration of myosin cross bridges by phosphorylation of myosin-binding protein C in cardiac muscle. *Proc. Natl. Acad. Sci. U. S. A.* 93, 8999–9003.
- Weisberg, A., and Winegrad, S. (1998). Relation between crossbridge structure and actomyosin ATPase activity in rat heart. *Circ. Res.* 83, 60–72.
- Weiss, K.M., and Clark, A.G. (2002). Linkage disequilibrium and the mapping of complex human traits. *Trends Genet. TIG* 18, 19–24.

- Welikson, R.E., and Fischman, D.A. (2002). The C-terminal IgI domains of myosin-binding proteins C and H (MyBP-C and MyBP-H) are both necessary and sufficient for the intracellular crosslinking of sarcomeric myosin in transfected non-muscle cells. *J. Cell Sci.* 115, 3517–3526.
- Wigginton, J.E., and Abecasis, G.R. (2005). PEDSTATS: descriptive statistics, graphics and quality assessment for gene mapping data. *Bioinforma. Oxf. Engl.* 21, 3445–3447.
- Wigle, E.D., Sasson, Z., Henderson, M.A., Ruddy, T.D., Fulop, J., Rakowski, H., and Williams, W.G. (1985). Hypertrophic cardiomyopathy. The importance of the site and the extent of hypertrophy. A review. *Prog. Cardiovasc. Dis.* 28, 1–83.
- Willis, M.S., Rojas, M., Li, L., Selzman, C.H., Tang, R.-H., Stansfield, W.E., Rodriguez, J.E., Glass, D.J., and Patterson, C. (2009). Muscle ring finger 1 mediates cardiac atrophy in vivo. *Am. J. Physiol. Heart Circ. Physiol.* 296, H997–H1006.
- Winegrad, S. (1999). Cardiac myosin binding protein C. *Circ. Res.* 84, 1117–1126.
- Witt, C.C., Burkart, C., Labeit, D., McNabb, M., Wu, Y., Granzier, H., and Labeit, S. (2006). Nebulin regulates thin filament length, contractility, and Z-disk structure in vivo. *EMBO J.* 25, 3843–3855.
- Witt, C.C., Witt, S.H., Lerche, S., Labeit, D., Back, W., and Labeit, S. (2007). Cooperative control of striated muscle mass and metabolism by MuRF1 and MuRF2. *EMBO J.* 27, 350–360.
- Witt, S.H., Granzier, H., Witt, C.C., and Labeit, S. (2005). MURF-1 and MURF-2 target a specific subset of myofibrillar proteins redundantly: towards understanding MURF-dependent muscle ubiquitination. *J. Mol. Biol.* 350, 713–722.
- Wu, F., and Mo, Y.-Y. (2007). Ubiquitin-like protein modifications in prostate and breast cancer. *Front. Biosci. J. Virtual Libr.* 12, 700–711.
- Xiao, R.P. (2001). Beta-adrenergic signaling in the heart: dual coupling of the beta2-adrenergic receptor to G(s) and G(i) proteins. *Sci. STKE Signal Transduct. Knowl. Environ.* 2001, re15.
- Yamaguchi, O. (2003). Targeted deletion of apoptosis signal-regulating kinase 1 attenuates left ventricular remodeling. *Proc. Natl. Acad. Sci.* 100, 15883–15888.
- Yamamoto, K. (1984). Characterization of H-protein, a component of skeletal muscle myofibrils. *J. Biol. Chem.* 259, 7163–7168.
- Yamamoto, K., and Moos, C. (1983). The C-proteins of rabbit red, white, and cardiac muscles. *J. Biol. Chem.* 258, 8395–8401.

- Yanazume, T., Hasegawa, K., Morimoto, T., Kawamura, T., Wada, H., Matsumori, A., Kawase, Y., Hirai, M., and Kita, T. (2003). Cardiac p300 is involved in myocyte growth with decompensated heart failure. *Mol. Cell. Biol.* 23, 3593–3606.
- Yasuda, M., Koshida, S., Sato, N., and Obinata, T. (1995). Complete primary structure of chicken cardiac C-protein (MyBP-C) and its expression in developing striated muscles. *J. Mol. Cell. Cardiol.* 27, 2275–2286.
- Yeh, E.T.H. (2009). SUMOylation and De-SUMOylation: wrestling with life's processes. *J. Biol. Chem.* 284, 8223–8227.
- Ylä-Anttila, P., Vihinen, H., Jokitalo, E., and Eskelinen, E.-L. (2009). 3D tomography reveals connections between the phagophore and endoplasmic reticulum. *Autophagy* 5, 1180–1185.
- Yorimitsu, T., and Klionsky, D.J. (2005). Autophagy: molecular machinery for self-eating. *Cell Death Differ.* 12, 1542–1552.
- Yoshioka, K. (2003). A role for LIM kinase in cancer invasion. *Proc. Natl. Acad. Sci.* 100, 7247–7252.
- Zaykin, D.V., Westfall, P.H., Young, S.S., Karnoub, M.A., Wagner, M.J., and Ehm, M.G. (2002). Testing association of statistically inferred haplotypes with discrete and continuous traits in samples of unrelated individuals. *Hum. Hered.* 53, 79–91.
- Zeng, X., Overmeyer, J.H., and Maltese, W.A. (2006). Functional specificity of the mammalian Beclin-Vps34 PI 3-kinase complex in macroautophagy versus endocytosis and lysosomal enzyme trafficking. *J. Cell Sci.* 119, 259–270.
- Zhang, K., and Sun, F. (2005). Assessing the power of tag SNPs in the mapping of quantitative trait loci (QTL) with extremal and random samples. *BMC Genet.* 6, 51.
- Zhang, Y.-Q., and Sarge, K.D. (2008). Sumoylation regulates lamin A function and is lost in lamin A mutants associated with familial cardiomyopathies. *J. Cell Biol.* 182, 35–39.
- Zhang, L., Ding, L., Cheung, T.H., Dong, M.-Q., Chen, J., Sewell, A.K., Liu, X., Yates, J.R., 3rd, and Han, M. (2007). Systematic identification of *C. elegans* miRISC proteins, miRNAs, and mRNA targets by their interactions with GW182 proteins AIN-1 and AIN-2. *Mol. Cell* 28, 598–613.
- Zhang, Q.-J., Chen, H.-Z., Wang, L., Liu, D.-P., Hill, J.A., and Liu, Z.-P. (2011). The histone trimethyllysine demethylase JMJD2A promotes cardiac hypertrophy in response to hypertrophic stimuli in mice. *J. Clin. Invest.* 121, 2447–2456.
- Zhang, Z.-Y., Zhou, B., and Xie, L. (2002). Modulation of protein kinase signaling by protein phosphatases and inhibitors. *Pharmacol. Ther.* 93, 307–317.

- Zhao, X.L., Gutierrez, L.M., Chang, C.F., and Hosey, M.M. (1994). The alpha 1-subunit of skeletal muscle L-type Ca channels is the key target for regulation by A-kinase and protein phosphatase-1C. *Biochem. Biophys. Res. Commun.* 198, 166–173.
- Zheng, Q., and Wang, X. (2010). Autophagy and the ubiquitin-proteasome system in cardiac dysfunction. *Panminerva Med.* 52, 9–25.
- Zheng, Q., Li, J., and Wang, X. (2009). Interplay between the ubiquitin-proteasome system and autophagy in proteinopathies. *Int. J. Physiol. Pathophysiol. Pharmacol.* 1, 127–142.
- Zhu, L., Santos, N.C., and Kim, K.H. (2009). Small ubiquitin-like modifier-2 modification of retinoic acid receptor-alpha regulates its subcellular localization and transcriptional activity. *Endocrinology* 150, 5586–5595.
- Zinchuk, V., Zinchuk, O., and Okada, T. (2007). Quantitative Colocalization Analysis of Multicolor Confocal Immunofluorescence Microscopy Images: Pushing Pixels to Explore Biological Phenomena. *Acta Histochem. Cytochem.* 40, 101–111.
- Zodorky, B.N.M. and El-Kadi, A.O.S. (2007). H9c2 cell line is a valuable in vitro model to study the drug metabolizing enzymes in the heart. *J. Pharmacol. Toxicol. Methods.* 56, 317–322.
- Zoghbi, M.E., Woodhead, J.L., Moss, R.L., and Craig, R. (2008). Three-dimensional structure of vertebrate cardiac muscle myosin filaments. *Proc. Natl. Acad. Sci. U. S. A.* 105, 2386–2390.
- Zolk, O., Schenke, C., and Sarikas, A. (2006). The ubiquitin–proteasome system: Focus on the heart. *Cardiovasc. Res.* 70, 410–421.
- Zou, P., Pinotsis, N., Lange, S., Song, Y.-H., Popov, A., Mavridis, I., Mayans, O.M., Gautel, M., and Wilmanns, M. (2006). Palindromic assembly of the giant muscle protein titin in the sarcomeric Z-disk. *Nature* 439, 229–233.